Polyploid phasing algorithms and applications

Omar Abou Saada

Université de Strasbourg

UNIVERSITY OF STRASBOURG

École Doctorale des Sciences de la Vie et de la Santé STRASBOURG

DOCTORAL SCHOOL ED414

UMR7156 Genomics, Molecular Genetics, Microbiology

Doctoral dissertation presented by:

Omar ABOU SAADA

defended on: September 27th, 2021

In partial fulfillment of the requirements of a degree of: **Doctor of Philosophy**

Discipline/Specialty: Bioinformatics

Polyploid phasing algorithms and applications

Ph.D. advised by:

FRIEDRICH Anne	Associate professor, University of Strasbourg
SCHACHERER Joseph	Professor, University of Strasbourg

REPORTER:

WEIGEL Detlef	Professor, University of Tübingen
WOLFE Ken	Professor, University College Dublin

OTHER MEMBERS OF THE COMMITTEE:

AURY Jean-Marc	Researcher, Genoscope
LECOMPTE Odile	Professor, University of Strasbourg

Université de Strasbourg

UNIVERSITÉ DE STRASBOURG

École Doctorale des Sciences de la Vie et de la Santé STRASBOURG

ÉCOLE DOCTORALE ED414

UMR7156 Génétique Moléculaire, Génomique, Microbiologie

THÈSE présentée par:

Omar ABOU SAADA

soutenue le : September 27th, 2021

pour obtenir le grade de : **Docteur de l'Université de Stasbourg**

Discipline/Spécialité: Bioinformatique

Algorithmes de phasage de polyploides et leurs applications

THÈSE dirigée par:

FRIEDRICH Anne	Maître de conférences, Université de Strasbourg
SCHACHERER Joseph	Professeur, Université de Strasbourg

RAPPORTEURS:

WEIGEL Detlef	Professeur, Université de Tübingen
WOLFE Ken	Professeur, University College Dublin

AUTRES MEMBRES DU JURY:

AURY Jean-Marc	Chercheur, Genoscope
LECOMPTE Odile	Professeur, Université de Strasbourg

Acknowledgements

The following work has been completed at the department of molecular genetics, genomics and microbiology, UMR7156/CNRS, University of Strasbourg, under the co-supervision of Pr. Anne Friedrich and Pr. Joseph Schacherer.

I thank the members of the committee, Mr. Jean-Marc Aury, Pr. Odile Lecompte, Pr. Detlef Weigel and Pr. Ken Wolfe for agreeing to judge this work. I would also be remiss not to thank Dr. Anais Bardet, Dr. Todd Blevins and Dr. Olivier Poch for the valuable comments and advice they provided during my mid-thesis committees.

My co-supervisors, Anne and Joseph, have consistently maintained a very welcoming, constructive environment in which I had the autonomy to make mistakes and their support and wisdom to show me how to overcome any challenge. I never felt like there was something that could not be done, an idea that could not be pursued, and they have always figured out how to steer me back into the right direction.
Thank you Anne for always finding the time to discuss my ideas and all of your helpful comments, especially for nPhase, and for being patient with my writing.
Thank you Joseph for trusting me to dig just a little bit deeper in projects, to always try one more thing to solve a problem, and for providing consistently actionable ideas and criticism.

Over the course of this thesis I have felt listened to, valued, supported and encouraged to pursue projects I found interesting, and I cannot imagine a better work environment.
I would like to thank everyone in the lab for contributing to this great environment: Jackson for being kind enough to leave me with a survival guide to perform GWAS

using the 1,011 data, Jean-Seb for bringing life to the office I shared with him for a time, Elodie who endured a thesis at the same time as me and, being far more serious and competent than me, was always a lifesaver for administrative questions, Téo for his ridiculously good sense of visual design, Sabrina for being so funny, the lab hasn't been the same without you! Of course, I also thank Fabien for always transcending concepts, Claudia for very kindly asking me every now and then how I'm doing, and bringing a lot of energy into the office, Emilien for that time he helped me with that thing in that place for the guy, and to which he is now sworn to secrecy, Elie for helping me coax people from the lab into going out to karaoke, and having a ton of fun in the process, Marion for soon enthusiastically making the mistake of joining us for karaoke, Andreas for all your hard work sequencing and selecting these beer strains with me, and hopefully soon for all your hard work drinking the fruit of their labor with me, Chris for just generally being such an open and kind person, Abhishek for his seriously impressive knowledge of the literature, encouraging me to want to be able to be a tenth as knowledgeable as him, Jing for just being an actual, real-life legend of the lab, Emna for bringing such a cool project to the lab, and last but not least, Claudine, whose project on retrotransposons was my introduction to the lab!

There have been others I haven't mentioned here, who did not stay as long but left their own unique impressions and contributed to a lively lab.

I also want to thank the people I've had the opportunity to work with, in particular but not limited to: Gilles Fischer, Gianni Liti, Samuel O'Donnel, Jia-Xing Yue, Maitreya Dunham and Chris Large. Thank you for your comments and collaboration.

I've been incredibly lucky in my education. I would like to thank my parents for listening to their scared 5-year-old child, intimidated by the large classrooms typical

of public education in Egypt. Thank you Josiane, my first elementary school teacher, for confidently telling my mom that I would go far in education. Thank you Pr. Bourguet, my high school biology teacher, for sparking my interest in molecular genetics. Thank you, Pr. Potier, for welcoming us all into the community of scientists and biologists in the first university class of the first year. Thank you Pr. Jossinet and Dr. Lescure for convincing me to pursue bioinformatics. Thank you, Dr. Bardet, for all that you've helped me learn during the Master's degree project you supervised.

Thank you, Arielyn, for sharing so much with me, including our passion for data analysis and puzzle pieces that can fit together in different ways.
Thank you, Justine, for agreeing to get on this rollercoaster with me and inspiring me with your true strength and determination.

Thank you to my parents and sister for always being supportive, and Chadi for being such a cool addition to the family. I'm always lost in my projects, and I don't call nearly as much as I should, but knowing I have a home in you all has always been a source of confidence and serenity for me. Thank you to my uncle Pierre and his wife Rosie for helping me get my bearings when I moved to France. I also want to thank the rest of my family, in France and in Egypt, for their love, support, and patience after asking me "So what do you do?".

Finally, I want to thank all of the people whose paths I've crossed who I haven't mentioned directly here. The list is too long.

Thank you meme Sausan for letting me win at tawla when I was a kid.

I miss you.

Table of Contents

STATE OF THE ART

The genomic era and associated promises of population genomics

The completion of the Human Genome Project in 2003[1] was a massive achievement which marked the beginning of the genomic era. This era is defined by the availability not only of the human genome but also of reference sequences for other model organisms, namely *Saccharomyces cerevisiae*[2], *Arabidopsis thaliana*[3] and *Mus musculus*[4] among many others. The availability of these reference sequences was accompanied by the dramatic decrease in sequencing costs which enabled the rise of several -omic strategies such as the eponymous genomics, but also transcriptomics, epigenomics and associated high-throughput strategies such as ChIP-seq and Chromatin Conformation Capture. At that time, sequencing projects continued establishing reference sequences for more and more species, bringing the genetic diversity of life into focus[5] and greatly enriching the field of comparative genomics[6,7]. Sequencing multiple individuals of the same species enabled studies to start assessing the genetic diversity within a species, to investigate a population's evolutionary history and to identify commonly shared polymorphisms. Individuals of a species present phenotypic variability, part of which is heritable and must be driven in part by genetic differences. Uncovering the genetic part of heritability became possible with recently established reference sequences and increasing amounts of sequenced individuals. The prospect of deciphering the genetic information of species stirred interest in larger datasets of genomes, motivated in part by the idea that obtaining a wide range of genomes and associated phenotypes would help uncover genotype-phenotype relations. The sequencing costs continued decreasing until sequencing hundreds, even thousands of individuals was no longer prohibitively expensive, prompting the start of large population sequencing projects.

Consequently, the limiting factor has strongly shifted from our ability to generate biological data to our ability to analyze it. In 2014, the 3,000 rice genomes project called upon the international community to analyze their dataset[8]. In 2015, the 1000 Genomes Project provided 2504 human genome sequences and their associated variants[9], including structural variants[10] (SVs). Their paper and more importantly, its associated data, has been cited over 6000 times as of 2021. The 1001 Genomes Consortium published its study of 1,135 genomes of *Arabidopsis thaliana* in 2016, reconstructing its natural history and emphasizing how well the population is adapted for statistical association of genotype-phenotype relations[11]. In 2018, 1,011 strains of the model organism *Saccharomyces cerevisiae* were published in the context of the 1002 Yeast Genomes Project, characterizing the diversity of the species, noting the phenotypic effects of Copy Number Variants (CNVs) and providing a resource for population genomic studies in *S. cerevisiae*[12].

Population genomic studies survey the genetic and phenotypic diversity within a species. This variability can then be leveraged to identify genetic elements that are statistically associated with phenotypic states. To this end, the Genome-Wide Association Studies (GWAS) was developed, typically modelling the genetic architecture of phenotypes as consisting of additive effects. GWAS seeks to statistically infer genotype-phenotype relations using a phenotyped and genotyped population of individuals of the same species. To have sufficient statistical power, a large number of individuals is required, typically in the order of hundreds, or thousands. A major risk factor for age-related macular degeneration, a cause of irreversible loss of vision, was identified by a GWAS study on 226 individuals of Chinese descent using 100,000 SNPs[13]. Another early success for GWAS identified a gene associated with elevated risk of myocardial infarctions[14]. While a highly successful strategy for monogenic traits, it soon became apparent that for many common, highly heritable and complex traits, the alleles identified by GWAS

accounted for far less variability than was previously known to be heritable. The genetic part of the heritability of complex diseases such as the highly studied Alzheimer's Disease (AD) had been inferred by sibling and twin studies, setting a target of the heritability to explain. Still today, our understanding of the genetic basis of AD is incomplete. This progressive neurological disorder comes in two forms: the rare Early-Onset Alzheimer's Disease (EOAD), which comprises 5% of cases of AD, and Late-Onset Alzheimer's Disease (LOAD). LOAD affects individuals over the age of 65 and is estimated to be 58-79% heritable, while the heritability of EOAD is estimated at >90%[15]. 58 risk loci are associated with AD, capturing around 50% of the heritability of LOAD, with the remaining 50% still unaccounted for as of 2021[16].

Implementations of the GWAS method initially only considered common variants, though the inability to fully capture the genetically heritable part of phenotypic variability prompted a continual increase in the level of detail at which these genomes are characterized. Population genomic studies provide resources of unprecedented scale to the scientific community, with no signs of slowing down. The pilot phase of the GenomeAsia 100K project was recently published[17] and in 2019 the Sanger Institute announced it would sequence half a million whole human genomes from the UK biobank by 2021.

Missing nuances of population genomic studies

By their nature, large-scale population genomic studies provide more data than can be analyzed, and have yet to be fully exploitable. These population genomics efforts, and in particular their staple GWAS method have repeatedly exposed the gaps in our ability to link genotype and phenotype through such statistical associations. Phenotypic variance not explained by the set of significantly associated alleles, such as the missing 50% of heritability in LOAD, has been referred to as the missing

heritability. Behind the issue of extracting as much information as possible from such large datasets is the issue of the approximations used to simplify the problem. The typical, basic GWAS implementation does not take rare variants or ploidy into account, instead approximating the genome to a series of independent, common, biallelic variants. The initial focus on common variants was motivated by the prohibitive costs of sequencing enough individuals to have sufficient statistical power to identify rare variants associated with phenotypes. This focus lends itself well to testing the Common Disease, Common Variant hypothesis, but precludes it from testing the Common Disease, Rare Variant hypothesis[18]. The missing heritability can be reduced by analyzing the data with increasingly complex models which account for more of the variability observed in the genomes of a population. These models are improved by including data that would otherwise be discarded or unexplored, such as polyallelic sites, indels, SVs, CNVs and their allelic dosage or by increasing the statistical power of the study enough to include rare, high-effect variants[19]. In other words, all of the approximations and omissions leading up to a GWAS analysis can contribute to obscuring a non-negligible part of the heritability.

Empowering GWAS studies with more types of genetic variation reduces the missing heritability. In the 1,011 *S. cerevisiae* genomes study, GWAS analysis incorporating CNV information was performed for 35 phenotypes. The significantly associated CNVs accounted for an order of magnitude more of the phenotypic variability than significantly associated SNPs (36.8% and 4.5%, respectively). For example, the phenotype of resistance to copper sulfate was significantly associated with CNV of the *CUP1* locus, explaining 45% of phenotypic variation.

However, some of the genetic variability is omitted due to technical limitations of the short read sequencing technology. Most population genomic studies are based on high-throughput short read sequencing methods, which are limited by their short read

length. Short reads alone are unable to resolve large repetitive regions or complex SVs such as translocations or inversions and have limited potential to distinguish between alleles in a diploid or polyploid.

Fortunately, much longer reads have recently become available through single molecule sequencing technologies such as those provided by Oxford Nanopore and Pacific Biosciences, collectively referred to as long-read sequencing methods. While more error-prone, these technologies have the potential to overcome all of the limitations of short reads in a single sequencing step. These technologies directly sequence the native DNA molecule, without resorting to an amplification step like high-throughput short read sequencing methods. This allows them to avoid the phase error, significantly increasing read length and direct identification of modified bases such as cytosine methylation. Using long reads, repetitive regions can be sequenced end to end and placed within their genomic context, structural variants can be fully captured by individual reads and genomes of low heterozygosity can be phased by reads which link together distant heterozygous variants.

Phasing genomes unlocks explanatory potential

When compared to each other, genomes of the same species are very commonly reduced to sets of independent variable elements. A Single Nucleotide Polymorphism (SNP) is not considered in relation to the other SNPs around it on the same molecule, it is considered alone and independent (population structure concerns excluded). Long-read sequencing methods are particularly well-suited to addressing questions of phasing due to their ability to link many variable elements together. Haplotype phase information has not been consistently exploited for diploid species, much less for the more complex genomes of polyploids. Yet

haplotypes have known biological effects and should be included in models and studies which seek to uncover genotype-phenotype relations.

Hybrid organisms sometimes outperform both parents in terms of fitness in a phenomenon termed heterosis. The genetic basis of heterosis is dissected in a study of maize by phasing generated hybrids, estimating most of the heterosis they observe is due to complementation of recessive deleterious alleles, but not all[20]. The grapevine cultivar, Chardonnay, is a cross between Gouais blanc and Pinot noir and presents another example of heterosis[21]. By constructing a diploid-aware *de novo* reference sequence using long reads, it was possible to identify gene families which were expanded in one or the other haplotype. These expanded gene families, revealed by phasing, improve the fitness of the hybrid through complementary synergy.

Allele-Specific Expression (ASE), the preferred transcription of one allele over others, has been linked in humans to cancer susceptibility and progression[22], and complex diseases such as asthma and Parkinson's, among others[23]. Such far-ranging effects of ASE on phenotype can be identified more precisely if the genomes are phased, in particular for more complex polyploid samples in which the exact allele being preferentially expressed cannot always be determined from its SNPs.

Compound heterozygosity, an effect observed when harboring different alleles of the same gene, typically describes cases where two alleles in a diploid are recessive due to different mutations. In these situations it is crucial to know if both deleterious mutations are on the same copy of a gene or different ones. In 2011 a Gujarati Indian individual's genome was phased using fosmid libraries and short read sequencing methods[24]. Using unphased data, this individual would present 44 cases of potential compound heterozygosity. Upon phasing, only 10 cases of compound heterozygosity

were confirmed. This concept can easily be extended to other ploidies, or genes with CNVs, such that the effect of compound heterozygosity is increasingly manifest based on the proportion of non-functional copies. The compound heterozygosity model has been proposed as a way to model complex diseases in GWAS and is claimed to significantly reduce the missing heritability[25]. Use of this model motivated the development of a new tool which takes compound heterozygosity into account and led to the identification of enrichment in compound heterozygosity for genes involved in neuronal development and growth[26].

Modifications to the standard GWAS strategy to incorporate haplotype information have also been implemented, resulting in increased statistical power in simulated datasets[27,28] and has been successfully applied to identify agriculturally relevant traits in soybean[29].

In addition to improving the predictive and explanatory power of statistical analyses, phasing a polyploid population can be crucial in understanding its evolutionary origins. Polyploids can be autopolyploid, obtaining multiple copies of their genome through genome duplication, or allopolyploid, obtaining multiple copies through hybridization. Phasing was crucial to uncovering the nature of the polyploidy of two tetraploid Mediterranean shrubs, revealing them to be allopolyploids[30]. Population genomic studies can uncover interesting patterns connecting ploidy to specific environments, or reveal admixtures or hybrid individuals. The effects and analyses discussed here can bring significant value to our understanding of the populations we sequence.

Saccharomyces cerevisiae, model organism, model population

Yeasts are a good genetic model, these unicellular eukaryotes grow quickly and in environments which are easy to control, making it possible to significantly limit the role of the environment in phenotypic variability. *S. cerevisiae* in particular is a highly studied model organism. Its small, compact genome of 12.5 Mb split among 16 chromosomes is well annotated. Genetic modification methods of *S. cerevisiae* are well-established and the laboratory strains are very well characterized. It was not only domesticated by scientists to serve as a genetic box to query and through which to decipher genetic mechanisms, it was also domesticated in several human environments and helps produce dairy, bread, wine, beer and bioethanol. Not all isolates of *S. cerevisiae* are domesticated, however, and wild strains can be isolated from environments such as forests or the surfaces of bruised fruits and the insects that visit them. Its well-annotated genome, ecological and geographical diversity, along with its history of multiple independent domestication events, make the population of *S. cerevisiae* isolates a good model for population genomics studies.

The most complete study of this species to date is the 1,011 *S. cerevisiae* genome population survey which sequenced the entire genomes of geographically and ecologically diverse strains of *S. cerevisiae*, characterizing populations of wild and domesticated strains at a fine level[12]. This analysis established the pangenome of the species – the full set of genes found within the species. The reference genome of a species is not fully representative of the genomic content of the population. Some strains or subpopulations may have genes or other genetic elements not found in the rest of the population, and more crucially, not found in the reference. Identifying those genes then becomes necessary by assembling them *de novo*. The full set of genes that can be found in a population is the pangenome, which contrasts with the minimal set of genes shared within a population, the core genome. In the 1,011

dataset, the pangenome is a set of 7800 Open Reading Frames (ORFs), subdivided into 5000 ORFs of the core genome and 2800 variable ORFs that complete the pangenome. A significant proportion of the variable ORFs was found to correspond to introgressions from *Saccharomyces paradoxus*, a closely related species with orthologous genes introgressed into the genomes of *S. cerevisiae* strains.

The wide sampling of the diversity of the species also made it possible to retrace the evolutionary history of the species to a single origin marked by several independent domestication events. The evolution of wild isolates is characterized by SNP accumulation, while domesticated isolates have evolutionary histories also marked by variable ploidy, aneuploidy events and expanded gene families. The expanded gene families are probably an adaptation to the human-shaped environments these domesticated clades were identified in. Domesticated clades also display considerable variation in CNVs, again likely adaptations to these artificial environments. Evidently the highly specialized environments associated with human domestication, such as brewing, baking or winemaking have necessitated specific adaptations. The multiple independent domestication events and the clear differences in genomic content between wild and domesticated strains provides a particularly interesting view into the effects of domestication on genomic structure.

The untapped potential of polyploid beer isolates of *Saccharomyces cerevisiae*

While classically thought of as a diploid species, the 1,011 *S. cerevisiae* genome population survey identified that 11.5% of the isolates were polyploid (>2n). Polyploidy was not evenly distributed within the population, instead strongly associated with specific domestication environments: all of the ale beer strains and the large majority of African beer strains were polyploid (Figure 1). Additionally, nearly 20% of isolates presented aneuploidy, again strongly associated with human environments, mainly affecting the ale beer and sake clades. The strong link between

polyploidy in *S. cerevisiae* and the brewing environment is particularly interesting given that beer-brewing *S. cerevisiae* strains are a polyphyletic group[31] consisting of at least three different clades. The polyploid ale beers, polyploid African beer strains and partially polyploid mosaic beers suggest that polyploidy is important to *S. cerevisiae* in the brewing environment and developed independently. Raising further questions, not all domesticated environments lead to polyploidy, nor do domesticated environments which lead to high ethanol concentrations. The wine and bioethanol strains are typically diploids.

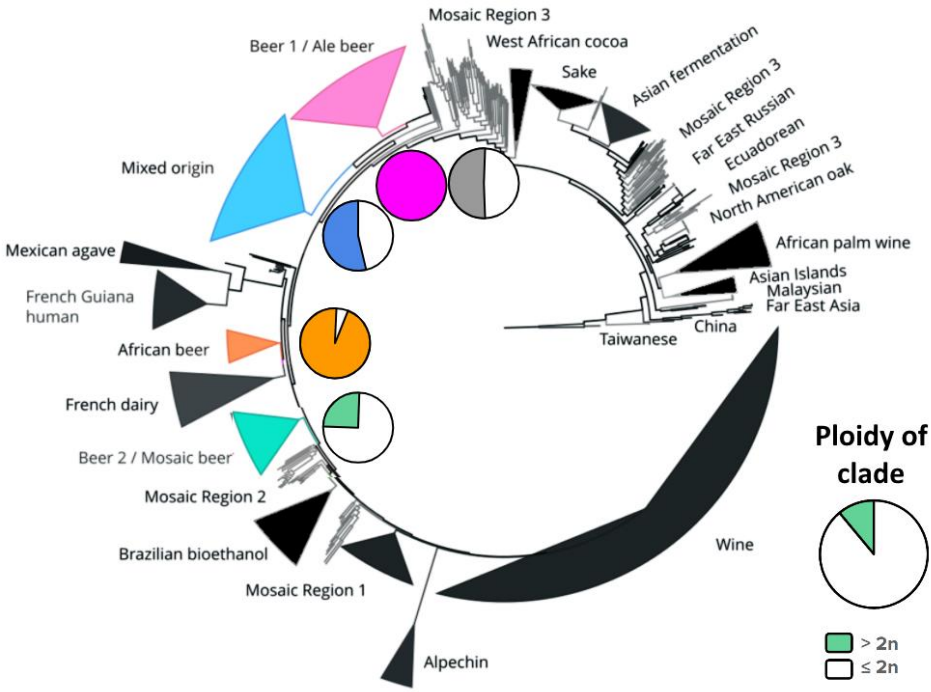

Figure 1 - Distribution and fraction of polyploids in the SNP dendrogram of 1,011 *Saccharomyces cerevisiae* isolates
This dendrogram is based on the genomic SNPs of 1,011 isolates of *S. cerevisiae* from diverse geographical and ecological origins, including human environments. Nearly 12% of these 1,011 strains are polyploid (>2n), and interestingly these polyploids are not equally distributed among the different subpopulations. All ale beer strains, most African beer strains, and a large fraction of the mixed origin and mosaic strains are polyploid, while all remaining subpopulations are 2n or lower. The grey pie chart represents mosaic region 3. Tree based on data from Peter *et al.* (2018), figure adapted from Krogerus *et al.* (2019).

The ale beer strains have been shown through phasing to be a polyploid admixture of Asian and European wine strains[32]. This answers the historical question of the nature of the polyploidy of these strains. Ale beer strains are mainly tetraploid and seem to derive from a hybrid of two diploid strains. The origins of the other beer groups have not yet been elucidated. The apparent link between beer brewing and polyploidy, along with the frequent aneuploidy events make it particularly interesting to interrogate these strains through phasing.

Independent hybridization events in *Brettanomyces bruxellensis*

Other, non-model yeasts such as *Brettanomyces bruxellensis* can also be of significant interest due to their complex genomes, population structure and economic importance. This yeast species is found in breweries of some specialty Belgian beers[33] such as Lambic and is one of the species in the symbiotic film associated with kombucha production[34]. *B. bruxellensis* also gained notoriety in the wine industry due to its spoiling effect in wine production[35]. Its genome was only assembled at near-chromosome scale (15 contigs for 8 chromosomes) in 2015[36] and at chromosome scale (8 contigs) in 2017[37]. Both of these attempts to establish a high quality *de novo* reference used long read sequencing to achieve their goal. Its current reference genome is 13 Mb large, split unevenly among 8 chromosomes. Due to its economic importance, large collections of *B. bruxellensis* were readily available and interest in this species has been high despite not being as well-studied or widely adopted for analysis as the model yeast *S. cerevisiae*.

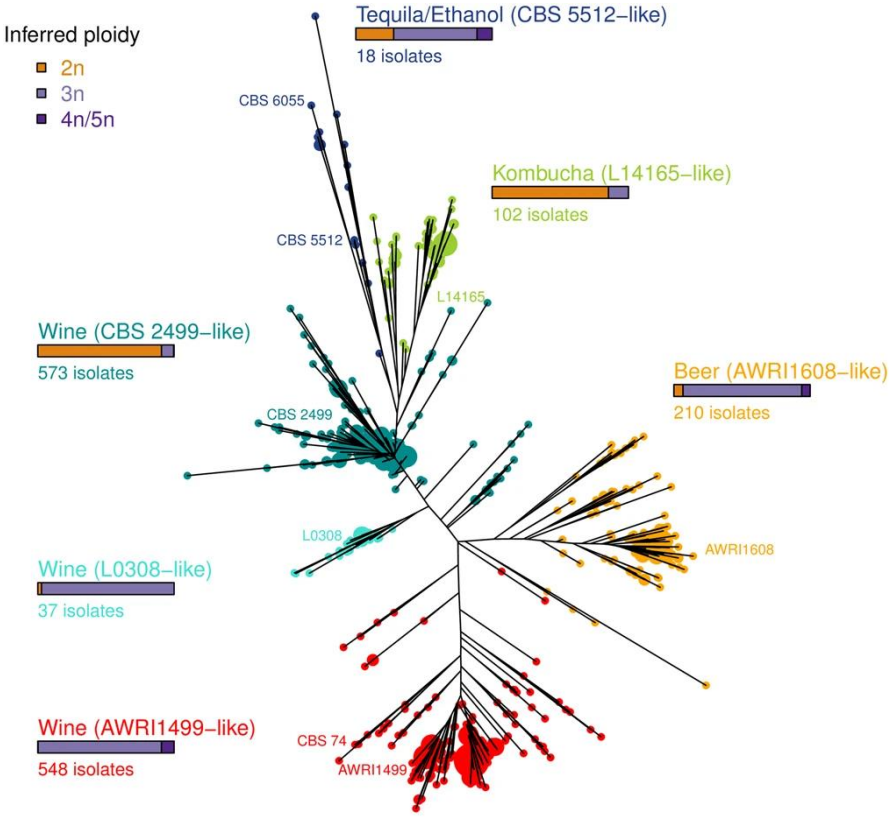

Figure 2 - Distribution of polyploids in dendrogram of 1488 *Brettanomyces bruxellensis* isolates based on 12 microsatellite markers
This dendrogram, based on 12 microsatellite markers, provides an initial estimate of the population structure of 1488 strains of *B. bruxellensis* representative of the diversity of the species. The inferred ploidy of these strains suggests a high degree of polyploidy, particularly within certain populations such as beer and AWRI1499-like wine strains. Figure adapted from Avramova *et al.* (2018).

In 2018, a genetic survey based on 12 microsatellites in 1488 isolates of the highly diverse population of *B. bruxellensis* revealed the structure of its genome is closely linked to ploidy level, geographical origin and the substrate it was isolated from[38]. In this study approximately 60% of the strains surveyed are estimated to be polyploid[38] (Figure 2). The majority of these polyploids are triploids, split into two major groups: beer strains and wine strains. It had previously been reported that some

isolates of *B. bruxellensis* are polyploid as a result of hybridization[39] (Figure 3). This study described two different cases of *B. bruxellensis* triploids, each having hybridized with a different still unidentified but related species. These unidentified species were named *"Brettanomyces x*" and "*Brettanomyces y*", owing to their genetic closeness to *Brettanomyces bruxellensis*. These triploids are therefore allopolyploids, or hybrids, with 2n+1n genomes. The two isolates in which *Brettanomyces x* and *Brettanomyces y* were identified, AWRI1499 and AWRI1608, are the basis for the two major groups of triploids observed. The nature of these unidentified species in AWRI1499-like wine strains and the AWRI1608-like beer strains presents itself as an interesting genomic mystery to be solved through phasing.

In addition to elucidating the nature of the hybridization, a recent survey of 53 strains from diverse geographical and ecological origins cemented the notion that *B. bruxellensis* has a complex genomic architecture with frequent aneuploidies, high levels of structural variation and significant heterozygosity (up to 3.5% in some triploids, significantly higher than the maximum 1.8% divergence between the most distant strains of *S. cerevisiae*)[40]. This complex genomic architecture undoubtedly has phenotypic consequences and must be taken into account for a complete understanding of this organism's biology.

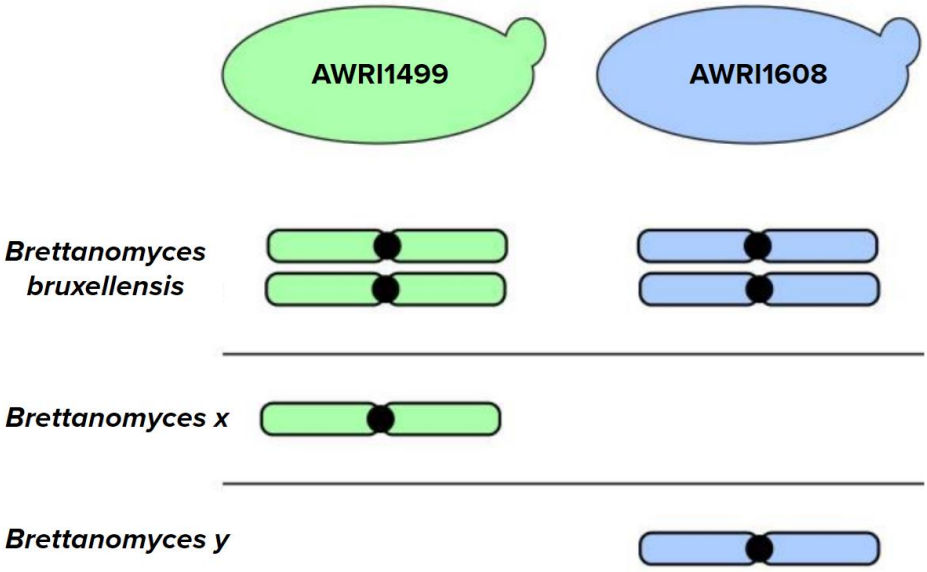

Figure 3 - Triploid *Brettanomyces bruxellensis* strains are suspected of being hybrids (2n+1n)

Previous reports indicate that triploid *B. bruxellensis* strains appear to be hybrids containing a core diploid genome and a more distantly related 1n genomic copy. The nature of this third copy is unknown and it in fact appears that some strains harbor an extra genomic copy here named *Brettanomyces x*, while other strains harbor a different extra copy, *Brettanomyces y*. Figure adapted from Borneman et al., (2014).

Polyploid genomes and the phasing out of approximations

To better retrace the evolutionary history of a population and to assess the phenotypic consequences of genetic sequences more accurately, it is important to take the entire genome into account, in all its complexity and detail. In *S. cerevisiae*, the polyphyletic group of beer strains presents higher ploidies, suggesting polyploidy is a common adaptation to the brewing environment and raising the question of the origins of these different beer groups. For *B. bruxellensis* the complex genomic architecture and the mystery over the other species involved in the apparent multiple independent hybridizations encourage a much closer look at the genomes of this species. To fully explore both of these examples, as well as any other biological system of a higher ploidy, would require phasing sequenced polyploid genomes. The current processes to sequence a genome all involve a step which fragments the DNA molecules. To obtain phase information, these DNA fragments, also called "reads", must then be pieced back together into the original chromosomes. For heterozygous organisms, this fragmentation makes it difficult to know which SNPs co-occur on the same chromosome. The phasing problem is the challenge of determining the original sequences of the chromosomes, known as haplotypes.

However, phasing has historically been difficult due to the read length of short read sequencing methods being shorter than the distance between variants (Figure 4). Long reads have led to highly performant methods for diploid phasing, notably through the alignment-based method WhatsHap[41] and the diploid aware *de novo* assembly tool, Falcon Unzip[42]. However, polyploid phasing presents significant additional complexity which is more difficult to resolve, even with long reads. Crucially, for a heterozygous diploid, solutions to the problem can exploit an obvious symmetry: finding the sequence of one haplotype necessarily leads to knowing the sequence of the other. The polyploid phasing problem, however, does not display

this symmetry, which greatly increases its complexity. Knowing the sequence of one haplotype still leaves uncertainty over the two or more remaining haplotypes. Consequently, the field of polyploid phasing has lagged behind diploid phasing, limiting our understanding of polyploid genomes.

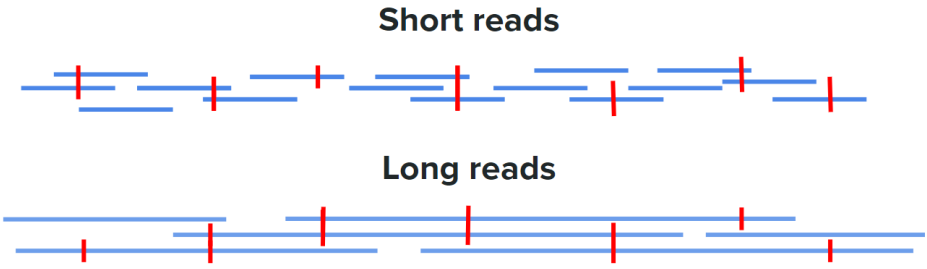

Figure 4 - Long reads overcome the inter-variant distance limitations of short reads
In order to phase a genome, it is necessary to link together variable positions, or SNPs, represented here by vertical red bars. Short reads face a serious limitation for phasing when the distance between SNPs is greater than the length of the reads or greater than the insert size for paired end reads. Long reads, with their significantly higher read length which can reach hundreds of kb, are able to link together even very distant SNPs. However long reads are also more error-prone, a drawback that must be taken into account.

Polyploid phasing methods

Solutions to the polyploid phasing problem can be categorized into three main strategies: Physical separation methods, *de novo* haplotype assembly, and alignment-based phasing. Briefly, physical separation methods attempt to only sequence one chromosome at a time, side-stepping the polyploid phasing problem by sequencing individual chromosomes[43]. *De novo* haplotype assembly methods ambitiously attempt to simultaneously recreate the different haplotypes and resolve the structure of the genome, typically relying on long-range sequencing methods such as Hi-C[44]. Alignment-based phasing methods map the sequencing reads to a reference sequence and identify variable positions, which are then used as input to a phasing algorithm that outputs predicted haplotypes.

Here, we discuss the different paradigms in the field of alignment-based polyploid phasing methods and how the performance of these methods is evaluated. We also propose that it would greatly benefit the field to standardize the performance metrics used to evaluate proposed methods, including the generation of gold standard datasets to systematically benchmark against.

Trends in polyploid phasing solutions

All alignment-based phasing methods share the same pre-processing steps. First, a reference sequence must be chosen or assembled *de novo*, to serve as a guide. Then, the sequenced reads are mapped to this reference sequence and variable positions are identified. Finally, the dataset of reads, reduced to their variable, phase-informative positions, is used as input for the phasing method (Figure 5). The methods proposed as solutions to the polyploid phasing problem are highly varied in their approaches

and mathematical and conceptual underpinnings. To provide a coherent framework for this review, we delineate the development and usage of different strategies, identifying four major trends:

Population inference methods, which leverage mapped reads of known genotypes in related individuals or in a population to infer the haplotypes in a sample.

Objective function optimization methods, which typically represent the mapped reads as a matrix and seek to minimize an objective function which typically represents the amount of discrepancy between the predicted haplotypes and the observed sequencing data.

Graph partitioning methods, which convert the mapped reads to a graph and seek to split the graph into subgraphs that correspond to the haplotype predictions.

Cluster building methods, which rely on the similarity between mapped reads to group them into clusters that correspond to predicted haplotypes.

We discuss these four paradigms, their implementations and limitations.

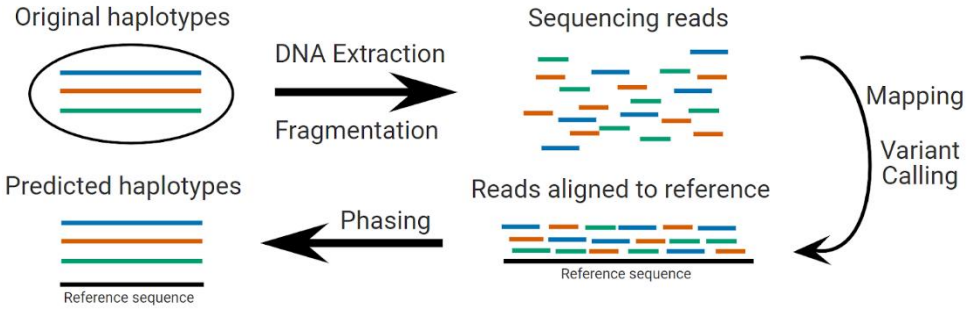

Figure 5 - Alignment-based phasing

Alignment-based phasing methods invariably require the following steps: DNA sequencing of the sample, which fragments the DNA into sequenced reads. The reads are then mapped to a reference sequence and heterozygous sites are identified by variant calling. The dataset of reads associated with their variable positions is then input to a phasing method and predicted haplotypes are output. These predicted haplotypes therefore conform to the structure of the reference sequence that was aligned to initially.

A - Population inference

To solve the polyploid phasing problem, population inference methods rely on the availability of significant amounts of genomic data. Rather than attempt to phase each genome individually, these methods leverage the genetic information of several individuals to inform the phasing (Figure 6). The choice of population is important to the strategy, and can range from large, non-specific populations of individuals of the same species[45–49], to highly specific, smaller populations such as parents or siblings[50–52].

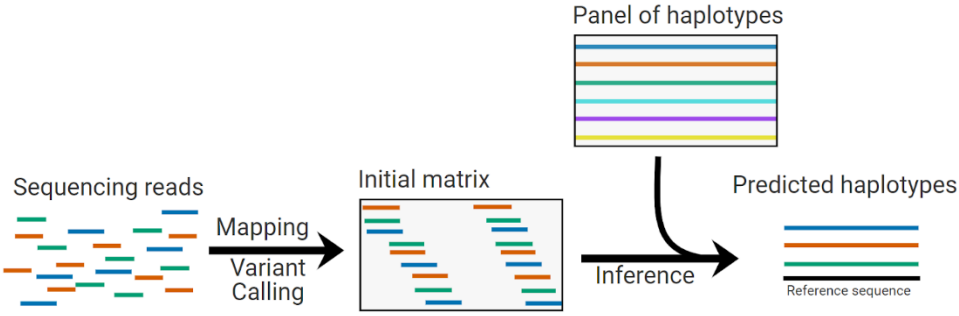

Figure 6 - Population inference strategy
Population inference methods typically cast the mapped reads to a matrix and compare them to a panel composed of haplotype information obtained from sequencing either a large population of individuals, or a smaller group of individuals related to the sample. Haplotypes are predicted through statistical inference based on the frequency of jointly observed genotypes.

The first such methods, SATlotyper[45] and polyHap[46], used large populations of unrelated individuals, while later methods such as TriPoly[50], PopPoly[51] and mapPoly[52] exploit pedigree information to inform their predictions. The methods employed to leverage population data for phasing are highly varied: SATlotyper casts the polyploid phasing problem as a boolean satisfiability problem[45], polyHap[46]

and mapPoly[52] both use Hidden Markov Models to leverage the statistical information in populations of individuals, superMASSA[47] frames it as a graphical Bayesian problem, SHEsisPlus[48] developed a formulation of the Expectation Maximization algorithm to predict the most likely haplotypes, and TriPoly[50] and PopPoly[51] both leverage pedigree information and Mendelian laws of inheritance to phase haplotypes. Finally, while Poly-Harsh[49] is not fully a population inference algorithm, its authors describe a clustering algorithm using population inference to connect fragmented phase blocks, improving the contiguity of phasing.

Population inference methods are particularly powerful when it comes to extending the reach of short read sequencing using statistical information. This has a very positive effect on contiguity without requiring the use of other sequencing methods. The public availability of a significant amount of sequencing data for various organisms is a very valuable resource for this method, though applying it to less studied organisms can prove more costly than other strategies presented here. One of the notable limitations inherent to population inference methods is the requirement of a sequenced population. For the methods which require large populations, the material and labor cost of obtaining and sequencing a large number of individuals can be a significant limiting factor. For those which require fewer but related individuals, the difficulty can lay in the existence or availability of such individuals. This renders these methods inappropriate for situations with limited resources, such as any study of a single individual, particularly if it is an individual of a species which is not extensively studied and sequenced.

The choice of the reference sequence against which to map the population is also a crucial one for these methods. The mapping and variant calling operations can be computationally expensive, and their quality is dependent on the quality of the reference sequence in use. Here, a seemingly intractable problem is apparent for some applications of population inference methods. Any species with a propensity

for structural variation would be difficult to phase with these methods, as the architecture of their genomes does not lend itself well to using the same reference for all individuals of the population. This makes it impossible to pick a reference sequence which accurately represents the population, and difficult to obtain sufficiently many distinct individuals with the same genomic architecture. Not all organisms have extensive structural variations within their population, however, and for populations which maintain highly similar genomic architectures, this strategy remains appropriate.

B - Objective function optimization

The objective function optimization strategy seeks to solve the phasing problem for single individuals. This method defines an objective function, which it then implements an algorithm to minimize (Figure 7). The objective function is typically a measurement of how well the predicted haplotypes correspond to the reads in the dataset. For example, for MEC (Minimum Error Correction) optimization, the objective function counts how many mismatches there are between the predicted haplotypes and the set of mapped reads. The intuition is that a low MEC score implies a highly accurate phasing. Another variant of this method is the MFR (Minimum Fragment Removal) method, in which the objective function is minimized when the predicted haplotypes and the set of mapped reads are in perfect agreement after the removal of as few reads as possible. Typically, but not always, objective function optimization methods cast the dataset of reads as a matrix and implement known or novel algorithms and heuristics intended to minimize the chosen objective function in the matrix.

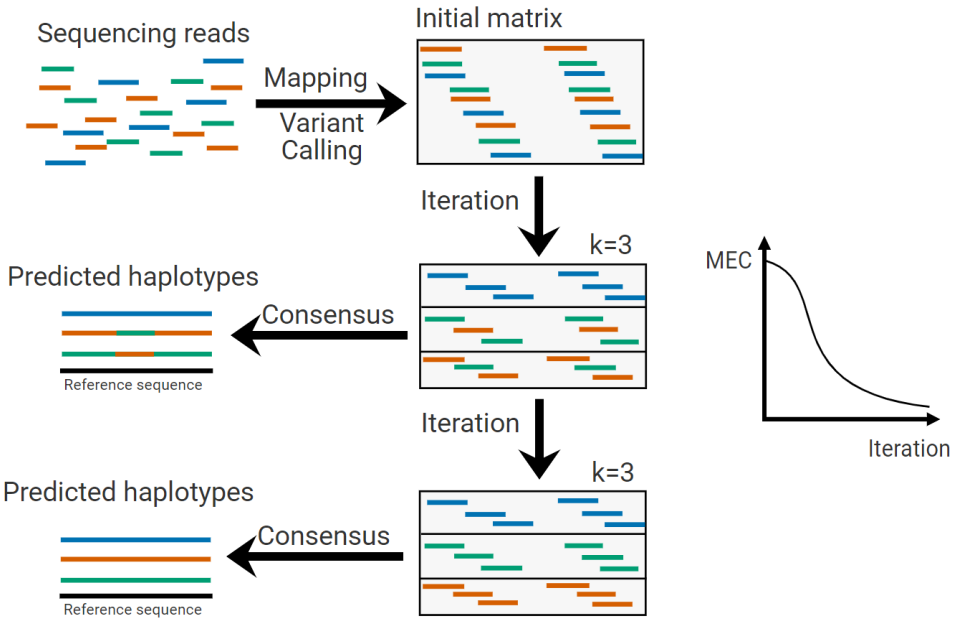

Figure 7 - Objective function optimization strategy

Objective function minimization strategies define a function which has a high score when the sample is not phased, and an increasingly lower score as the phasing improves. In theory such a function should lead to increasingly accurate haplotypes, until finally reaching a good haplotype prediction when minimized. In this figure we used the dominant MEC function as an example, though other functions can be used in this strategy. The objective function minimization strategy treats the polyploid phasing problem as an optimization problem which splits the matrix into *k* submatrices and applies various optimization methods to solve it. Each submatrix is then converted to a haplotype prediction through consensus of the reads.

Objective function optimization methods showcase a variety of heuristics and statistical methods. The first full application of the objective function optimization method for higher ploidies is found in HapTree[53], which uses a relative likelihood function to phase polyploid genomes. However, the most common objective function is the MEC[49,54–59]. The first polyploid application which optimizes the MEC function, GTIHR[54], uses a genetic algorithm which only applies to triploids. It was followed by SDhaP[55], whose authors developed a novel convex optimization method to minimize the MEC for higher ploidies. SCGDhap[56], BFBP[57], AltHap[58] and Poly-Harsh[49] all also use the MEC function and attempt to optimize it using various approaches, such as BFBP's belief propagation algorithm derived from communication theory and Poly-Harsh's Gibbs sampling method. EHTLD[59] extends the MEC function by applying additional genetic constraints, naming it the MEC with Genotype Information (MEC/GI), but it only applies to triploids. Finally, HaplotypeAssembler[60] uses the MFR objective function and optimizes it using integer linear programming.

The approach of objective function optimization is dominated by the MEC function yet remains very varied in the methods implemented to solve it. In contrast with the preceding population inference strategy, these methods aim to phase individual genomes, relying solely on the mapped reads to inform the reconstruction of the haplotypes. This, however, puts the objective function optimization and other strategies at a disadvantage when the sequencing data is not sufficiently informative to overcome low levels of phasing information. This would be the case of genomes with very low levels of heterozygosity or datasets in which the sequencing data consists of reads that are shorter than the distance between heterozygous positions, inevitably leading to fragmented haplotypes. Long reads are particularly interesting for phasing applications due to how phase-informative they are. Each long read can contain significantly more heterozygous positions than its short read counterparts.

However, none of the objective function optimization methods cited here take long reads into account. The intuition behind the optimization of an objective function is typically guided by the notion that the predicted haplotypes must conform in some way to the information present in the set of mapped reads. This assumption holds fairly well only if the read dataset is known to be of high quality and not error-prone. These methods are more appropriate for relatively error-free reads.

Objective function minimization strategies do not suffer from the same issues with complex genomic architectures as the population inference methods do. However, they all coerce the reads into a selectable ploidy *k*, which is incompatible with the biological reality that a polyploid genome of ploidy *n* does not necessarily have *n* haplotypes throughout its genome. For example, it may have an extra copy of one of its chromosomes, with its own unique haplotype. Alternatively, it may have the exact same haplotype for a large region of two of its chromosomes, effectively presenting only *n*-1 haplotypes for that region. An algorithm that coerces exactly *k* haplotypes on the entire genome will provide erroneous results if these edge cases are not considered and explicitly handled in some way. For polyploid genomes with simpler genomic architectures, where the ploidy and number of haplotypes remain stable, these methods remain appropriate.

C - Graph partitioning

The graph partitioning strategy casts the dataset of mapped reads as a graph. Typically, each mapped read is a node and each edge represents how similar two nodes are. The goal is then to determine the optimal way to split the graph into subgraphs that represent the different predicted haplotypes (Figure 8). It departs from the objective function strategy by seeking to group similar mapped reads together, away from dissimilar mapped reads, rather than seeking to optimize for coherence of the predicted haplotypes with the set of mapped reads. It achieves this through the use of the graph model and its associated mathematical tools and algorithms. To this end, graph partitioning algorithms are implemented or developed and applied, outputting subgraphs which are then converted to haplotype sequences, usually through majority voting.

Typical graph partitioning solutions to the polyploid phasing problem cast the mapped reads as nodes and give weights to overlapping nodes which penalize differences between them. Then a graph partitioning algorithm is applied to the graph in order to obtain the subgraphs which correspond to the haplotype predictions. In HapColor[61], the weight between mapped reads corresponds to the number of mismatches between them. It then applies the DSatur (Degree of saturation) algorithm, obtaining a high number of subgraphs, which it then iteratively merges until only k subgraphs remain. For PolyCluster[62], Hap10[63], ComHapDet[64] and WhatsHap Polyphase[65], the nodes are also mapped reads, and the weights are negative if there are many mismatches between reads, and positive if there are many matches. This then encourages their respective graph partitioning algorithm to cut the graph along the lines of negatively weighted disagreement. Hap10 and WhatsHap Polyphase distinguish themselves through their use of long reads. Hap10 uses 10X linked reads and applies a max-k-cut algorithm, while WhatsHap Polyphase uses

PacBio and Oxford Nanopore long reads and applies heuristics to solve the cluster editing problem. Notably, the initial cluster editing step of WhatsHap Polyphase is ploidy agnostic, meaning it is not biased towards a specific ploidy. However, WhatsHap Polyphase still coerces a specific ploidy, but it does so while explicitly taking into account the edge case of local regions of similarity between haplotypes in a process it terms haplotype threading.

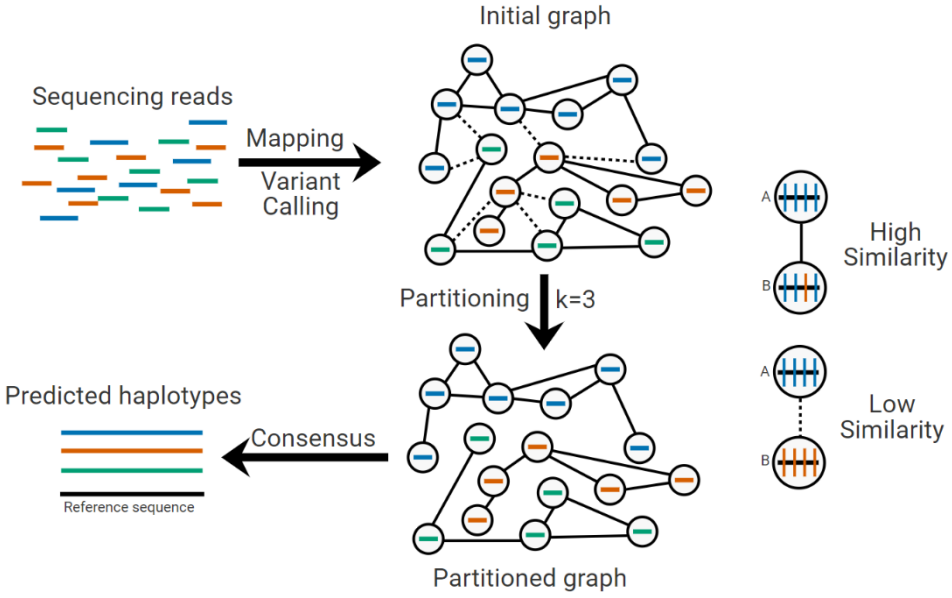

Figure 8 - Graph partitioning strategy

Graph partitioning strategies cast the mapped reads to a graph in which typically the reads are nodes and the edges between them correspond to a measure of how similar or dissimilar the reads are to each other based on the variants they carry. The goal is to identify *k* subgraphs of reads derived from the same haplotype, and to that end various graph partitioning methods are applied. Each subgraph is then converted to a haplotype prediction through consensus of the reads.

There have been two other graph partitioning methods which cast the mapped reads to a graph in a different way. The first application of graph partitioning methods to the polyploid phasing problem was an extension to HapCompass[66] which made it applicable to polyploids. Under the HapCompass model, each node is a SNP, and the mapped reads are edges. The use of SNPs as nodes is uncommon, but observed again recently with HRCH[67], another non-standard example of a graph partitioning method. HRCH uses a weighted SNP hypergraph, which it then partitions into predicted haplotypes using the hypergraph partitioning algorithm hMETIS.

The graph partitioning strategy relies on the notion that reads which derive from the same haplotype will be similar to each other, and dissimilar to reads derived from other haplotypes. They should then naturally form tightly connected graphs if attributed weights which correspond to their similarity (or dissimilarity). This strategy leverages well-established algorithms which efficiently split graphs into well-connected components. WhatsHap Polyphase's application of a graph partitioning strategy to long read datasets and its handling of part of the complexity brought on by the variability in genomic architectures is encouraging for the handling of the more complex problems of polyploid phasing. However, most graph partitioning algorithms, and all methods presented here, coerce the graph into k subgraphs. This leads to the same pitfalls as discussed for the objective function strategy, notably with structural variants and aneuploidies. While it may be possible to handle all edge cases in post-processing steps, careful consideration should be placed upon the sample being studied and the limitations and biases inherent to the phasing algorithm being used. There may be an existing or yet to be developed graph partitioning method which is intrinsically capable of resolving complex genomes containing aneuploidies, structural variants and a variable number of local haplotypes, however this has not yet been shown. This strategy may prove to be the

model of choice for resolving complex polyploid genomes, particularly when combined with long reads.

D - Cluster building

The cluster building strategy groups methods which do not appear to have a favored way of representing the data. Instead, these methods iteratively create and extend clusters of similar reads using heuristics (Figure 9). These methods are related to the graph partitioning methods in that they establish a way to cluster similar reads together, and dissimilar reads apart. However, they either do not explicitly cast the mapped reads to a graph, or they do not use graph partitioning algorithms. Another notable aspect of the methods in this strategy is the interest displayed in leveraging long reads to improve phasing quality.

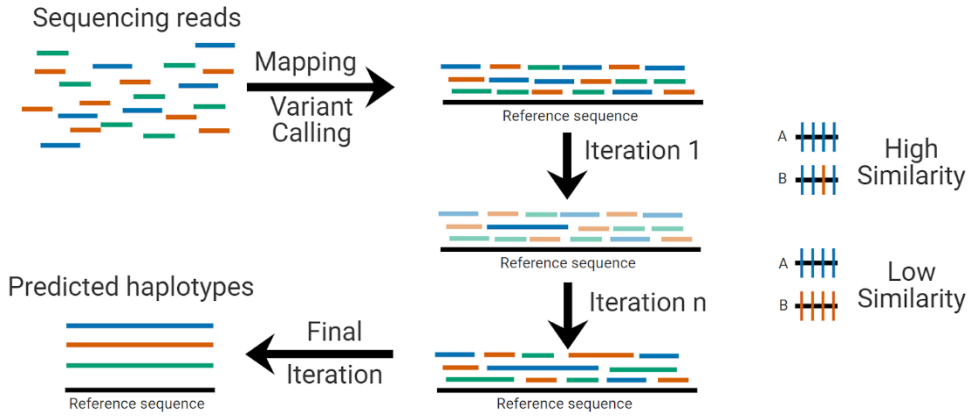

Figure 9 - Cluster building strategy
Cluster building strategies do not appear to have a favored model to which to cast the set of mapped reads. These methods typically score the similarity and dissimilarity between overlapping reads and iteratively build local clusters from the most similar pairs of reads. This strategy has led to ploidy agnostic methods, which cluster reads until the remaining clusters are too dissimilar rather than cluster them until the remaining clusters fit *k* haplotype predictions.

H-Pop and H-PopG[68] represent the read data as a matrix and seek to split the matrix into *k* parts, with each part corresponding to a group of reads with maximal similarity. Each group then represents a different haplotype, and it therefore introduces a diversity measure, which seeks to maximize the difference between the *k* groups, or predicted haplotypes. Similarly, Ranbow[69] uses a seed and extend paradigm to locally, iteratively cluster reads together based on similarity and dissimilarity measures. While it does coerce *k* haplotypes, it also handles the edge case where the number of haplotypes is less than *k*. While Ranbow is described only for short reads, its authors express interest in extending it to use long reads.

All of the cluster building methods which do use long reads are ploidy agnostic, meaning they do not coerce a specific ploidy. Chaisson *et al., 2018* propose a correlation clustering method to solve the polyploid phasing problem using long reads, however it is designed to only phase parts of the genome, intended to resolve multicopy duplications, and no tool was released.[70] This is the first ploidy agnostic phasing method applied to part of a genome. In an unnamed method[32], Fay *et al., 2019* describe a custom phasing algorithm they developed in order to analyze admixed polyploid yeasts. Using mapped long reads, they score similar reads positively, and dissimilar ones negatively, then proceed to iteratively merge long reads together for three rounds. This is the first example of a ploidy agnostic method applied to entire genomes, though it is not compared to other methods or released as a tool for the community to use. Finally, nPhase[71], a method we recently developed, solves the polyploid phasing problem by iteratively clustering similar reads together until only unique haplotypes remain. It is the first ploidy agnostic phasing method applicable to entire genomes to be released as a tool.

The cluster building strategy shares the same intuition that drives the graph partitioning strategy. Reads derived from the same haplotype will resemble each other and be different from reads derived from another haplotype. However, in

contrast with the graph partitioning strategy, these methods do not cast the set of mapped reads to a graph. Instead, the cluster building methods are defined by the strategy of iteratively growing clusters of reads while maintaining the diversity of the clusters. Interestingly, this strategy has led to three ploidy agnostic phasing methods, all of which leverage long reads. Ranbow handles the edge case where the number of haplotypes is locally lower than the ploidy, and the ploidy agnostic methods in theory adapt to the shape of the genomic architecture. While it should be expected that ploidy agnostic methods are capable of handling aneuploidies and local changes in the number of haplotypes, they do not provide any handling of other structural variants such as heterozygous inversions and translocations. This is partly a consequence of the nature of all of these strategies as alignment-based phasing methods, since they are limited to the genomic architecture imposed by the haploid reference sequence. However, long reads can provide a significant amount of information about structural variants, notably through split reads. No method of polyploid phasing attempts to use split reads to resolve heterozygous structural variation. The development of such a method would be a significant step towards complete polyploid phasing methods. For complex genomes, cluster building methods, and in particular ploidy agnostic phasing methods are appropriate. However, one major drawback of ploidy agnostic methods is the interpretability of the results. It is less straight-forward to manipulate ploidy agnostic phasing results than phasing results which neatly fit an expectation of k haplotypes.

Overview

The four strategies we described attempt to solve the same problem, and there are large interfaces between them. The way a problem is modeled influences the solution space that is intuitive and the mathematical tools which are at our disposal to solve it. We find that the field of alignment-based polyploid phasing algorithms has evolved to tackle increasingly complex formulations of the problem, using increasingly sophisticated strategies and tools, yet still has significant room for improvement. In particular, long reads are under-exploited despite representing a very significant tool to obtain large amounts of phase information. The polyploid phasing problem also needs to explicitly tackle and resolve the problems of heterozygous structural variants, aneuploidies and local variations in the number of haplotypes. The ploidy agnostic methods tackle some of the complexity of genomic architecture, but not all. For brevity, we did not discuss whether or not each method phases only biallelic SNPs, or also phases indels and multiallelic SNPs. However, it is clear that the majority of methods limit themselves to only phasing biallelic SNPs, sometimes also multiallelic SNPs, and indels seem to only be phased by Ranbow. We also discussed the importance of the chosen reference sequence, and it may become common practice to perform a collapsed *de novo* assembly to generate an appropriate reference for each sample prior to alignment-based phasing. However, this also entails having to generate a new genome annotation for downstream analyses and can unnecessarily complicate comparisons between samples. Overall, there is still room for improvement in the field of polyploid phasing algorithms and recommended practices.

Validation datasets and performance metrics

Once a polyploid phasing method has been developed, its performance must be evaluated. To that end, a validation dataset which corresponds to a set of reads obtained from a polyploid must be given as input to the phasing method, and the output haplotype predictions must be evaluated by performance metrics.

The validation dataset can be simulated or real. In the case of simulated datasets, it is possible to know the optimal phasing result, which allows for the use of detailed metrics to better understand the performance of the polyploid phasing algorithm. A validation dataset can be fully simulated, such as in Haptree[53], which randomly generates haplotypes and simulates reads derived from these haplotypes. Validation datasets can also be partially simulated, or reconstructed. This is the case for WhatsHap Polyphase and nPhase, which both merge real sequencing reads of organisms with known haplotypes. WhatsHap Polyphase combines human datasets with known haplotypes, while nPhase combines *S. cerevisiae* datasets of haploid and homozygous diploid individuals. Fully simulated datasets have a high degree of control over all characteristics of the genome, which allows them to test the effects of different ploidy levels, heterozygosity levels, genome architectures, coverage levels. However, these methods are highly dependent on the accuracy of their simulations of genomes and sequencing results. Partially simulated datasets are more faithful simulations of real haplotype phasing scenarios as they use real genomes, with real SNPs and real sequencing reads. However, these genomes are still artificially produced, typically presenting relatively uniform distance between haplotypes, and there is less control over their characteristics, which limits the testing space. Some parameters, such as the effects of coverage level and heterozygosity rate, can still be queried by downsampling the number of reads or the variable

positions input to the phasing algorithm, however this process is less straight-forward than it is for a fully simulated dataset.

For all simulated datasets, the ground truth is known and can be used to evaluate the predicted haplotypes. A variety of metrics have been implemented, here we discuss those most commonly used in the field.

The MEC score is not only an objective function used in a number of phasing methods, but also a metric which has been routinely used as evidence of good phasing. The MEC score, as a performance metric, has received some criticism in the context of the polyploid phasing problem. In their paper on Ranbow, Moeinzadeh *et al.* note that the MEC metric is incomplete, only considering sequencing errors[69], while in their paper for WhatsHap Polyphase, Schrinner *et al.* point out that low MEC scores can be obtained with objective worse phasing result[65]. Due to the significantly higher error rate of long read sequencing, any method relying on these reads will necessarily obtain worse MEC scores despite the obvious advantages of long reads, further limiting the usefulness of this metric for the evaluation of polyploid phasing methods.

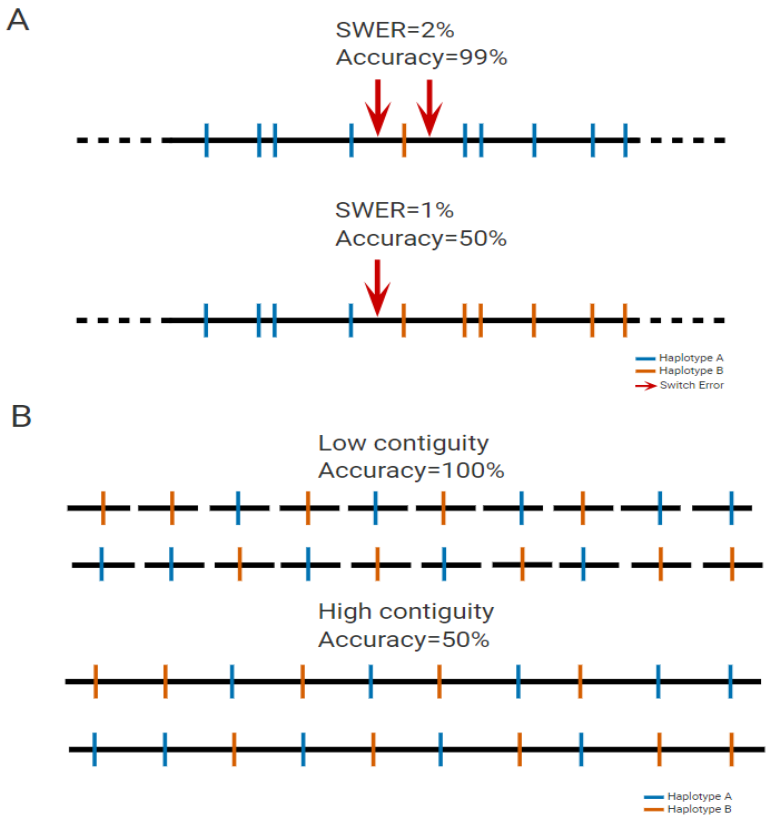

Figure 10 - Behavior of the SWER and contiguity performance metrics

A We illustrate the unpredictable nature of the SWitch Error Rate (SWER) metric with two examples. In both cases we suppose we have a haplotype prediction of 100 variants. In the first, top case, two consecutive switch errors lead to a 2% SWER, but due to being consecutive the accuracy is at a very high 99%. In the second, lower case, there is only one switch error, giving a better SWER score of 1%, however the accuracy is reduced by half to 50% due to it occurring in the middle of the prediction. This behavior of the SWER metric makes it unpredictable and unreliable. **B** We illustrate the importance of contiguity to the interpretation of accuracy results with two examples. In both cases we show haplotype predictions for a diploid sequence. In the first, low contiguity example, we illustrate how it can be trivial to obtain extremely accurate predictions if they are sufficiently fragmented. Through the second, high contiguity example, we show how the accuracy of the previous example could dramatically decrease by increasing contiguity.

The Switch Error Rate (SWER), also described as the Vector Error Rate (VER), measures how frequently the predicted haplotype switches between true phases (Figure 10A). Optimization of this metric does not necessarily lead to improved phasing accuracy, as a single vector can reduce the accuracy by half. In a real use case, the presence of a switch error has a much more significant consequence than the presence of a few point errors. As we argued in our paper on nPhase[71], the interpretability of the SWER is further complicated by the fact that the presence of more switch errors can result in significantly better phasing results, rendering the metric fundamentally unpredictable. The use of this metric is no doubt motivated by the observation that it is possible to phase several SNPs very well, yet a single switch error can reduce the accuracy by up to 50%. Hence methods which produce longer phase blocks, more susceptible to switch errors, may appear to have worse accuracy despite having large stretches of correctly phased blocks. However, this metric remains flawed and does not behave predictably. Some possible replacement metrics would be to report the mean length of unbroken phase blocks, or the minimal unbroken phased block length to cover 90% of the SNPs.

The accuracy, also described as the Reconstruction Rate or Hamming distance measures how accurate the phasing is globally. Accuracy can be defined in two forms. The first is the prediction accuracy, which at 99% can state that for every 100 SNP predictions it makes, on average 1 SNP will be in the wrong phase. The second is the reconstruction accuracy, which at 99% states that for every 100 SNPs in the genome, on average 1 SNP will be in the wrong phase or not phased. The latter is more stringent by taking the missing rate into account. In both cases, the accuracy metric gives an important notion of how accurate the predictions are, making it a crucial performance metric to evaluate.

Accuracy on its own, however, is not a sufficient marker of how informative a phasing result is. Without an indication of how contiguous the results are, the accuracy metric can be highly misleading (Figure 10B). A good haplotype prediction must be accurate and contiguous. However, the definition of contiguity is not straight-forward. Definitions based on the number of phased blocks per chromosome can be used to compare methods to each other, but due to the variability of genome sizes they do not provide an intuitive understanding of how good the phasing is. Taking inspiration from the metrics used to assess the contiguity of genome assemblies, contiguity can be defined as the minimum number or length of haplotype blocks to cover 50% or 90% of the SNPs. This is done by some methods, such as Hap10 which determined the N50 haplotype block length[63]. Highly different standards of what constitutes a good contiguity should be expected when comparing short and long read methods due to the ability of long reads to phase very distant SNPs.

These metrics are all applicable when the ground truth is known, which is the case for simulated datasets. However, it is less straight-forward to evaluate the performance of these methods with real polyploid data due the absence of a ground truth. A few proxies have been developed to tackle this problem. We have already discussed the MEC metric, which is one of the main metrics used to evaluate performance on real polyploids. Ranbow[69] phases the sweet potato, *Ipomoea batatas*, and uses long, accurate Roche 454 reads to validate its haplotype predictions. WhatsHap Polyphase and nPhase both phase the autotetraploid potato plant, *Solanum tuberosum*, and show qualitatively that its genes appear well-phased[65,71].

In their paper[72], Motazedi *et al.* develop haplosim, a simulation pipeline which can generate simulated haplotypes and associated reads. This tool has been used by several polyploid phasing methods for their validation steps, such as Hap10[63] and

Ranbow[69]. However, there is no widely used benchmarking dataset which can systematically be compared against, and haplosim does not appear to have been updated in the past three years to reflect the significant improvements in quality achieved in long read sequencing methods. A well-maintained gold standard benchmark would be of benefit to the field of polyploid phasing. It would be interesting for such a resource to carefully consider the performance metrics to evaluate, the diversity of read sequencing methods and the effects of variable ploidy, genome architecture, heterozygosity level, genome size, structural variation, indels, polyallelic sites and local variations in the number of haplotypes.

References

1. International Human Genome Sequencing Consortium. Finishing the euchromatic sequence of the human genome. Nature 431, 931–945 (2004).
2. Mewes, H. W. et al. Overview of the yeast genome. Nature 387, 7–8 (1997).
3. The Arabidopsis Genome Initiative. Analysis of the genome sequence of the flowering plant Arabidopsis thaliana. Nature 408, 796–815 (2000).
4. Chinwalla, A. T. et al. Initial sequencing and comparative analysis of the mouse genome. Nature 420, 520–562 (2002).
5. Delsuc, F., Brinkmann, H. & Philippe, H. Phylogenomics and the reconstruction of the tree of life. Nat. Rev. Genet. 6, 361–375 (2005).
6. Miller, W., Makova, K. D., Nekrutenko, A. & Hardison, R. C. Comparative genomics. Annu. Rev. Genomics Hum. Genet. 5, 15–56 (2004).
7. Alföldi, J. & Lindblad-Toh, K. Comparative genomics as a tool to understand evolution and disease. Genome Res. 23, 1063–1068 (2013).
8. The 3, 000 rice genomes project. The 3,000 rice genomes project. GigaScience 3, 7 (2014).
9. Auton, A. et al. A global reference for human genetic variation. Nature 526, 68–74 (2015).
10. Sudmant, P. H. et al. An integrated map of structural variation in 2,504 human genomes. Nature 526, 75–81 (2015).
11. Alonso-Blanco, C. et al. 1,135 Genomes Reveal the Global Pattern of Polymorphism in Arabidopsis thaliana. Cell 166, 481–491 (2016).
12. Peter, J. et al. Genome evolution across 1,011 Saccharomyces cerevisiae isolates. Nature 556, 339–344 (2018).
13. DeWan, A. et al. HTRA1 Promoter Polymorphism in Wet Age-Related Macular Degeneration. Science 314, 989–992 (2006).
14. Ozaki, K. et al. Functional SNPs in the lymphotoxin-alpha gene that are associated with susceptibility to myocardial infarction. Nat. Genet. 32, 650–654 (2002).
15. Sims, R., Hill, M. & Williams, J. The multiplex model of the genetics of Alzheimer's disease. Nat. Neurosci. 23, 311–322 (2020).
16. Raybould, R. & Sims, R. Searching the Dark Genome for Alzheimer's Disease Risk Variants. Brain Sci. 11, 332 (2021).
17. Wall, J. D. et al. The GenomeAsia 100K Project enables genetic discoveries across Asia. Nature 576, 106–111 (2019).
18. Schork, N. J., Murray, S. S., Frazer, K. A. & Topol, E. J. Common vs. Rare Allele Hypotheses for Complex Diseases. Curr. Opin. Genet. Dev. 19, 212–219 (2009).
19. Génin, E. Missing heritability of complex diseases: case solved? Hum. Genet. 139, 103–113 (2020).
20. Yang, J. et al. Incomplete dominance of deleterious alleles contributes substantially to trait variation and heterosis in maize. PLOS Genet. 13, e1007019 (2017).

21. Roach, M. J. et al. Population sequencing reveals clonal diversity and ancestral inbreeding in the grapevine cultivar Chardonnay. PLOS Genet. 14, e1007807 (2018).
22. Robles-Espinoza, C. D., Mohammadi, P., Bonilla, X. & Gutierrez-Arcelus, M. Allele-specific expression: applications in cancer and technical considerations. Curr. Opin. Genet. Dev. 66, 10–19 (2021).
23. Vohra, M., Sharma, A. R., B, N. P. & Rai, P. S. SNPs in Sites for DNA Methylation, Transcription Factor Binding, and miRNA Targets Leading to Allele-Specific Gene Expression and Contributing to Complex Disease Risk: A Systematic Review. Public Health Genomics 23, 155–170 (2020).
24. Kitzman, J. O. et al. Haplotype-resolved genome sequencing of a Gujarati Indian individual. Nat. Biotechnol. 29, 59–63 (2011).
25. Sanjak, J. S., Long, A. D. & Thornton, K. R. A Model of Compound Heterozygous, Loss-of-Function Alleles Is Broadly Consistent with Observations from Complex-Disease GWAS Datasets. PLOS Genet. 13, e1006573 (2017).
26. Cox, A. J. et al. In trans variant calling reveals enrichment for compound heterozygous variants in genes involved in neuronal development and growth. Genet. Res. 101, (2019).
27. Zhang, Z. et al. Ancestral haplotype-based association mapping with generalized linear mixed models accounting for stratification. Bioinformatics 28, 2467–2473 (2012).
28. Hamazaki, K. & Iwata, H. RAINBOW: Haplotype-based genome-wide association study using a novel SNP-set method. PLOS Comput. Biol. 16, e1007663 (2020).
29. A Genome-Wide Association Study for Agronomic Traits in Soybean Using SNP Markers and SNP-Based Haplotype Analysis. https://www.ncbi.nlm.nih.gov/pmc/articles/PMC5289539/.
30. Eriksson, J. S. et al. Allele phasing is critical to revealing a shared allopolyploid origin of Medicago arborea and M. strasseri (Fabaceae). BMC Evol. Biol. 18, 9 (2018).
31. Gallone, B. et al. Domestication and Divergence of Saccharomyces cerevisiae Beer Yeasts. Cell 166, 1397-1410.e16 (2016).
32. Fay, J. C. et al. A polyploid admixed origin of beer yeasts derived from European and Asian wine populations. PLOS Biol. 17, e3000147 (2019).
33. Steensels, J. et al. Brettanomyces yeasts — From spoilage organisms to valuable contributors to industrial fermentations. Int. J. Food Microbiol. 206, 24–38 (2015).
34. Teoh, A. L., Heard, G. & Cox, J. Yeast ecology of Kombucha fermentation. Int. J. Food Microbiol. 95, 119–126 (2004).
35. Conterno, L., Joseph, C. M. L., Arvik, T. J., Henick-Kling, T. & Bisson, L. F. Genetic and Physiological Characterization of Brettanomyces bruxellensis Strains Isolated from Wines. Am. J. Enol. Vitic. 57, 139–147 (2006).
36. Olsen, R.-A. et al. De novo assembly of Dekkera bruxellensis: a multi technology approach using short and long-read sequencing and optical mapping. GigaScience 4, 56 (2015).

37. Fournier, T. et al. High-Quality de Novo Genome Assembly of the Dekkera bruxellensis Yeast Using Nanopore MinION Sequencing. G3 GenesGenomesGenetics 7, 3243–3250 (2017).
38. Avramova, M. et al. Brettanomyces bruxellensis population survey reveals a diploid-triploid complex structured according to substrate of isolation and geographical distribution. Sci. Rep. 8, 4136 (2018).
39. Borneman, A. R., Zeppel, R., Chambers, P. J. & Curtin, C. D. Insights into the Dekkera bruxellensis Genomic Landscape: Comparative Genomics Reveals Variations in Ploidy and Nutrient Utilisation Potential amongst Wine Isolates. PLOS Genet. 10, e1004161 (2014).
40. Gounot, J.-S. et al. High Complexity and Degree of Genetic Variation in Brettanomyces bruxellensis Population. Genome Biol. Evol. 12, 795–807 (2020).
41. Patterson, M. et al. WhatsHap: Weighted Haplotype Assembly for Future-Generation Sequencing Reads. J. Comput. Biol. 22, 498–509 (2015).
42. Chin, C.-S. et al. Phased diploid genome assembly with single-molecule real-time sequencing. Nat. Methods 13, 1050–1054 (2016).
43. Ruo-Nan, Z. & Zan-Min, H. The Development of Chromosome Microdissection and Microcloning Technique and its Applications in Genomic Research. Curr. Genomics 8, 67–72 (2007).
44. Zhang, X., Zhang, S., Zhao, Q., Ming, R. & Tang, H. Assembly of allele-aware, chromosomal-scale autopolyploid genomes based on Hi-C data. Nat. Plants 5, 833–845 (2019).
45. Neigenfind, J. et al. Haplotype inference from unphased SNP data in heterozygous polyploids based on SAT. BMC Genomics 9, 356 (2008).
46. Su, S.-Y., White, J., Balding, D. J. & Coin, L. J. Inference of haplotypic phase and missing genotypes in polyploid organisms and variable copy number genomic regions. BMC Bioinformatics 9, 513 (2008).
47. Serang, O., Mollinari, M. & Garcia, A. A. F. Efficient Exact Maximum a Posteriori Computation for Bayesian SNP Genotyping in Polyploids. PLOS ONE 7, e30906 (2012).
48. Shen, J. et al. SHEsisPlus, a toolset for genetic studies on polyploid species. Sci. Rep. 6, 24095 (2016).
49. He, D., Saha, S., Finkers, R. & Parida, L. Efficient algorithms for polyploid haplotype phasing. BMC Genomics 19, 110 (2018).
50. Motazedi, E. et al. TriPoly: haplotype estimation for polyploids using sequencing data of related individuals. Bioinformatics 34, 3864–3872 (2018).
51. Motazedi, E., Maliepaard, C., Finkers, R., Visser, R. & de Ridder, D. Family-Based Haplotype Estimation and Allele Dosage Correction for Polyploids Using Short Sequence Reads. Front. Genet. 0, (2019).
52. Mollinari, M. & Garcia, A. A. F. Linkage Analysis and Haplotype Phasing in Experimental Autopolyploid Populations with High Ploidy Level Using Hidden Markov Models. G3 GenesGenomesGenetics 9, 3297–3314 (2019).

53. Berger, E., Yorukoglu, D., Peng, J. & Berger, B. HapTree: A Novel Bayesian Framework for Single Individual Polyplotyping Using NGS Data. PLOS Comput. Biol. 10, e1003502 (2014).
54. Wu, J., Chen, X. & Li, X. Haplotyping a single triploid individual based on genetic algorithm. Biomed. Mater. Eng. 24, 3753–3762 (2014).
55. Das, S. & Vikalo, H. SDhaP: haplotype assembly for diploids and polyploids via semi-definite programming. BMC Genomics 16, 260 (2015).
56. Cai, C., Sanghavi, S. & Vikalo, H. Structured Low-Rank Matrix Factorization for Haplotype Assembly. IEEE J. Sel. Top. Signal Process. 10, 647–657 (2016).
57. Puljiz, Z. & Vikalo, H. Decoding Genetic Variations: Communications-Inspired Haplotype Assembly. IEEE/ACM Trans. Comput. Biol. Bioinform. 13, 518–530 (2016).
58. Hashemi, A., Zhu, B. & Vikalo, H. Sparse Tensor Decomposition for Haplotype Assembly of Diploids and Polyploids. BMC Genomics 19, 191 (2018).
59. Wu, J. & Zhang, Q. A fast and accurate enumeration-based algorithm for haplotyping a triploid individual. Algorithms Mol. Biol. 13, 10 (2018).
60. Siragusa, E., Haiminen, N., Finkers, R., Visser, R. & Parida, L. Haplotype assembly of autotetraploid potato using integer linear programing. Bioinformatics 35, 3279–3286 (2019).
61. Mazrouee, S. & Wang, W. HapColor: A graph coloring framework for polyploidy phasing. in 2015 IEEE International Conference on Bioinformatics and Biomedicine (BIBM) 105–108 (2015). doi:10.1109/BIBM.2015.7359663.
62. Mazrouee, S. & Wang, W. PolyCluster: Minimum Fragment Disagreement Clustering for Polyploid Phasing. IEEE/ACM Trans. Comput. Biol. Bioinform. 17, 264–277 (2020).
63. Majidian, S., Kahaei, M. H. & de Ridder, D. Hap10: reconstructing accurate and long polyploid haplotypes using linked reads. BMC Bioinformatics 21, 253 (2020).
64. Sankararaman, A., Vikalo, H. & Baccelli, F. ComHapDet: a spatial community detection algorithm for haplotype assembly. BMC Genomics 21, 586 (2020).
65. Schrinner, S. D. et al. Haplotype threading: accurate polyploid phasing from long reads. Genome Biol. 21, 252 (2020).
66. Aguiar, D. & Istrail, S. Haplotype assembly in polyploid genomes and identical by descent shared tracts. Bioinformatics 29, i352–i360 (2013).
67. Olyaee, M. H., Khanteymoori, A. & Khalifeh, K. A chaotic viewpoint-based approach to solve haplotype assembly using hypergraph model. PLOS ONE 15, e0241291 (2020).
68. Xie, M., Wu, Q., Wang, J. & Jiang, T. H-PoP and H-PoPG: heuristic partitioning algorithms for single individual haplotyping of polyploids. Bioinformatics 32, 3735–3744 (2016).
69. Moeinzadeh, M.-H. et al. Ranbow: A fast and accurate method for polyploid haplotype reconstruction. PLOS Comput. Biol. 16, e1007843 (2020).
70. Chaisson, M. J., Mukherjee, S., Kannan, S. & Eichler, E. E. Resolving Multicopy Duplications de novo Using Polyploid Phasing. in Research in Computational Molecular

Biology (ed. Sahinalp, S. C.) 117–133 (Springer International Publishing, 2017). doi:10.1007/978-3-319-56970-3_8.
71. Abou Saada, O., Tsouris, A., Eberlein, C., Friedrich, A. & Schacherer, J. nPhase: an accurate and contiguous phasing method for polyploids. Genome Biol. 22, 126 (2021).
72. Motazedi, E., Finkers, R., Maliepaard, C. & de Ridder, D. Exploiting next-generation sequencing to solve the haplotyping puzzle in polyploids: a simulation study. Brief. Bioinform. 19, 387–403 (2018).

Project summary

Phasing, and in particular polyploid phasing, have been challenging problems held back by the limited read length of high-throughput short read sequencing methods which can't overcome the distance between heterozygous sites and the financial and labor high cost of alternative methods such as the physical separation of chromosomes or use of fosmid libraries. Recently developed single molecule long-read sequencing methods provide much longer reads which overcome this previous limitation at reasonable costs. However, the accuracy of these methods has been lower than that of the previous short read methods, despite rapid and frequent improvements. Significant strides in the diploid phasing problem were achieved by leveraging the long read length of long-read sequencing methods. For diploid phasing, each variable position can only have one of two states, to place in one of two haplotypes. This simplifies the task by making it possible to deduce one phase by knowing the other. Tools such as the alignment-based WhatsHap[1] and the *de novo* assembly tool Falcon-Unzip[2] exploit this inherent symmetry to provide good phasing results for diploids. Efforts to solve polyploid phasing, where the absence of symmetry greatly complexifies the problem, still need to resolve significant technical roadblocks. A large proportion of polyploid phasing methods designed for short read data relied on the high accuracy of these reads and cannot be directly applied or easily modified to accommodate the error profiles of long read methods. The complex genomic architectures of polyploids such as the presence of aneuploidies and regions of variable numbers of haplotypes also still need to be addressed in order to obtain an accurate view of the structure of their genomes. The absence of a reliable polyploid phasing strategy also translates to a dearth in applications of polyploid phasing methods to populations of individuals.

In this context, we decided to develop a polyploid phasing algorithm which we describe in **Chapter I**. Our tool, named nPhase, is a pipeline which takes as input a reference sequence, a set of short reads and a set of long reads. The pipeline will align the long and short read sequences to the reference, and it will variant call the mapped short reads. Then this dataset is phased by our ploidy agnostic cluster building method which adapts to the ploidy of the dataset and natively handles aneuploidy and variations in the number of distinct haplotypes. Our method has a few adjustable parameters and we describe how we selected the default parameters through extensive testing on a simulated validation dataset. We also describe the heuristics we developed to clean up raw phasing results obtained with nPhase. Finally, we apply our algorithm to a triploid strain of the yeast species *Brettanomyces bruxellensis* and to chromosome two of the autotetraploid plant *Solanum tuberosum.* We also describe our observations regarding ways to validate results obtained on real datasets, notably by introducing a new way to evaluate the quality of a phased cluster based on the allelic frequencies observed within.

Having developed this ploidy agnostic phasing method, we then set out to apply it to two real datasets. First, a large collection of 1,011 isolates of the yeast species *Saccharomyces cerevisiae* were recently sequenced[3]. It was found that 11.5% of the strains are polyploids. These polyploid isolates were not uniformly distributed throughout the population, only affecting a few subpopulations. In particular we note that the polyphyletic group of beers, mainly distributed across three main clades (Beer 1, Beer 2 and African Beer), all were composed of a significant proportion of polyploid strains. In **Chapter II**, we therefore sequenced 35 beer strains of *S. cerevisiae* with Oxford Nanopore technology, obtaining long reads which we used to phase this population with nPhase. We found that the three main beer yeast subpopulations appear to derive from different admixtures of other populations. As previously reported, strains of the Beer 1 clade were an admixture of Asian and

European wine strains. We found that strains of the Beer 2 clade were also composed of a similar admixture, only with a higher proportion of European wine alleles. We therefore renamed the Beer 1 and Beer 2 clades to the more evocative Asian dominant and European dominant, respectively. Finally, the African Beer strains mainly exhibited European wine alleles, with a background of French dairy alleles. The phased data made it possible for us to estimate the genetic divergence of haplotypes within and between strains. By comparing all haplotypes of genes and selecting those with the highest levels of divergence (>4%), we identified significant GO term enrichment for carbon metabolism, dehydrogenase activity, cell wall remodeling and transporter activity. A deeper look at individual phased genes also revealed different evolutionary trajectories of individual genes across subpopulations, showing that the inactivation of the beer off-flavor forming gene *FDC1* was independently inactivated in the Asian dominant and African Beer groups. We also found that the *ADH2* and *SFA1* genes which participate in the formation of fusel alcohols, another source of off-flavors in beer, are inactivated in Asian dominant strains.

Another species with an interesting polyploidization history is *Brettanomyces bruxellensis*. This yeast species is used to brew some specialty Belgian beers and participates in the microbial community that makes kombucha, but is also notorious for contaminating bioethanol plants and wine. A very large collection of 1,500 isolates of *B. bruxellensis* was recently surveyed using microsatellite data and it was identified that nearly 60% of isolates are polyploid[4]. It was previously known that some triploid strains of *B. bruxellensis* genomes exhibit an interesting profile, their genomes being composed of a core diploid genome and a distant third set of chromosomes, likely obtained through hybridization with a sister species[5]. We therefore sequenced 71 diverse strains of *B. bruxellensis* using short- and long-read sequencing to phase these strains in **Chapter III**. In this chapter, we developed

another phasing strategy intended to separate reads from polyploid hybrids in which some of the genomic copies are obtained from hybridization with a different species. We found that each of the four triploid subpopulations (wine 2, wine 3, beer and tequila/bioethanol) has a unique polyploidization history with a distinct trajectory. Based on genetic distance, we determined that the wine 2 group likely underwent autopolyploidization and that allopolyploidization occurred independently for the wine 3, beer and the tequila/bioethanol subpopulations. We also identified that hybridization of the allopolyploids occurred with a different species each time. We ruled out known sister species of *B. bruxellensis* such as *Brettanomyces anomala* and *Brettanomyces nanus* by sequencing them and assembling their genomes *de novo*, finding that they were too distant to the genetic material we observe in our allopolyploids. Finally, we also detail extensive loss of heterozygosity events which shape the genomic architecture of these subpopulations.

Overall, in this project we first sought to develop a novel polyploid phasing algorithm, opting for a ploidy agnostic method which adapts to the shape of the data. Then, once the method was established, its application was explored in the contexts of two different populations with contrasting polyploidization histories: on one hand the *S. cerevisiae* beer strains, a polyphyletic group of strains which cluster into three main clades, all of which have adapted to the brewing environment and on the other hand the *B. bruxellensis* subpopulations which have adapted to different environments and for the most part been derive from independent hybridization events with different, still unknown species.

References

1. Patterson, M. et al. WhatsHap: Weighted Haplotype Assembly for Future-Generation Sequencing Reads. J. Comput. Biol. 22, 498–509 (2015).
2. Chin, C.-S. et al. Phased diploid genome assembly with single-molecule real-time sequencing. Nat. Methods 13, 1050–1054 (2016).
3. Peter, J. et al. Genome evolution across 1,011 Saccharomyces cerevisiae isolates. Nature 556, 339–344 (2018).
4. Avramova, M. et al. Brettanomyces bruxellensis population survey reveals a diploid-triploid complex structured according to substrate of isolation and geographical distribution. Sci. Rep. 8, 4136 (2018).
5. Borneman, A. R., Zeppel, R., Chambers, P. J. & Curtin, C. D. Insights into the Dekkera bruxellensis Genomic Landscape: Comparative Genomics Reveals Variations in Ploidy and Nutrient Utilisation Potential amongst Wine Isolates. PLOS Genet. 10, e1004161 (2014).

Chapter I – nPhase: an accurate and contiguous phasing method for polyploids

Abstract

While genome sequencing and assembly are now routine, we do not have a full, precise picture of polyploid genomes. No existing polyploid phasing method provides accurate and contiguous haplotype predictions. We developed nPhase, a ploidy agnostic tool that leverages long reads and accurate short reads to solve alignment-based phasing for samples of unspecified ploidy (https://github.com/OmarOakheart/nPhase). nPhase is validated by tests on simulated and real polyploids. nPhase obtains on average over 95% accuracy and a contiguous 1.25 haplotigs per haplotype to cover more than >90% of each chromosome (heterozygosity rate ≥0.5%). nPhase opens the door to population genomics and hybrid studies of polyploids.

Background

Studying genotype-phenotype relations is contingent on having an accurate view of the genetic variants. To that end, various sequencing strategies and ways to analyze them have been developed. The ultimate goal is to faithfully determine the precise sequence of the DNA molecules contained within the cell. In practice this level of precision is rarely necessary and approximations are routinely used when they can be afforded. Aligning the sequencing data to a reference genome is a good approximation to identify genetic variants such as Single Nucleotide Polymorphisms (SNPs) but a poor one to identify Structural Variants (SVs)[1]. By contrast, the generation of *de novo* assemblies using the sequencing data is a good approximation to identify SVs[1] but, without significant polishing work[2], usually leads to a lower quality sequence. One enduring approximation is the reduction of the genome to a single sequence, even if the organism does not have a haploid or rigorously homozygous genome. A diploid or higher ploidy genome can be heterozygous. Identifying the heterozygous positions, or variants, is known as genotyping. Linking these variants together to establish which variants co-occur on the same strand of DNA is known as haplotyping or phasing. There is increasing interest in phasing genomes for diverse reasons, such as to obtain more accurate reference genomes[3], better study population genomics[4], improve the accuracy of GWAS studies[5], study the effects of compound heterozygosity[6], investigate Allele-Specific Expression patterns[7], gain insight into polyploid evolution[8,9], better understand the mechanisms of heterosis[10] and dissect the origins of hybrid species[11].

Phased genomes can be obtained either by physically separating entire chromosomes[12] (or significantly large portions of chromosomes) prior to sequencing[13] or by separating them bioinformatically after sequencing the whole genome[14]. The length of reads is a significant limiting factor in the ability to bioinformatically separate reads into their corresponding haplotypes. One very

successful method that overcame that limitation was trio binning[15], which circumvented the importance of long reads by leveraging information from parental whole genome sequencing. Other methods have been explored but cannot overcome the short read length limitation particularly well[16]. One solution has been to resort to imputing haplotypes through reference panels[17]. Despite a higher error rate, diploid phasing of long reads has been solved by existing methods such as WhatsHap[18], an alignment-based phasing tool and Falcon-Unzip[19], an assembly-based phasing tool. Assembly-based phasing attempts to generate a *de novo* assembly for each haplotype directly, without relying on a reference sequence. Alignment-based phasing uses a reference genome as support to identify heterozygous positions and then attempts to link positions together based on the co-occurrence of heterozygous SNPs on overlapping reads. For diploids each variable position can only be one of two possible bases. Knowing one haplotype allows to deduce the other. This allows diploid phasing methods to be relatively simple and straight-forward. For polyploids, however, a variable position can be one of two or up to six possible states (all four bases, a deletion or an insertion) and this deduction is no longer possible, rendering the task of phasing significantly more complex. Some methods currently exist to phase polyploids but mainly using short read sequencing and leading to a low accuracy and contiguity phasing[20,21,22,23].

Here, we developed nPhase to address the lack of a polyploid phasing method that outputs accurate, contiguous results and does not require prior knowledge of the ploidy of the sequenced genome. The required inputs are a reference sequence as well as long and short read sequencing data. The pipeline performs the mapping, variant calling, phasing and outputs the phased variants and a fastQ file for each predicted phased haplotype, or haplotig. The nPhase algorithm is ploidy agnostic, meaning it does not require any prior knowledge of ploidy and will not attempt to guess the ploidy of the sample. Instead, it will separate the reads into as few distinct haplotigs as possible. The nPhase algorithm has three modifiable parameters, we

have evaluated the effects of these parameters on the results and provide a default set of parameters, which we predict to be appropriate for all cases, along with some recommendations on how to modify these parameters for genomes that are more difficult to phase, *i.e.* low heterozygosity and high ploidy genomes.

Using yeast as an *in silico* model, we validated the performance of nPhase on simulated *Saccharomyces cerevisiae* genomes (2n, 3n and 4n) of varying heterozygosity levels (0.01%, 0.05%, 0.1% and 0.5% of the genome) as well as on a triploid *Brettanomyces bruxellensis* sample and chromosome 2 of the autotetraploid potato plant, *Solanum tuberosum*. Based on our simulated tests we found that nPhase performs very well in terms of accuracy and contiguity. We obtained an average of 93.9% accuracy for all diploids, 92.3% for all triploids, and 94.5% for tetraploids with a heterozygosity level of at least 0.5%, or 87.3% accuracy when we include the lowest heterozygosity level tetraploids. All results are very contiguous, with an average of between 2.4 and 4.1 haplotigs per haplotype, bringing us very close to the ideal result of one haplotig per haplotype.

Results

Phasing pipeline and strategy

We developed the nPhase pipeline, an alignment-based phasing method and associated algorithm that run using three inputs: highly accurate short reads, informative long reads and a reference sequence. The pipeline takes the raw inputs and processes them into data usable by the nPhase algorithm. Unlike other existing methods, our algorithm is designed for ploidy agnostic phasing. It does not require the user to input a ploidy level and it does not contain any logic that attempts to estimate the ploidy of the input data. The idea at the core of the algorithm is that if you iteratively cluster the most similar long reads and groups of long reads together you will naturally recreate the original haplotypes.

For the first step of the pipeline, the long and short reads are aligned to the reference, then the aligned short reads are variant called to identify heterozygous positions and generate a high quality dataset of variable positions (Figure 1). Each long read is then reduced to its set of heterozygous SNPs according to the previously identified variable positions. We also collect long read coverage information to allow the level of representation of a haplotype in the data to influence its likelihood of being properly phased (see Methods).

The reduced long reads and the coverage information are then passed onto the nPhase algorithm, an iterative clustering method. On the first iteration, nPhase clusters together the two most similar long reads, then it checks that the cluster identities are maintained, *i.e.* it checks that merging these two long reads together does not significantly change the information they each contain individually, and finally it generates a consensus sequence representative of the group of these two reads. The next iteration will be exactly the same with N-1 reads. nPhase will run until all

remaining clusters are sufficiently different from each other to fail the cluster identity maintenance check. These remaining clusters represent the different haplotypes within the original dataset.

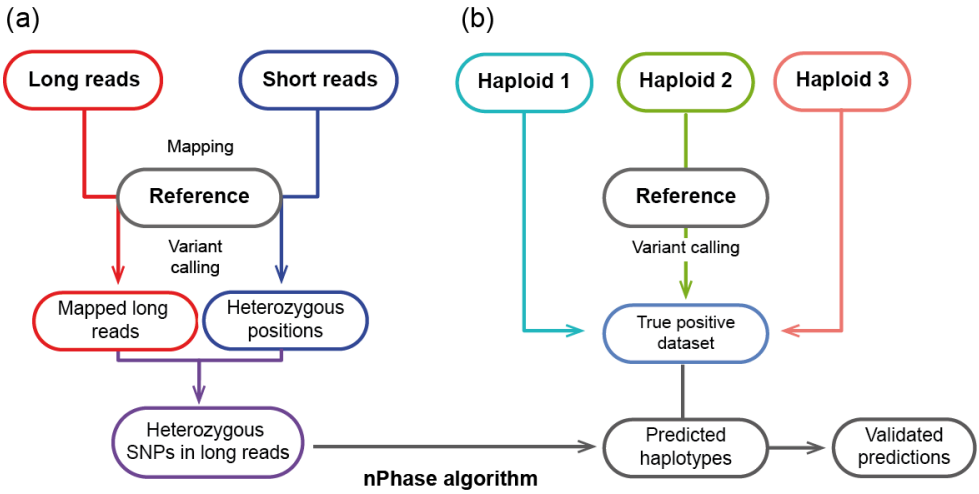

Figure 1 - nPhase pipeline and verification process. (**a**) The nPhase pipeline requires three inputs: a long read dataset, a short read dataset and a reference genome sequence. Both sequencing datasets are mapped to this reference genome, then the short reads are variant called in order to identify heterozygous positions. The long reads are reduced to only their heterozygous positions, and this set of linked heterozygous positions is phased by the nPhase algorithm and outputs phased haplotypes. (**b**) In parallel with running the virtual polyploids through the nPhase pipeline, we map the original strains to the same reference and variant call them to identify their haplotypes. This generates the true positive dataset against which we will compare the haplotypes predicted by nPhase in order to assess the accuracy of our algorithm.

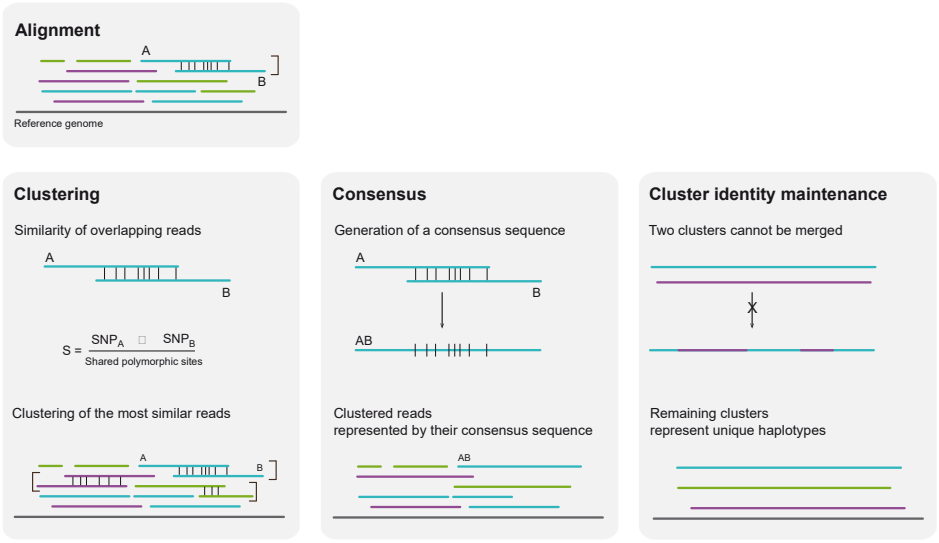

Figure 2 - nPhase algorithm. Here we represent how a triploid's reads could align to a reference sequence. Each read is one of three colors, one for each haplotype. The clustering, consensus and cluster identity maintenance steps are iteratively repeated until all remaining clusters are forbidden to merge. **Clustering**: Each vertical line represents a SNP; different colors signify different haplotypic origins. Only two reads are clustered at a time, here we show three clusters, so this is the result of the third step of nPhase's iterative clustering. **Consensus**: A consensus sequence is generated by allowing every read in the cluster to vote for a specific base for a given position. Votes are weighted by the pre-calculated context coverage number to discourage sequencing errors. The consensus sequences that represent clusters are treated just like aligned long reads and continue to be clustered. **Cluster identity maintenance**: When all remaining clusters are very different from each other, they are not allowed to merge, this is to prevent the algorithm from always outputting only one cluster per region. The remaining clusters and their consensus sequences should correspond to the haplotypes present in the original dataset.

nPhase, a ploidy agnostic phasing algorithm

As described earlier, nPhase is an iterative clustering algorithm. It is composed of three main ideas: (i) clustering, which ensures that similar reads are clustered together, (ii) cluster identity maintenance, which ensures that only similar clusters are merged into larger ones and finally (iii) consensus, a way to reduce a cluster to a consensus sequence in order to easily compare it to other clusters (Figure 2).

Each step of the clustering algorithm starts by calculating the similarity between every overlapping pair of reads (Figure 2a). By default, the minimal overlap is 10 heterozygous positions. Similarity is defined as $S = N_{\text{shared variants}}/N_{\text{shared positions}}$. The pair of reads with the highest similarity is clustered together. If there is a tie, then we cluster together the pair of reads with the most variable positions in common. If there is again a tie, then we select a pair randomly. By default, the algorithm will not attempt to merge two sequences with less than 1% similarity.

The pair that was selected now forms a cluster of two reads (Figure 2b). In order to continue this iterative algorithm, we need to define a way to calculate the similarity between a read and a cluster of reads, and the similarity between two clusters of reads. We do so by computing a consensus sequence for each cluster of reads and we use the consensus sequence to calculate the similarity as defined above. For each position, the consensus is defined as the base which has the most support from the reads in the cluster. Each read gets a vote equal to the context coverage of the base it supports. If there is a tie then all tied bases are included in the consensus sequence.

As defined, the clustering algorithm will continue to iterate, merging clusters together until all available options are exhausted and output only one cluster per region (Figure 2c). The solution is to set restrictions on which clusters are allowed to be merged in the clustering step. We consider that each cluster has its own "identity" defined by the population of reads that comprise it. If merging two clusters has a significant effect on the identity of both clusters then the merge is not allowed.

We calculate how much merging of two clusters would change them. The amount of change allowed is limited by the ID parameter. In order to quantify the amount of change to a cluster's identity we keep track of the "demographics" of each position, *i.e.* how strongly represented each base is for that position in that cluster. We differentiate positive identity changes from negative identity changes: (i) if a merge of two clusters results in increased support for their consensus sequence bases then that change is considered positive, (ii) if the merge results in decreased support for a consensus sequence base then that change is considered negative and we calculate how many votes the base lost, even if it remains the consensus base after the merge. The number of votes lost is divided by the total number of votes in the region that both clusters have in common to obtain the cluster identity change percentage. By default, if it is higher than 5% we do not allow the two clusters to merge. Once all remaining clusters fail this test, the algorithm stops. The resulting clusters represent the different haplotypes that nPhase found and are output as different sets of reads, heterozygous SNPs, and consensus sequences.

Validation of the nPhase algorithm by combining reads of non-heterozygous individuals

To test and validate the performance of nPhase, we decided to combine sequencing datasets of haploid and homozygous diploid organisms into virtual polyploid datasets. We selected four natural *S. cerevisiae* isolates as the basis for our virtual genomes: ACA, a haploid strain, and three homozygous diploid strains: CCN, BMB and CRL (Additional File 1: Table S1). These four strains have different ecological and geographical origins and are sufficiently distinct from each other to allow us to evaluate the performance of nPhase at heterozygosity levels of up to 1% of the genome[24].

We sequenced these strains using an Oxford Nanopore long-read sequencing strategy and obtained Illumina short-read data from our 1,011 yeast genomes

project[24]. Since these strains do not have any heterozygosity, we could map their short reads to the *Saccharomyces cerevisiae* reference genome and variant call them to obtain their haplotypes (Figure 1). We then used these haplotypes as a truth set to assess the performance of nPhase. With this truth set, we tested the influence of dataset characteristics: coverage, ploidy, heterozygosity level and the inclusion or exclusion of reads that map to distant regions of the genome, hereafter described as split reads. We also investigated the influence of parameters that modulate the behavior of the nPhase algorithm: minimum similarity, minimum overlap and maximum ID change (for a description of them see **Available Parameters** in Methods).

To assess the influence of ploidy, we used the three constructions of the different virtual genomes previously mentioned. We also randomly sampled 6250, 12500, 62500 and 125000 heterozygous SNPs from each virtual genome to simulate datasets where 0.05%, 0.1%, 0.5% and 1% of the positions in the genome are heterozygous. This equates to three different ploidies and four heterozygosity levels, or 12 polyploid genomes to test.

By running a total of 6000 validation tests on varying ploidy, heterozygosity, and coverage levels exploring the parameter space, we determined default parameters of nPhase (see Methods). According to these tests, the parameters that result in optimal results in terms of accuracy and contiguity are the following: 1% minimum similarity, 10% minimum overlap and 5% maximum ID (see **Identifying optimal parameters** in Methods). We then ran nPhase with these default parameters on our previously described optimal datasets of varying ploidy (2n, 3n and 4n) and heterozygosity levels (0.05%, 0.1%, 0.5% and 1%) of 20X long reads per haplotype with split read information (Additional File 1: Table S2).

As an example, we phased the tetraploid genome showing a heterozygosity level of 0.5% using nPhase (Figure 3). Since we know the ground truth, we can assign each

haplotig to the strain whose haplotype it most closely represents and we can calculate our accuracy metrics.

Figure 3 - Predicted haplotypes for the tetraploid genome with a 0.5% heterozygosity level. The result of this test was an accuracy of 93.7%, an error rate of 4.0%, and a missing rate of 2.2% with an average of 2.4 haplotigs per haplotype. Each subgraph displays the predicted haplotigs for a different chromosome, each predicted haplotig is on a different row on the Y axis, and the X axis displays the position along the chromosome. All predicted haplotigs are color coded according to the haplotype they are the closest to.

In order to measure accuracy we distinguish between two forms of errors: standard errors, *i.e.* heterozygous SNPs erroneously attributed to the wrong haplotype, and missing errors, *i.e.* heterozygous SNPs which we know are present but which were erroneously not represented in the predictions. The accuracy is the percentage of all SNPs which were correctly attributed to their haplotype. The error rate is the percentage of all predictions which were incorrect. The missing rate is the percentage

of all heterozygous SNPs which were never attributed to their haplotype. We use the following formula:

$$Accuracy=TP/(TP+FP+FN)$$

TP=True Positive; the SNP was attributed to the correct haplotype
FP=False Positive; the SNP does not belong in this haplotype
FN=False Negative; the SNP is not represented in the results.

The result of this test was an accuracy of 93.7%, an error rate of 4.0%, and a missing rate of 2.2% with an average of 2.4 haplotigs per haplotype. Seven of the sixteen chromosomes have an L90 of 1, meaning that for all four haplotypes, more than 90% of the heterozygous SNPs were assigned to one haplotig. For the nine remaining chromosomes, seven have at least two chromosome-length haplotigs. In all cases, the chromosomes are nearly fully covered by haplotigs that represent the four different haplotypes, as confirmed by the low missing haplotype prediction rate (2.2%). As a ploidy agnostic tool, nPhase was not given any information about the ploidy of this sample and does not attempt to estimate its ploidy. Despite that, nPhase reached a high accuracy (93.7%) and contiguity (2.4 haplotigs per haplotype), demonstrating its ability to reliably phase a tetraploid of that heterozygosity level. The same representation is available for the other datasets of different ploidy and heterozygosity levels (Additional File 2: Fig S1).

Across the 12 phased genomes with variable ploidy and heterozygosity levels, we noted little variation in terms of contiguity as we obtained between 2.4 and 4.3 haplotigs per haplotype (Figure 4a). At a heterozygosity level of 0.05%, the least contiguous genomes are observed with around 4 haplotigs per haplotype (Figure 4a). The triploid genomes decrease to around 3 haplotigs per haplotype for heterozygosity levels greater than 0.1% (Figure 4a). The tetraploid tests continue the

trend of higher ploidies becoming more stable and contiguous as the heterozygosity level increases, dropping to 3.1 haplotigs per haplotype at the 0.1% heterozygosity level and then stabilizing at 2.4 haplotigs per haplotype at the 0.5% and 1% heterozygosity levels (Figure 4a). This could be explained by the availability of more haplotigs to potentially merge with each other as ploidy increases.

Regarding the accuracy, we observed that for heterozygosity levels greater than 0.5%, the accuracy appears stable and high across ploidies with a minimum of 93.56% for the diploid (2n) at a 0.5% heterozygosity level, and a maximum of 96.70% accuracy for the triploid (3n) at a 1% heterozygosity level (Figure 4b). For lower heterozygosity levels ($\leq 0.1\%$), we have results that are more variable between ploidies (Figure 4b). Diploid tests retain a high 95.32% accuracy for the 0.1% heterozygosity level but drop to 90.34% accuracy for the 0.05% heterozygosity level. For triploid genomes, the results drop to 90.70% accuracy for the 0.1% heterozygosity level, then down to 87.00% at 0.05% heterozygosity level. Continuing the trend of higher ploidies performing worse with lower heterozygosity levels, the accuracies for the 0.1% and 0.05% heterozygosity levels for the tetraploid tests output 81.65% and 78.62% accuracy, respectively.

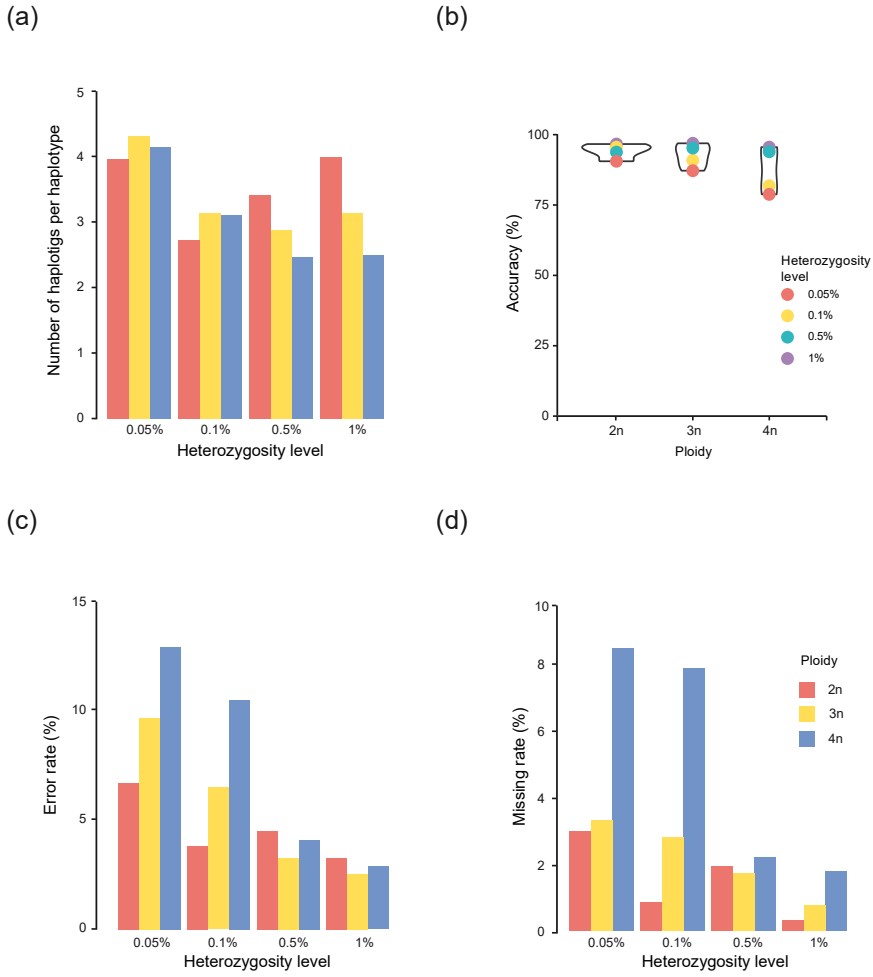

Figure 4 - Effects of ploidy and heterozygosity levels on accuracy and contiguity. Through these graphs we show the effects of sample properties (heterozygosity level and ploidy) on nPhase's accuracy metrics when run with default parameters. (a) Each bar displays the contiguity of a different test result. The least contiguous heterozygosity level is 0.05%, likely related to its also yielding the least accurate results. Overall, we note little absolute variation in the contiguity. Interestingly, contiguity at higher heterozygosity levels appears to be a function of ploidy. Higher ploidies seem less likely to become less contiguous as a result of increasing the heterozygosity level, while the diploid tests are more affected. We also note that tetraploids of high heterozygosity level are the most contiguous. (b) Each bar displays the accuracy of a different test result. As ploidy increases, the accuracy tends to

decrease. It also appears to decrease faster for tests on low heterozygosity level constructions. (c and d) Each bar displays our evaluation of the effects of ploidy and heterozygosity level on the error and missing rates, respectively, for our 12 tests using optimal parameters. Overall, we see that the error rate is always higher than the missing rate across these conditions. As the heterozygosity level increases, the error and missing rates decrease along with the gap between ploidies. We also find that more difficult phasing problems (high ploidy and low heterozygosity level) yield much higher error and missing rates, and that the low heterozygosity tetraploids seem to be particularly sensitive to missing calls.

In addition, we observed that errors are more frequent in all tests than missing calls (Figures 4c and 4d). For higher heterozygosity levels ($\geq 0.5\%$), these two forms of error are stable and very low. The error rate is set between a minimum of 2.53% for the 1% heterozygosity level triploid and a maximum of 4.51% for the 0.5% heterozygosity level diploid. And the missing rate is set between a minimum of 0.31% for the 1% heterozygosity level diploid and a maximum of 2.21% for the 0.5% heterozygosity level tetraploid. For lower heterozygosity levels ($\leq 0.1\%$), both the error and missing rates increase with ploidy, suggesting both types of errors may be linked. If we set aside the 0.1% heterozygosity level diploid which has an error and missing rates of 3.82% and 0.86%, respectively, the error rates have a wide range with a minimum error of 6.49% for the 0.1% heterozygosity level triploid and a maximum error of 12.91% for the 0.05% heterozygosity level tetraploid. Similarly, the missing rates range from a minimum of 2.97% for the 0.05% heterozygosity level diploid to a maximum of 8.46% for the 0.05% heterozygosity level tetraploid, again adding to the trend of lower heterozygosity levels coupled with higher ploidies yielding worse results.

Benchmarking nPhase against other polyploid phasing tools

Some methods currently exist to phase polyploids using long read data such as WhatsHap polyphase[20], as well as other methods which were mostly designed to work with short read sequencing data but can sometimes use long reads as input[21,22,23]. Because nPhase is a phasing tool that leverages the linking power of long reads to achieve its high accuracy and contiguity metrics, we did not benchmark it against tools that rely exclusively on short reads for phasing, since these are inherently limited by the size of their reads. We also did not benchmark nPhase against tools that can only phase diploid genomes as this is not the intended use case for our algorithm. We therefore compare nPhase to the recently released WhatsHap polyphase, to our knowledge the only other polyploid phasing algorithm that handles long reads.

We compared the results nPhase (default parameters) with WhatsHap polyphase on the same samples (Figure 5). Since WhatsHap polyphase has a parameter named "--block-cut-sensitivity" that can be set to determine the tradeoff between accuracy and contiguity, we tested WhatsHap polyphase using all possible values for this parameter (integers from 0 to 5) to compare all possible results to nPhase's default results. A value of 0 for this parameter means that WhatsHap polyphase will generate the most contiguous results possible, and 5 means that it will generate the most accurate results possible.

The performance of WhatsHap polyphase was measured in terms of switch error rate and N50 block lengths. Instead we will talk about accuracy and average number of haplotigs per haplotype, two metrics that are more direct representations of the performance of the algorithms and answer two important questions: "How reliable are the results?", *i.e.* what are the proportions of accurate, erroneous and missing calls? And "How informative are they?", *i.e.* by how many haplotigs is each haplotype represented? nPhase and WhatsHap polyphase were both applied to our 20X test datasets of different ploidy and heterozygosity levels. nPhase was tested

using its default parameters and WhatsHap polyphase was tested with all six possible values of its adjustable sensitivity parameter. We report here the average accuracy, error and missing rates, as well as the average number of haplotigs obtained for the genome, normalized by the ploidy.

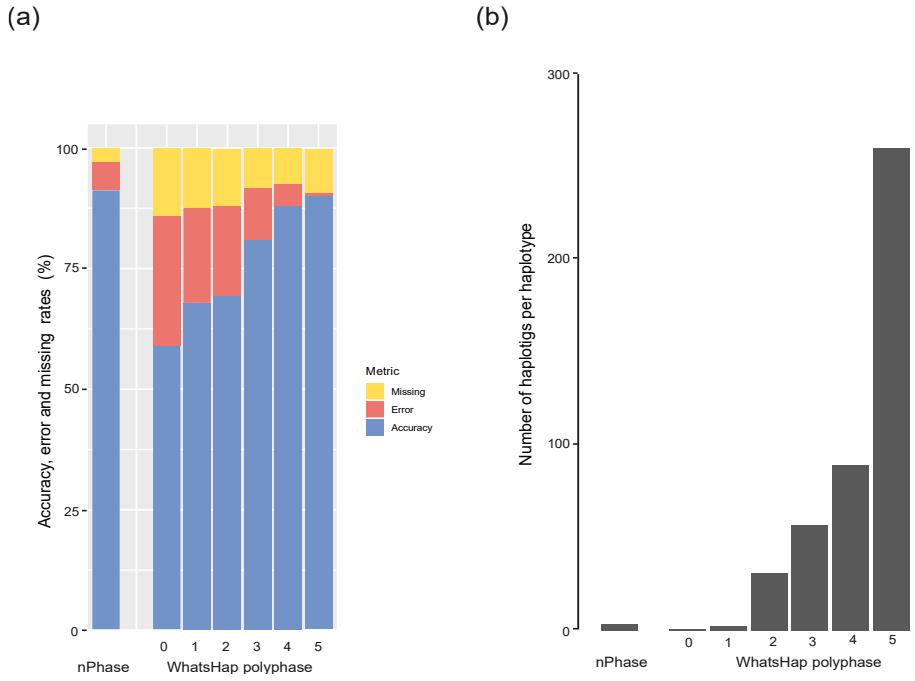

Figure 5 - Error types and number of haplotigs for nPhase and WhatsHap polyphase. nPhase and WhatsHap polyphase were both applied to our 20X test datasets of different ploidy and heterozygosity levels. nPhase was tested using its default parameters and WhatsHap polyphase was tested with all six possible values of its adjustable sensitivity parameter. This graph compares both tools using the following metrics: average number of haplotigs obtained for the genome, normalized by the ploidy, average accuracy, average error rate and average missing rate. (**a**) Average accuracy, error and missing rates for all tests using nPhase and WhatsHap polyphase on different sensitivity levels. The error rate for WhatsHap polyphase increases dramatically as the sensitivity level decreases, illustrating the tool's tradeoff between accuracy and contiguity. (**b**) Average number of haplotigs per chromosome per haplotype for all tests using nPhase and WhatsHap polyphase on different sensitivity levels. The very high number of haplotigs per chromosome per haplotype for the highest sensitivity levels (5 and 4) shows that despite being highly accurate, they are not contiguous enough to be informative. Based on our results, nPhase outperforms WhatsHap polyphase in all of our tests. The tradeoff between accuracy and contiguity is extreme in WhatsHap polyphase, either the results are very accurate but so fragmented as to be uninformative, or they are about as contiguous as nPhase but less than 65% accurate.

In our tests nPhase has an average accuracy of 91.2%, slightly outperforming WhatsHap polyphase's most sensitive setting (5), which yields an average accuracy of 90.1%, and its second most sensitive setting (4) which yields an average accuracy of 88.9% (Figure 5a). Lower sensitivity levels for WhatsHap polyphase quickly lose accuracy, with the next lowest setting yielding only 81.1% accuracy on average, and its least sensitive setting only reaching 59% accuracy.

In addition to its high accuracy, nPhase is highly contiguous, outputting these accurate results, on average, in 3.4 haplotigs per chromosome per haplotype (Figure 5b). The highly accurate WhatsHap polyphase sensitivity levels (5 and 4) output their results in a highly discontiguous 258.7 and 88.9 haplotigs per haplotype, respectively. In order to output results of similar contiguity to nPhase, WhatsHap polyphase must sacrifice accuracy and drop to a sensitivity level of 1 or 0, which output 2.5 and 0.9 haplotigs per chromosome per haplotype, respectively. This tradeoff between accuracy and contiguity performed by WhatsHap polyphase does not appear to have a useful middle ground and nPhase demonstrates that it is not necessary to make a choice given that it simultaneously achieves both.

Validation of the nPhase algorithm on a real *Brettanomyces bruxellensis* triploid strain

We further tested nPhase by running it on a real triploid organism. We selected GB54, a triploid strain of the yeast species *Brettanomyces bruxellensis* with a 0.7% heterozygosity level. GB54 was sequenced by Oxford Nanopore long-read sequencing and Illumina short-read sequencing, then processed through the nPhase pipeline. Since we know that this strain is a triploid strain, we should expect a successful phasing to reflect that triploid nature by outputting three haplotypes per region. In our results we observe that most regions have been phased into two or three haplotypes, with few small exceptions (Figure 6).

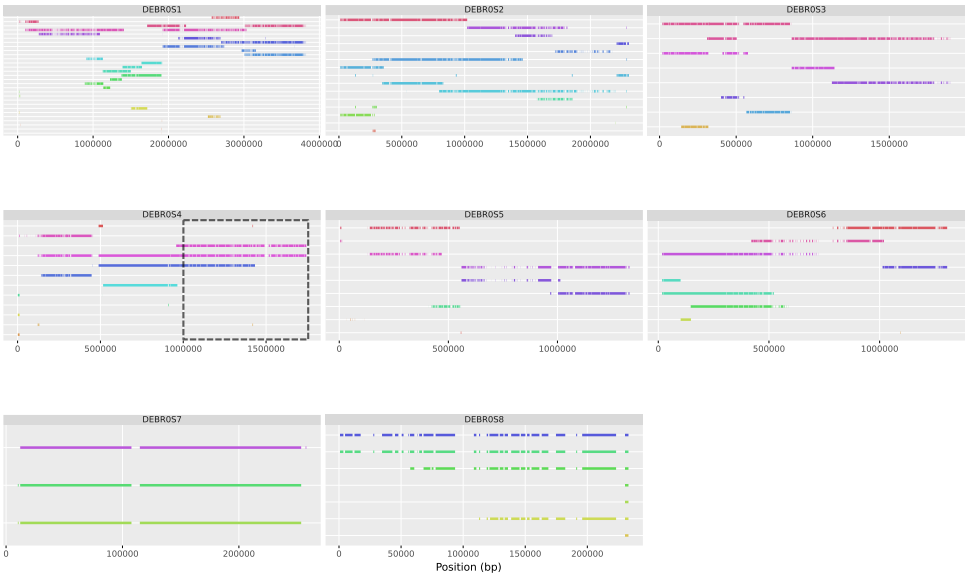

Figure 6 - Predicted haplotypes for the *Brettanomyces bruxellensis* strain. Each subgraph displays the predicted haplotigs for a different chromosome of this 0.7% heterozygosity level triploid, each predicted haplotig is on a different row on the Y axis, and the X axis displays the position along the chromosome. All predicted haplotigs are color coded randomly as the ground truth is not known. We observe that while the strain is a known triploid, nPhase did not exclusively predict three haplotypes per region. We also note that some regions such as the end of chromosome 2 or center of chromosome 6 have a very low level of heterozygosity.

The regions that output more or less than three haplotypes are unexpected and potentially represent a phasing failure. For example, the highlighted region in Figure 6, on chromosome 4 transitions from three haplotypes to only two haplotypes. By remapping each haplotig's reads back to the reference and viewing the coverage, we note that regions phased into only two haplotigs have a coverage distribution consistent with the presence of only two haplotypes but three genomic copies (Figure 7). One haplotig accounts for 2/3 of the coverage and the other haplotig accounts for the remaining 1/3 of the coverage. In Figure 7, we highlighted the previously described region of chromosome 4, showing us that the three haplotigs in the first

triploid region have roughly equal coverage, and in the region with only two haplotigs one of them is twice as covered as the other.

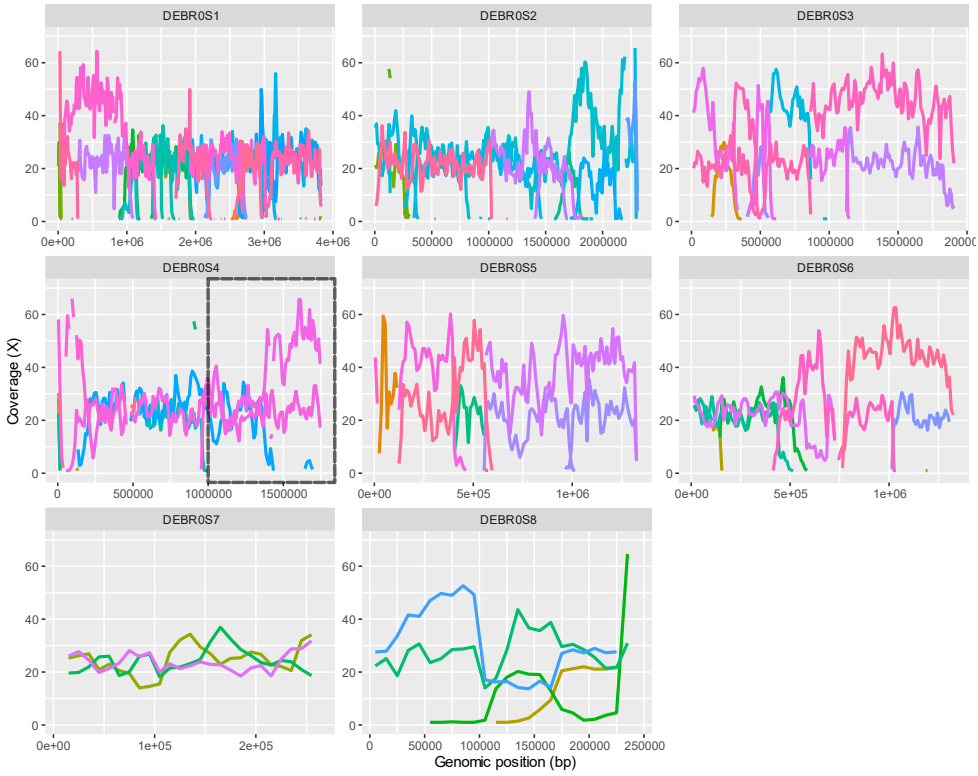

Figure 7 - Coverage level of predicted haplotigs for the *Brettanomyces bruxellensis* strain. Each subgraph displays the coverage level of predicted haplotigs for a different chromosome of this 0.7% heterozygosity level triploid, the Y axis is the coverage level and the X axis displays the position along the chromosome. All predicted haplotigs are color coded randomly as the ground truth is not known. We observe that in regions covered by only two haplotigs, one will be covered roughly twice as much as the other, whereas regions covered by three haplotigs tend to be equally covered.

The haplotigs that represent 2/3 of the reads in the region they cover either represent one single haplotype which is present in two copies, or they represent two very similar haplotypes that were erroneously clustered into one by nPhase. By looking at the distribution of the heterozygous allele frequency within each haplotig's corresponding cluster of reads, we show that few clusters are clearly enriched in

allele frequencies around 50% (Figure 8). Two of these clusters correspond to regions erroneously predicted to contain only one haplotig (Additional File 2: Fig S2), confirming that the allele frequency within a haplotig cluster can reveal chimeric clusters. The absence of a noticeable enrichment in the allele frequencies of other clusters is further evidence that the predictions made by nPhase are highly accurate.

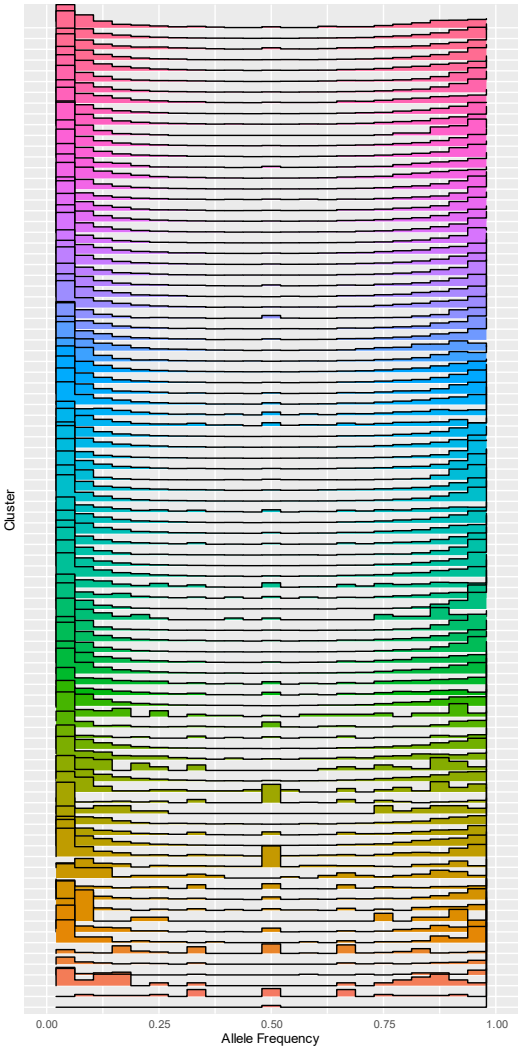

Figure 8 - Allele frequency distribution of predicted haplotigs for the Brettanomyces bruxellensis strain. Each line displays the allele frequency distribution of predicted haplotig clusters. the height of each bar is the relative proportion of all heterozygous SNPs in that cluster and the X axis displays the allele frequency. All predicted haplotig clusters are color coded randomly as the ground truth is not known. We identify two clusters as having a heterozygous SNPs with a slightly high proportion of allele frequencies around 50%, one in green and one in orange towards the bottom of the figure.

Implementing automated cleaning steps

We observed in our initial *in silico* results that nPhase outputs many shorter haplotigs which consequently do not contain much phasing information. With our test on the *Brettanomyces bruxellensis* strain we identified that we can use haplotig cluster allele frequency as a proxy for phasing quality. We also noted that, by design, nPhase will only output unique haplotypes which sometimes means that a region will be phased into fewer copies than might be naively expected based on ploidy. Finally, we also find that raw nPhase results can sometimes appear to be too fragmented.

To provide a method that begins addressing these issues, we developed a series of three steps intended to automatically clean nPhase's raw results without significantly affecting accuracy:

1. Merging as many remaining haplotigs as possible together
2. Filtering out haplotigs that account for less than 1% of all coverage
3. Redistributing the reads of highly covered haplotigs

These steps are further described in the **Automated Cleaning** section in Methods. We checked the effect of these steps on accuracy and number of haplotigs by applying them to the results of running nPhase with default parameters on all our virtual polyploids (10X and 20X coverage). Overall, our raw results had an average of 4.03 haplotigs per haplotype (Figure 9A) and an average accuracy of 88.6% (Figure 9B). After cleaning we observed an average of 2.37 haplotigs per haplotype and an average accuracy of 87.4%. If we only consider our tests at 0.5% heterozygosity or higher, then our raw results had an average of 3.81 haplotigs per haplotype and an accuracy of 91.49%. After cleaning we had an average of 1.87 haplotigs per haplotype with an accuracy of 91.44%.

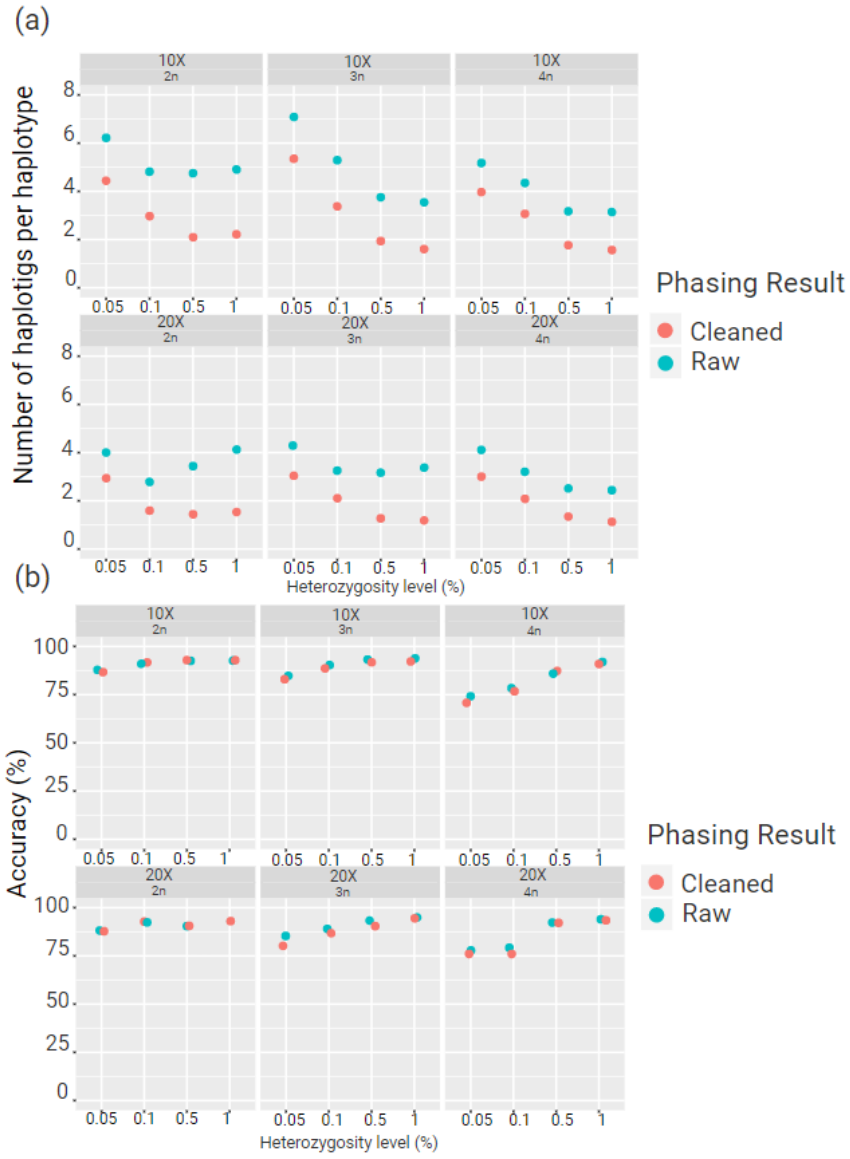

Figure 9 - Contiguity and accuracy of nPhase results on virtual polyploids before and after automated cleaning. Each subgraph compares performance metrics for raw nPhase results with their automatically cleaned counterparts. Each point corresponds to a virtual genome of a given ploidy (n), coverage (X) and heterozygosity level **(a)** We compare here the number of haplotigs per haplotype in all these conditions. We find a significant reduction in the number of haplotigs per haplotype for our cleaned results in all cases. **(b)** We compare here the accuracy (%) in all conditions. We find that the automated cleaning process has a small, negligible negative effect on accuracy in most cases, though not all.

We tested this method on our results with GB54 and observe a significantly more contiguous phasing (Figure 10). The cleaning process successfully redistributed the reads in the previously highlighted region of chromosome 4 (Additional File 2: Fig S3) and merged haplotigs together in a way that renders the results much easier to interpret. The number of haplotigs has been reduced from 93 to 33, greatly reducing noise. We expect the accuracy not to have been negatively affected by this step based on the way the read coverage of cleaned haplotig clusters is distributed (1/3, 1/3, 1/3 coverage or 2/3, 1/3 coverage) and the allele frequency distributions of the cleaned haplotigs (Additional File 2: Fig S4).

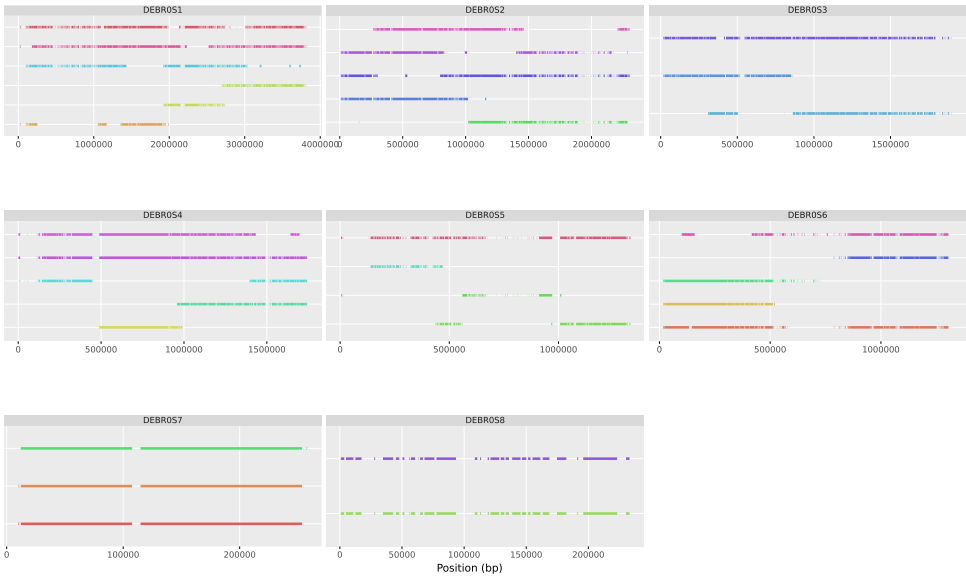

Figure 10. Automatically cleaned predicted haplotypes for the *Brettanomyces bruxellensis* strain. This figure represents an automatically cleaned version of Figure 6. We note the presence of significantly fewer haplotigs, a higher contiguity and the filling of the gap observed in the chromosome DEBR0S4. One notable change observed with the cleaned step is that chromosome 8 is predicted to have only two different haplotypes, which was not evident based on the raw results. For any sensitive application it would be necessary to further scrutinize this prediction since the automated cleaning process is less rigorously validated.

Running the nPhase algorithm on chromosome 2 of the potato plant species *Solanum tuberosum*

We also tested nPhase on one chromosome of a larger, more repetitive plant genome. We used the autotetraploid *Solanum tuberosum* (potato) dataset generated for the WhatsHap polyphase paper[20]. We used the latest version of the DM1–3 516 R44 assembly as a reference (v6.1)[25]. We chose to limit this section to phasing chromosome 2. At 46 Mb it is the shortest chromosome in the reference assembly (chromosome 1 is the largest with an 88 Mb chromosome) and is 30x larger than the longest chromosome in *S. cerevisiae* (chromosome 4, 1.5 Mb). We observe a 2.4% heterozygosity level for chromosome 2 based on Illumina data, more than twice as high as our most heterozygous test case (1%).

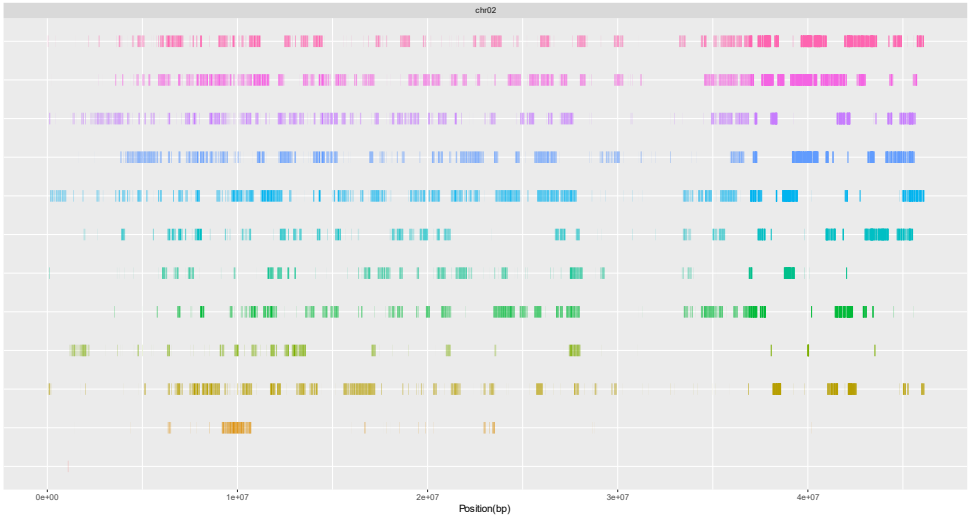

Figure 11. Automatically cleaned predicted haplotypes for the *Solanum tuberosum* strain. This figure represents automatically cleaned phasing results for chromosome 2 of *Solanum tuberosum*. 99% of phasing predictions are contained within the 12 largest haplotigs displayed here (the 12th is so sparse it isn't visualized here). The cleaned result is significantly more contiguous than the raw 1129 haplotigs obtained directly from nPhase. Only around 16% of positions are covered by more than 4 haplotigs, likely in large part where one haplotig drops off in coverage while another starts increasing.

To reduce computation time, we used a randomly sampled subset of heterozygous variants, effectively phasing at a 0.5% heterozygosity level. The raw results of nPhase yielded 1129 haplotigs, which were reduced to 25 haplotigs by a modified version of the automated cleaning steps; the final gap filling step was disabled in light of the fragmented nature of our raw results (Figure 11). Of the 25 cleaned haplotigs output, we find 90% of predicted variants in the 9 largest cleaned haplotigs, and 99% of predicted variants in the 12 largest cleaned haplotigs. The remaining 13 cleaned haplotigs account for less than 0.6% of predictions made and could reasonably be filtered out.

We note that the haplotigs obtained skip around the chromosome, which may either be due to structural variation or to long reads being mapped in error to the wrong repetitive regions, thereby giving the illusion of widespread structural variation. We also checked the phasing predictions for the 5 longest genes of chromosome 2 (Additional File 2: Fig S5) and found that they are coherent with our expectations for an autotetraploid.

Discussion

We developed nPhase, an algorithm that relies on a few intuitive rules to process an input dataset of long reads, reduced to heterozygous positions, outputting as few clusters as possible which we have shown correspond to the true haplotypes with >90% accuracy. By not specifying the ploidy of the sample in any step, we allow nPhase to adapt to the particularities of the dataset and do not run the risk of forcing an incorrect result to fit such an arbitrary algorithmic constraint. We provide nPhase as part of a pipeline that enables anyone to use their short and long read sequences of the same sample as inputs and obtain a list of SNPs and a fastQ file for each predicted haplotig.

Through our validation tests, we determined that there is a set of parameters for nPhase that performs optimally in nearly all of our test cases and that the algorithm performs well even with very low levels of genetic distance between haplotypes. We found that as little as 10X coverage can yield satisfying results. More complex cases, such as when there is a high ploidy coupled with a low heterozygosity, should benefit from higher coverage and a more stringent parameter for the minimum overlap (0.25 for example). Further investigation would be needed in order to more adequately define how these difficult samples should be treated. We also demonstrated with our benchmarking tests that nPhase outputs far more accurate and contiguous haplotigs than alternative polyploid phasing methods, and that this contiguity can be greatly improved at a very small cost to accuracy by using our simple automated cleaning process.

By testing nPhase on a triploid strain of the yeast species *Brettanomyces bruxellensis* we were able to demonstrate that our method can be used on a real polyploid sample and provides a previously inaccessible insight into its haplotypic composition. We were able to show through the chosen sample the usefulness of a ploidy agnostic

method which can adapt to a genome with a variable number of haplotypes. In the process of validating this real test case, we established two ways of qualitatively assessing phasing quality: checking the coverage plots of re-mapped haplotig reads and checking the allele frequency of reads that comprise a cluster. Our automated cleaning process yielded satisfying results, visibly improving the contiguity of the phasing, reducing noise, and filling some of the gaps observed in the raw phasing results.

We also tested nPhase on a much larger example, the 44 Mb long chromosome 2 of the potato plant species *Solanum tuberosum*, 30 times longer than the longest chromosome of *Saccharomyces cerevisiae*. This is a highly heterozygous autotetraploid with a highly repetitive genome and represents an important test case for nPhase. Despite the significantly increased complexity, we found that by using nPhase coupled with our cleaning steps we were able to produce a remarkably contiguous phasing prediction using only a fraction of the available data. The genes in particular we expect to be correctly phased, while we did not test the effects of nPhase on a highly repetitive test case with a known ground truth, limiting our certainty that the phasing was equally accurate in repetitive regions of the genome. In our analysis we did not take any extra steps to address the repetitive nature of the potato genome: we used a reference in which the repeats were not masked, we used all mapped reads, including those with low mapQ scores, and we did not check if variants called by short reads were reflected in the long reads. These are a few areas in which steps can be taken to improve the quality of the phasing. We also only used a fraction of all available heterozygous positions, and devoting more computing power and time to exploit more of that very relevant phasing information would presumably yield even better results.

As an alignment-based phasing algorithm, the performance of nPhase is going to be highly dependent on read length and the quality of the reference genome being mapped against. Consequently, structural variants between the sample and the

reference, or even structural variants within the sample are presently not explicitly identified and phased by the algorithm. In order to resolve structural variants between the sample and the reference or even between haplotypes in the sample, we need to rely on the information in split reads. Here, we used a simple strategy to stitch together some of the haplotigs we obtain without using all of the information contained within split reads. Leveraging the full potential of split reads is a crucial next step to improve the contiguity of phased blocks. The main difficulty in using split reads appears to be that these alignments are significantly less reliable and will need to be processed differently to account for that.

We made the choice not to base our phased blocks on insertion or deletion information. This information can still be obtained in the phased blocks by generating a *de novo* assembly using nPhase's fastQ output for the relevant haplotig and could be integrated in future developments.

The rarity of raw accuracy numbers in the polyploid phasing literature derives from the observation that a single well-placed haplotype switching error has the potential to reduce the accuracy of a phased block by half. This led to the widespread adoption of using the SWitch Error Rate (SWER) or Vector Error Rate (VER) as the performance metric by which to compare polyploid phasing methods. This metric is only relevant to methods that accept the inevitability of switch errors, for which the raw measurement of the accuracy of predictions will not speak by itself. nPhase has achieved a very high level of accuracy (>95%) and contiguity (1.25 haplotigs per haplotype) across most of our validation tests (in particular where the heterozygosity rate is of 0.5% of higher). The principal interest of providing performance metrics is to make it easy to assess the trustworthiness of a method's results. For these reasons, we did not include the SWER in our performance metrics.

With the nPhase algorithm we believe that the problem of switch errors in polyploid phasing is largely solved, the next important hurdle for polyploid phasing is finding

an appropriate way to handle split reads to solve the remaining problems of contiguity and structural variants both within a sample and between the sample and the reference we align to. nPhase can still be used as a preprocessing step for any study of phased polyploid SVs and indels since that information is partially held within its output of fastQ files of phased reads.

Overall, nPhase provides, for the first time, an accurate and contiguous picture of polyploid genomes using only a reference genome and short and long reads. It paves the way for a better understanding of the origins of hybrid polyploid organisms, the true diversity of polyploid populations with potential hints on their origins and their relation to other diploid or haploid strains, and provides a clearer picture to investigate phenotypic effects tied to alleles which were previously inaccessible.

Methods

Total DNA extraction

Single colonies of each natural isolate were isolated by streaking on YPD media, containing ampicillin (50 µg/mL). Cells from one colony of each isolate were grown in 60 mL of YPD at 30°C for 24 hours. We extracted the total DNA of each isolate using the QIAGEN Genomic-tip 100/G kit, according to manufacturer's instructions.

Library preparation and sequencing

The kit NEBNext Ultra™ II DNA Library Prep Kit (Ipswich, USA) for Illumina (San Diego, USA) was used for short read library preparation of the GB54 *Brettanomyces bruxellensis* isolate. The sample was sequenced on a single lane of NextSeq (Illumina) at the European Molecular Laboratory (EMBL) in Heidelberg, Germany. The strategy of sequencing was 75 paired-end (75PE).

For long read sequencing, we used the EXP-NBD104 native barcoding kit (Oxford Nanopore) and the protocol provided by the manufacturer to barcode the total DNA of each of the isolates. The barcoded DNA was then quantified with a Qubit® 1.0 fluorometer (Thermo Fisher) and pooled together with an equal amount of DNA coming from each isolate. We then used the SQK-LSK109 ligation sequencing kit (Oxford Nanopore) to finish the library preparation. Finally, the library was loaded to a R9.3 flow cell for a 72 hour run.

Data pre-processing

The short reads are mapped to a reference genome using bwa[26] with the command bwa mem -M. We ran GATK[27] MarkDuplicates then variant called with GATK 4.0's HaplotypeCaller --ploidy 2 to identify heterozygous positions. Long reads are basecalled, adapter trimmed and demultiplexed by Guppy. They are then mapped to

the same reference using NGMLR[28]. We keep only primary alignments and split reads with the samtools[29] flag 260.

We determine the positions of heterozygous SNPs from the VCF obtained by GATK by looking for positions where AF=1.00 in the file. We reduced each long read to the set of variable positions it overlaps (Additional File 2: Fig S6a). To simplify later computational steps, we remove long reads that are subsets of other long reads.

nPhase is only capable of phasing SNPs if they are identified by the variant calling step. This is not necessarily always the case, and the accuracy metrics are based on the total number of SNPs identified in the polyploid sample by the variant calling step. However, unidentified SNPs will still exist in the reads, so if the algorithm performs a proper clustering of the reads the information will still be available and readily extracted by a closer view of the results.

Context coverage

Long reads are error-prone but it is important not to perform any form of error correction to ensure that the heterozygosity is not incorrectly flattened or mis-assigned. The nPhase pipeline works with raw long reads. In order to minimize the influence of these errors we consider that SNP coverage is a useful indicator of quality. We count the number of times each heterozygous SNP is present in a specific context in our dataset. We define context as being the closest flanking heterozygous SNPs (two heterozygous SNPs upstream and two heterozygous SNPs downstream). The context information will be used to better inform the nPhase algorithm and allow it to escape the situation where a sequencing error randomly converts a well-supported SNP to another SNP that is well-supported in another haplotype (Additional File 2: Fig S6b).

Output results

Once nPhase is done running it outputs several files:

(i) A fastQ file for each haplotig containing all of the reads that have been clustered together for this haplotig, this file can then be used with a *de novo* assembly or alignment tool for further analysis.

(ii) A tab separated file listing the consensus base for each heterozygous position contained within each haplotig. There are three columns: chromosome, position and consensus base. If two different bases are equally represented for a given position and equally well supported within the cluster they will both be represented in this file on separate lines. This file is sorted by position.

(iii) A plot representing the different haplotigs along the reference genome, similar to the one displayed in Figure 3 but lacking the haplotype color code since the ground truth is not known in a typical use case of nPhase.

nPhase parameter description

nPhase has a total of 4 parameters which can be adjusted to better fit the sample. These parameters are the following (Additional File 2: Fig S7):

S, the minimum fraction of similarity between two reads. When two reads overlap with each other we calculate their similarity by dividing the number of heterozygous SNPs they share by the number of heterozygous positions they both cover. If that fraction is smaller than the parameter S, then we will consider that these two reads cannot be part of the same haplotype. This parameter can be set to any fraction between 0 and 1, by default it is set at 0.01, or 1% similarity.

O, the minimum fraction of overlap between two reads. When two reads overlap with each other we can count the number of heterozygous positions they both cover. If they both cover more than 100 heterozygous positions, this parameter is ignored.

If they cover fewer than 100 heterozygous positions then we calculate the overlap by dividing the number of heterozygous positions the two reads have in common by the total number of heterozygous positions covered by the smaller of the two reads. In this case, smaller does not necessarily mean a shorter read, it means a read that covers fewer heterozygous positions. If this overlap is smaller than the parameter O, then we consider that these two reads do not overlap enough for us to conclusively determine if they're part of the same haplotype. This parameter can be set to any fraction between 0 and 1, by default it is set at 0.1, or 10% overlap.

L, the minimum number of reads supporting a haplotig. Once nPhase has clustered all of the reads into different haplotigs, the user may want to filter out all haplotigs that are supported by fewer than N reads. This parameter can be set to any integer $N \geq 0$, by default it is set at 0. If set to N, it will not output any cluster supported by fewer than N reads.

ID, the maximum amount of change when merging clusters. When nPhase considers merging two clusters of reads into one new cluster it must determine if these two clusters are similar enough to warrant merging them together or if they should remain unique clusters, representative of unique haplotypes. Since these are clusters, every heterozygous position is potentially covered multiple times, sometimes with different reads in the same cluster indicating conflicting bases for the same position. We can calculate the number of reads voting for each base in a given cluster and determine the "demographics" for that position. We can take this further and have an overview of every heterozygous position in the cluster and how well-supported each base is. The base that has the majority of support is considered to be the "true" base for that cluster. When we merge two clusters together, we potentially change these "demographics". These changes either further strengthen the position of the majority base for a given position, in which case there is no negative change in the cluster's "identity" or they weaken the majority base's position and cause a negative change to the cluster's "identity". When there are

negative changes to the cluster's "identity" we can calculate the amount of change that has occurred and if that amount is too high the clusters are not allowed to merge. This parameter can be set to any fraction between 0 and 1, by default it is set at 0.05, or a 5% ID change tolerance.

These parameters are set by default, though they can be modified if needed. The nPhase algorithm will use these parameters as limitations to determine which reads it is allowed to cluster together into haplotigs and which clusters of reads it can merge together into longer haplotigs. Ideally, only the ID parameter needs to be modified, keeping all other parameters very low and forcing the algorithm to merge clusters as aggressively as allowed by the ID parameter.

Identifying optimal parameters

In order to determine which parameters nPhase should use by default, it is important to understand how these parameters affect the results. Ideally, we will find that there is a set of parameters which is optimal for all possible combinations of ploidy and heterozygosity level, such a set would then become the default recommended parameters for nPhase. If no such set of parameters appears to exist, the next best case is to minimize the impact of as many of the available parameters as possible in order to reduce the parameter a user would need to explore when using nPhase to phase their dataset.

Through our tests, we find that there is a narrow range in the parameter space that results in the optimal performance of nPhase. Intuitively, the optimal strategy appears to be to set the minimum similarity and minimum overlap parameters down to a low value so that all of the reads in the dataset are allowed to merge into a cluster, and to only worry about finding an appropriate threshold for the ID change parameter. Since the ID change parameter controls how dissimilar two clusters need to be in order to be considered two different haplotypes, it is fitting for this parameter

alone to have the most pronounced impact on the quality of results. If set too low nPhase will consider small sequencing errors to be evidence of alternate haplotypes, and if set too high it will allow different haplotypes to merge into chimeric and wrong results.

To demonstrate this, we ran nPhase 125 times on 24 different samples of varying coverage, ploidy and number of heterozygous SNPs for a total of 3000 tests. These 125 tests represent every possible combination of the minimum similarity S, minimum overlap O, and maximum identity change ID parameters for the following values: 0.01, 0.05, 0.1, 0.15, 0.25.

The L parameter was set to 0 for these tests since it's intended for use to clean up results by removing small, lowly supported haplotigs and we wanted to determine how nPhase performs without throwing away any of the data.

We found that S, the minimum similarity parameter, had no influence on the results at these levels (Additional File 2: Fig S8a). O, the minimum overlap parameter, needs to be at least at 0.1 and seems to show very minor improvements in accuracy at higher levels (Additional File 2: Fig S8b). The ID parameter has the most influence on the accuracy of the results, with values of 0.05 and 0.1 yielding the best results (Additional File 2: Fig S8c).

We then looked at the effects of O and ID on the average number of haplotigs per chromosome per parent. We found that the number of haplotigs slightly increases with O (Additional File 2: Fig S9a), while ID has a strong effect on the contiguity of the results (Additional File 2: Fig S9b). A higher value for ID leads to a more contiguous assembly, though this comes at the cost of accuracy (Additional File 2: Fig S9c). We again find that values held between 0.05 and 0.1 provide good results. If we separate our tests by ploidy we can see that, as the ploidy increases the optimal choice for the ID parameter narrows down around 0.05 (Additional File 2: Fig S10).

Based on our tests, we find that the following set of parameters is the best adapted to handle any sample: S=0.01, O=0.1, L=0, ID=0.05. We use these as our default parameters.

Influence of coverage

We sought to establish the effects of coverage on the quality metrics of nPhase's predictions. To do so we performed our tests on a 10X per haplotype dataset and a 20X per haplotype dataset. We found that both accuracy and contiguity are improved by the higher coverage level of 20X per haplotype (Additional File 2: Fig S11). This effect is observed across ploidy and heterozygosity levels, though the accuracy effects are more pronounced for higher ploidy, lower heterozygosity level samples.

A low number of haplotigs per haplotype is not always a good sign of high contiguity as it can be compatible with a high rate of chimeric haplotigs. Therefore, we looked at the contiguity effects of coverage for our tests using default parameters, which we have previously determined output accurate results. Based on these tests we were able to confirm that the 20X dataset is more contiguous than the 10X dataset (Additional File 2: Fig S11b). We therefore used the 20X datasets as part of our default analysis.

Split read stitching step

Some reads align to two or more very distant sequences in the reference genome. These reads can represent a structural variation between the sample and the reference being mapped to. We split them into the different segments that align to the reference and refer to them to as split reads.

Split reads can be very misleading and trusting them blindly would result in chimeric haplotigs. We developed a simple pre-processing strategy to integrate part of the information contained by these split reads.

We run nPhase a first time to obtain our initial haplotigs. We expect some of the edges of haplotigs to correspond to structural variants such as inversions or large indels so we identify the SNPs at the edges of these clusters. These are the SNPs which we expect to be included in the split reads that can connect two haplotigs separated by a structural variant, so they are the most trustworthy SNPs in our split read dataset. We reduce each split read to only the heterozygous SNPs that overlap with these regions and re-run the nPhase algorithm with these reads included. Clusters are currently not allowed to combine reads from different reference chromosomes, so split reads can only be used to improve the contiguity of haplotigs on the same reference chromosome.

As described, nPhase does not exploit the information contained in split reads to the fullest extent, only attempting to improve contiguity by stitching together haplotigs on the same chromosome. Once there are only a few remaining haplotigs, further improving contiguity necessarily means stitching longer haplotigs together. This presents a very real danger of creating chimeric haplotigs that have very strong negative effects on accuracy. To validate the usefulness of these steps and this method of using the split read data we ran 3000 tests of nPhase both with split read information and 3000 tests without in order to determine the effects of our split read stitching strategy on both contiguity and accuracy. We found that the contiguity did significantly improve across all of our tests that included split read information, compared to those that did not (Additional File 2: Fig S12a). Encouragingly, when comparing the accuracy distributions of the two sets of tests they are virtually identical (Additional File 2: Fig S12b). The tests that used split reads were very slightly less accurate than their counterparts but much more contiguous, motivating our decision to integrate the use of split read information in nPhase.

Automated Cleaning

We established a three step automated cleaning procedure to quickly reduce noise and improve the contiguity of raw nPhase results. These steps have a negligible negative effect on accuracy in our *in silico* tests while greatly reducing the number of haplotigs per haplotype.

The first step of the automated cleaning process is the merging step. We first calculate, for every raw cluster output by nPhase, the proportion of bases that disagree with the consensus base. We call this the discordance level of the cluster, and it is equivalent to the summed minor allele frequencies represented in this cluster. We calculate the mean level of discordance across all clusters output by nPhase and we use this number as our stopping point. Our goal is to find pairs of clusters that merge together without increasing our risk of merging two different haplotypes into one. For each pair of clusters, we calculate the discordance level that we would obtain if we merged them together. If that discordance level is lower than the average discordance level calculated previously, then we can allow the merge to occur. If it is higher then we do not allow the merge. Once there are no pairs of clusters left that are allowed to merge, we end this step.

The second step is a filtering step. We sort all remaining clusters by the total coverage they represent, and we only remove clusters that account for the smallest 1% of coverage. This allows us to get rid of the small noisy clusters we have observed in our results.

The third and final step is the filling of gaps. We calculate, for each chromosome, the average coverage level of all the haplotigs (each haplotig counts as 1X, we are not looking at the coverage level of the reads contained within the clusters that define the haplotigs). We round this coverage level, and if it is rounded up to *n* (from 2.6 to 3 for example), then we identify the regions of the chromosome that are covered less than *n* times. For each such region we identify the most covered cluster, split its reads

in half, and redistribute them such that we have effectively filled the gap. This step presumes that the gap is due to a large region of the chromosome having the same haplotype in at least two copies of the genome (as evidenced by the coverage level being twice as high, for example).

We validated these steps by running them on our virtual polyploids and comparing the accuracy and contiguity results to the raw nPhase results.

Performance limits

With default parameters the nPhase algorithm took between 1 minute and nearly 5 hours of runtime on a single CPU (the nPhase algorithm has not been parallelized), and between 0.6 GB and 31.8 GB of memory (Additional File 1: Table S3). The runtime and memory usage are clearly tied to the ploidy and heterozygosity level. A higher ploidy and higher heterozygosity level translates to a significant increase in runtime and memory usage. Each diploid test, up to 1% heterozygosity, ran in less than an hour and ten minutes and used less than 8 GB of memory. Triploid tests took a minimum of 3.5 minutes of CPU time and 0.9 GB of memory to run for the 0.05% heterozygosity level example, and a maximum of three hours and ten minutes of CPU time and 19 GB of memory for the 1% heterozygosity level test. The tetraploid examples were the most resource intensive, using up a minimum of 6 minutes of CPU time and 1.25 GB of memory for the 0.05% heterozygosity level, and a maximum of four hours and fifty minutes of CPU time and 31.8 GB of memory to run. nPhase can output results in a reasonable time using moderate memory resources. If run on a particularly large genome in a time-sensitive context, nPhase could be applied to individual chromosomes in parallel. It's also reasonable to consider down-sampling the number of SNPs to a heterozygosity level of around 0.5% given the results obtained are comparable and run in less than half the time as the 1% heterozygosity level tests. All of the heterozygous SNPs would still be

present in the long reads and could be recovered from the fastQ files associated to the predicted haplotypes.

Assessing the quality of the *Brettanomyces bruxellensis* phasing

We used the nPhase pipeline to phase a triploid *Brettanomyces bruxellensis* strain. nPhase predicted that a number of regions had three haplotypes, and that others had only two. In order to verify the accuracy of these predictions we visualized our data in two complementary ways.

First we checked the coverage levels of the predicted haplotigs. We mapped the fastQ files generated by nPhase back to the same reference genome, then generated coverage plots using a 5kb window (the genome is 13 Mb long). In order to minimize the visual noise in Figure 7, we only displayed the longest haplotigs that account for 90% of all coverage.

Second we checked the allele frequency distribution within each cluster. We cross-referenced the file generated by nPhase in the VariantCalls/LongReads folder containing a list of reads and the identity of every base at each heterozygous position with the file generated in the Phased folder containing a list of the final haplotig clusters and the list of reads that comprise them. Using both files we were able to determine the allele frequency for each position within every haplotig cluster. We selected only the positions covered by at least 20 reads to generate Figure 8.

Phasing an autotetraploid strain of *Solanum tuberosum* with nPhase

We obtained whole genome Oxford nanopore and Illumina read data for an autotetraploid strain of *Solanum tuberosum* from the WhatsHap polyphase paper under accession number PRJEB39456. We used v6.1 of the DM1–3 516 R44 assembly as a reference, selecting the version without any repeat masking. We mapped all the reads to the full genome, but we then extracted all of the reads which

mapped to chromosome 2 to run the phasing algorithm on. Of the 2.4% of heterozygous positions observed in chromosome 2 according to variant calling on Illumina data, we only kept a randomly sampled 0.5% for the phasing in order to save calculation time.

Once we obtained raw nPhase results, we ran our automated cleaning steps in order to improve contiguity and reduce the complexity of our results.

Supplementary Material

Fig S1 - Graphical representations of nPhase output results for every genome analyzed. For each of the 16 chromosomes of *S. cerevisiae*, every predicted haplotig is on a different y axis.

2n dataset, 0.1% heterozygosity level

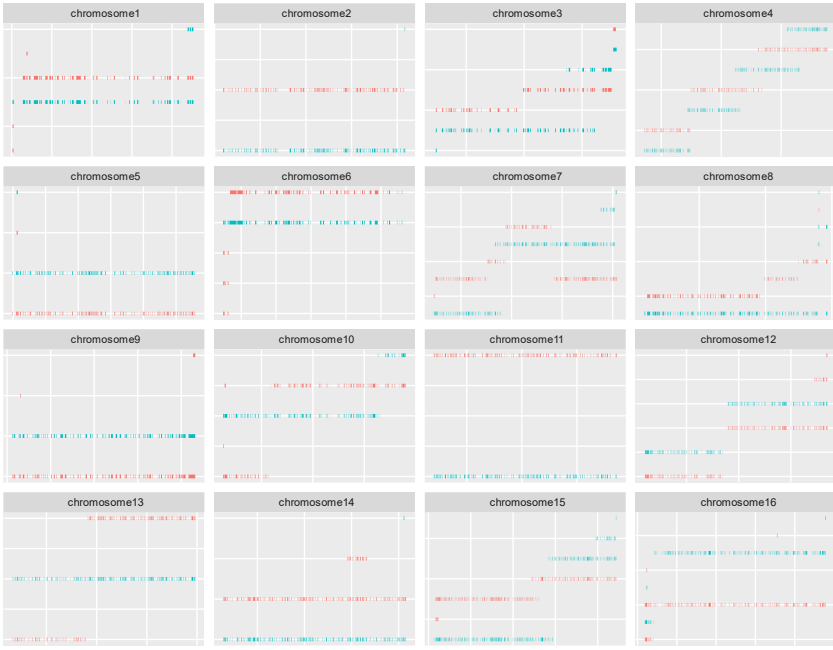

2n dataset, 0.5% heterozygosity level

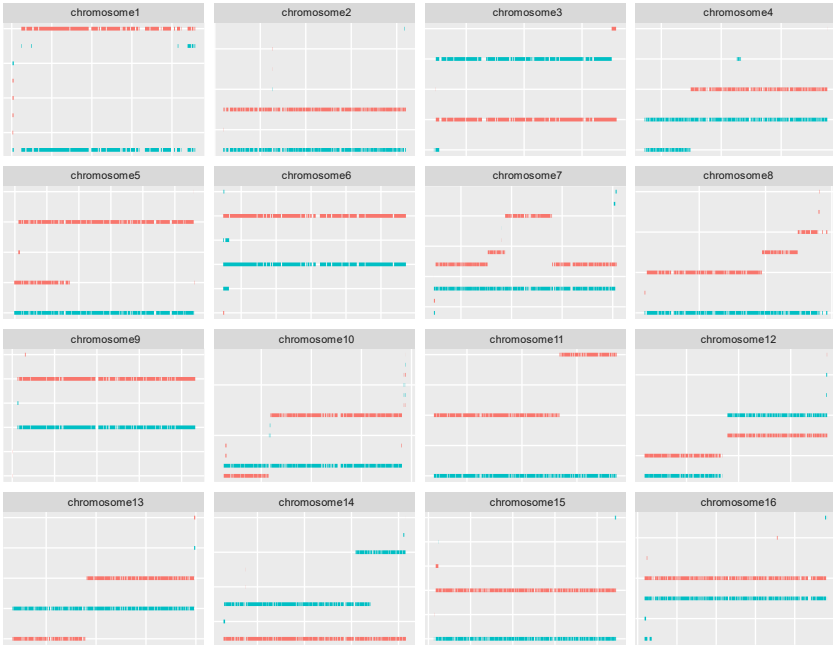

2n dataset, 1% heterozygosity level

3n dataset, 0.05% heterozygosity level

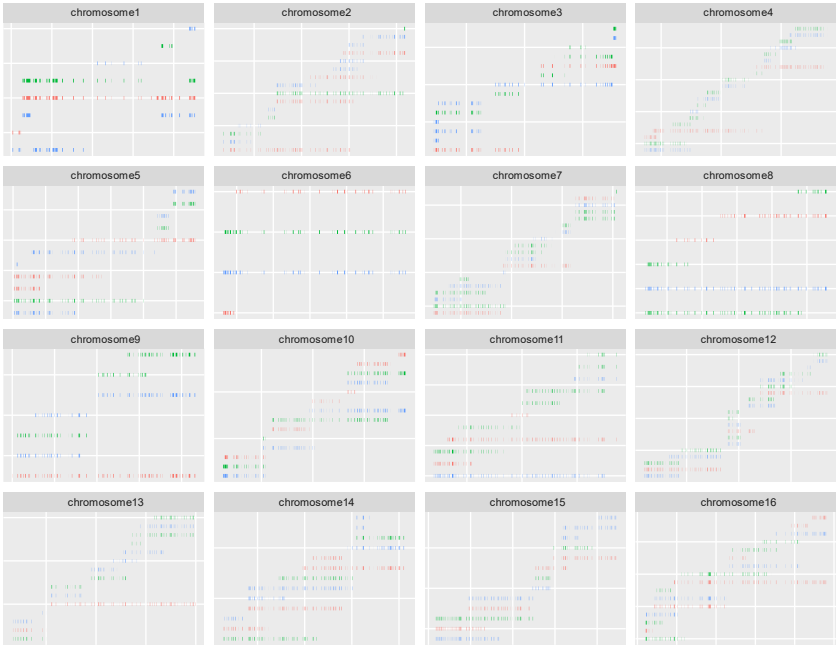

3n dataset, 0.1% heterozygosity level

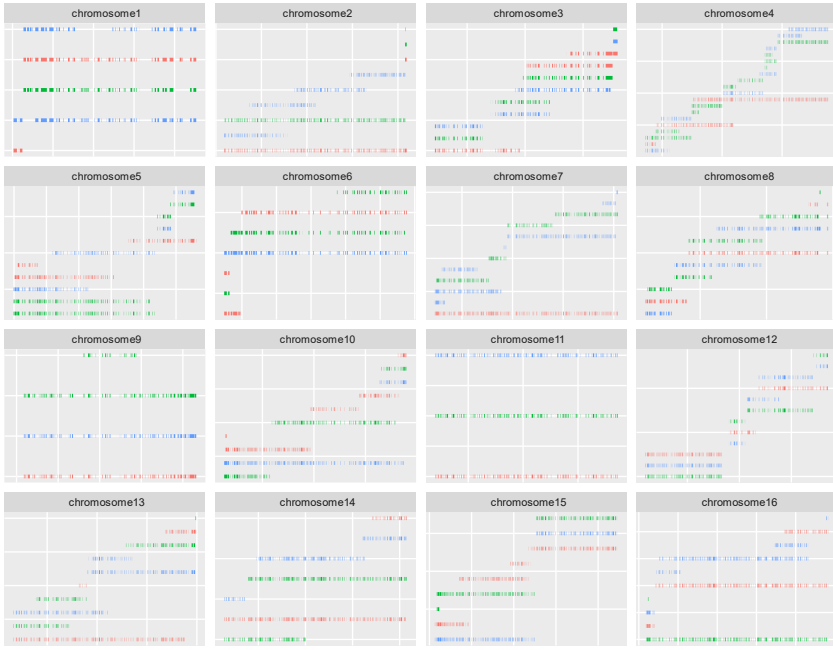

3n dataset, 0.5% heterozygosity level

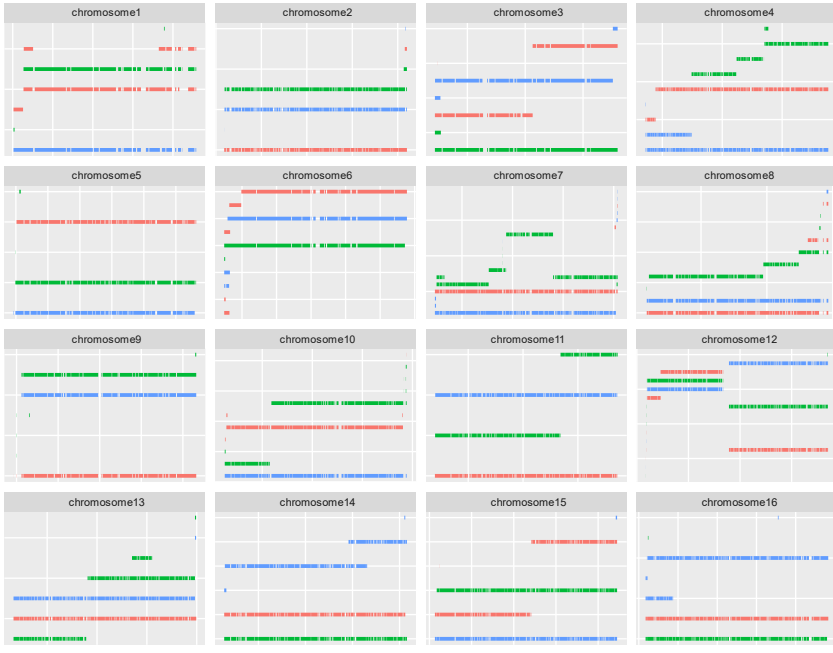

3n dataset, 1% heterozygosity level

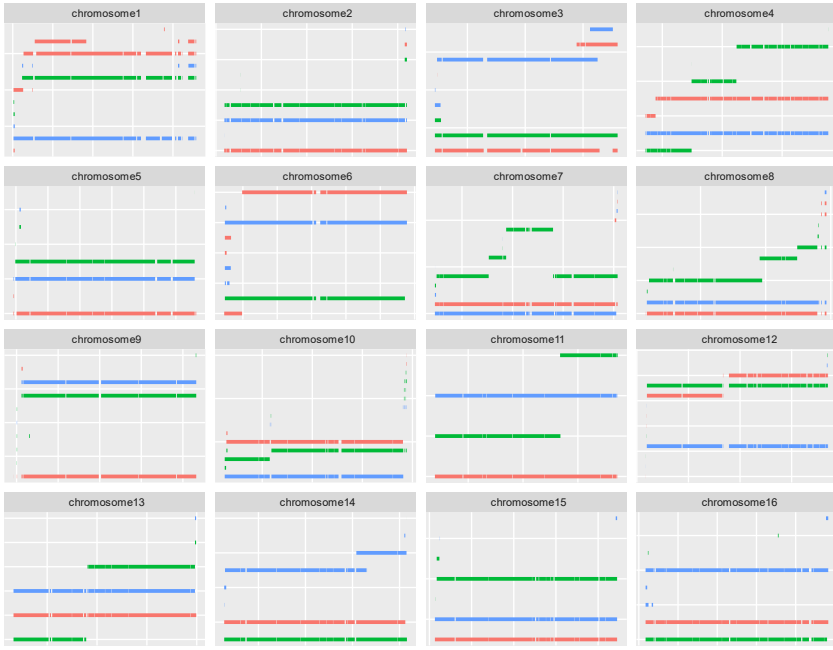

4n dataset, 0.05% heterozygosity level

4n dataset, 0.1% heterozygosity level

4n dataset, 0.5% heterozygosity level

4n dataset, 1% heterozygosity level

(a)

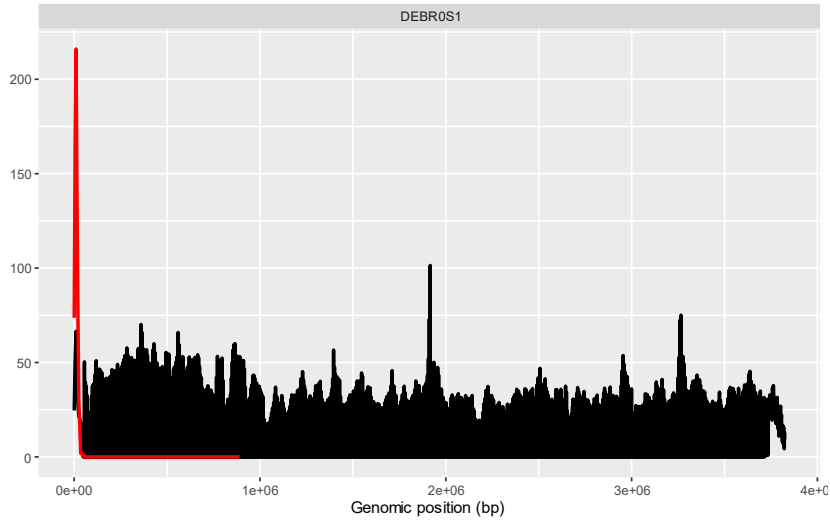

(b)

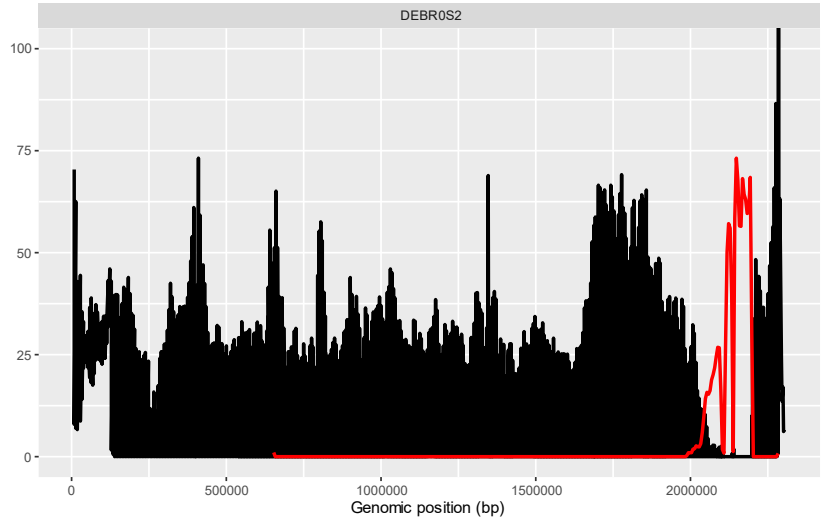

Fig S2 - Coverage of chimeric haplotigs. Through our allele frequency analysis, we identified two haplotigs which had clearly been badly phased by our method. We show in red the coverage of the chimeric haplotig and in black the coverage of other haplotigs in the chromosome.

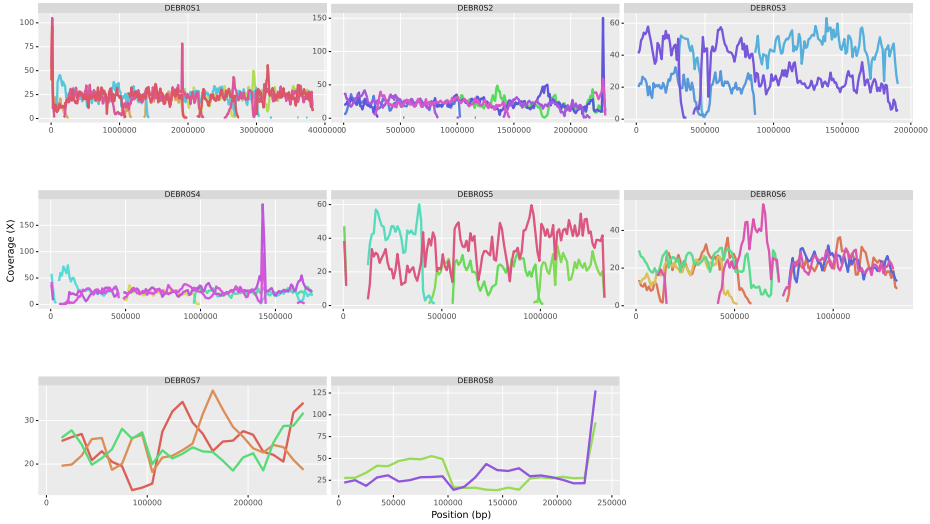

Fig S3 - Coverage level of GB54 haplotigs after automated cleaning. After automatically cleaning the raw output of nPhase, we observed much fewer haplotigs. We observe here the coverage level of these haplotigs and can confirm we kept the 2/3, 1/3 coverage distribution of chromosomes which were predicted to have only two haplotypes, and a 1/3, 1/3, 1/3 coverage distribution for chromosomes predicted to have three haplotypes.

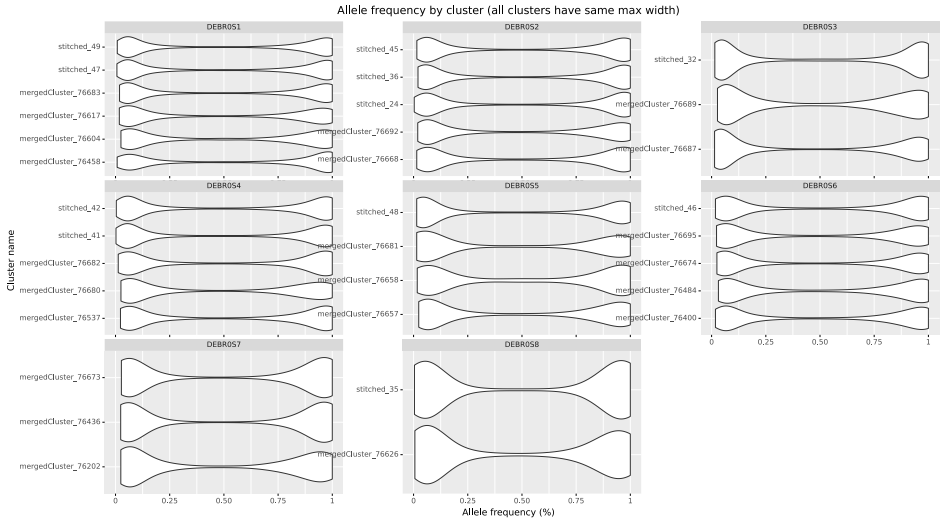

Fig S4 - Allele frequency distribution of GB54 haplotigs after automated cleaning. After automatically cleaning the raw output of nPhase, we observed much fewer haplotigs. We observe here the allele frequency distributions of these haplotigs and do not observe any significant enrichment in allele frequencies around 50%, supporting the hypothesis that these clusters each represent only one haplotype.

Fig S5 - Five longest genes in chromosome 2 of *Solanum tuberosum* phased by nPhase. The cleaned phasing results of the five longest genes of chromosome 2 of *Solanum* tuberosum are shown here in order from longest to shortest. On the left we have the phased heterozygous positions, with the haplotig as the Y axis and the position along the genome as the X axis. On the right we have the corresponding coverage of the haplotigs shown, with the Y axis displaying the coverage level (X). We note that we do not always obtain 4 unique haplotypes, though we can observe that, for example in the fifth gene, we have only three haplotigs but one is twice as covered as the other two, thereby account for four genomic copies. We also note that some predicted haplotigs are very lowly covered, and may not represent true haplotypes, such as the shorter cluster in the longest gene.

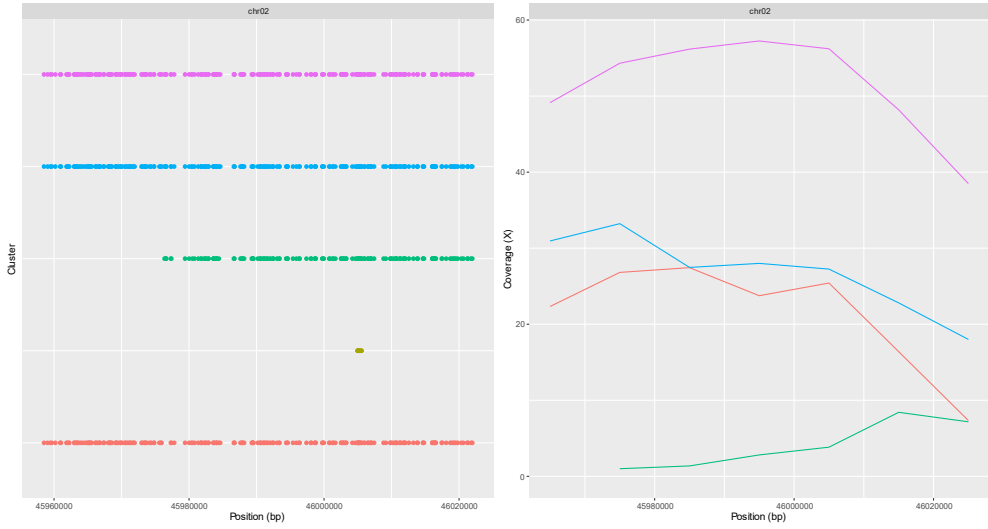

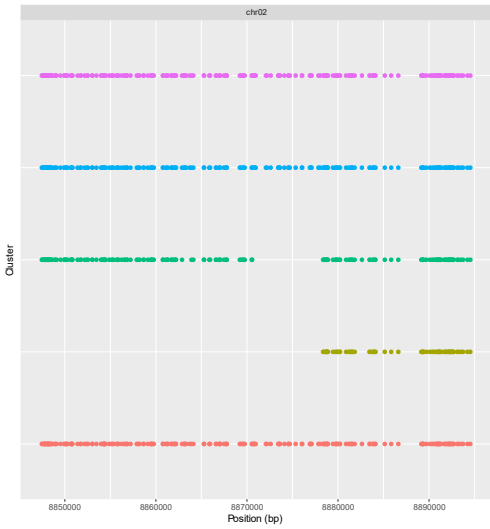
chr02
Cluster
8850000
8860000
8870000
8880000
8890000
Position (bp)

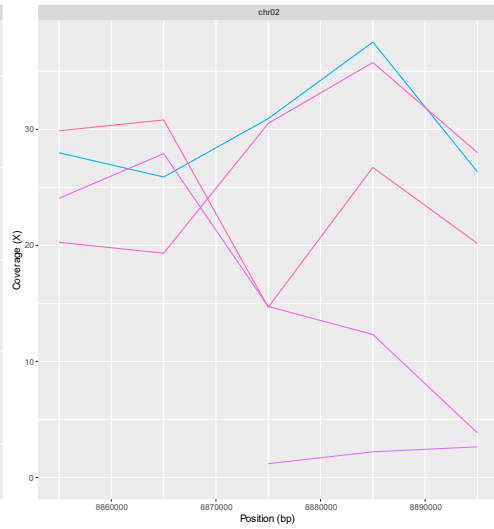
chr02
Coverage (X)
30
20
10
0
8860000
8870000
8880000
8890000
Position (bp)

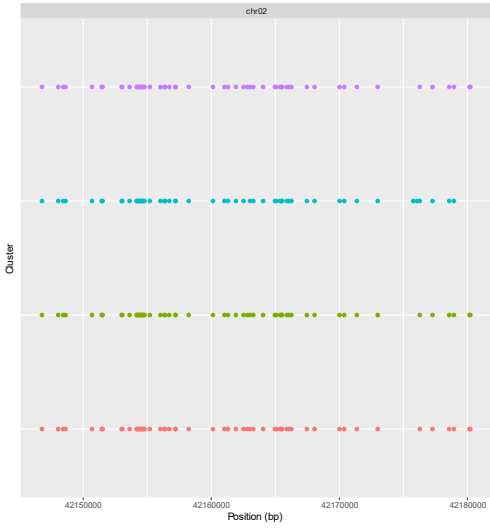
chr02
Cluster
42150000
42160000
42170000
42180000
Position (bp)

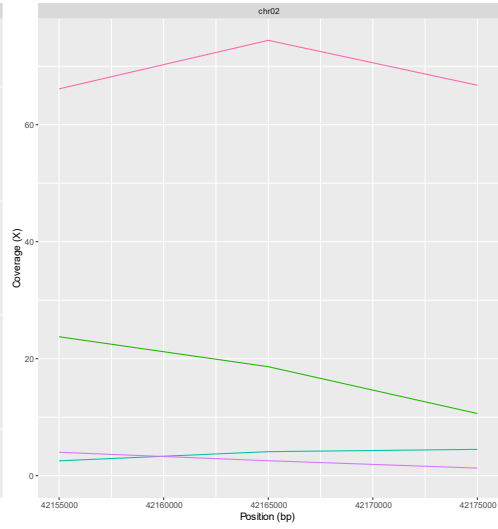
chr02
Coverage (X)
60
40
20
0
42155000
42160000
42165000
42170000
42175000
Position (bp)

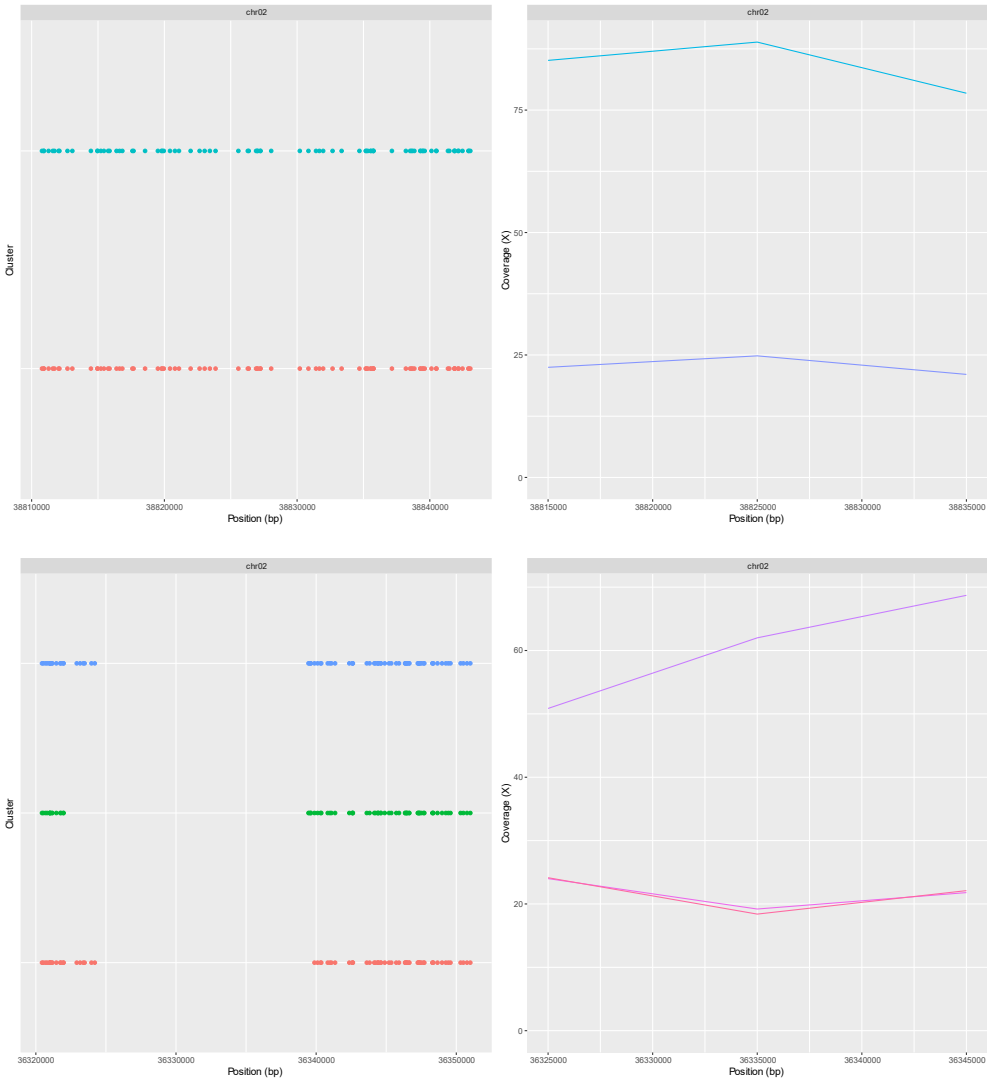
chr02
Cluster
38810000
38820000
38830000
38840000
Position (bp)
chr02
Coverage (X)
75
50
25
0
38815000
38820000
38825000
38830000
38835000
Position (bp)
chr02
Cluster
36320000
36330000
36340000
36350000
Position (bp)
chr02
Coverage (X)
60
40
20
0
36325000
36330000
36335000
36340000
36345000
Position (bp)

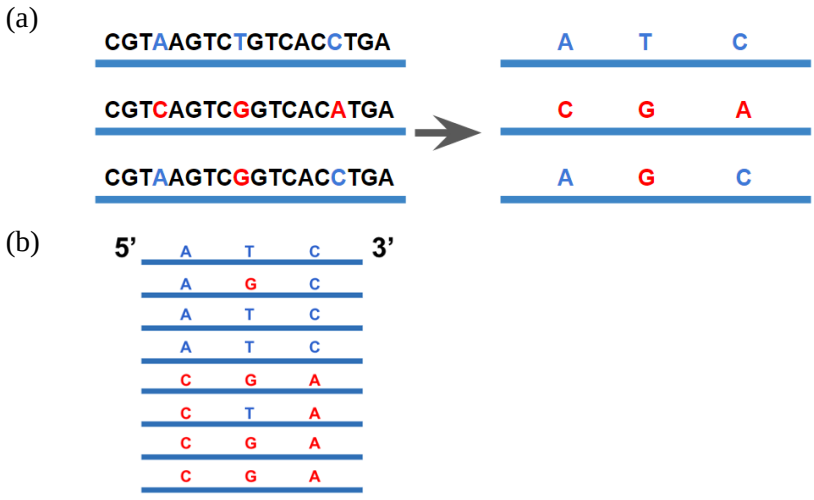

Fig S6 - Long read pre-processing steps. (**a**) Simplifying long reads**.** Each long read is reduced to the set of variable positions it overlaps. Hence the first sequence becomes ATC, the second becomes CGA and the third becomes AGC. We keep track of the position and chromosome on which each SNP is found. (**b**) Context coverage**.** **T** and **G** are equally covered without context, but with context we see that **AGC** and **CTA** are not as highly covered as **ATC** and **CGA**.

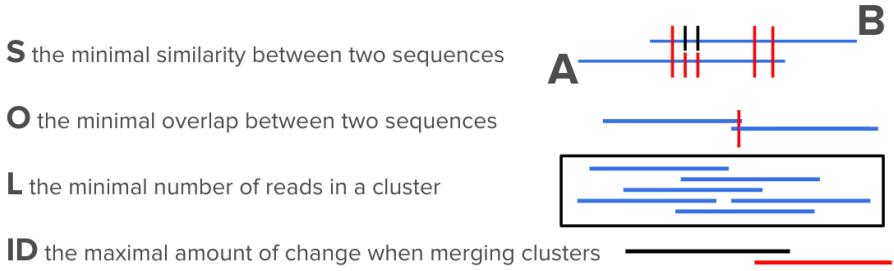

Fig S7 - nPhase parameters. The parameters S, O, L and ID are the only parameters that can be user-set in the nPhase algorithm.

(a)

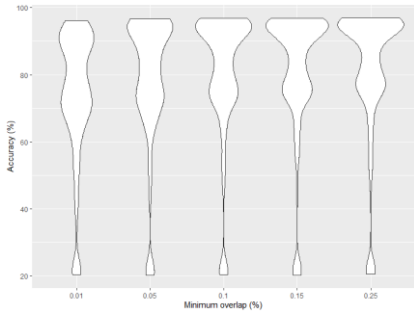

(b)

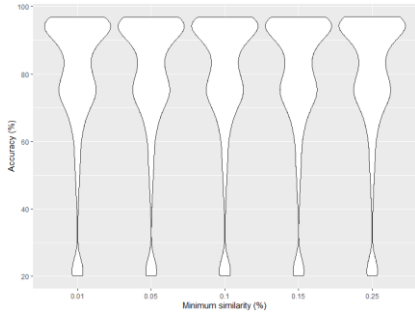

(c)

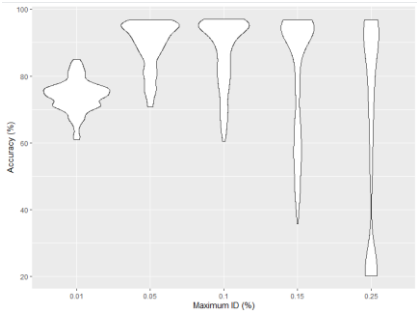

Fig S8 - Effects of parameters on prediction accuracy. We ran a total of 3000 tests using different nPhase parameters in order to evaluate their effects on the accuracy of the results. We found that the minimum overlap and minimum similarity parameters had minimal effects as shown by these violin plots of the accuracy for different values of each parameter, whereas the maximum ID parameter was much more influential. (**a**) The violin plots display an optimal performance for minimum overlap values of at least 0.1 , which corresponds to the presence of at least 10% of heterozygous SNPs in common between two clusters. This parameter only has an effect concerning clusters that have fewer than 100 heterozygous SNPs in common. (**b**) The violin plots for the different possible values attributed to the minimum similarity parameter are all the same, suggesting that at these values the parameter has no effect. (**c**) Based on these violin plots we found that, overall, the most reliable value for this parameter is 0.05, i.e. two clusters can only merge if it does not change their demographics by more than 5%. A value of 0.01 led to overall worse results, and higher values seem to split into two groups, with one that maintains a high accuracy and another that further falls as the ID parameter is set to higher and more lenient values.

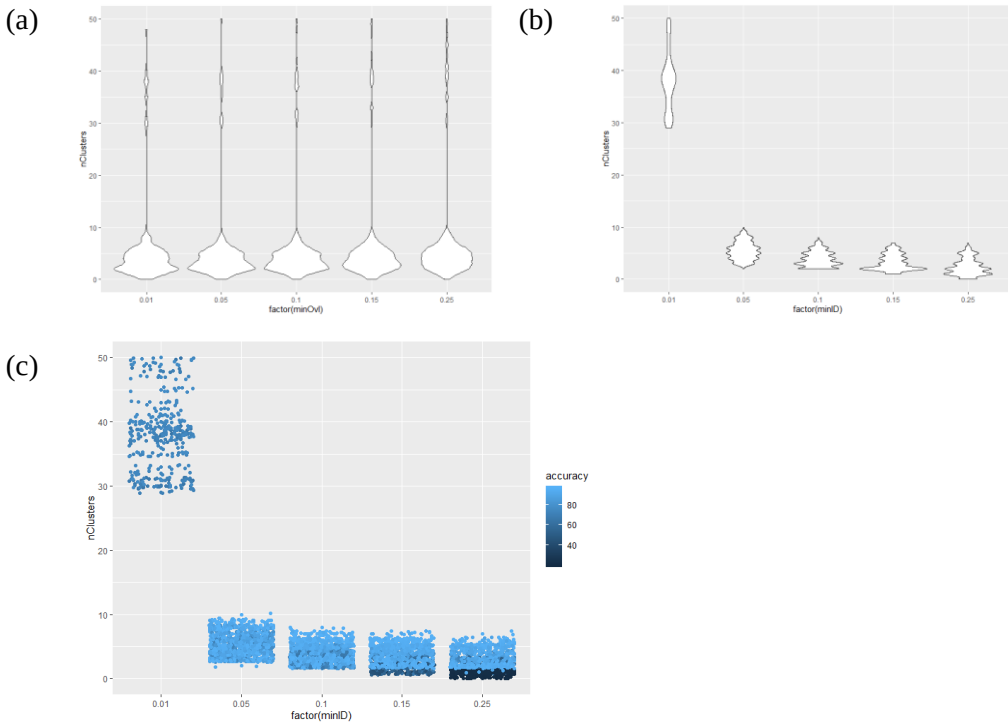

Fig S9 - Effects of parameters on contiguity. We ran a total of 3000 tests using different nPhase parameters in order to evaluate their effects on the contiguity of the results. We found that the minimum had a small effect, whereas the maximum ID parameter was much more influential. (**a**) These violin plots show how different values for the minimum overlap parameter affect the number of haplotigs. The Y axis displays the number of haplotigs per chromosome normalized by the number of haplotypes. We see a weak but predictable increase in the number of haplotigs as we increase this value and make it more stringent, though all parameter values shown here result in very comparable distributions. (**b**) These violin plots show how different values for the maximum ID parameter affect the number of haplotigs. The Y axis displays the number of haplotigs per chromosome normalized by the number of haplotypes. We observe here that the 0.01 value for this parameter, previously shown to lead to inaccurate results, also displays a significantly higher number of haplotigs than other values tested. As we increase the value of the ID parameter, rendering it less stringent, we also lower the number of haplotigs obtained. (**c**) This graph is similar to the one shown in (a), showing the normalized number of haplotigs per chromosome on the Y axis and the different values for the ID parameter in the X axis. We also color coded the individual tests, a lighter color denotes a more accurate result, whereas a darker color denotes a less accurate result. As the maximum ID parameter increases and becomes more lenient, we see that the most contiguous results are significantly less accurate.

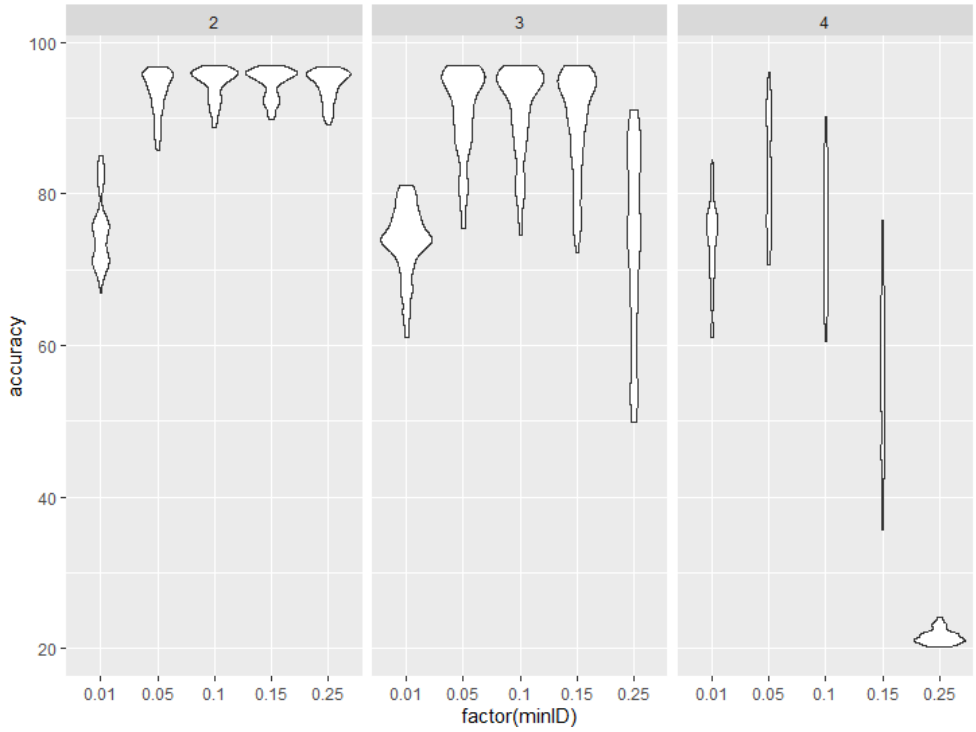

Fig S10 - Interaction between ploidy and ID parameter. This graph recalls the one in figure 1 in which we show how different values for the ID parameter lead to differences in accuracy. Her we display these same graphs separated by ploidy, showing that the three ploidies we tested (2n, 3n and 4n) are differently affected by the ID parameter value. As the ploidy increases, the range of values for the ID parameter that lead to accurate results narrows to around 0.05.

(a)

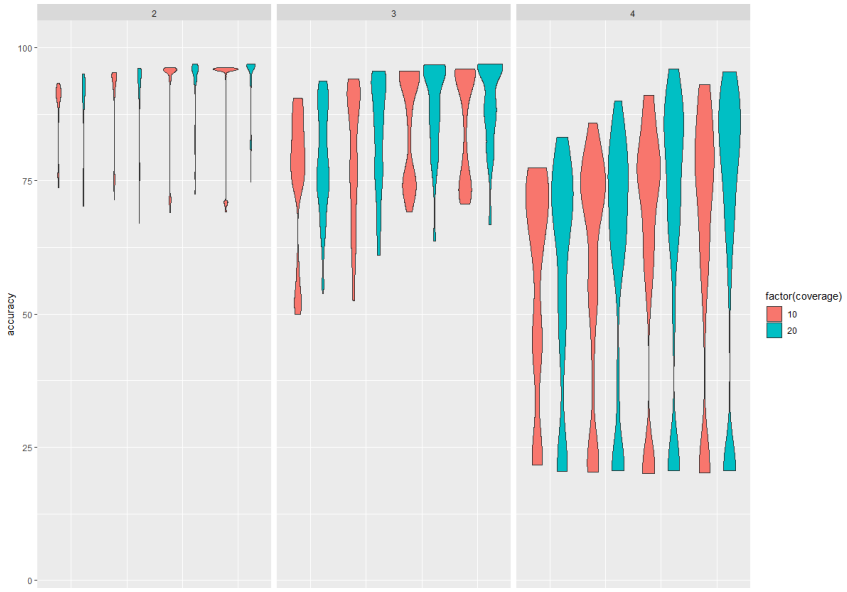
2
3
4
100
75
50
25
0
accuracy
factor(coverage)
10
20

(b)

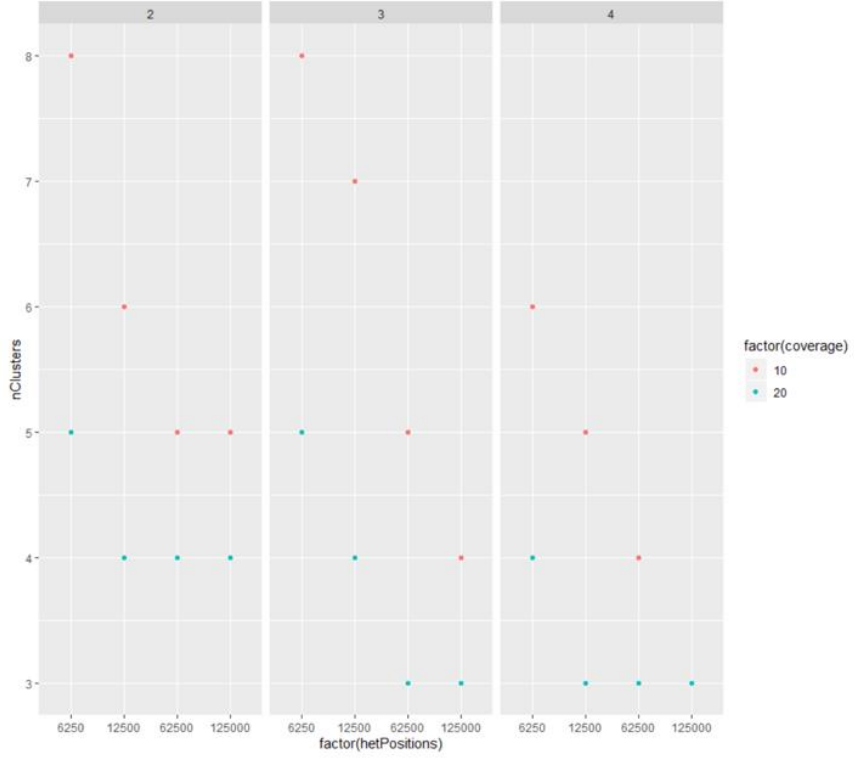
2
3
4
8
7
6
5
4
3
nClusters
6250
12500
62500
125000
factor(hetPositions)
factor(coverage)
10
20

Fig S11 - Effects of coverage on accuracy and contiguity. We compared the results of all 3000 tests performed on 10X datasets to the 3000 tests performed on their 20X counterparts and found that the 20X datasets had consistently more potential, reaching higher accuracy values and better contiguity across ploidy and heterozygosity levels. (a) Here we compare the accuracy distributions for tests of different ploidies and heterozygosity levels at the 10X and 20X coverage levels. We see that the 20X dataset is consistently able to reach higher accuracy levels, an effect which appears to be stronger when the ploidy is higher. (b) Since we are only interested in a high contiguity when it is coupled with a high accuracy, we will not look at a distribution of the number of haplotigs per haplotype across ploidy and heterozygosity levels at the 10X and 20X coverage levels, instead we're focusing on that contiguity metric for the tests using default parameters. We can clearly see a higher number of haplotigs per haplotype for the 10X dataset, with the gap between the 10X and 20X datasets deepening for lower heterozygosity level tests.

(a)

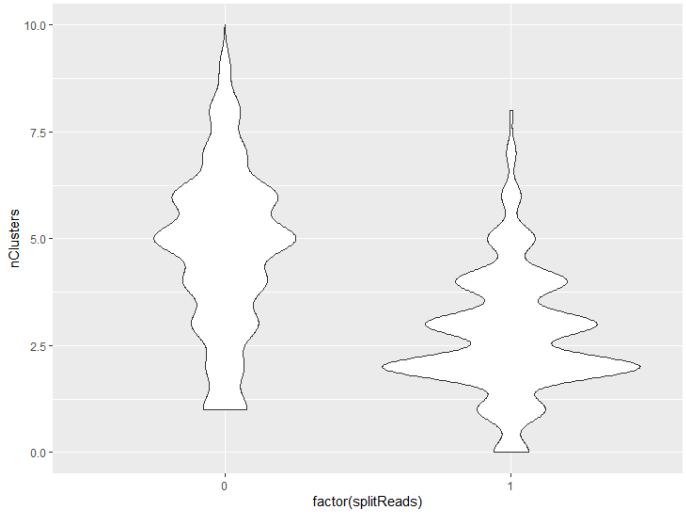

(b)

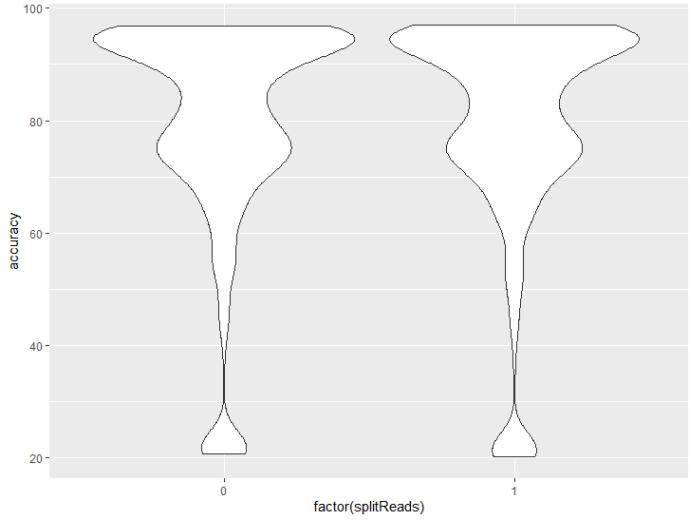

Fig S12 - Effects of including split reads. We ran 3000 tests on all parameter combinations without including split read information and 3000 tests with split read information. These violin plots show the impact of split read information on accuracy and contiguity. (**a**) Based on the violin plots, the results of tests that included split read information display significantly fewer haplotigs, indicative of a higher contiguity. (**b**) The accuracy of results for tests that included split reads is virtually identical to the accuracy of results without split reads.

Table S1: Origins and accessions of strains selected for validation testing

These strains, selected from the 1011 *S. cerevisiae* genome paper[1], were sequenced by MinION and their Illumina data was retrieved from the SRA data associated with the 1011 paper.

Isolate name	Standardized name	Isolation	Ecological origin	Geographical origin	Ploidy	Aneuploidy	Zygosity	Total number of SNPs	SRA Accession (Illumina reads)
VKM_Y-504:S	CCN	Berries of Viburnum Burejanum	Fruit	Russian Far East	2	Euploid	Homozygous	77912	ERR1308732
EM93_3	ACA	Rotting fig	Fruit	California, USA	1	Euploid	Homozygous	25551	ERR1309429
C-6	CRL	Wine conserved in amphora	Wine	Georgia	2	Euploid	Homozygous	38217	ERR1308952
UWOPS03-433.3	BMB	Nectar, bertam palm	Tree	Malaysia	2	Euploid	Homozygous	7822	ERR1308675

[1] Peter, J., De Chiara, M., Friedrich, A. *et al*. Genome evolution across 1,011 Saccharomyces cerevisiae isolates. Nature 556, 339–344 (2018). https://doi.org/10.1038/s41586-018-0030-5

Table S2: nPhase accuracy and contiguity metrics

Accuracy and contiguity metrics for nPhase run on all tests using optimal parameters

Sample Name	Ploidy	Number of heterozygous positions	Accuracy (%)	Error (%)	Missing (%)	Average number of clusters per chromosome per parent
CCN_BMB	2	125000	96.44	3.25	0.31	4
CCN_BMB	2	62500	93.57	4.51	1.92	4
CCN_BMB	2	12500	95.32	3.82	0.86	3
CCN_BMB	2	6250	90.34	6.69	2.97	4
CCN_ACA_BMB	3	125000	96.7	2.53	0.76	3
CCN_ACA_BMB	3	62500	95.02	3.26	1.72	3
CCN_ACA_BMB	3	12500	90.7	6.49	2.81	3
CCN_ACA_BMB	3	6250	87	9.69	3.31	4
CCN_ACA_BMB_CRL	4	125000	95.34	2.88	1.78	3
CCN_ACA_BMB_CRL	4	62500	93.72	4.07	2.21	3
CCN_ACA_BMB_CRL	4	12500	81.65	10.49	7.87	3
CCN_ACA_BMB_CRL	4	6250	78.62	12.91	8.46	4

Table S3: nPhase computational performance metrics
CPU time and memory resources used by the nPhase algorithm for different tests using optimal parameters

Construction	Ploidy	Heterozygosity level	CPU Used (HH:MM:SS)	CPU Used (Hours)	Memory used (GB)
CCN_BMB	2	0.05%	0:01:09	0.02	0.6
CCN_BMB	2	0.10%	0:04:11	0.07	1.34
CCN_BMB	2	0.50%	0:34:58	0.58	6.16
CCN_BMB	2	1%	1:07:27	1.12	7.91
CCN_ACA_BMB	3	0.05%	0:03:22	0.05	0.9
CCN_ACA_BMB	3	0.10%	0:13:38	0.22	2.04
CCN_ACA_BMB	3	0.50%	1:31:10	1.52	8.92
CCN_ACA_BMB	3	1%	3:08:38	3.14	18.9
CCN_ACA_BMB_CRL	4	0.05%	0:06:02	0.1	1.25
CCN_ACA_BMB_CRL	4	0.10%	0:27:28	0.45	2.83
CCN_ACA_BMB_CRL	4	0.50%	2:37:11	2.61	12.18
CCN_ACA_BMB_CRL	4	1%	4:50:15	4.83	31.78

Availability of data and materials

The nPhase algorithm and the nPhase pipeline are both available under the open source GNU General Public License v3.0 at:

https://github.com/OmarOakheart/nPhase[30]

Oxford Nanopore sequencing data is available under the study accession number PRJEB39456

Illumina short read data for the *Saccharomyces cerevisiae* strains are taken from the 1,011 yeast genomes project[24] and their SRA accessions are the following: ERR1308732[31], ERR1309429[31], ERR1308952[31], ERR1308675[31].

Illumina and Oxford Nanopore data for the *Brettanomyces bruxellensis* GB54 strain is available under the study accession number PRJEB40511.

Illumina and Oxford Nanopore data for the *Solanum tuberosum* strain used is available under the study accession number PRJNA587397[32].

References

1. Mahmoud, M. *et al.* Structural variant calling: the long and the short of it. *Genome Biol* **20**, (2019).
2. Sohn, J. & Nam, J.-W. The present and future of de novo whole-genome assembly. *Brief Bioinform* **19**, 23–40 (2018).
3. Kitzman, J. O. *et al.* Haplotype-resolved genome sequencing of a Gujarati Indian individual. *Nat. Biotechnol.* **29**, 59–63 (2011).
4. Roach, M. J. *et al.* Population sequencing reveals clonal diversity and ancestral inbreeding in the grapevine cultivar Chardonnay. *PLoS Genet.* **14**, e1007807 (2018).
5. Hamazaki, K. & Iwata, H. Haplotype-based genome wide association study using a novel SNP-set method : RAINBOW. *bioRxiv* 612028 (2019).
6. Sanjak, J. S., Long, A. D. & Thornton, K. R. A Model of Compound Heterozygous, Loss-of-Function Alleles Is Broadly Consistent with Observations from Complex-Disease GWAS Datasets. *PLOS Genetics* **13**, e1006573 (2017).
7. Benitez, J. A., Cheng, S. & Deng, Q. Revealing allele-specific gene expression by single-cell transcriptomics. *Int. J. Biochem. Cell Biol.* **90**, 155–160 (2017).
8. Wagner, N. D., He, L. & Hörandl, E. Relationships and genome evolution of polyploid Salix species revealed by RAD sequencing data. *bioRxiv* 864504 (2019).
9. Eriksson, J. S. *et al.* Allele phasing is critical to revealing a shared allopolyploid origin of Medicago arborea and M. strasseri (Fabaceae). *BMC Evol Biol* **18**, 9 (2018).
10. Yang, J. *et al.* Incomplete dominance of deleterious alleles contributes substantially to trait variation and heterosis in maize. *PLOS Genetics* **13**, e1007019 (2017).
11. Fay, J. C. *et al.* A polyploid admixed origin of beer yeasts derived from European and Asian wine populations. *PLOS Biology* **17**, e3000147 (2019).
12. Zhou, R.-N. & Hu, Z.-M. The Development of Chromosome Microdissection and Microcloning Technique and its Applications in Genomic Research. *Curr Genomics* **8**, 67–72 (2007).
13. Snyder, M. W., Adey, A., Kitzman, J. O. & Shendure, J. Haplotype-resolved genome sequencing: experimental methods and applications. *Nature Reviews Genetics* **16**, 344–358 (2015).
14. Zhang, X., Wu, R., Wang, Y., Yu, J. & Tang, H. Unzipping haplotypes in diploid and polyploid genomes. *Comput Struct Biotechnol J* **18**, 66–72 (2019).
15. Koren, S. *et al.* De novo assembly of haplotype-resolved genomes with trio binning. *Nat Biotechnol* (2018).
16. He, D., Saha, S., Finkers, R. & Parida, L. Efficient algorithms for polyploid haplotype phasing. *BMC Genomics* **19**, 110 (2018).
17. Browning, S. R. & Browning, B. L. Rapid and Accurate Haplotype Phasing and Missing-Data Inference for Whole-Genome Association Studies By Use of

Localized Haplotype Clustering. *The American Journal of Human Genetics* **81**, 1084–1097 (2007).
18. Patterson, M. *et al.* WhatsHap: Weighted Haplotype Assembly for Future-Generation Sequencing Reads. *Journal of Computational Biology* **22**, 498–509 (2015).
19. Chin, C.-S. *et al.* Phased diploid genome assembly with single-molecule real-time sequencing. *Nat. Methods* **13**, 1050–1054 (2016).
20. Schrinner, S.D., Mari, R.S., Ebler, J., Rautiainen, M., Seillier, L., Reimer, J.J., Usadel, B., Marschall, T., and Klau, G.W. (2020). Haplotype threading: accurate polyploid phasing from long reads. Genome Biology *21*, 252.
21. Xie, M., Wu, Q., Wang, J. & Jiang, T. H-PoP and H-PoPG: heuristic partitioning algorithms for single individual haplotyping of polyploids. *Bioinformatics* **32**, 3735–3744 (2016).
22. Motazedi, E., Finkers, R., Maliepaard, C. & de Ridder, D. Exploiting next-generation sequencing to solve the haplotyping puzzle in polyploids: a simulation study. *Brief. Bioinformatics* **19**, 387–403 (2018).
23. Moeinzadeh, M.-H. *et al.* Ranbow: A fast and accurate method for polyploid haplotype reconstruction. *PLOS Computational Biology* **16**, e1007843 (2020).
24. Peter, J. *et al.* Genome evolution across 1,011 *Saccharomyces cerevisiae* isolates. *Nature* **556**, 339–344 (2018).
25. Pham, G. M. *et al.* Construction of a chromosome-scale long-read reference genome assembly for potato. *GigaScience* **9**, (2020).
26. Li, H. & Durbin, R. Fast and accurate short read alignment with Burrows–Wheeler transform. *Bioinformatics* **25**, 1754–1760 (2009).
27. Van der Auwera, G. A. *et al.* From FastQ data to high confidence variant calls: the Genome Analysis Toolkit best practices pipeline. *Curr Protoc Bioinformatics* **43**, 11.10.1-11.10.33 (2013).
28. Sedlazeck, F. J. *et al.* Accurate detection of complex structural variations using single-molecule sequencing. *Nature Methods* **15**, 461–468 (2018).
29. Li, H. *et al.* The Sequence Alignment/Map format and SAMtools. *Bioinformatics* **25**, 2078–2079 (2009).
30. Abou Saada, O. *et al.* nPhase. Github. https://github.com/OmarOakheart/nPhase 10.5281/zenodo.4626656 (2021).
31. Peter, J. *et al.* Genome evolution across 1,011 *Saccharomyces cerevisiae* isolates. Subset of four *Saccharomyces cerevisiae* short read sequencing files (ERR1308732, ERR1309429, ERR1308952, ERR1308675). NCBI BioProject. https://www.ncbi.nlm.nih.gov/bioproject/PRJEB13017 (2018).
32. Seillier, L. *et al.* Solanum tuberosum genome sequencing. Oxford Nanopore and Illumina Data. NCBI BioProject. https://www.ncbi.nlm.nih.gov/bioproject/PRJNA587397 (2019).

Chapter II – Phased polyploid genomes provide deeper insights into the different evolutionary trajectories of the *Saccharomyces cerevisiae* beer yeasts

Abstract

Yeasts and in particular *Saccharomyces cerevisiae* have been used for brewing beer for thousands of years. Population genomic surveys highlighted that beer yeasts are polyphyletic with the emergence of different domesticated subpopulations characterized by high genetic diversity and ploidy level. However, the different origins of these subpopulations are still unclear as reconstruction of polyploid genomes is required. To have a better insight into the differential evolutionary trajectories, we sequenced the genomes of 35 *Saccharomyces cerevisiae* isolates coming from different beer-brewing clades using a long-read sequencing strategy. By phasing the genomes and using a windowed approach, we identified three main beer subpopulations based on allelic content (European dominant, Asian dominant, and African beer). They were derived from different admixtures between populations and are characterized by distinctive genomic patterns. By comparing the fully phased genes, the most diverse in our dataset are enriched for functions relevant to the brewing environment such as carbon metabolism, oxidoreduction and cell wall organization activity. Finally, independent domestication, evolution and adaptation events across subpopulations were also highlighted by investigating specific genes previously linked to the brewing process. Altogether, our analysis based on phased polyploid genomes has led to a new insight into the contrasting evolutionary history of beer isolates.

Background

The yeast *Saccharomyces cerevisiae* is a well-studied model organism with a long history of human domestication due to its fermentation ability. It has unknowingly been leveraged by early humans to ferment foods and has been domesticated in various ecological niches. Notably, there is evidence of the domestication of *S. cerevisiae* in the cheese, wine, bread, sake, cacao, coffee bean and beer industries [1–8]. The domestication process began long before Louis Pasteur's identification of the brewer's yeast *S. cerevisiae* and Emil Hansen's isolation of pure cultures for use in the Carlsberg brewery in 1883[9], likely accelerated through backslopping: the practice of collecting a part of the fermentation product which still contains living cells and using it to inoculate the next fermentation, thereby improving its efficiency. Backslopping is a driver of domestication which can accelerate the adaptation of yeasts to human preferences[10]. It is particularly illustrated through the widespread inactivation of two genes, *PAD1* and *FDC1*, whose product 4-Vinyl Guaiacol (4VG) produces an undesirable off-flavor in beer[4]. This adaptation is a striking example of domestication given that the yeasts used in beer brewing are a polyphyletic group, with some strains more closely related to European wine or sake isolates than to other beer strains[5]. Two main industrial beer subpopulations[4], named Beer 1 and Beer 2, were identified[4,5,8]. The Beer 1 group, mostly composed of polyploid ale strains, has been shown to derive from admixture between close relatives of European and Asian wine strains[8].

Industrialized beer brewing strains have had to adapt only to the brewing environment, which typically has high alcohol concentrations, high osmotic pressure and low pH. Adaptations can mean remodeling the cell wall[11,12], degrading protein aggregates[13] caused by ethanol denaturation, controlling pH by vacuolar acidification[14], controlling osmotic pressure via the inactivation of aquaporins[5].

However the life cycle of these industrialized strains also shields them from the wild, in which they have reduced fitness[4]. African beers, however, did not undergo the same industrialization processes. Similar to wine yeasts which cannot grow in grape must year-round and must maintain their ability to survive in vineyard environments, African beer yeasts must remain adapted to their local environments as traditional African fermentation methods offer far less stable environments than industrial methods. Traditional African beer-making methods rely on the presence of native *S. cerevisiae* (and other yeasts) on the brewing ingredients. The fermentation processes for African beers typically start with an initial spontaneous fermentation usually driven by lactic acid bacteria (LAB)[15,16]. An alcoholic fermentation follows, either spontaneously[16,17], by explicit back-slopping methods[18], or indirect back-slopping methods such as the reuse of tools or containers that allow well-adapted microorganisms from successful previous fermentations to drive the fermentation process[15,16]. The life cycle of African beer yeasts contrasts with the industrialized, highly specialized beer brewing yeasts grown as pure cultures[19,20]. Backslopping, a known driver of domestication[4], has certainly shaped the genomes of industrialized beer brewing yeasts, and very plausibly that of African beer yeasts as well, though less extensively. Comparing the two groups may reveal genes relevant to adaptations to brewing environments and uncover convergent evolution processes.

In this study we further characterize the origins of modern industrial ale-brewing strains, finding that the previously described Beer 1 and Beer 2 groups differ in the proportion of European/Asian alleles, renaming the groups to Asian dominant and European dominant, and show that the alleles of the African beer strains are closest to European wine and French dairy. We also phase the genomes of all 35 strains and determined the genetic distances between strains and between groups, finding that the mean divergence between African beer strains and modern ale-brewing strains is under 0.35%. Using phased genome data, we calculated the intra-strain divergence and found that the Asian dominant strains have the highest mean intra-strain

divergence at 0.21%, followed closely by European dominant and African beer strains at 0.20% and 0.16% divergence, respectively. By comparing the fully phased genes in our dataset, we determined the level of divergence between gene haplotypes and identified those that reach the highest level of pairwise diversity. We detected genes of interest such as *ROQ1*, required for denatured protein degradation, *YPS* genes, involved in cell wall remodeling and several *IMA* genes, which are involved in isomaltose utilisation[13,12,21]. Finally, we also investigated genes that present evidence of domestication (*MAL11*, *PAD1*, *FDC1*, *GAL2*, *ADH2* and *SFA1*) and provided evidence of convergent evolution in the loss of function of the *FDC1* gene in African beer and Asian dominant groups. We also found that the *ADH2* and *SFA1* genes appear to be undergoing the same human selection as the *PAD1* and *FDC1* genes to suit human preferences of beer flavor by reducing fusel alcohol formation[22], a source of off-flavors in beer when present in high concentrations[23].

Results

Selection of beer isolates, sequencing and genome phasing

To dissect the genetic diversity and genomic architecture of beer-brewing yeasts, we selected 35 strains from diverse clades based either on their known use in fermenting beers or on their high genetic similarity to beer-brewing strains (Supplementary Table S1). Beer-brewing strains of *S. cerevisiae* are polyphyletic, forming at least three distinct clades: one clade of African beer strains and two clades of modern ale strains named Beer 1 and Beer 2, which are believed to have different origins[4]. It has been shown that Beer 1 strains are a polyploid admixture of European and Asian wine strains[8]. The African beer and Beer 1 groups typically have higher ploidies, between 3n and 5n for the African beer group and typically 4n for the Beer 1 group. Strains from the Beer 2 group are not typically polyploid. Adding to the diversity and complexity of the population of beer yeasts, some isolates used in breweries have genomes consistent with European wine strains, and others have genomes that cluster with other strains of mixed origins. For our study, we selected 8 African beer strains, 16 Beer 1 strains, and 5 Beer 2 strains. We also selected 6 beer-brewing strains from outside of these three clades, including 2 European wine strains isolated from breweries, 3 strains from the Mixed origin clade and 1 from the Mosaic Region 1 clade[6].

Given the polyploid nature of a majority of the strains selected, we sequenced all 35 strains with Oxford Nanopore long reads in order to phase their genomes. We used publicly available short read data for nearly all of the strains selected[6,8] (Supplementary Table S2). Only strain YMD4285 was sequenced by Illumina for this study. We aimed to obtain at least 80X theoretical coverage with our long reads for most strains in order to obtain accurate and contiguous phasing results. We reached the target of 80X coverage in 26 out of 35 strains, with the remaining 9

ranging from 14.4X theoretical coverage to 77.6X (Supplementary Table S2). Whenever possible, we downsampled our long-read data to 80X of the best reads, obtaining mean read lengths up to 37.7 kb (mean 21.2 kb) and mean read quality scores up to 15.9 (mean 14.4). In cases where we could not downsample to 80X, we used all of the sequencing reads for our analyses. The Illumina short read data we used ranges from 144X to 368X (mean 281X), with mean quality scores ranging from 28.8 to 34.8 (mean 32.9).

We recently developed a phasing algorithm and pipeline, nPhase[24], which phases a genome using short reads, long reads and a reference sequence. The short reads are mapped to the reference sequence and variant called, which serves as a list of high-confidence SNP positions. The long reads are also mapped to the same reference sequence and iteratively clustered together according to the similarity between reads at these previously defined SNP positions. The iterative clustering ends when only distinct clusters remain, which are different from each other. nPhase is a ploidy agnostic phasing method, it makes no attempt to coerce the results to a given or estimated ploidy, it only detects when the existing clusters should not be merged together. nPhase also provides a cleaning algorithm which removes small clusters and attempts to improve the contiguity of phasing results and reduce noise at little cost to accuracy by applying simple heuristics[24]. We used our dataset of accurate short reads and phase-informative long reads to phase all 35 strains using nPhase[24] and used the nPhase cleaning algorithm to improve the contiguity of our results (Supplementary Figures S1 and S2).

Without a ground truth, we cannot assess the accuracy of our phasing results, however we can assess their contiguity. We use the L90 metric which we define here as the minimal number of haplotigs to cover at least 90% of all reads, and the L90 per chromosome, which is simply the L90 divided by the number of chromosomes times the ploidy. The L90 per chromosome for the phasing of a triploid strain of *S.*

cerevisiae is therefore the L90 divided by 3*16. If the value is close to 1, we have close to a contiguous phasing, if it is much higher, the phasing is increasingly fragmented, and if much lower, increasingly likely not to have correctly distinguished between haplotypes. We report in our raw results an L90 per chromosome that ranges from 1 to 2.6 (with an outlier at 4.3 due to low long read coverage), with a mean L90 per chromosome of 1.6 (Supplementary Table S3). After applying the cleaning pipeline available for nPhase we improved the contiguity, reducing the range of L90 per chromosome to between 0.8 and 2.3 (with the same outlier at 3.6). The cleaning step also substantially reduced the average total number of haplotigs from 198 to 100.

Aneuploidy information for most strains was obtained from Peter *et al.* 2018. For the 7 remaining strains aneuploidy was determined based on allele frequency plots (Supplementary Figure S3). The phasing correctly predicted a number of suspected and known aneuploidies such as the 6 different chromosome losses of the tetraploid strain BBG and the extra copy of chromosome 3 in the diploid strain CPB, though not all, with aneuploidies in strains such as CFM remaining unclear after phasing, potentially due to lower read lengths (Supplementary Table S4).

Inter-strain divergence reveals three groups of strains

The standard way of estimating the divergence between two strains uses unphased genomes to calculate their distance based on allelic differences. Using this method, we obtain a mean inter-strain divergence of 0.58% across all strains, with a maximum divergence of 1% when comparing AVS and YMD4285 (Supplementary Table S5). This method is not well adapted to polyploidy, as it does not take into account the complexity of these genomes, leading to inaccurate representations of the differences in genetic content between strains. It does not, for example, reveal if two strains may have a subgenome or haplotype in common. There are two main barriers to obtaining this type of information: it requires access to phased haplotypes,

and the question is complicated by recombination events and Loss of Heterozygosity (LOH) events. Using our dataset of phased haplotypes, we propose a more accurate metric of inter-strain divergence for polyploids that takes their haplotypes into account. For each pair of strains, A and B for example, we calculate the distance between 10 kb regions of all haplotypes, keeping only the match with the lowest divergence. We allow a 10 kb region of a haplotype in strain B to match with several 10 kb regions in strain A's haplotypes. This allows us to estimate divergence based on the allelic content of each strain (Figure 1). Using this method, we updated our mean inter-strain genetic divergence numbers from 0.58% to 0.36% and the highest level of inter-strain divergence drops to 0.56%, obtained when comparing strains ANL and YMD4285 (Supplementary Table S6). The previously most divergent strains AVS and YMD4285 are 0.55% divergent using this calculation method.

This inter-strain divergence based on haplotypes reveals three main groups of strains in our dataset defined by a higher similarity to each other than to other strains: the African beer group (s8 strains), the Beer 2 group to which we can add two European wine strains and the Mosaic Region 1 strains (8 strains), and finally the Beer 1 group to which we can add the 3 mixed origin strains (19 strains). Two of the three mixed origin strains, CFP and CFN, could arguably be assigned to either group though the third, BDL, resembles the Beer 1 group more closely. Despite the polyphyletic nature of the population, we can reorganize the strains in our dataset into three major groups.

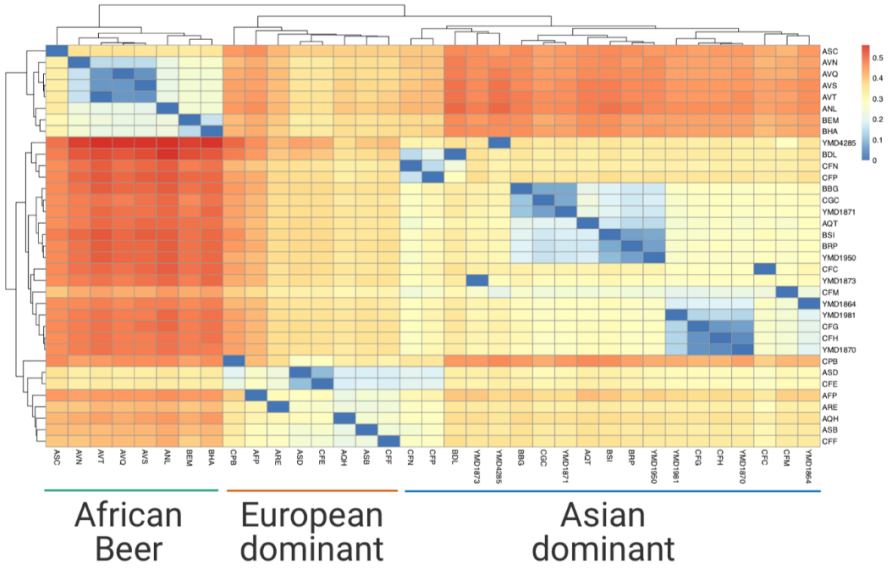

Figure 1 - Inter-strain divergence levels using 10 kb haplotype windows
This heatmap represents the mean inter-strain divergence between each pair of the 35 strains used in this study. The values were calculated by comparing all 10 kb haplotype windows between strains and range from 0% divergence for strains compared to themselves to 0.56% between the most different strains. Hierarchical clustering was performed and suggests the strains can be divided into three main groups, with strains CFP and CFN attributed to the right-most group despite an ambiguous profile suggesting close similarity to the group at the center of the heatmap.

Three main groups differ by proportions and origin of allele content

In order to elucidate the difference between the Beer 1 and Beer 2 groups, and to start characterizing the allele content of African beers, we used a windowed approach to compare each strain's haplotypes to their closest match in the clades described in the 1,011 *S. cerevisiae* genomes survey[6]. For each of these previously described clades, we identified the polymorphisms that are specific to it according to the sequencing data of the population[6]. Then, for each strain, we divided each of its haplotypes into 20 kb windows and identified all of the clade-specific

polymorphisms in the window. We assigned each 20 kb region of each haplotype to the clade which had the highest signal. We did not use all of the clades described in the 1,011 yeast genomes survey[6]. We excluded clades known to derive from older populations, such as Brazilian bioethanol, which shares a close relationship with European wine[25], and West African cocoa which is an admixture of European wine, Asian fermentation and North American oak[3]. We also excluded clades for which our dataset had too few strains to contribute much data, this excludes clades such as Ecuadorean and Far East Russian for which we have fewer than 10 strains each. Finally, we obviously excluded the clades we are trying to study. We did not include the beer clades we are investigating as well as the mosaic or mixed origin clades. We therefore limited our allele content comparison to the six following clades: European wine (for which we merged all wine clades), North American oak, Asian fermentation (we merged sake and Asian fermentation), French dairy, African palm wine and the French Guiana subpopulations.

Through this windowed approach we can confirm the reorganization of our strains into three groups based on their similar origin profiles (Figure 2A). British and Belgian/German ales and mixed origin strains (i.e., the Beer 1 group) have the same origin profile (Supplementary Figure S4), mainly composed of European wine and Asian fermentation alleles, with the largest signal of Asian fermentation markers out of all three groups, forming the Asian dominant group. This method of estimating the origin of the allele content of these strains corroborates the admixed origin previously described[8] (Supplemental Figure S5). African beers have a large signal of European wine alleles, and differ from the other two groups by their higher signal of French dairy alleles. The final group, containing all of the mosaic beers and two European wine strains (i.e., the Beer 2 group), is characterized by its high level of European wine and low but still significant Asian fermentation signal, and resembles the profile of Asian dominant strains where the balance between Asian fermentation and European wine alleles has been inverted.

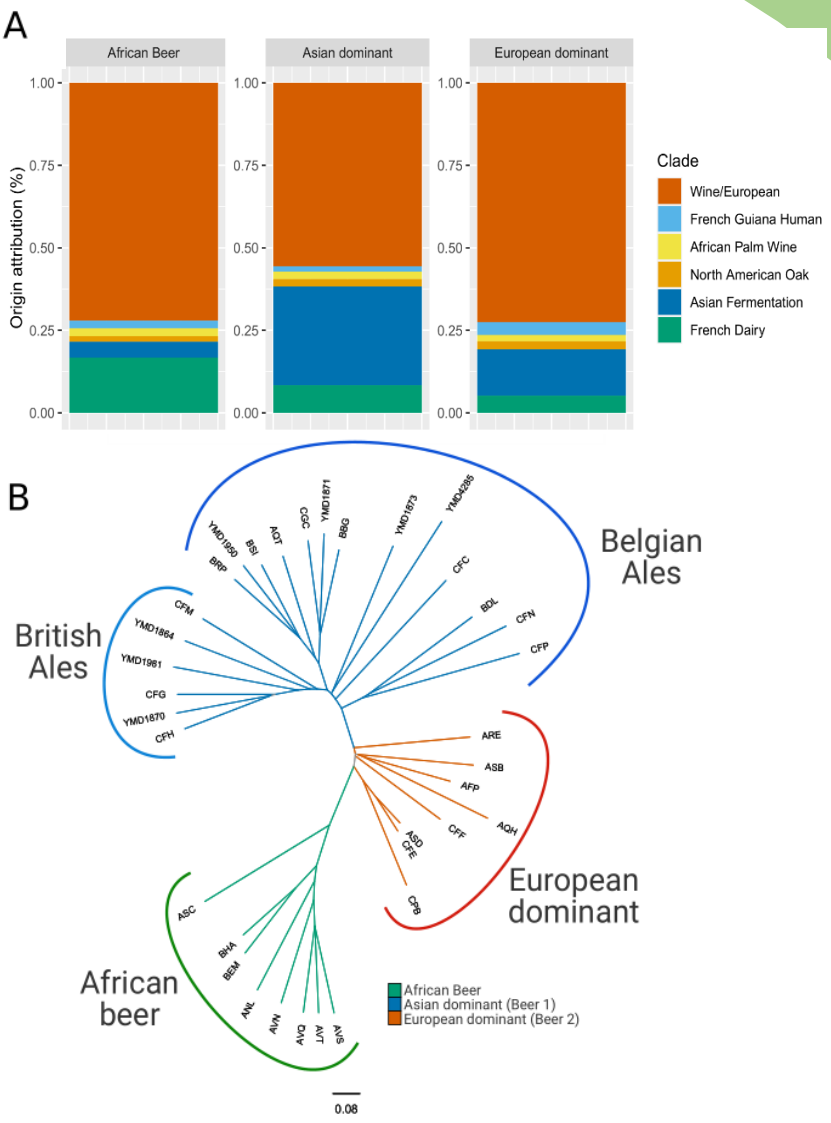

Figure 2 - Three groups of beer strains differ by allelic origin
We phased the genomes of all 35 strains and for each haplotype we identified SNPs that are markers of known clades such as French Dairy or European Wine. We then attributed each haplotype to the clade with the highest signal, in blocks of 20 kb, finding 3 different profiles: African Beer, European dominant, and Asian dominant. A In this figure we show that all three groups have a high European Wine signal. Strains attributed to the African Beer also have a high French Dairy signal, while the difference between the Asian dominant and European dominant strains is their level of Asian Fermentation alleles. The Asian dominant group has a higher signal for Asian Fermentation then the European dominant group. B This dendrogram, generated from a SNP matrix using Illumina data, has been colored to represent the origin group attributed to each strain, and shows the European dominant group is between the Asian dominant and African beer groups.

We then generated a dendrogram based on all genomic SNPs to place the strains in relation to each other (Figure 2B). We find that the European dominant group is in between the African beer group and the Asian dominant group. Consistent with previous reports we also distinguish two ale groups that correspond to geographical origin, British ales (CFG, CFH, YMD1864, YMD1870 and YMD1981) which cluster together on one branch of the dendrogram along with USA strain CFM, and Belgian/German ales which cluster on the adjacent branch (BRP, YMD1950, BSI, AQT and YMD1871), alongside CGC, a USA strain isolated from an olive fly and BBG, a strain isolated from the water of the Morava river in Slovakia. The Belgian/German strains YMD1873, CFC and CFF are also found along the main branch of the Asian dominant group on this dendrogram, alongside YMD4285, BDL and CFN. We will hereafter refer to the 5 British strains and the USA strain that clusters with them as the British ales, and all other Asian dominant strains as the Belgian/German Ales.

We can modify the previously described method of calculating inter-strain divergence to calculate intra-strain divergence, comparing haplotypes within a strain to each other. Using this method, we found that overall African beers are the least self-diverse, with 0.16% mean self-divergence, likely owing to their highly polyploid nature. The most self-diverse are Asian dominant strains with 0.21% self-divergence and the European dominant strains are not far behind with 0.20% mean self-divergence. The Asian dominant and European dominant strains reach slightly higher self-divergence levels than African beers. The lower extremes of African beer strains are likely due to its higher ploidy, and therefore higher likelihood for each 10 kb region not to be too distant from one of the several other haplotypes.

Intra-strain divergence of African beers varies from 0.12% in the least self-divergent strain to 0.17% in the most self-divergent strain. In European dominant it varies from 0.05% to 0.27%. The two least self-divergent European dominant strains are at

0.05% and 0.09%, with the third least at a much higher 0.21%. In Asian dominant strains the self-divergence levels vary from 0.09% to 0.35%, though the minimum and maximum are slightly extreme outliers, with the next least self-divergent and next most self-divergent strains at 0.16% and 0.28%, respectively (Supplementary Table S7).

Genes with highest divergence enriched in functions relevant to brewing environment

We phased the genomes of 35 strains of *S. cerevisiae* associated with beer brewing, selected from a diverse set of isolates comprising three main clades and three associated clades. All of these isolates have had to adapt to the brewing environment or are very closely genetically related to beer brewing strains. The main groups have adapted independently to the brewing environment, and we expect that a survey of the genes with the most diverse haplotypes in our dataset will reveal genes which have undergone rapid deterioration due to being redundant, pseudogenes which are under no selective pressure, and genes of interest for adaptation to the brewing environment which were put under selective pressure.

To investigate this, we extracted all of the fully phased genes in our dataset and calculated the pairwise divergence between all phased copies (Figure 3). Phased African beer genes are on average 0.23% divergent from each other, slightly lower than the average 0.24% of European dominant strains and 0.32% of Asian dominant strains. In all groups, a minority of genes show significant divergence levels within their group, reaching over 4% divergence levels. When all phased copies are compared to each other, the average divergence level rises to 0.36%, and a few more gene alleles are found with a pairwise divergence level over 4%, pointing to genes which have very divergent haplotypes across different groups but not necessarily within them.

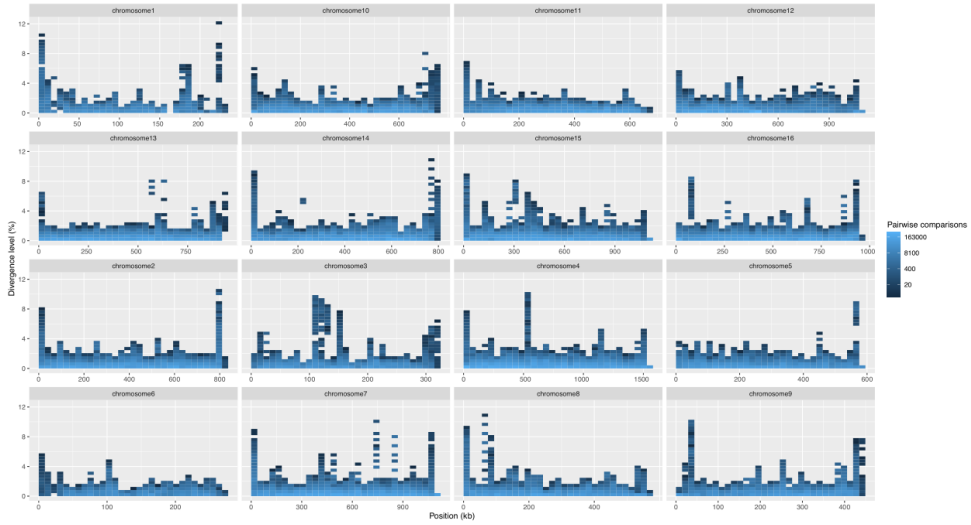

Figure 3 - Distribution of divergence levels for fully phased genes using all strains
We identified all of the fully phased genes in our dataset and compared them to each other in a pairwise manner, then plotted the divergence levels and their distribution along the genome as a heatmap. The y axis represents the divergence level as a percentage, and the x axis is the position along the chromosome. The color represents the number of supporting pairwise comparisons, implemented here using a log scale for visual clarity. We observe that more highly divergent genes tend to be less frequent and rarely reach above 4% divergence. The subtelomeric appear to have more highly divergent genes, however we also observe many other regions within the chromosomes with high levels of divergence so they are not limited to the telomeres.

We then identified the 144 genes which have a pairwise divergence level of 4% or higher (Supplementary Table S8). Of these 144 genes, 57 had a verified annotation, 54 were uncharacterized and the remaining 33 were dubious genes. We subjected our list of 57 verified genes to a GO term finder analysis to identify enrichment in processes, function and cellular component localization. We found that our list of 57 highly divergent genes is enriched for carbon metabolic processes for various carbon sources (e.g., maltose, galactose, sucrose), galactose transport and cell wall organization. These genes are also enriched in cell wall structural constituents, dehydrogenase activity and transmembrane sugar transporters and enriched in genes

whose products localize to the cell periphery, cell wall and vacuoles (Supplementary Table S9).

Notable genes of interest include *ROQ1*, which directs the SHRED pathway to degrade proteins denatured by high alcohol concentrations[10], *YPS* genes involved in cell wall remodeling to resist oxidative and osmotic stress[12,26], and *CTT1*, a catalase expressed in response to oxidative stress[27]. Deeper investigation into the genes highlighted and the diverse haplotypes observed and their potential functional consequences would be of significant interest for further understanding the changes required for wild yeast to adapt to the brewing environment, examples of convergent and/or divergent evolutionary trajectories.

Industrial domestication markers: the *MAL11*, *PAD1* and *FDC1* genes

Our dataset corroborates and expands on previously reported findings for the *MAL11*, *PAD1* and *FDC1* genes[4]. These genes, highlighted in Gallone *et al.* 2016, are evidence of the domestication of beer yeasts to suit industrial needs and human flavor preferences. We describe here our observations for these genes in our dataset (Supplementary Table S10).

Maltose utilization is an industrially relevant phenotype in beer brewing, due to the high maltose content obtained after malting grain. Maltose is typically the main fermentable carbon source in wort, the brewing solution to undergo fermentation. The *MAL11* gene codes for an effective maltose transporter, shown to be present in the Asian dominant strains but inactivated in the European dominant group by frameshift-inducing indels[4]. There are two reported frameshift-inducing indels, 1772CA➞C and 1175A➞AT. We report that *MAL11* is present and intact in half of the African beer strains and absent in the others (Supplemental Figure S6). In our dataset, *MAL11* suffered inactivation by homozygous frameshift-inducing indels in all European dominant strains, except for ARE, which displays both known

frameshift-inducing indels heterozygously, and ASD which is intact. Similarly, all of the Belgian ale strains have at least a heterozygous indel except for BBG which is intact. Finally, we find that none of the British ale strains in our dataset display any frameshift-inducing indels.

The *PAD1* and *FDC1* genes code for proteins which participate in the formation of 4VG, a compound that yields a potent off-flavor in beer[4], and their function therefore leads to an inferior product by human standards. The inactivation of these genes has previously been identified as evidence of human domestication of beer yeasts due to their effects on beer flavor[4]. In our dataset we make corroborating observations. In fact, the *PAD1* gene presents no frameshift-inducing indels, and appears intact in all European dominant and African Beer strains, however it is fully inactivated by nonsense mutations in all haplotypes of British ale strains and in over half of the Belgian ale strains. In addition, the *FDC1* gene appears to be intact in European dominant strains. In Asian dominant strains it is inactivated through the frameshift-inducing indel 495T➞TA. This indel is present homozygously in all haplotypes of British ale strains, and in the majority of Belgian ale strains. Only three Belgian ale strains appear to have intact copies of *FDC1*. African beers also present a frameshift-inducing indel which inactivates their copy of *FDC1*, however it's a different indel than the one observed in Asian dominant strains. In African beers we have the indel 35AC➞A which is present at least heterozygously in half of the strains in our dataset. The other African beer strains have an intact copy of *FDC1*.

Overall, we find that the African beer strains bear previously reported markers of domestication through the presence of *MAL11* and the independent inactivating indel observed in *FDC1* for some of the strains. In contrast, the industrialized Beer 2 strains do not present the industrially favorable genotypes, consistent with the previously reported observation that they exhibit fewer signs of domestication than

Beer 1 strains[4]. These results further support the notion that traditional beer brewing methods such as those used in African beer brewing are a driver of domestication.

Phasing diverse populations reveals distinct evolutionary trajectories

To leverage the diversity of our dataset and explore some of the highly divergent genes described above, we calculated, for each full gene haplotype, the mean distance to all of the haplotypes of each group. This gave us insight into the conservation and divergence of genes among all strains. We describe our observations for *GAL2, ADH2* and an associated gene, *SFA1* (Supplementary Table S10).

Haplotypes of the *GAL2* gene are highly diverse in African beer strains

The fermentation environment of African Beer strains is known to typically harbor a variety of Lactic Acid Bacteria (LAB) strains which proliferate during the initial spontaneous fermentation. French dairy strains, which also share their environment with LAB strains, compete with them by consuming all of the available sugars faster. However, the typical *GAL* pathway in *S. cerevisiae* is repressed by the presence of glucose, a more efficient sugar which the yeast will metabolize first. Once the environment is depleted of glucose, growth stalls as the yeast cells switch to galactose utilization. Adaptations to the *GAL* pathway which address this competitive disadvantage have been shown in French dairy strains. The high affinity glucose/galactose transporter *GAL2* has been shown not to undergo glucose repression and allow for the simultaneous assimilation of both glucose and galactose. These modifications permit them to avoid the shift that occurs when switching from glucose to galactose, thereby improving their competitive fitness[28,29].

In our dataset, copies of *GAL2* are very similar to each other and present no frameshifts in European dominant and Asian dominant strains, however, we observe a spectrum of copies of *GAL2* in African strains ranging from 1.56% genetic

divergence to the closest non-African versions of *GAL2* to 4.05% genetic divergence with the most distant versions (Supplementary Table S11, Supplementary figure S7). Four African beer strains harbor haplotypes at divergence levels with non-African strains between 1.5% and 4.0% (Supplementary figure S8). The remaining four African beer strains all have a narrower range of haplotype divergence, around 2.5% for one and over 3.0% for the other three. The four strains with the higher range of diversity between their own haplotypes are the same ones harboring frameshift-inducing indels, homozygously for one strain and heterozygously for the other three (Supplementary Table S10).

This diversity in copies and the inactivation of certain alleles of *GAL2* exclusively found in African beer strains may represent adaptations to sharing their environment with LAB strains which would parallel but remain independent with the adaptations observed in French dairy strains.

The *ADH2* and *SFA1* genes present further evidence of domestication in Asian dominant and European dominant strains

At high concentrations, fusel alcohols are considered a potent off-flavor in beer. *S. cerevisiae* has six genes involved in the final step of the Ehrlich pathway for fusel alcohol formation[22], the *ADH* alcohol dehydrogenase family *ADH1* to *ADH5*, and *SFA1*, an alcohol dehydrogenase and glutathione-dependent formaldehyde dehydrogenase. *ADH1*, *ADH3*, *ADH4* and *ADH5* convert acetaldehyde to ethanol, however *ADH2* performs the inverse reaction and oxidizes ethanol into acetaldehyde.

In our dataset, all African beer strains and British ale strains have at least one intact copy of *ADH2*. Half of the European dominant strains and the majority of Belgian ale strains suffer from homozygous deletions. And 9 Belgian ale strains and one European dominant strain all present a homozygous deletion of approximately 26 bp

in the middle of *ADH2*, which is much larger in strains CFN and YMD1873 (Figure 4). A different deletion of about 25 bp at the beginning of the gene is observed in three European dominant strains. The *ADH2* gene has previously been a target for inactivation for industrial beer brewing purposes owing to its role in forming the off-flavors acetaldehyde and diacetyl and reducing alcohol content[30]. These observed deletions and high genetic diversity may reflect evidence of domestication.

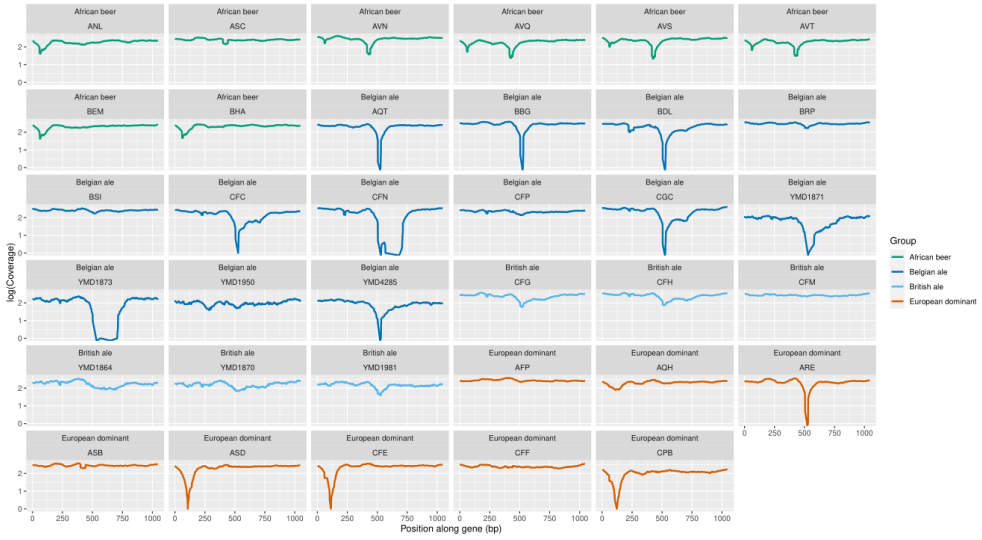

Figure 4 - Coverage levels of the *ADH2* gene reveal homozygous internal deletions
We extracted the coverage levels of Illumina reads in the region corresponding to the gene *ADH2* (chromosome XIII: 873291-874337). This graph shows the coverage level of *ADH2* for each strain, using a log scale on the Y axis to represent coverage for ease of interpretation. The X axis represents the position along the gene, starting at 0 for the first position of the CDS. The strains are colored according to the group, except for the Asian dominant group which is subdivided into British ales and Belgian ales. We observe a shared homozygous deletion in the middle of *ADH2* among 9 of the 13 Belgian ale strains and one of the European dominant strains. We also note the presence of a shared homozygous deletion in the beginning of *ADH2* in 3 of the 8 European dominant strains.

This potential domestication event does not affect British ale strains. However, we make complementary in our dataset, as all strains appear to have intact copies of the *SFA1* gene except for 4 of 6 British ale strains. These strains present either a deletion leading to a frameshift and a subsequent premature stop or have at least one haplotype with a nonsense mutation. This inactivation of several alleles of *SFA1* only in British ale strains may be evidence of a domestication event that runs parallels and complements the disruption of *ADH2* in Belgian ale and European dominant strains, likely in connection to their role in fusel alcohol production[23].

Discussion

We phased 35 strains of *S. cerevisiae* which are either used in beer brewing, or are in clades that have a large proportion of beer brewing strains according to the 1,011 *Saccharomyces cerevisiae* genomes survey[6]. A little under a quarter strains are diploids (n=8), all others being polyploids that range from 3n to 5n. We phased all 35 strains using nPhase, obtaining contiguous results with an average of 1.2 haplotigs per chromosome to phase 90% of reads.

We used a windowed approach on these phased haplotypes to estimate their pairwise divergence levels based on phased genetic content, revealing that our dataset seems to comprise three large groups of strains that are more similar to each other than to other strains. Using a different windowed approach, we then estimated the allelic origins of these beer strains by assigning their haplotypes to different clades[6]. We found that they all contain an important proportion of European wine alleles, and that we can categorize them into the same three distinct groups, this time based on their allelic origin profiles: Asian dominant strains, European dominant strains, and African beer strains. The Asian dominant strains correspond to the previously defined Beer 1 group[4] and whose origin as a polyploid admixture of Asian and European wine alleles has previously been described[8]. The European dominant group corresponds to the previously defined Beer 2 group[4], and is again an admixture of Asian and European wine, however it differs from the Asian dominant group by its lower proportion of Asian fermentation alleles. Finally, we characterize the allele content of the African Beers as having a strong European wine signal, and a higher French dairy signal than the other groups.

African beer brewing methods are significantly less industrialized and typically follow traditional means[15], which for *S. cerevisiae* translates to a mode of life that must remain adapted to the wild and to environments with other microorganisms,

notably the LAB which proliferate during the initial spontaneous fermentation step that typically precedes *S. cerevisiae*'s alcoholic fermentation[15,16]. French dairy strains of *S. cerevisiae* which share an environment with LAB have been shown to adapt their *GAL* pathway to disable its glucose repression and more rapidly drain the environment of sugar to outcompete other organisms [28,29]. We find possible evidence of a similar adaptation to sharing an environment with LAB in the extensive changes to *GAL2* we observe in African Beer strains, and the presence of multiple different haplotypes of *GAL2* within each strain. We propose that these modifications may disable or attenuate glucose repression, or confer some other advantage to *S. cerevisiae* strains sharing an environment with LAB.

We also found that despite less obvious domestication pressures, some African beer strains show known signs of domestication. It has been shown that the *FDC1* gene is inactivated in a large number of industrialized beer strains, and not in wild strains, due to its role in forming the undesirable off-flavor compound 4VG[4]. In half of the African beer strains in our dataset, we observed that *FDC1* was inactivated by a frameshift mutation different from the one that affects Asian dominant strains, suggesting an independent domestication event for this gene.

Finally, we propose that two complementary domestication events occurred in European dominant strains and British and Belgian ale strains. The alcohol dehydrogenases *SFA1* and *ADH2* can both contribute to the last step of the formation of fusel alcohol[22], which in high concentrations are undesirable[23] (in fact, fusel is a German word for bad or cheap liquor). A deletion in the middle of *ADH2* is widely present in Belgian Ale strains and at the beginning of *ADH2* in half of the European dominant strains in our dataset, while premature stops in *SFA1* are observed in British Ale strains, suggesting independent and complementary domestication events which should have a similar effect of lowering the overall concentration of fusel alcohol in the final brew.

Methods

Selection of strains, DNA extraction and sequencing

For this study, we focused on a subset of 35 of *Saccharomyces cerevisiae* isolates from diverse clades based either on their known use in fermenting beers or on their high genetic similarity to beer-brewing strains (Supplementary Table S1).

The DNA of 35 strains was extracted from 30 mL cultures (single colony, 48h growth at 30°C) using the QIAGEN Genomic-tip 100/G kit with the recommended manufacture's genomic DNA buffer set. The manufacture's protocol was followed as recommended and final DNA was eluded in 100-200 µl water. DNA was quantified with the broad-range DNA quantification kit from Qubit. Genomic DNA was migrated on a 1.5% agarose gel to check for degradation.

For the long-read sequencing we used the Oxford Nanopore Technology (Oxford, UK). Libraries for sequencing using the MinION and were prepared as described in Istace et al.[31] using the Ligation Sequencing Kit SQK-LSK109. We barcoded strains with the Native Barcoding Expansion 1-12 (EXP-NBD104) to multiplex up to 12 samples per sequencing reaction.

Phasing and cleaning using nPhase

We used filtlong v0.2.0 (https://github.com/rrwick/Filtlong) to subset our nanopore long reads to 80X (estimated as 12 500 000 * 80 bases), then used the nPhase pipeline[24] v1.1.3 with default parameters to phase each strain using its long and short reads and the R64 reference sequence of *S. cerevisiae*. Once we obtained raw results using the nPhase pipeline command, we ran the nPhase cleaning command using default parameters to improve contiguity and eliminate short, uninformative haplotigs.

Calculating pairwise haplotype divergence between strains within strains

nPhase outputs a file with the suffix ".variants.tsv" which indicates, for each predicted haplotig, the SNPs that were phased. We use this file along with the reference sequence of *S. cerevisiae* to infer the full sequences of our haplotypes and split them into 10kb windows. Then, for each pair of strains, we compared every full 10 kb haplotype window to all of the haplotypes fully covering the same window in the opposite strain and only kept the lowest divergence value.

This method extends to the calculation of internal divergence levels, with the difference that instead of comparing the haplotypes of one strain to the haplotypes of another, we compared the haplotypes of one strain to each other. We again keep the lowest value, but we do not allow a 10 kb haplotype block to compare to itself.

Being ploidy agnostic, nPhase tends to group homozygous regions together so there may be an over-estimation of divergence, however nPhase also doesn't take indels into account so there may be an under-estimation of divergence. It's unclear which bias has the stronger effect, or the extent of the effect of these limitations.

Dendrogram creation

A genotyping matrix was constructed with the GenotypeGVCFs function of GATK[32] that was run on individual gvcf files generated by GATK's HaplotypeCaller method. This matrix was used to build a neighbor-joining tree with the R packages ape[33] and SNPrelate[34]. To that end, the gvcf matrix was converted into a gds file and individual dissimilarities were estimated for each pair of isolates with the snpgdsDiss function. The bionj algorithm was then run on the obtained distance matrix.

Pairwise differences between the studied strains was estimated from the non-shared SNPs positions obtained with bcftool[35] isec with -n -1 -c all options run on individual gvcf files.

Allele content origin attribution

In order to investigate the origins of these beer strains we used a windowed approach to split the haplotypes predicted by nPhase into 20 kb windows and compared them to 6 of the clades described in Peter *et al.* 2018: European wine (we merged all of the European wine subclades), the clinical French Guiana human, African palm wine, North American Oak, Asian fermentation (we merged the Sake and Asian fermentation clades) and French Dairy.

For each clade, we consider that a position is a marker of this clade if it has a Minor Allele Frequency (MAF) ≥ 25% within the clade and is not present in more than one of the other 5 clades at a MAF ≥ 25%. Then for each 20kb window of each haplotype we attributed the clade with the highest number of markers.

Calculating divergence between gene haplotypes

To calculate the pairwise divergence between genes we used the latest annotation of *S. cerevisiae* available on SGD (Release 64-2-1 of the S288C reference genome[36]) and extracted the positions of genes. We then extracted each gene's sequence in the reference genome and for each strain we used the strainName.variant.tsv file generated by nPhase to extract all predicted haplotypes, only keeping the variants that fall within each gene's sequence and inferring them into the reference sequence. We only kept gene haplotypes which had full predictions, we did not keep any incompletely inferred genes. We then proceeded to a pairwise comparison of every gene haplotype in our dataset, calculating the divergence as the number of mismatching positions divided by the length of the gene.

Gene Ontology Term Finder calculations on SGD

Based on the divergence calculations described above, we then identified all genes for which at least one pairwise comparison led to a divergence level ≥ 4%. We only keep genes whose ORF classification is listed as "Verified" in the annotation, not

"Uncharacterized" or "Dubious". Then we input that list with default parameters into the Gene Ontology Term Finder[37] available on the *Saccharomyces* Genome Database (SGD) website at the following url: https://www.yeastgenome.org/goTermFinder

Identifying frameshifts & premature stops

We identified indels that cause frameshift mutations by manual inspection of the Illumina VCF files generated by the nPhase pipeline using bwa-mem[38] for mapping and GATK 4.0[32] for variant calling. Premature stops were identified by identifying stop codons in the previously generated inferred gene haplotypes.

Coverage plots for the *MAL11*, and *ADH2* genes

We generated the data for our gene coverage plots of *MAL11* and *ADH2* using bamCoverage[39] v3.5.0 with a window size of 1.

Data visualization tools

The heatmap with clustering (Figure 1) was generated using pheatmap v1.0.12 (https://cran.r-project.org/web/packages/pheatmap/index.html), the dendrogram is viewed in FigTree v1.4.4 (http://tree.bio.ed.ac.uk/software/figtree/) and other figures were generated using ggplot2 v3.3.3 (https://ggplot2.tidyverse.org) on the R programming language v4.0.2 (https://www.r-project.org/about.html). We used a color palette intended for interpretability by people with colorblindness[40].

Supplementary Material

Supplementary figure S1: Raw phasing results for all 35 strains

We present the three plots generated for each strain's raw nPhase phasing predictions. For each strain, the first plot shows the coverage of each predicted haplotig, the second plot shows the discordance level of each predicted haplotig, and the final plot shows an overview of where the haplotigs are along the genome.
Only strain AQH is shown here, the file containing figures for all strains can be found in the companion document accessible from the appendices.

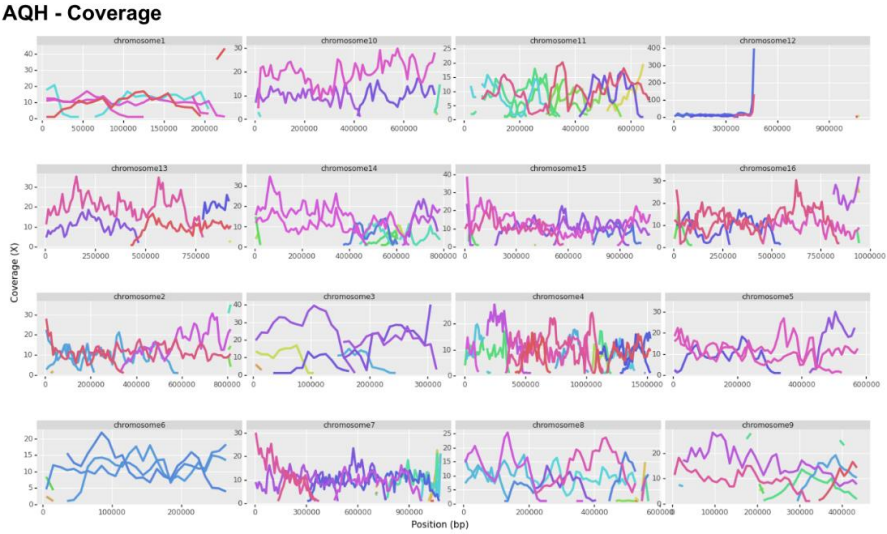

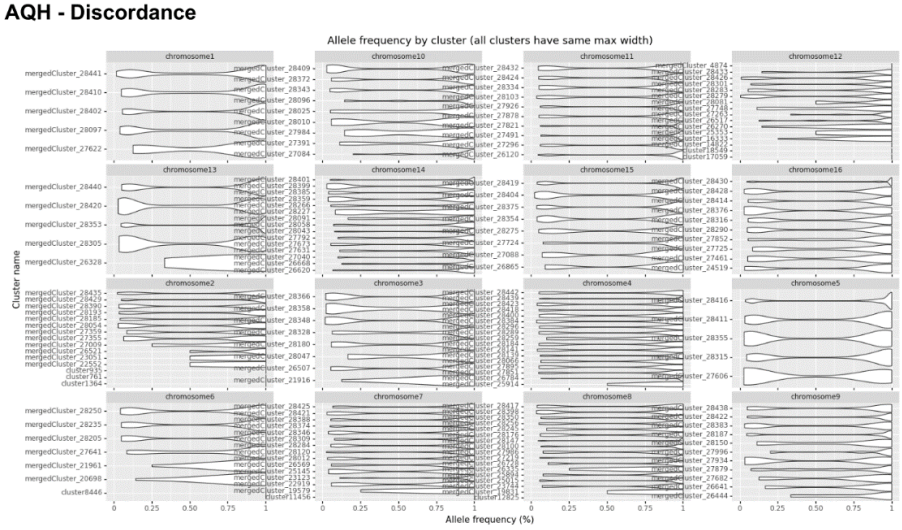

AQH - Phased

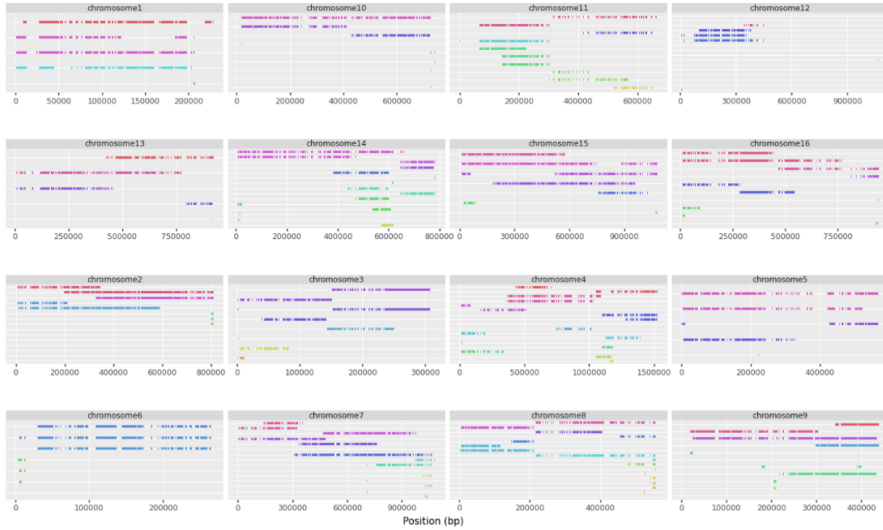
chromosome1
chromosome10
chromosome11
chromosome12
chromosome13
chromosome14
chromosome15
chromosome16
chromosome2
chromosome3
chromosome4
chromosome5
chromosome6
chromosome7
chromosome8
chromosome9
Position (bp)

Supplementary figure S2: Cleaned phasing results for all 35 strains

We present the three plots generated for each strain's cleaned nPhase phasing predictions, generated from the raw predictions. For each strain, the first plot shows the coverage of each predicted haplotig, the second plot shows the discordance level of each predicted haplotig, and the final plot shows an overview of where the haplotigs are along the genome.

Only strain AQH is shown here, the file containing figures for all strains can be found in the companion document accessible from the appendices.

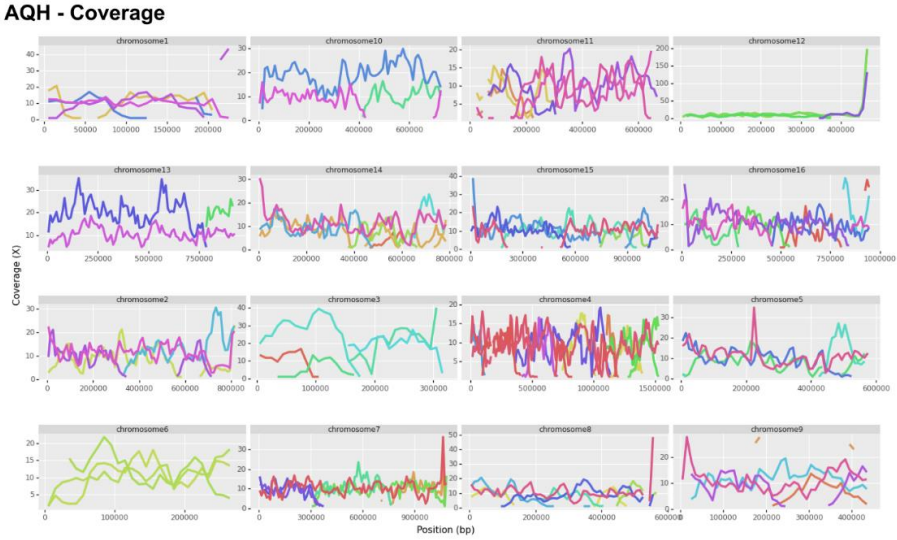

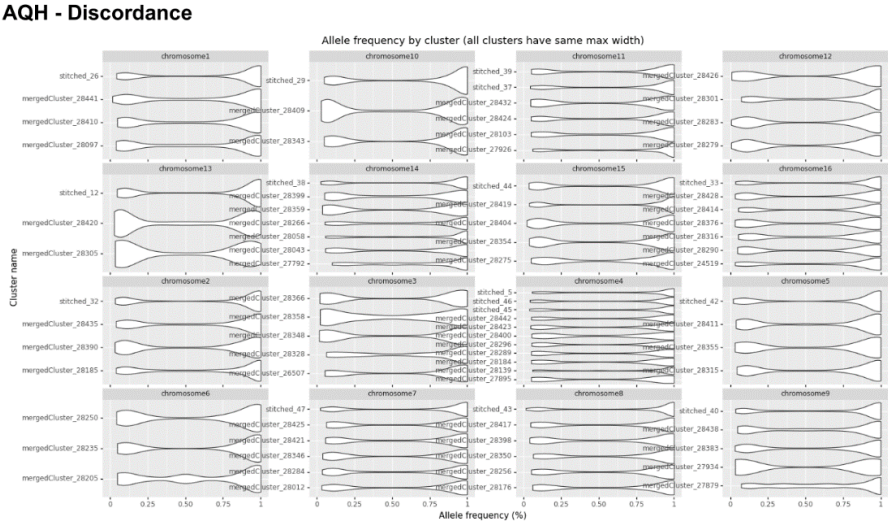

AQH - Phased

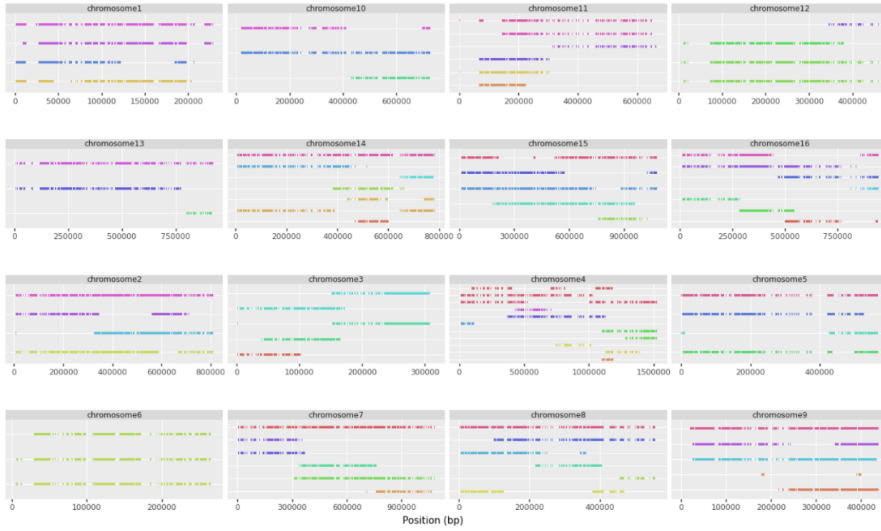
chromosome1
chromosome10
chromosome11
chromosome12
chromosome13
chromosome14
chromosome15
chromosome16
chromosome2
chromosome3
chromosome4
chromosome5
chromosome6
chromosome7
chromosome8
chromosome9
Position (bp)

Supplementary figure S3: Allele frequency plots

These allele frequency plots were generated for the 7 strains not included in the 1,011 paper by Peter *et al.* and were used to identify clear aneuploidies by manual visual inspection. For each plot we specify the aneuploidies called.

Only strains YMD1864 and YMD1870 are shown here, the file containing figures for all strains can be found in the companion document accessible from the appendices.

YMD1864

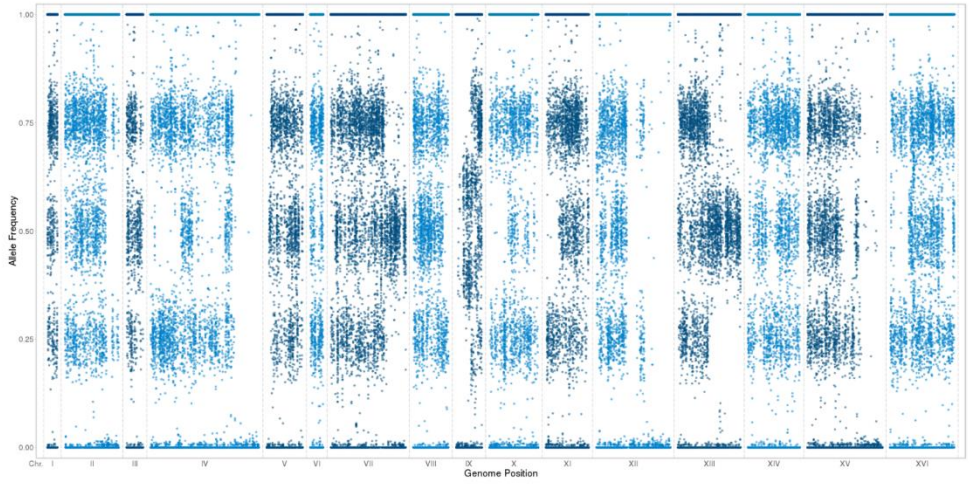

Aneuploidies observed: +1*9

YMD1870

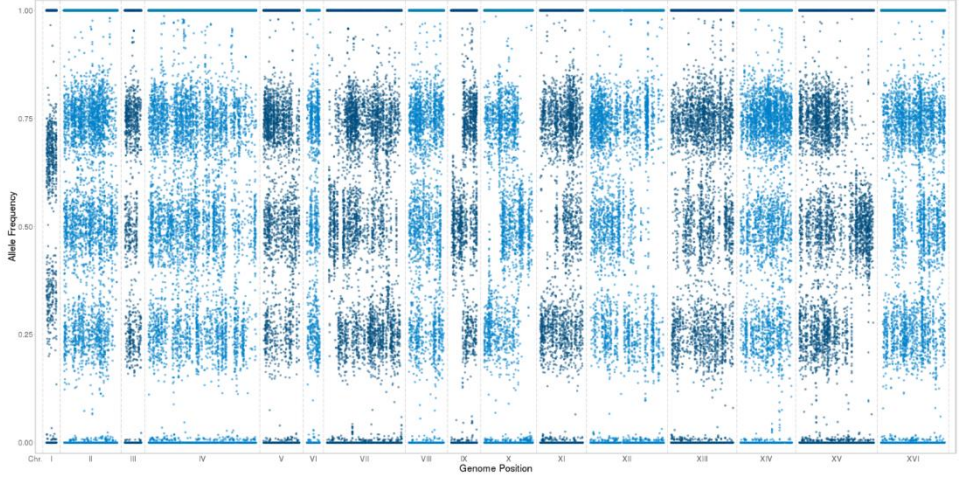

Aneuploidies observed: -1*1

Supplementary figure S4 - Origin profiles per strain per group

For each strain, we attributed 20kb regions of its haplotypes to the clade with the highest similarity. This figure shows, for each strain, the proportion of regions attributed to each clade. Each page corresponds to one of the three groups we identified based on these profiles: European dominant strains, Asian dominant strains, and African beer strains. Strains within the same group have very similar profiles.

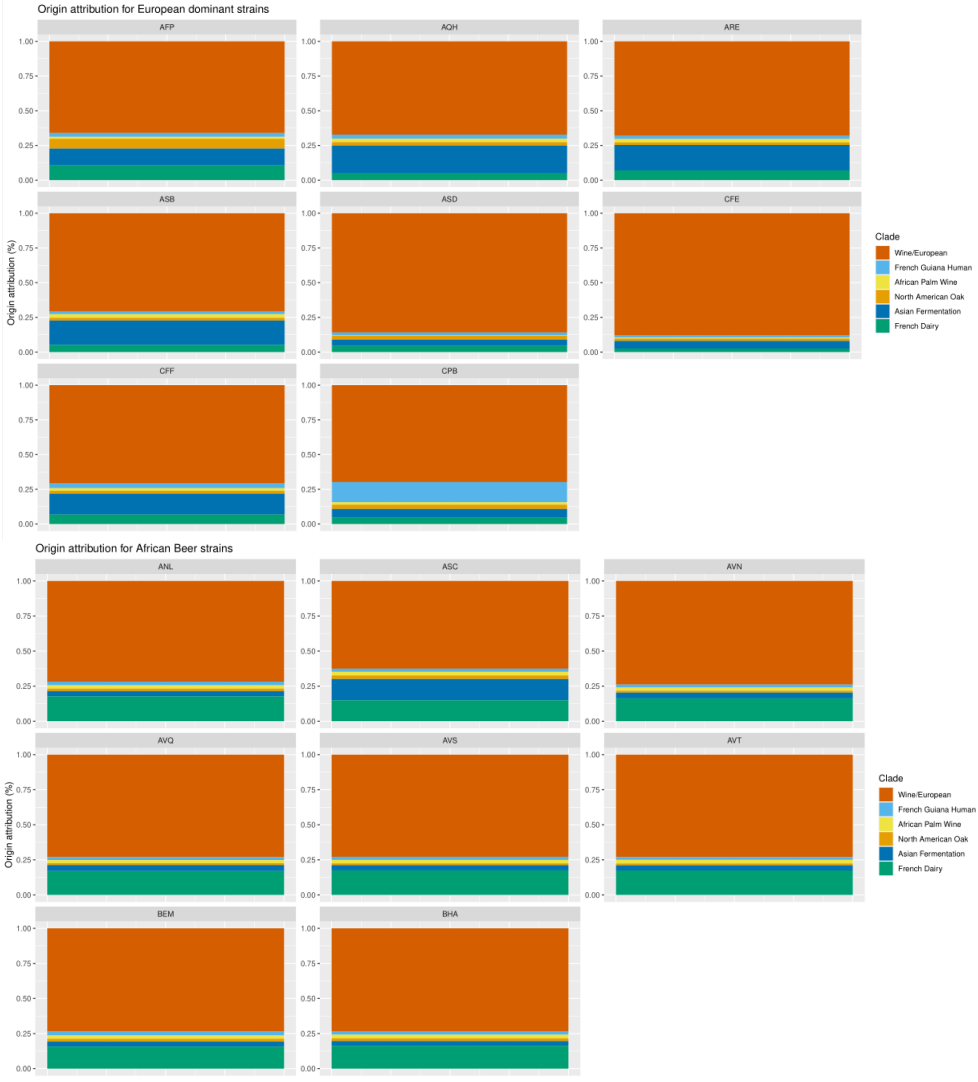

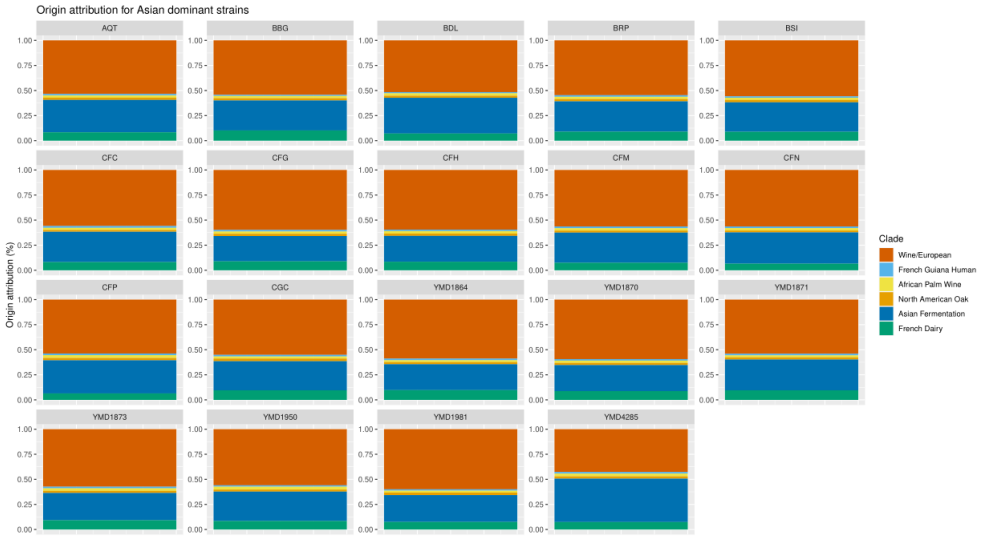
Origin attribution for Asian dominant strains
AQT
BBG
BDL
BRP
BSI
CFC
CFG
CFH
CFM
CFN
CFP
CGC
YMD1864
YMD1870
YMD1871
YMD1873
YMD1950
YMD1981
YMD4285
Origin attribution (%)
1.00
0.75
0.50
0.25
0.00
Clade
Wine/European
French Guiana Human
African Palm Wine
North American Oak
Asian Fermentation
French Dairy

Supplementary figure S5 - Allele similarity across the genome for different groups

Once each strain's different haplotypes have been assigned to a clade, we can generate a graph that shows, for each 20kb window along the genome, what proportion of haplotypes support each allelic origin. This representation reveals which parts of the genome are mostly similar to one or the other clade, and gives a general overview of the allele content of each group, showing them to have very different profiles. The Asian dominant group and European dominant group look similar, though with almost inverted proportions of European Wine alleles and Asian Fermentation alleles, and the African Beer group has the highest proportion of French dairy, but also appears to have less contested origins.

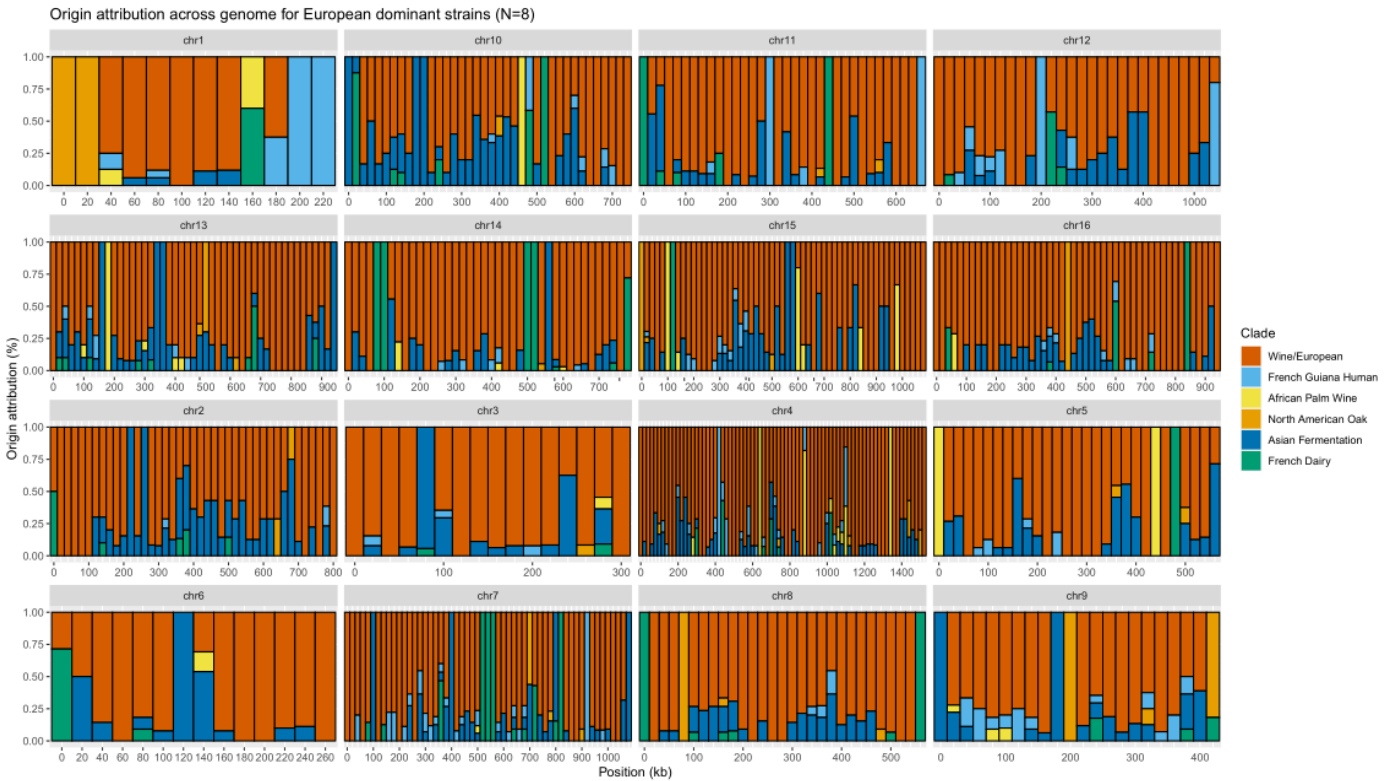

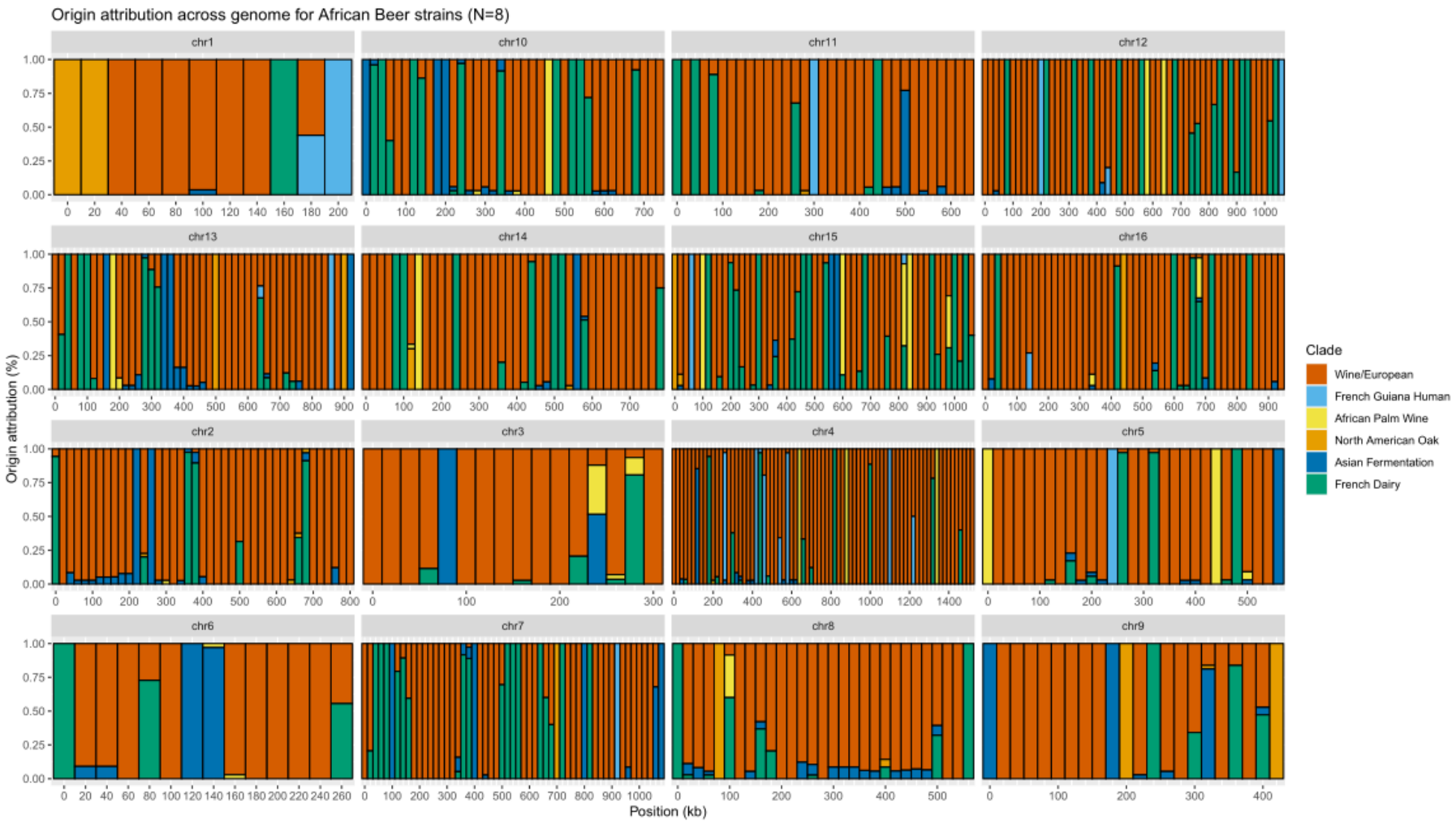
Origin attribution across genome for African Beer strains (N=8)
chr1
chr10
chr11
chr12
chr13
chr14
chr15
chr16
chr2
chr3
chr4
chr5
chr6
chr7
chr8
chr9
Origin attribution (%)
Position (kb)
Clade
Wine/European
French Guiana Human
African Palm Wine
North American Oak
Asian Fermentation
French Dairy

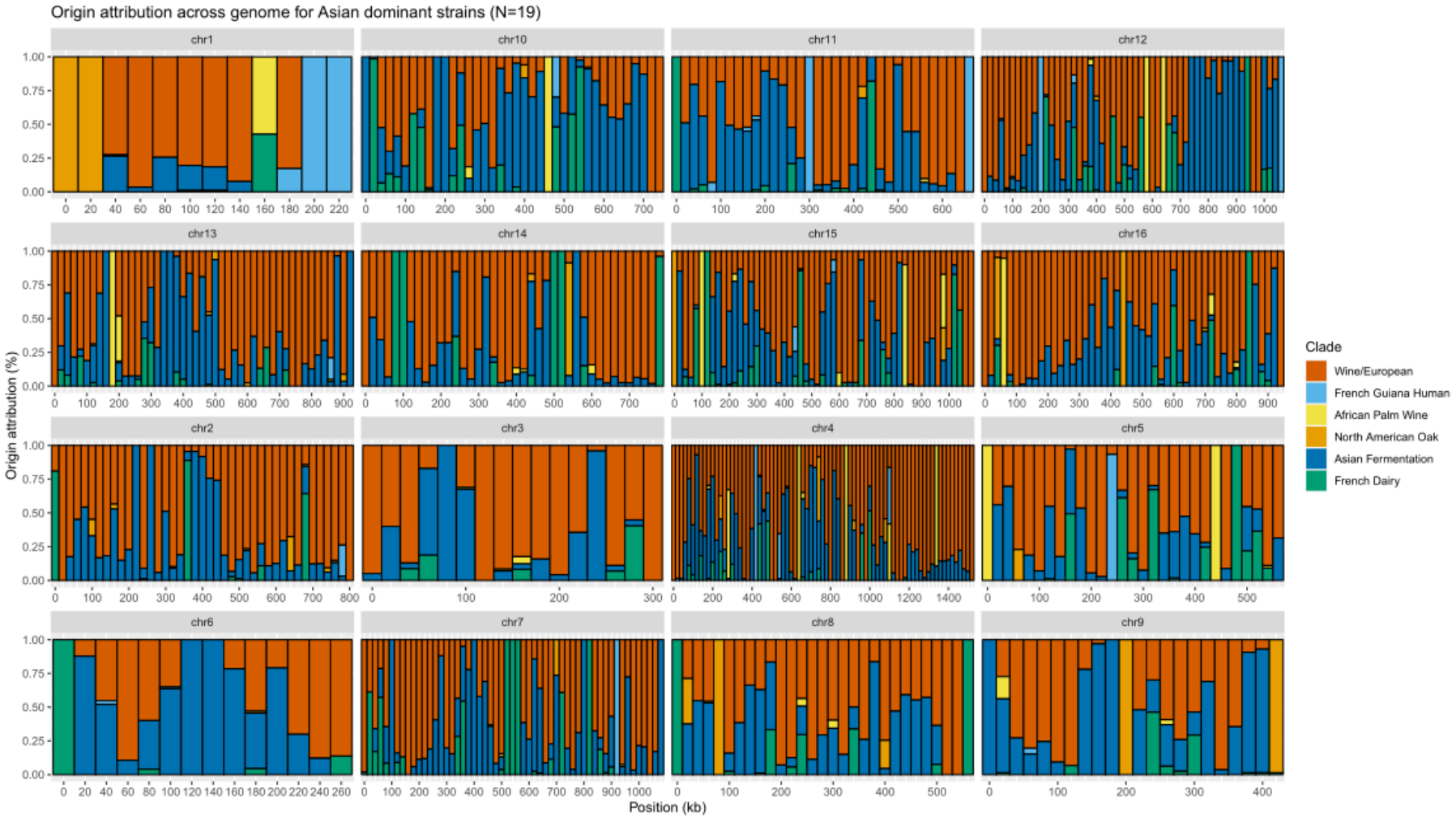
Origin attribution across genome for Asian dominant strains (N=19)
chr1
chr10
chr11
chr12
chr13
chr14
chr15
chr16
chr2
chr3
chr4
chr5
chr6
chr7
chr8
chr9
Origin attribution (%)
Position (kb)
Clade
Wine/European
French Guiana Human
African Palm Wine
North American Oak
Asian Fermentation
French Dairy

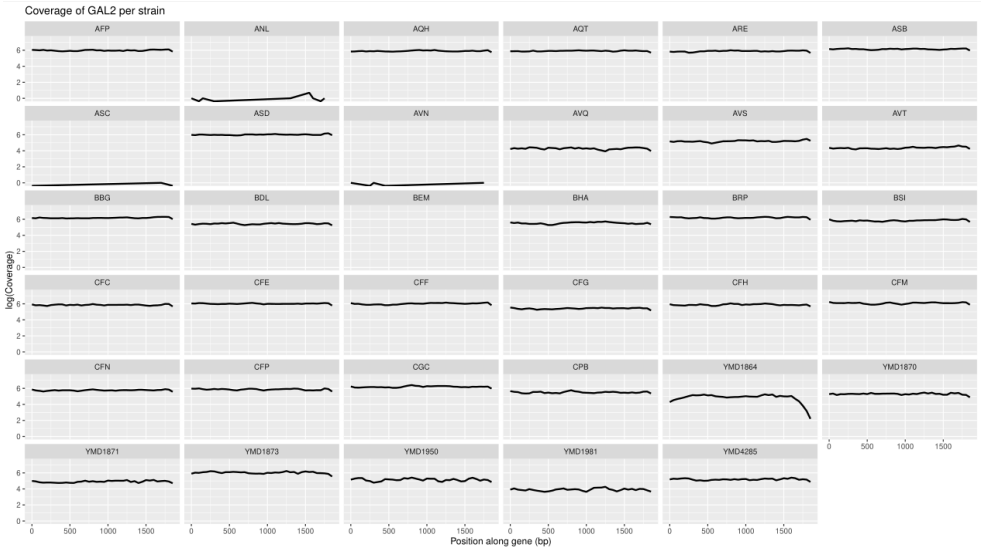

Supplementary figure S6 - *MAL11* coverage plots
We extracted the coverage levels of Illumina reads in the region corresponding to the gene *MAL11* (ChromosomeVII:1073963-1075813). This graph shows the coverage level of *MAL11* for each strain, using a log scale on the Y axis to represent coverage for ease of interpretation. The X axis represents the position along the gene, starting at 0 for the first position of the CDS. We note the extremely low coverage for strains ANL, ASC and AVN, and the total absence of coverage for strain BEM.

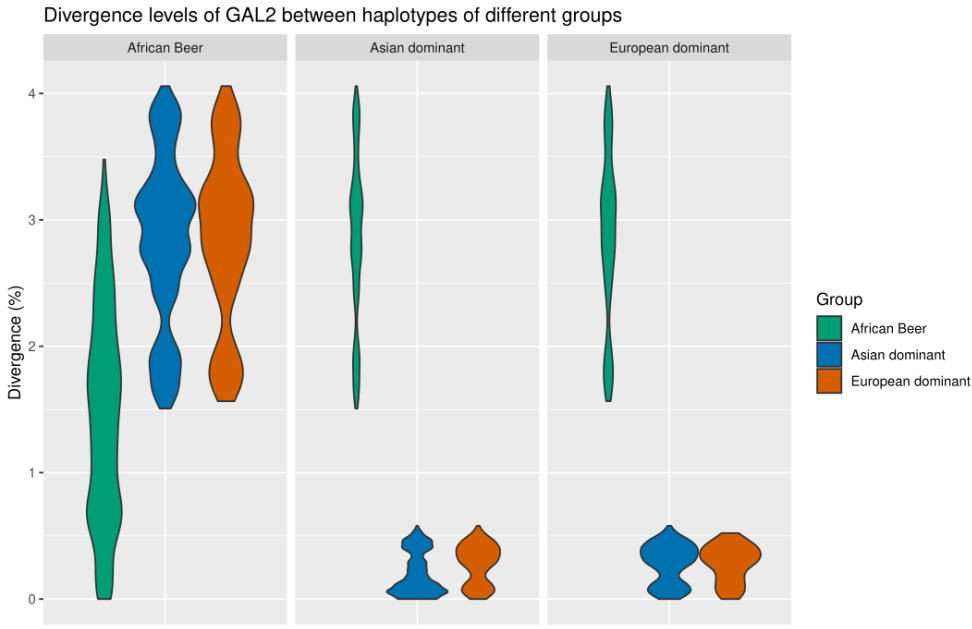

Supplementary figure S7 - Divergence levels of *GAL2* between haplotypes of different groups

This graph represents the divergence levels of *GAL2* obtained via pairwise comparisons of all fully phased haplotypes for this gene in our dataset. We note that the divergence level (y Axis, given as a percentage) is high when comparing African beer haplotypes of *GAL2* to other African beer haplotypes of *GAL2*, and even higher when compared to European dominant or Asian dominant copies of *GAL2*. The European dominant and Asian dominant haplotypes of *GAL2* are not very divergent from each other, with a maximum of 0.5% divergence. However the African beer haplotypes of *GAL2* are at minimum 1.5% divergent from European dominant and Asian dominant strains, and at most 4% divergent from them.

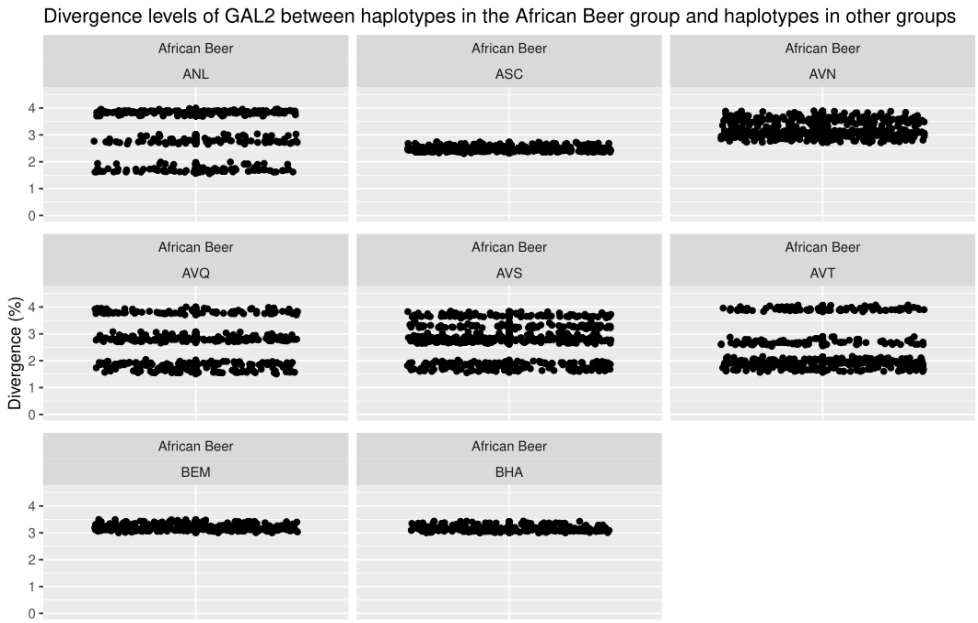

Supplementary figure S8 - *GAL2* haplotype divergence levels within African beer strains

This graph represents, for each African beer strain, the divergence levels of all of its haplotypes with the European dominant and Asian dominant haplotypes of *GAL2*. The Y axis represents the divergence level and each point represents a different pairwise comparison, the points are jittered for ease of interpretation. We observe that some strains, such as ANL, AVQ, AVS and AVT have multiple haplotypes of *GAL2*, with varying levels of divergence from the European dominant and Asian dominant haplotypes.

Supplementary Table S1: Descriptions of strains

Background information on the strains used in our analysis. The "Group" column refers to the assigned origin according to our observations of the allele content using a windowed method, described further in the results section.

Strain Name	Isolate name	Group	Ploidy (n)	Aneuploidy	Isolation	Ecological origins	Geographical origins	Clade
AFP	CBS6505	European Dominant	2	euploid	Cachaça	Beer	UK	Mosaic beer
ANL	A-6	African Beer	4	euploid	Sorghum beer	Beer	Ghana	African beer
AQH	CBS7957	European Dominant	3	aneu;+1*3;	Factory producing cassava flour	Industrial	Sao Paulo, Brazil	Mosaic beer
AQT	CBS1230	Asian Dominant	3	aneu;+1*6;	Beer	Beer	Belgium	Ale beer
ARE	CBS1398	European Dominant	2	aneu;+1*2; +1*3; +1*6; +4*9; +1*12; +1*14; +1*15;	Leaf of Eucalyptus sp.	Tree	NA	Mosaic beer
ASB	CBS4255	European Dominant	2	euploid	Sputum	Human, clinical	NA	Mosaic beer
ASC	CBS4455	African Beer	3	aneu;+1*1;	Kaffir beer	Beer	South Africa	African beer

ASD	CBS4507	European Dominant	2	euploid	Brewer's yeast, English top yeast	Beer	NA	Wine/European
AVN	CH02	African Beer	4	euploid	Pearl millet beer	Beer	Abengourou, Ivory Coast	African beer
AVQ	CH10	African Beer	5	aneu;+1*4;	Pearl millet beer	Beer	Abengourou, Ivory Coast	African beer
AVS	CH14	African Beer	5	aneu;+1*12; +1*13;	Pearl millet beer	Beer	Abengourou, Ivory Coast	African beer
AVT	CH13	African Beer	5	aneu;+1*2; +1*5;	Pearl millet beer	Beer	Abengourou, Ivory Coast	African beer
BBG	CCY_21-4-106	Asian Dominant	4	aneu;-1*1; -1*6; -1*8; -1*10; -1*14; -1*16;	River water (Morava)	Water	Devinska Nova Ves, Slovakia	Ale beer
BDL	CLQCA_10-386	Asian Dominant	2	euploid	Beer	Beer	Ecuador	Mixed origin
BEM	CLIB653	African Beer	4	euploid	Beer leaven for Bili Bili beer, brewery	Beer	Chad	African beer
BHA	CLIB655	African Beer	3	euploid	Beer leaven for Bili Bili beer, brewery	Beer	Chad	African beer
BRP	DBVPG6694	Asian Dominant	4	aneu;+1*1; -1*3;	Artois Peterman beer	Beer	Belgium	Ale beer

BSI	DBVPG6693	Asian Dominant	4	aneu;+1*1; +1*9; -1*14;	Beer	Beer	Belgium	Ale beer
CFC	4.5_WLP530	Asian Dominant	4	aneu;-1*12;	Carlsberg Beer, Abbey ale yeast (Westmalle brewery)	Beer	Westmalle, Belgium	Ale beer
CFE	4.9_WLP099	European Dominant	2	euploid	Carlsberg Beer, super high gravity	Beer	United Kingdom	Wine/European
CFF	6.2_WLP570	European Dominant	2	euploid	Carlsberg Beer	Beer	Belgium	Mosaic beer
CFG	1.6_Safale_S40	Asian Dominant	4	aneu;-1*6;	Carlsberg Beer	Beer	UK	Ale beer
CFH	Nottingham_ale 1.8_Lallemand	Asian Dominant	4	aneu;-1*1; -1*7;	Carlsberg Beer	Beer	UK	Ale beer
CFM	5.5_WLP090	Asian Dominant	4	aneu;-1*1; -1*5; -1*9;	Carlsberg Beer, "San Diego Super Yeast"	Beer	San Diego, USA	Ale beer
CFN	3.3_Safale_S-33	Asian Dominant	4	aneu;+1*2; +1*9;	Carlsberg Beer	Beer	NA	Mixed origin
CFP	3.4_Safbrew_T-58	Asian Dominant	4	euploid	Carlsberg Beer	Beer	NA	Mixed origin
CGC	UCD_06-645	Asian Dominant	4	euploid	Female olive fly	Fruit	Davis, CA, UCD	Ale beer

CPB	995	European Dominant	2	aneu;+1*3;	Fermented beverage from raisins and sugar	Beer	Hungary	Mosaic region 1
YMD1864	Wyeast1275	Asian Dominant	4	aneu +1*9;	Commercial Ale	Beer	England	Ale Beer
YMD1870	Wyeast1028	Asian Dominant	4	aneu -1*1;	Commercial Ale	Beer	Britain	Ale Beer
YMD1871	Wyeast2565	Asian Dominant	4	euploid	Commercial Ale	Beer	Germany	Ale Beer
YMD1873	Wyeast3068	Asian Dominant	4	aneu -1*10;	Commercial Wheat	Wheat Beer	Germany	Ale Beer
YMD1950	Wyeast 3463 Forbidden Fruit (Belgian wheat)	Asian Dominant	4	euploid	Commercial Wheat	Wheat Beer	Belgium	Ale Beer
YMD1981	Wyeast1968	Asian Dominant	4	aneu -1*5; -1*10; -1*12; -1*14;	Commercial Ale	Beer	England	Ale Beer
YMD4285	Stalljen	Asian Dominant	4	euploid	Beer	Farmhouse Beer	Norway	Ale Beer

Supplementary Table S2: Sequencing statistics

Sequencing data statistics for the MinION and Illumina sequencing runs of this study.

Strain	MinION sequencing							
	Mean read length (kb)	Mean read quality	Median read length (kb)	Median read quality	Number of reads	Read length N50 (kb)	Total bases (Gb)	Theoretical Coverage (X)
AFP	29.8	15.3	25.8	15.4	33607	37.3	1	80
ANL	23.8	15.2	19.8	15.2	42030	28.5	1	80
AQH	7.5	13.8	3.3	14	85081	18.9	0.64	51.2
AQT	28.1	15.5	24.5	15.5	35573	33.5	1	80
ARE	35.5	15.9	32	15.9	28148	40.4	1	80
ASB	29.7	14.8	24.5	14.9	33678	38	1	80
ASC	8.9	13.7	3.4	13.9	92824	24.7	0.82	65.6
ASD	17	14.8	12.5	15	58737	26.4	1	80
AVN	11.3	14.1	4.9	14.6	15854	27.1	0.18	14.4
AVQ	14.2	14.1	6.5	14.4	70327	30.5	1	80
AVS	14	14.6	10.7	14.8	71270	19.2	1	80
AVT	26.1	14.6	19.9	14.8	38297	37.7	1	80
BBG	37.7	15.4	35.4	15.4	26501	42.7	1	80
BDL	35.7	15.4	31.9	15.4	28023	40.9	1	80
BEM	10.4	14.1	6.8	14.3	95921	16.4	1	80
BHA	30.1	15.7	26.7	15.7	33272	35	1	80

BRP	22.9	14.5	19.1	14.6	43589	30.5	1	80
BSI	10.5	13.3	4	13.5	77702	27.8	0.82	65.6
CFC	33.7	14.8	28.9	15	29653	39.8	1	80
CFE	13.4	14.1	8.3	14.5	72588	25.9	0.97	77.6
CFF	24.4	15.3	20.4	15.4	41037	31.2	1	80
CFG	24.4	14.1	19.1	14.5	40928	32.8	1	80
CFH	33.1	15.3	30.1	15.3	30249	37.9	1	80
CFM	8.8	10.1	6.3	10.3	114245	12.2	1	80
CFN	22	13.2	18.2	13.3	45439	27.2	1	80
CFP	25.7	15.4	21.8	15.4	38944	29.4	1	80
CGC	29.2	14.6	25.6	14.7	34288	37.7	1	80
CPB	23.8	14.9	20.6	14.9	42100	29.7	1	80
YMD1864	9.8	13.3	5.2	13.7	84880	20.1	0.83	66.4
YMD1870	29.3	15.6	25.2	15.5	34180	32.9	1	80
YMD1871	12.8	13.4	6.2	13.8	54736	28.1	0.7	56
YMD1873	21.3	15.1	18.1	15.2	46951	25.8	1	80
YMD1950	11.8	13.4	5.8	13.8	66483	25.2	0.78	62.4
YMD1981	14.2	14.2	9.6	14.4	70280	23.7	1	80
YMD4285	12.3	13.4	6.1	13.8	71969	26.2	0.89	71.2
Total	21.2	14.4					0.9	74.6

Strain	Illumina sequencing			
	Mean read quality	Number of reads	Total bases (Gb)	Theoretical Coverage (X)
AFP	34.8	38302000	3.8	304
ANL	34.2	31573592	3.2	256
AQH	33.6	38258278	3.8	304
AQT	34.4	35911684	3.5	280
ARE	34.1	37465530	3.6	288
ASB	33.5	36669880	3.6	288
ASC	34.6	39670940	3.8	304
ASD	33.3	36915614	3.6	288
AVN	33.2	44874148	4.4	352
AVQ	33	33041378	3.2	256
AVS	32.9	38331296	3.8	304
AVT	33	35650262	3.6	288
BBG	34.3	41281728	4.2	336
BDL	35.2	36189032	3.6	288
BEM	35.2	33166312	3.4	272
BHA	33.9	35372210	3.6	288
BRP	33.2	46614138	4.6	368
BSI	31.8	40242854	4	320
CFC	33.8	32205534	3.2	256
CFE	32.8	42084090	4.2	336

CFF	32.4	39921422	4	320
CFG	34	42302044	4.2	336
CFH	33.5	45909668	4.6	368
CFM	33.8	40044236	4	320
CFN	33.7	45620516	4.5	360
CFP	32	35190058	3.5	280
CGC	34	46002610	4.6	368
CPB	32.1	27472676	2.7	216
YMD1864	30.9	23398040	2.4	192
YMD1870	30.9	25578302	2.6	208
YMD1871	29.7	19192418	2	160
YMD1873	30.8	24423424	2.4	192
YMD1950	29	27143926	2.8	224
YMD1981	29.9	20361912	2	160
YMD4285	28.8	12168130	1.8	144
Total	32.9		3.5	280.7

Supplementary Table S3: Phasing statistics

Summary statistics for all 35 phased strains. We provide them for the raw phasing results as well as the cleaned phasing results. L90 is the minimum number of haplotigs to phase 90% of the phase informative reads. This excludes reads which only cover homozygous positions or are subsets of other reads. The L90 per chromosome value is an estimate of phasing quality and is equal to the L90 divided by 16*ploidy, we do not take known aneuploidy into account for this value. A value close to 1 indicates a likely contiguous phasing.

Strain	Ploidy (n)	Number of heterozygous SNPs	Raw phasing results			Cleaned phasing results		
			L90	L90 per chromosome	Number of haplotigs	L90	L90 per chromosome	Number of haplotigs
AFP	2	5114	63	2	133	52	1.6	79
ANL	4	47229	66	1	172	55	0.9	83
AQH	3	53973	76	1.6	173	60	1.3	83
AQT	3	35315	84	1.8	199	57	1.2	87
ARE	2	20405	39	1.2	100	26	0.8	43
ASB	2	36576	46	1.4	146	31	1	54
ASC	3	38035	71	1.5	201	64	1.3	102
ASD	2	4132	81	2.5	142	71	2.2	106
AVN	4	44206	272	4.3	591	232	3.6	371
AVQ	5	49626	78	1	168	67	0.8	96
AVS	5	51635	99	1.2	211	77	1	112
AVT	5	49440	78	1	189	66	0.8	90
BBG	4	38434	75	1.2	184	59	0.9	81

BDL	2	45792	51	1.6	160	35	1.1	55
BEM	4	30249	98	1.5	208	76	1.2	114
BHA	3	22945	57	1.2	127	43	0.9	66
BRP	4	49642	98	1.5	214	76	1.2	106
BSI	4	43317	91	1.4	231	78	1.2	112
CFC	4	63692	83	1.3	181	67	1	93
CFE	2	9207	82	2.6	161	72	2.3	108
CFF	2	32544	57	1.8	148	37	1.2	57
CFG	4	58215	81	1.3	191	66	1	98
CFH	4	58666	79	1.2	190	57	0.9	80
CFM	4	42367	102	1.6	244	92	1.4	138
CFN	4	79737	83	1.3	233	70	1.1	100
CFP	4	79944	90	1.4	218	63	1	87
CGC	4	50930	86	1.3	210	68	1.1	91
CPB	2	21492	73	2.3	159	49	1.5	77
YMD1864	4	46430	104	1.6	230	82	1.3	121
YMD1870	4	55977	74	1.2	160	59	0.9	82
YMD1871	4	47434	84	1.3	230	76	1.2	111
YMD1873	4	40325	105	1.6	207	76	1.2	114
YMD1950	4	47256	82	1.3	180	69	1.1	98
YMD1981	4	54566	94	1.5	218	70	1.1	105
YMD4285	4	71777	77	1.2	217	71	1.1	103
Total			85	1.6	198	68	1.2	100

Supplementary Table S4: Aneuploidies

Aneuploidies were determined by manual inspection of the output plots given by nPhase for the raw phasing results as well as the cleaned phasing results. Presence of an additional haplotig or absence of a haplotig was observed in the phasing plot in corroboration with the coverage plot. For example a triploid with three haplotigs on a given chromosome for which one of the haplotigs is twice as covered as the others has a +1 aneuploidy.

Strain	Ploidy	Known aneuploidy	Aneuploidy observed in raw phasing	Aneuploidy observed in cleaned phasing
AFP	2	euploid	N/A	N/A
ANL	4	euploid	N/A	N/A
AQH	3	aneu;+1*3;	No	aneu;+1*3;
AQT	3	aneu;+1*6;	aneu;+1*6;	aneu;+1*6;
ARE	2	aneu;+1*2; +1*3; +1*6; +4*9; +1*12; +1*14; +1*15;	aneu;+1*3;	No
ASB	2	euploid	N/A	N/A
ASC	3	aneu;+1*1;	No	aneu;+1*1;
ASD	2	euploid	N/A	N/A
AVN	4	euploid	N/A	N/A
AVQ	5	aneu;+1*4;	No	No
AVS	5	aneu;+1*12; +1*13;	No	aneu;+1*13;
AVT	5	aneu;+1*2; +1*5;	aneu;+1*2; +1*5;	aneu;+1*2; +1*5;
BBG	4	aneu;-1*1; -1*6; -1*8; -1*10; -1*14; -1*16;	aneu;-1*1 ;-1*6; -1*8; -1*10; -1*14; -1*16;	aneu;-1*1; -1*6; -1*8; -1*10; -1*14; -1*16;
BDL	2	euploid	N/A	N/A
BEM	4	euploid	N/A	N/A
BHA	3	euploid	N/A	N/A
BRP	4	aneu;+1*1; -1*3;	aneu;-1*3	aneu;-1*3
BSI	4	aneu;+1*1; +1*9; -1*14;	No	No
CFC	4	aneu;-1*12;	aneu;-1*12;	aneu;-1*12;
CFE	2	euploid	N/A	N/A

CFF	2	euploid	N/A	N/A
CFG	4	aneu;-1*6;	aneu;-1*6;	aneu;-1*6;
CFH	4	aneu;-1*1; -1*7;	aneu;-1*7;	aneu;-1*7;
CFM	4	aneu;-1*1; -1*5; -1*9;	No	No
CFN	4	aneu;+1*2; +1*9;	No	No
CFP	4	euploid	N/A	N/A
CGC	4	euploid	N/A	N/A
CPB	2	aneu;+1*3;	aneu;+1*3;	aneu;+1*3;
YMD1864	4	From AF plots: aneu;+1*9;	No	No
YMD1870	4	From AF plots: aneu;-1*1;	No	No
YMD1871	4	From AF plots: euploid	N/A	N/A
YMD1873	4	From AF plots: aneu;-1*10;	aneu;-1*10;	No
YMD1950	4	From AF plots: euploid	N/A	N/A
YMD1981	4	From AF plots: aneu; -1*5; -1*10; -1*12; -1*14;	aneu;-1*5; -1*10; -1*14;	aneu;-1*5; -1*10; -1*12; -1*14;
YMD4285	4	From AF plots: euploid	N/A	N/A

Supplementary Table S5: Inter-strain divergence levels for all 35 strains based on SNP matrix

This table shows the inter-strain divergence between every pair of strains. Inter-strain divergence was calculated based on SNP content, without taking haplotypes into account. Indels were not included in our estimation of divergence.

This table can be found in the companion document accessible from the appendices.

Supplementary Table S6: Inter-strain divergence levels for all 35 strains based on haplotypes

This table shows the inter-strain divergence between every pair of strains. Inter-strain divergence was calculated based on a 10 kb window and is presented here as a percentage. Homozygous positions were used in the calculations, so the divergence between two strains with homozygous variants in the same 10kb window takes these variants into account for our calculation. Indels were not included in our estimation of divergence.

This table can be found in the companion document accessible from the appendices.

Supplementary Table S7: Mean intra-strain divergence levels for all 35 strains

This table shows the intra-strain divergence between the haplotypes of each strain. Intra-strain divergence was calculated based on the closest 10 kb pairs of haplotypes and is presented here as a percentage.

Group	Strain	Mean intra-strain divergence (%)
African Beer	BEM	0.12
	BHA	0.12
	ANL	0.17
	AVN	0.17
	AVQ	0.17
	AVS	0.16
	AVT	0.17
	ASC	0.17
	Total	0.16
European dominant	CFE	0.09
	ASD	0.05
	CPB	0.21
	CFF	0.26
	AFP	0.25
	AQH	0.22
	ARE	0.27
	ASB	0.23
	Total	0.2
Asian dominant	CFN	0.24
	CFP	0.28
	BDL	0.35
	CFC	0.24
	YMD1873	0.19
	BBG	0.19
	YMD1871	0.21
	CGC	0.2
	AQT	0.17
	BSI	0.16

Asian dominant	YMD1950	0.2
	YMD4285	0.26
	BRP	0.21
	CFG	0.21
	CFH	0.23
	CFM	0.09
	YMD1864	0.21
	YMD1870	0.22
	YMD1981	0.21
	Total	0.21
All	**Total (All)**	0.2

Supplementary Table S8: Highly divergent genes

Genes presenting >4% divergence in at least one pairwise comparison of haplotypes, either across all three groups, only exhibiting >4% divergence when comparing haplotypes of different groups ("All"), or within one of the groups (other three columns). We observe here well-known genes such as GAL2 and ADH2. Predictably, a significant number of these highly divergent genes are uncharacterized or dubious genes as these sequences are typically very short and annotated as possible genes despite presumably being under little to no selective pressure.

The full table can be found in the companion document accessible from the appendices.

Common name	Systematic name	Status	All (18)	European dominant (70)	Asian dominant (71)	African beer (46)
Unnamed	YAL067W-A	Uncharacterized	No	Yes	Yes	Yes
Unnamed	YAL068W-A	Dubious	No	No	Yes	Yes
PAU7	YAR020C	Verified	No	No	No	Yes
Unnamed	YAR029W	Uncharacterized	No	No	Yes	No
PRM9	YAR031W	Verified	No	Yes	Yes	No
Unnamed	YAR070C	Dubious	No	Yes	Yes	No
PHO11	YAR071W	Verified	No	Yes	Yes	No
PAU9	YBL108C-A	Verified	No	Yes	No	No

Supplementary Table S9: GO Term Finder results on verified highly divergent genes

These three tables are the result of GO Term Finder analysis on the 57 verified genes in our list of 144 highly divergent genes (>4% divergence). This excludes the genes listed as uncharacterized or dubious. Each table relates a different set of GO terms: Those related to processes, those related to function, and those related to the cellular components where the gene's protein localizes. We observe significant enrichment in various forms of carbon metabolism processes and in cell wall organization, dehydrogenase functions, carbon transport and oxidoreductases, and localization to the cell wall and vacuoles.

GOID	TERM	CORRECTED PVALUE	FDR RATE	EXPECTED FALSE POSITIVES	ANNOTATED GENES
GO:0000023	maltose metabolic process	8.13E-06	0.00%	0	YGR287C, YOL157C, YBR297W, YJL216C, YBR298C
GO:0005984	disaccharide metabolic process	1.25E-05	0.00%	0	YIL162W, YBR298C, YGR287C, YOL157C, YBR297W, YJL216C
GO:0009311	oligosaccharide metabolic process	2.47E-05	0.00%	0	YBR298C, YIL162W, YOL157C, YJL216C, YBR297W, YGR287C
GO:0005987	sucrose catabolic process	6.12E-05	0.00%	0	YGR287C, YOL157C, YJL216C, YIL162W
GO:0005985	sucrose metabolic process	0.000109586	0.00%	0	YIL162W, YOL157C, YJL216C, YGR287C
GO:0046352	disaccharide catabolic process	0.000607275	0.00%	0	YJL216C, YOL157C, YGR287C, YIL162W
GO:0009313	oligosaccharide catabolic process	0.000845157	0.00%	0	YOL157C, YJL216C, YGR287C, YIL162W
GO:0015757	galactose transport	0.002336796	0.00%	0	YJL219W, YLR081W, YOL156W

GO:0000025	maltose catabolic process	0.00406629	0.89%	0.08	YJL216C, YOL157C, YGR287C
GO:0031505	fungal-type cell wall organization	0.006022812	0.80%	0.08	YOL161C, YOL155C, YFL020C, YIR039C, YBL108C-A, YLR461W, YDR542W, YAR020C, YKL224C

Function

GOID	TERM	CORRECTED PVALUE	FDR RATE	EXPECTED FALSE POSITIVES	ANNOTATED GENES
GO:0047681	aryl-alcohol dehydrogenase (NADP+) activity	1.43E-07	0.00%	0	YDL243C, YJR155W, YCR107W, YOL165C, YNL331C
GO:0005199	structural constituent of cell wall	4.12E-06	0.00%	0	YAR020C, YDR542W, YOL161C, YLR461W, YFL020C, YBL108C-A, YKL224C
GO:0047834	D-threo-aldose 1-dehydrogenase activity	1.07E-05	0.00%	0	YNL331C, YOL165C, YDL243C, YJR155W, YCR107W
GO:0004564	beta-fructofuranosidase activity	2.41E-05	0.00%	0	YIL162W, YJL216C, YOL157C, YGR287C
GO:0004575	sucrose alpha-glucosidase activity	2.41E-05	0.00%	0	YIL162W, YJL216C, YOL157C, YGR287C
GO:0090599	alpha-glucosidase activity	0.000111628	0.00%	0	YOL157C, YGR287C, YJL216C, YIL162W
GO:0015926	glucosidase activity	0.000319537	0.00%	0	YOL157C, YGR287C, YOL155C, YJL216C, YIL162W
GO:0005354	galactose transmembrane transporter activity	0.000919703	0.00%	0	YOL156W, YLR081W, YJL219W

GO:0004556	alpha-amylase activity	0.001600387	0.00%	0	YGR287C, YOL157C, YJL216C
GO:0004574	oligo-1,6-glucosidase activity	0.001600387	0.00%	0	YJL216C, YGR287C, YOL157C
GO:0016160	amylase activity	0.001600387	0.00%	0	YOL157C, YGR287C, YJL216C
GO:0032450	maltose alpha-glucosidase activity	0.001600387	0.00%	0	YOL157C, YGR287C, YJL216C
GO:0033934	glucan 1,4-alpha-maltotriohydrolase activity	0.001600387	0.00%	0	YJL216C, YGR287C, YOL157C
GO:0004553	hydrolase activity, hydrolyzing O-glycosyl compounds	0.003810912	0.00%	0	YOL155C, YJL216C, YIL162W, YOL157C, YGR287C
GO:0005351	sugar:proton symporter activity	0.003938333	0.00%	0	YJL219W, YBR298C, YLR081W, YOL156W
GO:0005402	cation:sugar symporter activity	0.003938333	0.00%	0	YLR081W, YJL219W, YBR298C, YOL156W
GO:0051119	sugar transmembrane transporter activity	0.00539954	0.00%	0	YLR081W, YBR298C, YJL219W, YOL156W
GO:0016616	oxidoreductase activity, acting on the CH-OH group of donors, NAD or NADP as acceptor	0.005459304	0.00%	0	YNL331C, YOL165C, YMR303C, YJR155W, YCR107W, YDL243C
GO:0015144	carbohydrate transmembrane transporter activity	0.007221389	0.00%	0	YBR298C, YJL219W, YLR081W, YOL156W
GO:0016614	oxidoreductase activity, acting on CH-OH group of donors	0.00750681	0.00%	0	YOL165C, YNL331C, YDL243C, YCR107W, YJR155W, YMR303C

Component

GOID	TERM	CORRECTED PVALUE	FDR RATE	EXPECTED FALSE POSITIVES	ANNOTATED GENES
GO:0071944	cell periphery	2.20E-10	0.00%	0	YAR020C, YIL162W, YCR010C, YOL161C, YBR298C, YFL020C, YGL255W, YGL053W, YAR071W, YML125C, YIL169C, YOL155C, YCR002C, YLR461W, YCL008C, YDR542W, YOL156W, YKL224C, YLR081W, YAR031W, YJL219W, YIR039C, YCR009C, YOL159C, YBL108C-A, YIL166C, YCR004C, YOL158C
GO:0009277	fungal-type cell wall	6.09E-06	0.00%	0	YLR461W, YDR542W, YAR020C, YAR071W, YOL161C, YBL108C-A, YOL155C, YFL020C, YKL224C, YIR039C
GO:0005618	cell wall	9.30E-06	0.00%	0	YFL020C, YBL108C-A, YOL155C, YOL161C, YIR039C, YKL224C, YDR542W, YLR461W, YAR071W, YAR020C
GO:0030312	external encapsulating structure	9.30E-06	0.00%	0	YAR071W, YAR020C, YDR542W, YLR461W, YIR039C, YKL224C, YFL020C, YOL161C, YOL155C, YBL108C-A
GO:0005773	vacuole	0.003474722	0.00%	0	YCR010C, YKL224C, YFL020C, YOL161C, YIL162W, YDR542W, YLR461W, YOL158C, YIL166C, YCL001W, YHL048W, YGR295C, YJL219W, YCL005W-A
GO:0000322	storage vacuole	0.004817282	0.33%	0.02	YIL162W, YDR542W, YLR461W, YKL224C, YFL020C, YOL161C, YCL001W, YGR295C, YHL048W, YJL219W, YCL005W-A, YOL158C, YIL166C
GO:0000323	lytic vacuole	0.004817282	0.29%	0.02	YIL162W, YLR461W, YDR542W, YKL224C, YOL161C, YFL020C, YHL048W, YGR295C, YCL001W, YCL005W-A, YJL219W, YOL158C, YIL166C
GO:0000324	fungal-type vacuole	0.004817282	0.25%	0.02	YIL162W, YLR461W, YDR542W, YKL224C, YOL161C, YFL020C, YGR295C, YHL048W, YCL001W, YCL005W-A, YJL219W, YOL158C, YIL166C

Supplementary Table S10: Gene Status

Haplotype information for the 6 genes MAL11, PAD1, FDC1, GAL2, ADH2 and SFA1 for all 35 strains. The positions given are relative to reference sequence of the gene, starting with the first base of the CDS as base number 1.

Only MAL11 is shown here. The full table can be found in the companion document accessible from the appendices.

	Gene	MAL11			
Group	Strain	Intact	Inactivating Indel	Nonsense mutation	SV
African Beer	BEM	NA	NA	NA	Gene is absent
	BHA	Yes	None	None	None
	ANL	NA	NA	NA	Gene is absent
	AVN	NA	NA	NA	Gene is absent
	AVQ	Yes	None	None	None
	AVS	Yes	None	None	None
	AVT	Yes	None	None	None
	ASC	NA	NA	NA	Gene is absent
European dominant	CFE	No	hom 1772CA → C	None	None
	ASD	Yes	None	None	None
	CPB	No	hom 1772CA → C	None	None
	CFF	No	hom 1175A → AT	None	None
	AFP	No	hom 1772CA → C	None	None
	AQH	No	hom 1772CA → C	None	None
	ARE	No	het 1175A → AT; het 1772CA → C	None	None
	ASB	No	hom 1175A → AT	None	None
Asian dominant (Belgian)	CFN	No	het 1772CA → C	None	None
	CFP	No	het 1772CA → C	None	None
	BDL	No	hom 1772CA → C	None	None
	CFC	No	hom 1175A → AT	None	None
	YMD1873	No	het 1175A → AT	None	None

Asian dominant (Belgian)	BBG	Yes	None	None	None
	YMD1871	No	het 1175A → AT	None	None
	CGC	No	hom 1175A → AT	None	None
	AQT	No	het 1175A → AT	None	None
	BSI	No	het 1175A → AT	None	None
	YMD1950	No	het 1175A → AT	None	None
	YMD4285	No	het 1175A → AT	None	None
	BRP	No	het 1175A → AT	None	None
Asian dominant (British)	CFG	Yes	None	None	None
	CFH	Yes	None	None	None
	CFM	Yes	None	None	None
	YMD1864	Yes	None	None	None
	YMD1870	Yes	None	None	None
	YMD1981	Yes	None	None	None

Supplementary Table S11: GAL2 Diversity

Mean, minimum and maximum divergence levels observed within groups for the various haplotypes of GAL2 (%).

Group	African Beer	European dominant	Asian dominant
African Beer	1.46	2.84	2.84
European dominant	2.84	0.28	0.27
Asian dominant	2.83	0.27	0.20

Minimum divergence levels observed within groups for the various haplotypes of GAL2 (%).

Group	African Beer	European dominant	Asian dominant
African Beer	0.00	1.56	1.5
European dominant	1.56	0.00	0.00
Asian dominant	1.50	0.00	0.00

Maximum divergence levels observed within groups for the various haplotypes of GAL2 (%).

Group	African Beer	European dominant	Asian dominant
African Beer	3.47	4.05	4.05
European dominant	4.05	0.52	0.57
Asian dominant	4.05	0.57	0.57

Availability of data

Oxford Nanopore and Illumina sequencing data are available under the study accession number PRJEB46384.

Illumina short read data for the *Saccharomyces cerevisiae* strains is taken from the 1,011 yeast genomes project and their SRA accession numbers are given in Supplemental Table 1.

References

1. Legras, J.-L., Merdinoglu, D., Cornuet, J.-M. & Karst, F. Bread, beer and wine: Saccharomyces cerevisiae diversity reflects human history. Mol. Ecol. 16, 2091–2102 (2007).
2. Schacherer, J., Shapiro, J. A., Ruderfer, D. M. & Kruglyak, L. Comprehensive polymorphism survey elucidates population structure of Saccharomyces cerevisiae. Nature 458, 342–345 (2009).
3. Ludlow, C. L. et al. Independent Origins of Yeast Associated with Coffee and Cacao Fermentation. Curr. Biol. 26, 965–971 (2016).
4. Gallone, B. et al. Domestication and Divergence of Saccharomyces cerevisiae Beer Yeasts. Cell 166, 1397-1410.e16 (2016).
5. Gonçalves, M. et al. Distinct Domestication Trajectories in Top-Fermenting Beer Yeasts and Wine Yeasts. Curr. Biol. 26, 2750–2761 (2016).
6. Peter, J. et al. Genome evolution across 1,011 Saccharomyces cerevisiae isolates. Nature 556, 339–344 (2018).
7. Legras, J.-L. et al. Adaptation of S. cerevisiae to Fermented Food Environments Reveals Remarkable Genome Plasticity and the Footprints of Domestication. Mol. Biol. Evol. 35, 1712–1727 (2018).
8. Fay, J. C. et al. A polyploid admixed origin of beer yeasts derived from European and Asian wine populations. PLoS Biol. 17, e3000147 (2019).
9. Barnett, J. A. & Lichtenthaler, F. W. A history of research on yeasts 3: Emil Fischer, Eduard Buchner and their contemporaries, 1880-1900. Yeast Chichester Engl. 18, 363–388 (2001).
10. Steensels, J., Gallone, B., Voordeckers, K. & Verstrepen, K. J. Domestication of Industrial Microbes. Curr. Biol. 29, R381–R393 (2019).
11. Udom, N., Chansongkrow, P., Charoensawan, V. & Auesukaree, C. Coordination of the Cell Wall Integrity and High-Osmolarity Glycerol Pathways in Response to Ethanol Stress in Saccharomyces cerevisiae. Appl. Environ. Microbiol. 85, e00551-19 (2019).
12. Gagnon-Arsenault, I., Tremblay, J. & Bourbonnais, Y. Fungal yapsins and cell wall: a unique family of aspartic peptidases for a distinctive cellular function. FEMS Yeast Res. 6, 966–978 (2006).
13. Szoradi, T. et al. SHRED Is a Regulatory Cascade that Reprograms Ubr1 Substrate Specificity for Enhanced Protein Quality Control during Stress. Mol. Cell 70, 1025-1037.e5 (2018).
14. Charoenbhakdi, S., Dokpikul, T., Burphan, T., Techo, T. & Auesukaree, C. Vacuolar H+-ATPase Protects Saccharomyces cerevisiae Cells against Ethanol-Induced Oxidative and Cell Wall Stresses. Appl. Environ. Microbiol. 82, 3121–3130 (2016).

15. Holzapfel, W. H. Appropriate starter culture technologies for small-scale fermentation in developing countries. Int. J. Food Microbiol. 75, 197–212 (2002).
16. Johansen, P. G., Owusu-Kwarteng, J., Parkouda, C., Padonou, S. W. & Jespersen, L. Occurrence and Importance of Yeasts in Indigenous Fermented Food and Beverages Produced in Sub-Saharan Africa. Front. Microbiol. 10, 1789 (2019).
17. Adebo, O. A. African Sorghum-Based Fermented Foods: Past, Current and Future Prospects. Nutrients 12, 1111 (2020).
18. Bokulich, N. A. & Bamforth, C. W. The Microbiology of Malting and Brewing. Microbiol. Mol. Biol. Rev. 77, 157–172 (2013).
19. Lengeler, K. B., Stovicek, V., Fennessy, R. T., Katz, M. & Förster, J. Never Change a Brewing Yeast? Why Not, There Are Plenty to Choose From. Front. Genet. 11, (2020).
20. Whittington, H. D., Dagher, S. F. & Bruno-Bárcena, J. M. Production and Conservation of Starter Cultures: From "Backslopping" to Controlled Fermentations. in How Fermented Foods Feed a Healthy Gut Microbiota: A Nutrition Continuum (eds. Azcarate-Peril, M. A., Arnold, R. R. & Bruno-Bárcena, J. M.) 125–138 (Springer International Publishing, 2019). doi:10.1007/978-3-030-28737-5_5.
21. Teste, M.-A., François, J. M. & Parrou, J.-L. Characterization of a new multigene family encoding isomaltases in the yeast Saccharomyces cerevisiae, the IMA family. J. Biol. Chem. 285, 26815–26824 (2010).
22. Dickinson, J. R., Salgado, L. E. J. & Hewlins, M. J. E. The Catabolism of Amino Acids to Long Chain and Complex Alcohols in Saccharomyces cerevisiae *. J. Biol. Chem. 278, 8028–8034 (2003).
23. Hazelwood, L. A., Daran, J.-M., van Maris, A. J. A., Pronk, J. T. & Dickinson, J. R. The Ehrlich Pathway for Fusel Alcohol Production: a Century of Research on Saccharomyces cerevisiae Metabolism. Appl. Environ. Microbiol. 74, 2259–2266 (2008).
24. Abou Saada, O., Tsouris, A., Eberlein, C., Friedrich, A. & Schacherer, J. nPhase: an accurate and contiguous phasing method for polyploids. Genome Biol. 22, 1–27 (2021).
25. Jacobus, A. P. et al. Comparative Genomics Supports That Brazilian Bioethanol Saccharomyces cerevisiae Comprise a Unified Group of Domesticated Strains Related to Cachaça Spirit Yeasts. Front. Microbiol. 12, (2021).
26. Krysan, D. J., Ting, E. L., Abeijon, C., Kroos, L. & Fuller, R. S. Yapsins Are a Family of Aspartyl Proteases Required for Cell Wall Integrity in Saccharomyces cerevisiae. Eukaryot. Cell 4, 1364–1374 (2005).
27. Verbelen, P. J., Saerens, S. M. G., Van Mulders, S. E., Delvaux, F. & Delvaux, F. R. The role of oxygen in yeast metabolism during high cell density brewery fermentations. Appl. Microbiol. Biotechnol. 82, 1143–1156 (2009).
28. Duan, S.-F. et al. Reverse Evolution of a Classic Gene Network in Yeast Offers a Competitive Advantage. Curr. Biol. CB 29, 1126-1136.e5 (2019).

29. Boocock, J., Sadhu, M. J., Durvasula, A., Bloom, J. S. & Kruglyak, L. Ancient balancing selection maintains incompatible versions of the galactose pathway in yeast. Science 371, 415–419 (2021).
30. Wang, Z.-Y., Wang, J.-J., Liu, X.-F., He, X.-P. & Zhang, B.-R. Recombinant industrial brewing yeast strains with ADH2 interruption using self-cloning GSH1+CUP1 cassette. FEMS Yeast Res. 9, 574–581 (2009).
31. Istace, B. et al. de novo assembly and population genomic survey of natural yeast isolates with the Oxford Nanopore MinION sequencer. GigaScience 6, 1–13 (2017).
32. McKenna, A. et al. The Genome Analysis Toolkit: a MapReduce framework for analyzing next-generation DNA sequencing data. Genome Res. 20, 1297–1303 (2010).
33. Paradis, E., Claude, J. & Strimmer, K. APE: Analyses of Phylogenetics and Evolution in R language. Bioinformatics 20, 289–290 (2004).
34. Zheng, X. et al. A high-performance computing toolset for relatedness and principal component analysis of SNP data. Bioinformatics 28, 3326–3328 (2012).
35. Danecek, P. et al. Twelve years of SAMtools and BCFtools. GigaScience 10, giab008 (2021).
36. Engel, S. R. et al. The Reference Genome Sequence of Saccharomyces cerevisiae: Then and Now. G3 GenesGenomesGenetics 4, 389–398 (2013).
37. Boyle, E. I. et al. GO::TermFinder--open source software for accessing Gene Ontology information and finding significantly enriched Gene Ontology terms associated with a list of genes. Bioinforma. Oxf. Engl. 20, 3710–3715 (2004).
38. Li, H. Aligning sequence reads, clone sequences and assembly contigs with BWA-MEM. ArXiv13033997 Q-Bio (2013).
39. Ramírez, F. et al. deepTools2: a next generation web server for deep-sequencing data analysis. Nucleic Acids Res. 44, W160–W165 (2016).
40. Wong, B. Points of view: Color blindness. Nat. Methods 8, 441–441 (2011).

Chapter III – Different trajectories of polyploidization shape the genomic landscape of the *Brettanomyces bruxellensis* yeast species

Abstract

Polyploidization events are observed across the tree of life and occurred in many fungi, plant and animal species. During evolution, polyploidy is thought to be an important source of speciation and tumorigenesis. However, the origin of polyploid populations is not always clear and little is known about the precise nature and structure of their complex genomes. Using a long-read sequencing strategy, we sequenced 71 strains of the *Brettanomyces bruxellensis* yeast species, which is found in anthropized environments (*e.g.* beer, kombucha, ethanol production and contaminant of wine) and characterized by several distinct polyploid subpopulations. To reconstruct the polyploid genomes, we phased them by using different strategies and we found that each subpopulation had a unique polyploidization history with distinct trajectories. The polyploid genomes contain either genetically closely related copies (genetic divergence < 1%) or diverged copies (> 3%), indicating auto- as well as allopolyploidization events. Allopolyploidization has occurred independently for each polyploid subpopulation, involving a specific and unique donor each time. Our analysis rules out known *Brettanomyces* sister species as possible donors. Finally, loss of heterozygosity events have shaped the structure of these polyploid genomes and underline their dynamics. Overall, our study highlighted the multiplicity of the trajectories leading to polyploidy within the same species.

Introduction

Polyploidy, a state in which organisms carry more than two sets of chromosomes, is a phenomenon that can be observed throughout plant, animal and fungal species. Interest in polyploidization has increased due to its tremendous effects on the evolution of species or its involvement in cancerogenesis[1–3]. The most obvious and probably well studied polyploidization events in the tree of life are Whole Genome Duplication (WGD) events, which are usually followed by subsequent and massive diversification. One example is the series of two ancient WGD events that occurred in the lineage leading to the ancestor of all vertebrates ~450 million years ago, and have significantly contributed to the subsequent evolution of 60,000 extant species[4,5].

There are different mechanisms to become polyploid[6,7]. The doubling of one's own genome or the generation of a hybrid from individuals of the same species would both lead to multiple genomic copies of identical or similar descent, which defines the mechanisms of autopolyplodization. Alternatively, interspecific hybridization would cause the acquisition of additional chromosomal sets harboring higher genetic variation, which defines allopolyploidization. While it is well established that a polyploid state causes genomic conflicts, leads to genome instability, or reduces gamete formation, on the contrary, genomic reorganization can ultimately promote diversification through the additional genomic information[8–10]. Therefore, polyploidy can play a predominant role in bursts of adaptive divergence and speciation[11,12]. Polyploidy can be beneficial under certain environmental circumstances and increases the potential for adaptability, taking advantage of evolutionary innovations from neo- and sub-functionalization of duplicated genes[13,14]. Environmental changes that require a fast adaptation for example can trigger the prevalence of polyploids, which at least for short-term timescales may

provide an adaptive advantage through genomic flexibility rather than simply being the “dead-end”.

Some taxa are believed to be more stable in polyploid states than others. These are known to be found frequently among plants, which in contrast to animals are characterized by a development that seems to be more robust to genomic perturbations[15]. Studies suggest that up to 70% of flowering plants originate from polyploid ancestors, putting it as a major contributor in the evolution of species[16,17]. But it is also suspected in animals that polyploidization plays an even more prevalent role than currently shown, limited by the analytic tools and effort detecting them. While animals are characterized by less stability in polyploids, it is well established that most of the vertebrate species originate from ancient polyploidization events too[2,18]. At the same time, polyploidy is also increasingly observed in single-cell organisms such as yeasts[19–21], suggesting that this state can serve as a rapid response to ecological or human-made changes in artificial environments, coevolution or enable invasions by the acquisition or maintenance of additional full sets of chromosomes[10,22–24]. In the lineage leading to *Saccharomyces cerevisiae*, a hybridization event between two ancestral species has been followed by subsequent WGD, a means by which, in the subsequent process of extensive genome reorganization, high fertility could be retained[25–28]. Moreover, the prevalence of polyploidy, currently observed in *S. cerevisiae* is approximately 11.5%, as shown in a recent study of 1,011 whole-genome sequenced isolates[21]. Polyploids are particularly enriched in subpopulations associated with the production of beer or bread, highlighting that its domestication most likely triggered the appearance of polyploids to fulfil the desired requirements in industrial settings.

With polyploidization being recognized as a ubiquitous mechanism in nature with almost unpredictable consequences in terms of genomic conflicts or adaptability, we

are still starting to fully resolve and understand the genomic architecture of natural polyploid populations, their prevalence, and trajectories especially within the same species. Access to long-read sequencing data has accelerated research on polyploid and hybrid genomes. However, the biggest challenge is still the correct phasing of haplotypes, to separate the different sets of chromosomes without any prior knowledge of ploidy and levels of genetic variation between genomic copies (sometimes referred to as subgenomes). Here, we focused on the *Brettanomyces bruxellensis* yeast species, a genetically diverse species with different subpopulations of various levels of ploidy which allows us to shed light into several questions related to polyploidization. As seen for other yeasts of the *Saccharomycotina* subphylum, the link between ecological origin and genetic differentiation for the different *B. bruxellensis* clades is primarily supposed to be driven by its anthropogenic influences[29,30]. Multiple genetically distinct subpopulations (clusters) correspond to different ecological niches: wine, beer, tequila/bioethanol, kombucha and soft drinks[31].

To study their genomic complexity and allow a detailed view of their genomic architecture for the first time, we sequenced a subset of 71 *B. bruxellensis* strains from different subpopulations with long and short read sequencing strategies. By using two complex phasing strategies, we studied different trajectories of polyploidization in an ecological diverse population.

Results

Conserved clusters of polyploid isolates

Brettanomyces bruxellensis is known as a diverse species with genetically and ecologically distinct clusters, and various levels of ploidy[31–33]. To dissect the genomic architecture and further understand the origin as well as the trajectories of recently described polyploid groups, we selected 71 strains with 51 coming from subpopulations defined as polyploids[31] (Figure 1A; Supplementary Table S1). Most of the strains were isolated in Europe and stem from different ecological origins: beer (n=25), wine (n=36), tequila/bioethanol (n=7) and kombucha (n=3).

To have a deep insight into the population structure and ploidy levels, we first sequenced the 71 genomes using a whole genome Illumina short-read sequencing strategy with a 16.9-fold mean coverage. Using this dataset, we sampled 24,313 genetic variants evenly distributed across the genome and performed a phylogenetic analysis (Figure 1B). All 71 strains were clustered into six well-defined lineages which correlate with environmental niches, corroborating previous reports[31–33]. We then assigned a ploidy to each of the strains using SNP frequency distributions within the sequence reads. We categorized their level of ploidy as either being diploid (with SNPs at allele frequencies of 0.5 and 1), triploid (with SNPs at allele frequencies of 0.33 and 0.67) or tetraploid (with SNPs at allele frequencies of 0.25, 0.5, 0.75 and 1) (Supplementary Figure S1A). We found that the level of ploidy is conserved within, but varies across subpopulations (Figure 1B). The wine 1, wine 2 and beer subpopulations are triploid while the wine 3 and kombucha subpopulations are diploid. The exception is a single tetraploid kombucha strain (Supplementary Figure S1A). The teq/EtOH clade harbors one diploid and three triploid strains while the ploidy could not be assigned to three of the four other isolates (Supplementary Figure S1A). For one strain (I_H06_YJS78889), we could neither identify its ploidy, nor assign it to one of the six subpopulations. To exclude the possibility that aneuploidies

are causing the non-assignment of ploidy levels for the four strains, we looked at read coverage across their genome to identify regions that are absent or present in multiple copies (Supplementary Figure S1B-C). We showed that the coverage is stable and that these strains do not contain regions with varying coverage explaining our results.

Overall, we highlight that the level of ploidy is conserved within genetically diverged subpopulations, but not across them. We showed that the teq/EtOH strains are the most diverse subpopulation and confirmed previous data that additionally suggested this subpopulation as the oldest of the different *B. bruxellensis* clades[33]. The teq/EtOH strains stand in contrast to other subpopulations like wine 3, which shows the lowest degree of genetic variation, suggesting a single ancestral origin with a recent expansion.

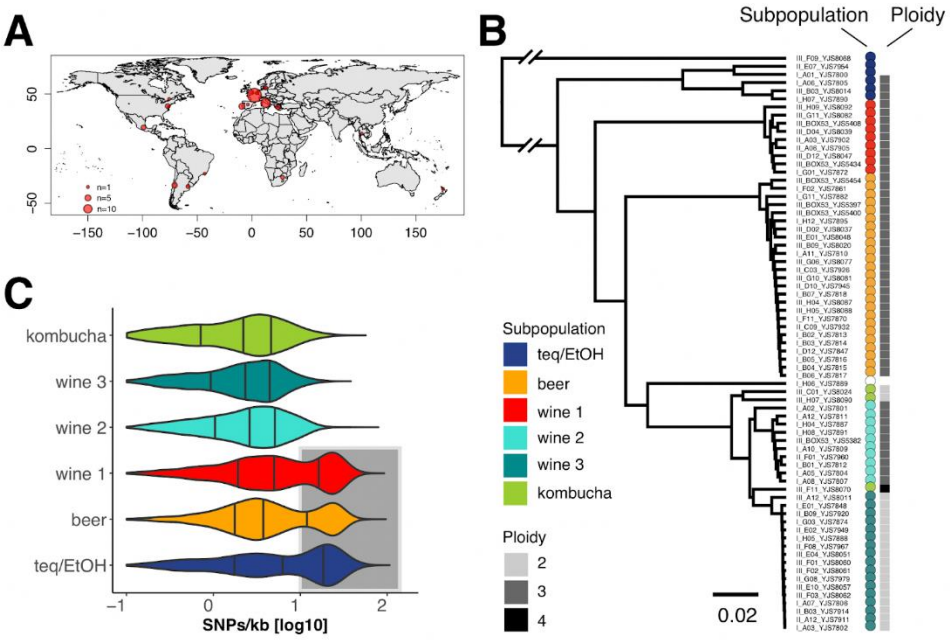

Figure 1 - Ploidy and intra-genomic variation

A. Strain collection. The 71 sequenced strains come from the collection of 1,500 isolates[31] and were isolated in different regions worldwide, where they are associated with anthropized environments such as tequila/bioethanol, beer, wine and kombucha production.

B. Genetic relationship and ploidy level. The sequenced strains, here clustered based on Illumina short read sequencing data (75PE), segregate into six genetically distinct subpopulations, namely tequila/bioethanol (teq/EtOH), beer, wine (1-3) and kombucha (based on 24,313 genome-wide distributed variants). Forty-eight strains were detected as triploids (69%) coming from five of the six subpopulations: teq/EtOH, beer, wine (1,2) and kombucha (inferred from genome-wide allele frequencies).

C. Genetic diversity within clades inferred from long-read sequencing data. The three subpopulations teq/EtOH (n=5), beer (n=22) and wine 1 (n=7) harbor strains with two clusters of reads bearing low and high genetic variation (underlaid in grey) compared to the reference genome *Brettanomyces bruxellensis*[36]. The subpopulation wine 2 (n=9), although being polyploid (B), lacks genomic regions with high genetic variation to the reference genome. The three lines within each distribution show the 25%, 50 and 75% quartiles.

Strategies used to phase the *B. bruxellensis* polyploid genomes

In order to resolve the genomic structure of polyploid isolates, we sequenced the genomes of the 71 strains using the Oxford Nanopore sequencing strategy. Long-read sequencing has become the strategy of choice to best resolve structural variation and build high quality *de novo* reference assemblies. The difficulty of resolving polyploid genomes, however, lies especially in the attempt to distinguish between the different haplotypes, which are present as independent genomic copies within the same genomes. We will hereafter refer to distinct genomic entities of different descendants within the same genome as genomic copies. While *de novo* assemblers are not capable of fully differentiating between different haplotypes in polyploids, seeking instead to provide collapsed haplotypes, several alignment-based algorithms have been developed recently to cope with the genomic architecture of polyploid genomes[34,35]. They all aim to phase haplotypes into independent entities, but they vary in performance based on factors such as ploidy, coverage, and the level of genetic divergence between genomic copies of the polyploid genomes.

To properly phase our polyploid genomes, we sought to apply different strategies depending on the level of divergence of the copies constituting these genomes to the *B. bruxellensis* reference genome[36]. Reasons to expect that there are different levels of variation relative to the reference have been identified by previous studies, which indicated that at least two individual polyploid isolates from the wine 1 and beer subpopulations have likely experienced polyploidization events by acquiring an additional genomic copy of high genetic variation[37].

To estimate the genetic divergence, we aligned the long reads of each strain to the *B. bruxellensis* reference genome (Supplementary Figure S2A). We identified three subpopulations (teq/EtOH, beer and wine 1) for which the genetic variation results in a bimodal distribution with a cluster of reads that have a low level of genetic

variation relative to the reference and a second cluster of reads that have a high genetic variation level relative to the reference (Figure 1C). These subpopulations stand in contrast to the other three subpopulations (wine 2, wine 3 and kombucha), which solely consist of low genetic divergence reads. Strikingly, wine 2 is the only polyploid subpopulation which bears reads with only low genetic diversity. It is hereafter assumed that "low genetic diversity/genomic variation" and "high genetic diversity/genomic variation" are understood to refer to the distance to the *B. bruxellensis* reference genome.

Given two types of polyploid subpopulations exhibiting either low or high genomic variation, we applied two different phasing strategies to study their genomic architecture.

(1) To resolve the origin of the genetic diversity, and to determine if the cluster with reads of high genetic variation corresponds to an additional genomic copy, we separated the long reads into distinct clusters based on their diversity level. We clustered reads with peaks of low genetic variation at 2 SNPs per kb and high genetic variation exhibiting 24.4 SNPs per kb, yielding a set of lowly divergent reads and one of highly divergent reads (Supplementary Figure S2A-B). Reads between the two distributions (*i.e.* with a variation between 10 and 14 SNPs per kb) were conservatively ignored due to the ambiguity of which cluster they should be assigned to (Supplementary Figure S2B). Using these two sets of reads, we generated *de novo* assemblies to recreate phased copies of these polyploid genomes.

(2) The low genetic variation observed in the polyploid wine 2 subpopulation did not allow us to separate reads based on their genetic divergence (Figure 1C). Consequently, we used nPhase, a phasing algorithm that we recently developed[35]. Briefly, nPhase resolves the genome into distinct haplotypes and provides accurate

and contiguous haplotype predictions using short and long read sequencing data without any prior information of the true ploidy. It accurately identifies heterozygous positions using highly accurate short reads and clusters long reads into haplotypes based on the presence of similar heterozygous SNP profiles[35].

Genomic architecture of the polyploid wine 2 subpopulation

We applied the nPhase phasing algorithm to the sequenced genomes of the wine 2 subpopulation which exhibit exclusively low intra-genomic variation. We focused on six of the ten strains for which we had high quality long and short read sequencing data, allowing us to phase their genome properly into independent haplotigs (Figure 2; Supplementary Figure S3A).

We observed that the chromosomes are phased into regions underlying in most cases two or three haplotigs (Supplementary Figure S3A). Some regions bear multiple and often small haplotigs, and underline the difficulty in phasing polyploid genomes with haplotypes that reflect high genetic similarity. In addition, the level of genetic divergence varies along the genomes of the six strains. Whenever nPhase resolves a region into two haplotigs, the genetic variation in these regions is lower compared to regions where it distinguishes between three haplotigs (Figure 2A). Here, the highest genetic variation in the presence of two haplotigs is 0.93%, while on average it is as low as 0.09% (Figure 2B, Supplementary Figure S3B). In the presence of a third phased haplotig, the genetic variation can be as high as 1.79% with an average genetic variation of 0.54% (Figure 2B, Supplementary Figure S3C). Consistent coverage levels support the hypothesis that the prediction of only two haplotypes is not due to the absence of a third copy for part of the chromosome (Figure 2A). Therefore, while the differentiation of three haplotigs underlines the existence of three genetically different genomic copies at that site, the phasing resolving into two

haplotigs represent a region with two identical haplotypes plus the existence of genetically different copy.

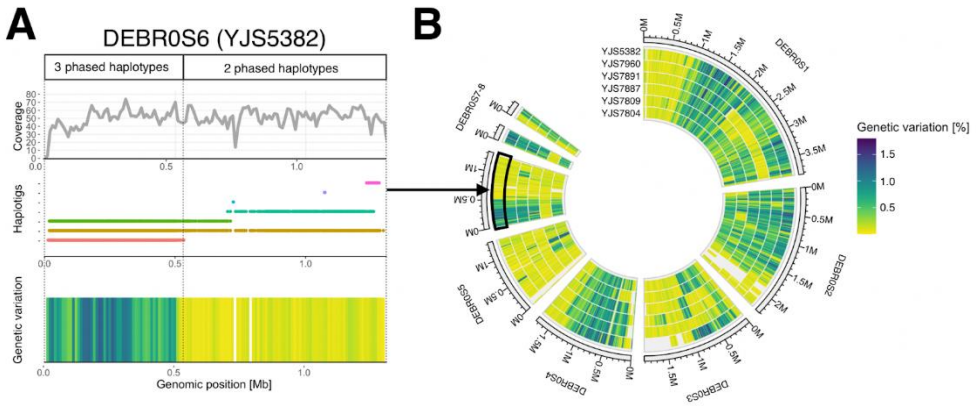

Figure 2 - Autopolyploidization for the wine 2 subpopulation
A Separation of haplotypes. Phasing the genomes of strains from the polyploid wine 2 subpopulation resolves the generally low intra-genomic variation into haplotigs along the genome. The presence of two haplotypes results in lower genetic variation as it does when three haplotigs are present at a given position. Maximal genetic variation between haplotypes increases from 0.93 % to 1.79 % with the presence of a third phased haplotype. To control that the variations in genetic difference are not artefacts caused by variable coverage along these regions, the genome-wide coverage was calculated. The coverage is consistent across regions that harbor either two or three phased haplotypes.
B. Conserved patterns of phased haplotypes along the genomes of six strains of the wine 2 subpopulation. Having either two or three phased haplotypes at a site is conserved among different strains from the same subpopulation.

Further, we can show the presence of conserved regions in all six strains that are characterized by the presence/absence of a third phased haplotype (Figure 2B; Supplementary Figure S3B-C). Some regions, for example the first 1 Mb on chromosome 1, are characterised by two identical copies and a non-identical copy, resolving into two phased haplotypes. This region is followed by another 1 Mb region, which is resolved into three haplotypes in all six strains. An explanation for the alternation of such regions phased into two or three haplotypes is the occurrence

of loss of heterozygosity (LOH) events. LOH events are characterized by the absence of polymorphic markers that distinguish different genomic copies in otherwise heterozygous diploid or polyploid individuals and consequently reduce the genetic variation. nPhase outputs only unique haplotypes present in the data, even if one haplotype contains twice the number of reads as the other, directly showing how LOH events shape the haplotypes found in a genome.

Moreover, the existence of the conserved regions of LOH events among the six strains could suggest hotspots for LOH events. Such hotspots have been shown in other species like *S. cerevisiae*[21] where they frequently reduce genetic variation. Alternatively, this conserved pattern could also hint at a recent common ancestor. However these strains were isolated from two countries on different continents (Supplementary Table S1), making this explanation less likely.

Overall, the utilization of long and short read sequences in combination with complex phasing strategies enables us to decipher the genomic structure of polyploid genomes of low genetic variation and allows us to study its dynamics. In the wine 2 subpopulation, the only polyploid clade with a low intra-genomic variation, the genomes of six strains revealed conserved regions having undergone LOH events.

Three polyploid clades contain a genetically diverged genomic copy

Next, we focused on the triploid genomes of the teq/EtOH, beer and wine 1 subpopulations, which exhibit genetically very heterogeneous genomes. To enable comparative analyses, we first separated long reads based on their genetic divergence compared to the reference genome (Supplementary Figure S2A). We clustered long reads from the bimodal distribution with reads bearing low genetic variation (peak at 2 SNPs per kb) and reads with high genetic variation (peak at 24.4 SNPs per kb) (Supplementary Figure S2B). As previously mentioned, reads with a variation between 10 and 14 SNPs per kb were ignored to avoid assigning reads to the wrong cluster. The determination of the ratio between the number of reads with a low genetic variation and the total coverage (all reads) within 10 kb windows across the genome allowed us to determine the average genomic ploidy level of each strain at a given genomic position (Supplementary Figure S4A). We identified that the three groups (teq/EtOH, beer and wine 1) contained two genomic copies with low genetic variation and a single genomic copy that exhibits a high genetic divergence (or vice versa), which on average complemented to 3n genome-wide (Supplementary Figure S4B).

The fact that the beer and wine 1 subpopulations contain isolates with higher genetic variation compared to the reference genome was already shown previously for a single strain from each subpopulation[37]. The authors claimed the possibility of interspecific hybridization events having taken place. We can, for the first time, highlight that this phenomenon of having a genetically different genomic copy within these subpopulations is frequent and conserved. Additionally, while previous analyses have underpinned the prevalence of polyploid strains in the teq/EtOH subpopulation, we can also show that teq/EtOH strains contain a genomic copy as genetically different to the reference genome of *B. bruxellensis* as in beer and wine 1 isolates.

To ultimately allow comparative studies between the different genomic copies among these genomes as well as with genomes from the other subpopulations, we first performed *de novo* genome assemblies using *SMARTdenovo*[38]. First, we used only the long reads that contained low genetic variation for all strains from the three subpopulations (teq/EtOH, beer and wine 1). We repeated this step independently for the long reads that were exclusively bearing high genetic variation to the reference genome to prepare *de novo* assemblies (Supplementary Figure S5; Supplementary Table S2). Then, we created group-specific reference genomes by concatenating the *de novo* assemblies generated from low and high genomic variation reads (See Material and Methods). This was done for a representative strain from each group. By performing a competitive mapping approach using these group-specific reference genomes with scaffolds made from low and high genetic variation, we separated the short reads for each strain from the three groups into two groups: short reads with low genetic variation and short reads with high genetic variation (teq/EtOH, beer and wine 1) (Supplementary Figure S5). Then, we aligned the short reads independently back to the *B. bruxellensis* reference genome. For strains that were either diploid, or polyploid with exclusively low genetic variation, we aligned short read sequences directly to the reference genome (wine 2, wine 3 and kombucha subpopulations).

First, we determined if there was any bias in the mapping rates of short reads to the reference genome/assemblies, comparing the high diversity strains aligned to the *de novo* assemblies and the low diversity strains aligned to the *B. bruxellensis* reference genome. Both showed similar alignment rates, respectively 94% and 92.5% indicating no bias in the alignment due to the applied phasing strategy. Then, we determined the genetic diversity of the 71 strains by performing a principal component analysis (Figure 3A). By looking at the first two principal components explaining 53.7% of the variation from 24,110 sampled genome-wide distributed

SNPs, we can show that the genomic copies with high genetic variation (‘High’) of 40 strains from the teq/EtOH, beer and wine 1 subpopulations are clearly distinct from the genomic copies with low genetic variation (‘Low’), and cluster in a group-specific way.

We then checked the genetic relationships of the genomic copies with only low genomic variation, since such genomic copies were present in all 71 strains (Figure 3B). We can show that the strains cluster in the six subpopulations as previously observed using raw Illumina data (Figure 1B). The strain I_H06_YJS7889, initially unable to be associated with a subpopulation, now clusters with other teq/EtOH strains.

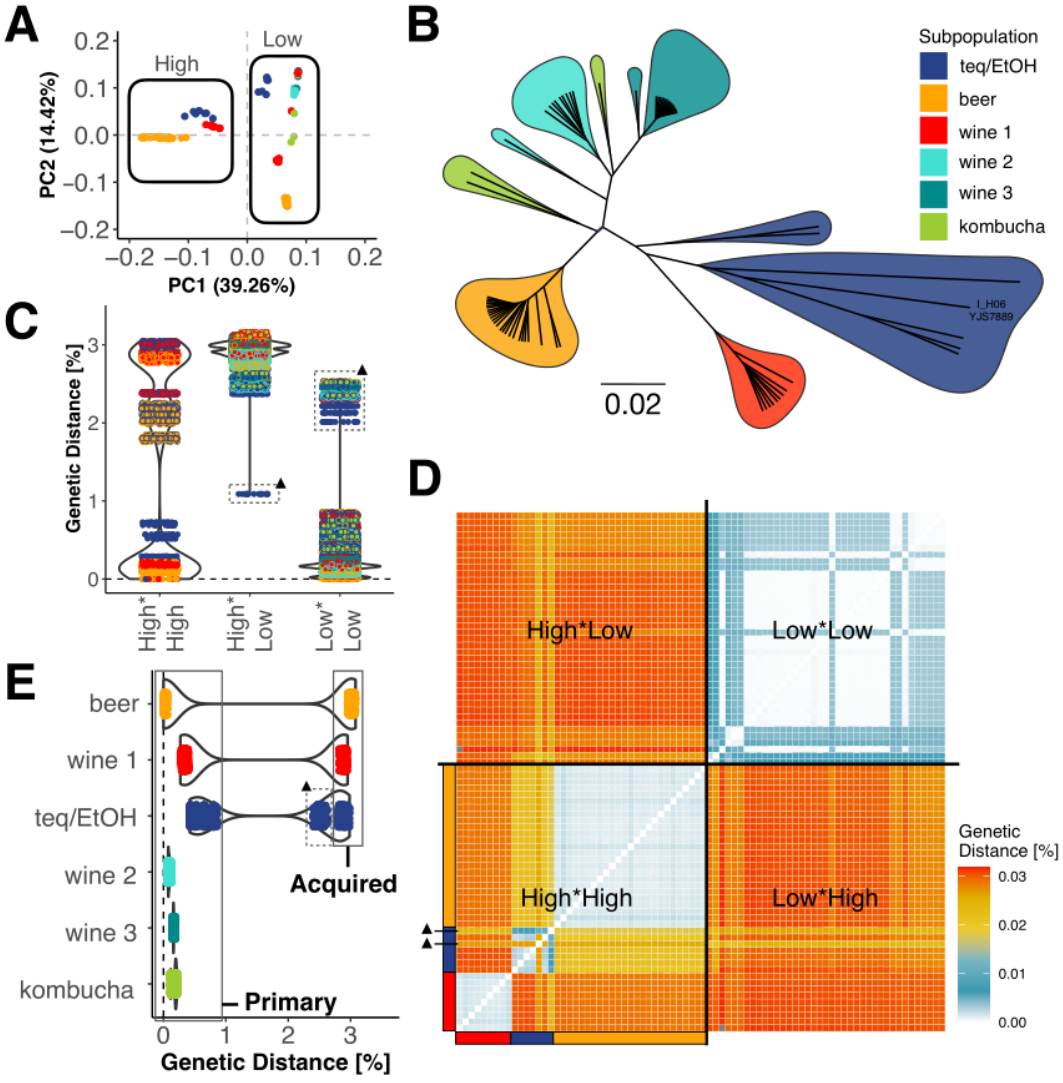
A
High
Low
PC2 (14.42%)
PC1 (39.26%)
B
Subpopulation
teq/EtOH
beer
wine 1
wine 2
wine 3
kombucha
0.02
C
Genetic Distance [%]
High* High
High* Low
Low* Low
D
High*Low
Low*Low
High*High
Low*High
Genetic Distance [%]
E
beer
wine 1
teq/EtOH
wine 2
wine 3
kombucha
Acquired
Primary
Genetic Distance [%]

Figure 3 - Three independent interspecific hybridization events

A. Three distinct clusters of genomic copies with high genetic variation. A principal component analysis shows that the genomic copies with high genetic variation to the reference genome of strains in the subpopulations teq/EtOH, beer and wine 1 are not only different to the genomic copy with low genetic variation, but are also genetically distinct between subpopulations (based on 24,110 genome-wide distributed SNPs).

B. Phylogenetic relationship from reads with low genetic variation to the reference genome. The genomic copies with low genetic variation are different between the six subpopulations teq/EtOH, beer, wine 1-3 and kombucha, which group according to their ecological origin (based on 24,110 genome-wide distributed SNPs).

C-E. Pairwise genetic diversity between genomic copies from imputed whole-genome sequences. C Left (High*High): Pairwise comparison of the genomic copies with high levels of intra-genomic variation between strains of the same subpopulations (single-colored dots) show a genetic diversity of less than 1% (average of 0.13%). Between strains from different subpopulations (two colored dots indicate the subpopulation dependency of the compared strains), this diversity varies between 1.76% and 3.05%. Middle (High*Low): The genetic distance between the genomic copies with low and high levels of variation, irrespective if it is within the same or between strains, is on average 2.92% (two colored dots indicate the subpopulation dependency of the compared strains). The strain III_F09_YJS8068 is an outlier (black triangle) as it appears to be an admixed diploid with only 1.1% divergence between the highly and lowly diverged parts of its genome. Right (Low*Low): Genetic distances between genomic copies of low intra-genomic variation is generally below (0.9%) between strains of the same or different subpopulations. The admixed strain III_F09_YJS8068 is the exception, since it also has the highest variation between the low intra-genomic of its genome and the low intra-genomic copies of other strains (>2%).

D. Heatmap showing the genetic distance between genomic copies of 40 polyploid individuals. The only strains whose genomic sequences (low intra-genomic variation and high intra-genomic variation) are similar is the admixed III_F09_YJS8068 (black triangle). Here, both genomic copies cluster together with all other genomic copies of high intra-genomic variation.

E. Acquired genomic copy of unknown origin. The genomic copies with low genetic variation were assigned as the primary genomic copies present in all individuals (2n-4n), while the genomic copies with high genetic variation were assigned as acquired genomic copies, only present in 40 polyploids of the subpopulations teq/EtOH, beer and wine 1. Pairwise genetic analysis with the primary genome of the beer subpopulation as a reference shows a clear gap between the genetic variation that defines the primary and the acquired genome. The primary genome of the beer subpopulation is similarly distant to its own acquired genomic copy as well as to the acquired genomic copies of the other two polyploid groups wine 1 and teq/EtOH. The two genetic clusters beyond the 0.9% for the teq/EtOH do not only comprise the pairwise comparison with the acquired genomic copies. The dotted rectangle corresponds to comparisons with the admixed diploid strain III_F09_YJS8068 (black triangle), for which both copies are equally distinct. Genetic distances were calculated pairwise per chromosome and then average per genome (JC69).

Acquired divergent copies highlight clade specific allopolyploidy events

To study the origin of the genetically divergent copies present in the three subpopulations, we imputed whole-genome fasta-alignment files for every individual. First, we compared the genomic copies with high genetic variation (High*High) within and between groups. We calculated pairwise genetic distances and found that the divergence between these copies within the subpopulations was 0.13% on average (Figure 3C, single-colored dots). By contrast, the genetic divergence of these copies across the subpopulations was 2.59% on average, ranging from 1.76% to 3.05% (two-colored dots).

When comparing the genetic distance between the lowly and highly (High*Low) diverged genomic copies across all the genomes, we observed that the genetic distance is 2.92% on average (Figure 3C, High*Low). The largest genetic distance is observed between the wine 1 and kombucha subpopulations, reaching 3.16%. The only outlier is the III_F09_YJS8068 strain (teq/EtOH) and has the closest genetic distance between its two genomic copies, at about 1.1% (Figure 3C, black triangle). With more than 2% distance, III_F09_YJS8068's low variation genome is also the most distant to all other low variation genomes (Figure 3C, Low*Low). This paints III_F09_YJS8068 as an admixed diploid whose two genomic copies are mixtures of lowly and highly diverged sequences, placing it between the highly diverged and lowly diverged genomes. The other genomes bearing low genetic variation are less than 1% diverged with each other (Low*Low). In fact, using the representation of pairwise distances in the heatmap format reasserts the three genetically distinct entities of the genomic copies with high genetic variation (Figure 3D, High*High), while the genomic copies with low genetic variation appear more similar (Figure 3D, Low*Low). Pairwise comparison using the lowly variable genomic copies of the beer clade as a reference confirm that inter-clade transfer of genomic copies can be excluded as a potential cause in the acquisition of additional genomic copies with

high genetic variation between the three polyploid subpopulations (Figure 3E). These three groups each have their own additional copy, and each group's additional copy is unrelated to the additional copies of other groups.

Since a closely related diploid genome is conserved across the isolates of the species, we define this part as the primary genome of *B. bruxellensis* (Figure 3E). It is present in all of the strains and harbors a genetic variation of less than 1% to the reference genome. The exception is the admixed strain III_F09_YJS8068 which groups within the teq/EtOH subpopulation and which is the only strain with a minimum genetic distance of 2.01% and maximum genetic distance of 2.53% to the other primary genomes. In addition to these primary genomic copies, a highly divergent copy is present in three groups (teq/EtOH, beer and wine 1 subpopulations) and was defined as a new or 'acquired' genomic copy (Figure 3E). The acquired genomic copies clearly exceed the genetic variation of the primary genome, raising the question of their origin and a possible acquisition by interspecies hybridization.

To test whether the additional copies have been acquired from sister species in the genus *Brettanomyces*, we sequenced and generated *de novo* genome assemblies for four of the sister species: *B. anomala*, *B. nanus*, *B. custerianus* and *B. acidodurans* (Supplementary Table S3, Supplementary Figure S6A-D). While we were able to show collinearity between the acquired copies and the reference genome of *B. bruxellensis* (Supplementary Figure S6E-F), the genomes of the sister species of *B. bruxellensis* were too dissimilar to retain any correlation using the same parameters. We were only able to show a correlation by lowering the parameters, which suggests less synteny paired with high genetic differentiation (Supplementary Figure S6G), as already shown by Roach and Bornemann (2020). With a genetic divergence of 2.5-3% between the acquired to the primary genomic copies, however, it seems

unlikely that sister species with a genetic similarity under 77% have been involved in the acquisition of the additional genomic copies[39].

Overall, we have shown that the triploid genomes of the wine 1, teq/EtOH, and beer subpopulation are composed of a part which is common to every *B. bruxellensis* isolates as well as a newly acquired divergent copy. These results strongly suggest that these events must have occurred independently with closer, so far unknown and far related isolates that we would, according to the genetic distance of ~3%, define as different species from *B. bruxellensis.*

LOH events shaping the genomic landscape of interspecific hybrids

Hybrid genomes are dynamic entities with LOH events playing an important role in their evolution[40,41]. As already seen for the triploid genomes of the wine 2 subpopulation, these events can cause the removal of genetic variation along the genomes in a conserved manner (Figure 2B). Moreover, these events would result in a difference of genomic content from the parental genomes. When preparing *de novo* assemblies from reads with either high or low intra-genomic variation, we observed significantly shorter assemblies (median 9.1 Mb) for the genomic copies harboring high intra-genomic variation, in comparison to *de novo* assemblies from reads with low intra-genomic variation and compared to the size of the reference genome of *B. bruxellensis*[36] (Supplementary Figure S7A, p-value = 1.3e-10). In fact, strains from different subpopulations showed a trend in which even assembly size seemed to be not only different but also conserved between subpopulations (Supplementary Figure S7B). Therefore, given the significantly shorter *de novo* assemblies of the acquired genomic copies, we hypothesized that these polyploid genomes with heterogeneous levels of genetic variation have undergone LOH events as well.

To check for LOH events along the polyploid genomes, we looked at the coverage from reads belonging to the primary and acquired genome, determined if they are complementary to the total coverage, and analyzed their proportion relative to the total coverage. Here, we used the coverage from the short reads, aligned to the reference genome of *B. bruxellensis* and previously separated using competitive mapping (Supplementary Figure S5) along the chromosomes to check for reciprocal shifts in coverage (Supplementary Figure S8A-B). We can show that regions that lack reads aligned to the acquired genomic copy display an increase in coverage at the primary genome complementing the total coverage. On the other hand, this also appears to be the case of several regions of the primary genome, where aligned reads represent only a single genomic copy (1/3 of the total coverage), while the acquired genomic copy appears to be represented by two genomic copies (2/3 of the total coverage). These results confirm the reorganization of polyploid genomes through LOH events in the subpopulations teq/EtOH, beer and wine 1.

Then, we used the primary genome as a reference and determined how many copies are present throughout the genome within the polyploid strains. We calculated its ratio per 10 kb non-sliding windows to the total coverage to assess its distribution. Our results show that the polyploids have undergone massive LOH events (Figure 4). Most regions appear to have been lost/gained within a subpopulation-specific pattern. On chromosome 1 for example, the beer and wine 1 subpopulations lack a significant part of the acquired genomic copy (1.7 Mb for beer strains and 1.2 Mb for wine 1 strains). Other, typically small events are private to individual strains.
Next, we checked if the parts absent from the acquired genomic copy in the three subpopulations complete the smaller *de novo* genome assemblies (Supplementary Figure S7). For the beer strains, we calculated that LOH events have caused the loss of 26.6% of regions on average from the acquired copy (Supplementary Figure S8A). This leaves 9.54 Mb of the acquired genomic copy intact, which is similar in size to

the *de novo* assembly of 8.9 Mb (Supplementary Figure S7B). For the wine 1 subpopulation, 22.3% of the acquired genomic copy is lost on average, leaving 10.1 Mb still present (Supplementary Figure S8B). Here, the *de novo* assembly size (10.1 Mb) matches exactly the size of retained regions in our analysis (Supplementary Figure S7B).

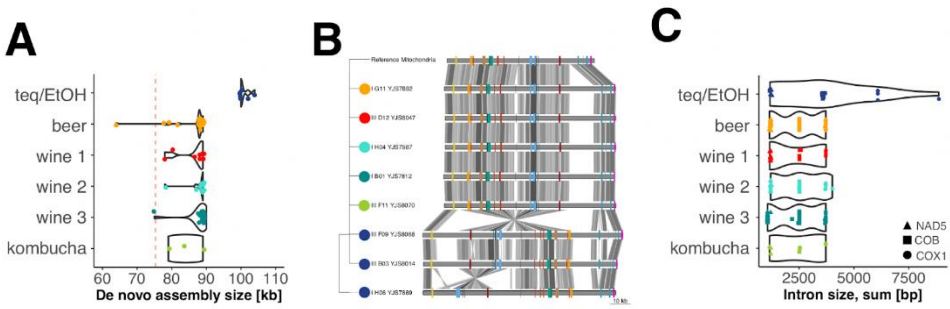

Figure 4 - Dynamic genomic landscape of polyploid strains
The polyploid genomes of the three subpopulations beer, wine 1 and teq/EtOH contain massive modifications through LOH events. The primary genome (low genetic variation) was used as a reference. Conserved patterns of modified regions for the primary genome were identified by determining the gain or loss of its copies in each strain, here varying between three (3×) and zero (0×). Only a few modified regions are unique to single or few strains. There are no common regions which show the same patterns across subpopulations. The teq/EtOH subpopulation shows a division into two clusters, each consisting of three individuals. The ploidy level was estimated in 10 kb windows.

The teq/EtOH strains display a pattern of loss/gain of genomic regions from the primary genome that enables the distinction of two subgroups, denoted as teq/EtOH 1 and teq/EtOH 2. The teq/EtOH 2 has almost entirely lost the second copy of the primary genome, replaced by a second copy of the acquired genome (Figure 4). Both subclades have lost 10.5% of the acquired genomic copy on average (12.1% for teq/EtOH 1 and 8.8% for teq/EtOH 2). The average of both (11.64 Mb) is comparable to the average *de novo* assembly size of 10.7 Mb.

The conserved patterns of LOH within each subpopulation raises the question of whether these patterns are the consequence of adaptation, random processes, or point at a recent shared ancestry. In the evolution of species, polyploidy has been shown to potentially play an important role in the acquisition of new traits or the amplification of already existing traits in the context of the acquisition of resistances[42,43], interactions[44,45], coping with changing environments[46], or the occupation of novel ecological niches[47]. The different environments *B. bruxellensis'* polyploid subpopulations are associated with such as bioethanol production, wine or beer fermentation, are harsh environments and require different adaptations such as a high tolerance to alcohol and acidity. As already seen for the polyploid wine 2 subpopulation, LOH events are shared among strains and, with LOH events at similar positions (*e.g.* DEBR0S1), hotspots for LOH might be involved.

Overall, the three subpopulations with polyploid genomes derived from interspecific hybridization events are highly dynamic, while LOH events have caused conserved patterns of low genetic diversity within each subpopulation. Further insight into how these variations at the gene level are expressed at a phenotypic level will have to be queried in future studies investigating the phenotypic landscape of the different subpopulations.

Discussion

The *Brettanomyces bruxellensis* yeast species is known to harbor subpopulations with various levels of ploidy[31–33]. For the first time, we provide a detailed insight into the complex genomic architecture of these polyploid subpopulations. Interestingly, we noticed that there is a high conservation of ploidy in each subpopulation and four of them, associated with three different ecological environments (tequila/ethanol production, wine making and beer brewing) are exclusively characterized by triploids.

Because polyploidy can be achieved in different ways (allopolyploidization or autopolyploidization), the final genomic composition might vary by distinct levels of intra-genomic information. At the same time, the intra-genomic variation will define the boundaries of genomic flexibility, and therefore drive evolution in almost unpredictable and different ways[46,48].

By using two different phasing strategies, we elucidated the genomic architecture of polyploid subpopulations of *B. bruxellensis* with various levels of intra-genomic variation. We highlighted that all six populations harbor a primary genome irrespective of their ploidy, which is defined as the genetic variation that does not go beyond 1% when compared to the reference genome of *B. bruxellensis*[36]. This is lower but in accordance with previous papers characterizing the genetic variation of *B. bruxellensis*, since they did not phase the genomes into distinct haplotypes (1.2%[32]). Furthermore, we show the existence of three allopolyploid subpopulations (teq/EtOH, beer, and wine 1) with an acquired genomic copy with a genetic divergence of about 3% compared to the reference genome. They clearly exceed the average intra-genomic variation of the primary genome, demonstrating the occurrence of interspecific hybridization events in these subpopulations. The known

sister species within the same genus are rejected as donors for the interspecific hybrids due to high genetic divergence of at least 23%[39].

We further highlight the fact that to our knowledge, the *B. bruxellensis* species is one (or the) rare case, in which these different scenarios, respectively allo- and autopolyploidy, can be observed in closely related subpopulations. We identified different trajectories for strains not only associated with different environments (teq/EtOH, beer and wine) but also associated with the same environment, while being part of a genetically distinct cluster. The "wine"-associated strains fall in three genetically diverged subpopulations. With the two subpopulations wine 1 and wine 2 being triploid and wine 3 being diploid, only wine 1 has acquired a third genomic copy from interspecific hybridization, while wine 2 has solely genetically similar haplotypes.

Different trajectories of polyploidization in nature were mostly studied (and observed) in plants, which yields no clues as to the importance or prevalence of polyploidization and its trajectories in animal or fungal systems[2,49,50]. These mechanisms, when observed and studied in extant polyploids, have mostly (when not exclusively) been determined between species, rather than within species. We highlight that future studies which screen individuals on a large scale to study prevalence and trajectories of polyploids across ecologically diverged, naturally occurring subpopulations are required, especially in the animal and fungi kingdom, Indications that polyploidy could be a more common state were shown by two recent studies, which genotyped more than 1,000 individuals from the *S. cerevisiae* and *B. bruxellensis* yeast species, with a prevalence of polyploids of 11.4%[21] and 54%[31], respectively.

Finally, we speculate that the different trajectories of polyploids in the subpopulations of *B. bruxellensis* are linked to the adaptation to the different anthropized environments. Polyploids in general have received a lot of attention in the context of adaptivity and diversification, in which many extant species originate from ancient polyploid states[25–28]. While a polyploid state itself can allow adaptability, it is often seen as a transient state which is followed by massive modifications to cope with genetic incompatibilities and to regain fertility in the long term. Evidence for this process has been gained through the detection of paralogous gene sets with different historical trajectories in many naturally diploid taxa, establishing the process of genomic modifications after polyploidization. With a prevalence of 54% polyploids, plus evidence for three independent interspecific hybridization events, polyploidy is abundant and most likely has significant effects for *B. bruxellensis.* The genomes of the allo- and autopolyploid subpopulations are characterized by massive genomic modifications, which have established a conserved pattern of rearranged blocks. These underline on the one hand the independent acquisition of genetically diverse genomic copies for the allopolyploid subpopulations, but most likely also reflect the recovery of fitness and overcoming of genomic incompatibilities. These acquired copies likely play a role in the adaptation of these subpopulations to the harsh and changing conditions of their anthropized environments. For example, sulfur dioxide is used to protect wine fermentation from spoilage by *B. bruxellensis.* The high tolerance against sulfur dioxide, mostly observed for the wine 1 subpopulation[30], could be the adaptation of this yeast to the recently increased usage of this agent in the industry.

Our study clearly highlights for the first time the coexistence of a large repertoire of evolution punctuated by various independent polyploidization events within a species and addresses the need to further resolve the genomic architecture of polyploid species complexes from diverse ecological settings.

Methods

Strain selection and DNA extraction

For this study, we focused on a subset of 71 strains of *Brettanomyces bruxellensis.* These strains are part of the collection of 1,500 strains[31] which was previously analyzed using microsatellites and partially with whole genome sequencing data[32]. The 71 strains were selected to represent the different clades of *B. bruxellensis* in terms of genetic diversity, ecological origin (origin of isolation) and variation in ploidy (Supplementary Table S1). Additional to 71 *B. bruxellensis* strains, four sister species (*B. anomala, B. custersianus, B. nanus, B. acidodurans*) including the reference strain of *B. bruxellensis* were selected for this study (Supplementary Table S3).

The DNA of 71 strains was extracted from 20ml cultures (single colony, 48h growth at 25°C) using the QIAGEN Genomic-tip 100/G kit (Hilden, Germany) with the recommended manufacturer's genomic DNA buffer set. The manufacturer's protocol was followed as recommended and final DNA was eluted in 100-200µl water. DNA was quantified with the broad-range or high-sensitivity DNA quantification kit from Qubit (Thermo Fisher Scientific, Waltham, USA) with the use of the automated plate reading platform from TECAN (Männedorf, Switzerland). Genomic DNA was migrated on a 1.5% agarose gel to check for degradation.

Library preparation and sequencing

The kit NEBNext® Ultra™ II DNA Library Prep Kit (Ipswich, USA) for Illumina® (San Diego, USA) was used for library preparation. The dual-barcoding strategy was applied and samples were sequenced on two lanes of NextSeq (Illumina®) at the European Molecular Laboratory (EMBL) in Heidelberg, Germany. The strategy of

sequencing was 75 paired-end (75PE) and sequences from two independent sequencing lanes were concatenated prior to any analysis.

For the long-read sequencing we used the Oxford Nanopore Technology (Oxford, UK). Libraries for sequencing using the MinION and were prepared as described in Istace *et al*. (2017)[51] using the Ligation Sequencing Kit SQK-LSK109. We barcoded strains with the Native Barcoding Expansion 1-12 (EXP-NBD104) to multiplex up to 12 samples per sequencing reaction.

Data analyses: long reads (Oxford Nanopore)

Base-calling, de-multiplexing and adapter trimming

Raw sequencing reads were processed as described in Fournier *et al*. (2017)[36]. Briefly, the base-calling and de-multiplexing steps were performed with guppy (https://nanoporetech.com/). Adapters were trimmed with Porechop (Porechop GitHub Repository https://github.com/rrwick/Porechop).

Separating reads with different degrees of genetic variation to the reference genome

We distinguish reads depending on their genetic distance to the reference genome *Brettanomyces bruxellensis*. For this, long reads of each sample were first aligned to the reference genome of *B. bruxellensis*[36] using NGM-LR[52] (v0.2.7). We separated reads into two groups based on their number of SNPs/kb. Here, reads comprising less than 10 variants per kb were assigned to the low intra-genomic variation cluster and reads with more than 14 variants per kb to the high intra-genomic variation cluster. Reads containing between 10 to 14 variants per kb were considered ambiguous and ignored to avoid misassignment which could strongly impact *de novo* genome assemblies.

Calculation of coverage for the low and high intra-genomic variation cluster sand their ploidy

The contribution to the total coverage was calculated for the reads that clustered in the low intra-genomic variation cluster and the high intra-genomic variation cluster. This was performed on 10kb windows and used as an approximate measurement of the average ploidy per strain (median coverage across strains and scaffolds: 68×). As an example, if the overall coverage for a certain region was calculated to be 60× (from reads with low and high intra-genomic variation), then a coverage of 40× for the reads with low intra-genomic variation and 20× for the reads with high intra-genomic variation would assume a triploid state at this locus, with a ratio of genomic copies of 2:1. This method was adapted to estimate different potential levels of ploidy (2n-5n).

Phasing the polyploid genomes of the wine 2 subpopulation

We phased six polyploid genomes of the wine 2 subpopulation with the nPhase pipeline as described in Abou Saada *et al*. (2021)[35]. For this, short and long reads were aligned to the *Brettanomyces bruxellensis* reference sequence and the mapped short reads were variant called. This data was then phased by the nPhase algorithm using default parameters.

To generate pairwise divergence plots, we cross-referenced two of the files output by nPhase in the Phased folder: (1) the *.clusterReadNames.tsv file, which contains the list of reads that comprise each cluster and (2) the *.variants.tsv file, which contains the list of heterozygous SNPs associated with each predicted haplotig. By combining the information in both files we were able to calculate the similarity between predicted haplotypes in 10kb windows.

In regions that have only two predicted haplotypes we have only one value, but in regions that have more than three predicted haplotypes we only kept the three longest

clusters and generated three similarity values through pairwise comparison (used for plotting maximal genetic distances between haplotypes).

De novo assemblies

Prior to the *de novo* assemblies, fastQ files containing the raw reads (respectively with low or high intragenomic variation to the reference genome) were corrected and cleaned using Canu -correct v.1.7[53]. *De novo* assemblies were performed with SMARTdenovo[38] and the parameters -J 1000 -c 1.

Collinearity and pairwise genetic identity of de novo assemblies

Collinearity between *de novo* assemblies of *B. bruxellensis* strains was checked using Mummer v.3 (https://doi.org/10.1093/nar/27.11.2369) and the following parameters nucmer --mum -l 200. To check for collinearity between different species, we lowered the values and stringency to --mum -l 20 -c 30 -b 100.

Data analyses: short reads (Illumina)

Genome-wide phylogeny and estimation of ploidy

Raw sequencing reads (not separated short reads) were aligned to the reference genome of *B. bruxellensis*[36] using BWA[54] v0.7.17 with the default settings (mem algorithm). File format conversions, the sorting and indexing of samples were performed using Samtools[55] v.1.9. Variant calling was done using the Genome Analysis Toolkit GATK[56] v4.1. The data from the variant calling in GATK was filtered and processed with VCFtools[57] and BCFtools[55] v1.9. We filtered out indels, kept only variants with a minimum coverage of 11 reads/site, removed individuals with more than 50% of missing data. The information of the Allele Balance for the Heterozygous sites (ABHet) was used to calculate the average allele frequencies in 10kb windows (non-sliding) in R v.3.3.3 (R Core Team 2019). Phylogenetic

Neighbor-Joining trees were performed with the R packages seqinr[58] and phangorn[59] using the substitution model JC69. The final trees were plotted with Figtree[60] v.1.4.3.

Genomic-copy specific alignments

A competitive mapping approach was used to distinguish short reads that represent the low and high intra-genomic variation. For this, the short reads of the 40 strains from the three polyploid subpopulations with low and high intra-genomic variation (teq/EtOH, beer, wine 1) were aligned to clade-specific reference genomes. These reference genomes were concatenated *de novo* assemblies, prepared from low and high intra-genomic variation (using long-read data) to the reference genome *B. bruxellensis*. These clade-specific reference genomes came from the polyploid strains YJS7895 (beer), YJS8039 (wine 1) and YJS7890 (teq/EtOH). Finally, to align all reads to the same reference genome and to perform comparative genomic analyses, the reads separated by the competitive mapping approach, which either mapped to the scaffolds from the low or the high intra-genomic *de novo* assemblies, were mapped back to the reference genome of *B. bruxellensis*[36]. The 31 strains, which did not show any signals of polyploidy (wine 3, kombucha) or high intra-genomic variation (wine 2) were mapped directly to the *B. bruxellensis* reference genome. In this way, all strains were ultimately aligned to the same reference facilitating the direct comparison of genetic variation. Alignments, file conversions, file sorting, file indexing and the calculation of coverage in 10kb windows were performed as described above.

Principal Component Analysis and phylogenetic analysis

Variant calling and filtering were done as described above. The program Adegenet[61] v2.1.0 was used to perform the Principal Component Analysis (PCA). Phylogenetic trees were generated and plotted as described above.

Pairwise distances

Samtools v1.9 and Bcftools[55] v1.9 were used to calculate the genotype likelihood from the bam-formatted alignment files, to call variants and to create single fasta files for each individual strain. Genetic distances were calculated in 50 kb windows in R with the package phangorn[59] (substitution model "JC69") and then averaged per individual.

Detection of regions underlying the variation in copy numbers

Variation in copies of the low intra-genetic variation along the polyploid genomes of the 40 allopolyploid strains was calculated in 10 kb windows from the ratio of the coverage of the primary genome to the total coverage. Ploidy levels were categorized as described above. Plots were generated with the R package ggbio[62].

Supplementary Material

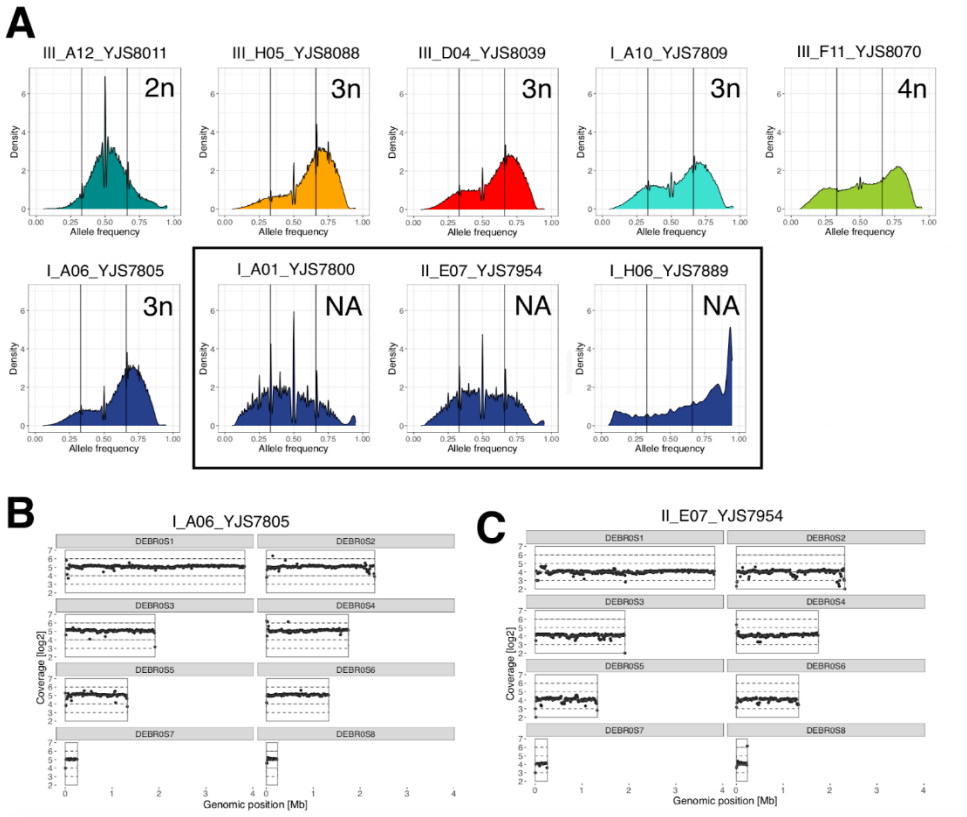

Figure S1: Allele frequencies and genome-wide coverage.
A Estimation of ploidy in 71 strains using short read sequencing data. Shown are examples of strains from each subpopulation. The level of ploidy varies between 2n (diploid) and 4n (tetraploid). For three individuals, ploidy could not be estimated based on 24,313 genome-wide distributed variants (framed in black). **B-C** Genome-wide coverage to detect potential aneuploidies. Coverage-based analysis did not show aneuploidies (segmental, chromosomal) that would explain the patterns of the three strains in (**A**), for which ploidy level failed to be determined by allele frequency. Shown are the strains I_A06_YJS7805 (**B**), for which ploidy could be determined (see Panel **A**), and II_E07_YJS7954 (**C**), where the usage of allele-frequencies was not sufficient to determine its ploidy.

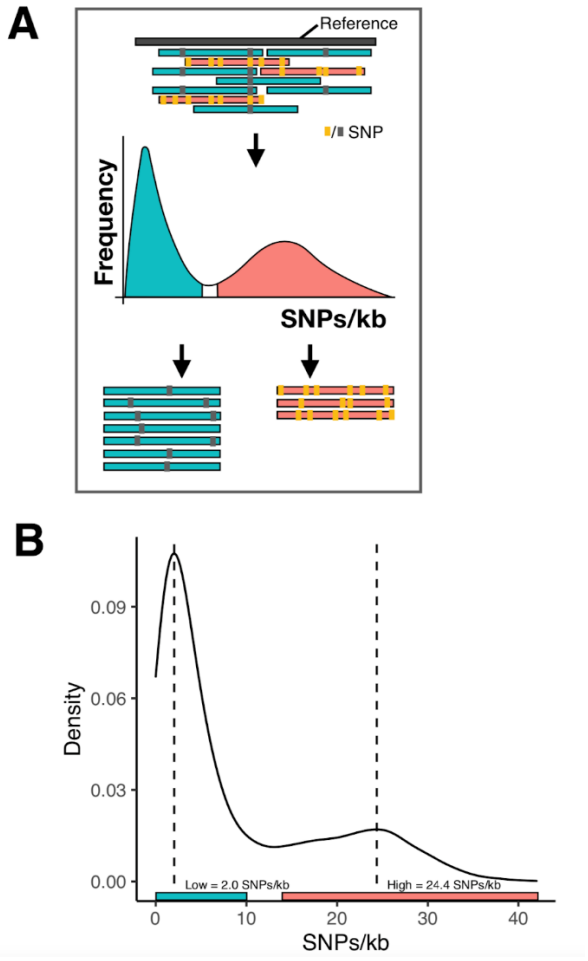

Figure S2: Separating sequencing reads based on intra-genomic variation to the reference genome.
A Long reads were first aligned to the reference genome of *B. bruxellensis* (Fournier *et al*., 2017) and separated based on their density of variation (SNPs/kb). Respectively, reads with low genetic variation to the reference genome were clustered and defined as low intra-genomic variation, reads with high genetic variation to the reference genome were clustered and defined as high intra-genomic variation.
B Three subpopulations with high intra-genomic variation. Shown is the intra-genomic variation from strains of the subpopulations teq/EtOH, beer and wine 1. These strains harbor, besides low intra-genomic variation with an average of 2.0 SNPs/kb, a cluster of reads with high intra-genomic variation (average 24.4 SNPs/kb) to the reference genome.

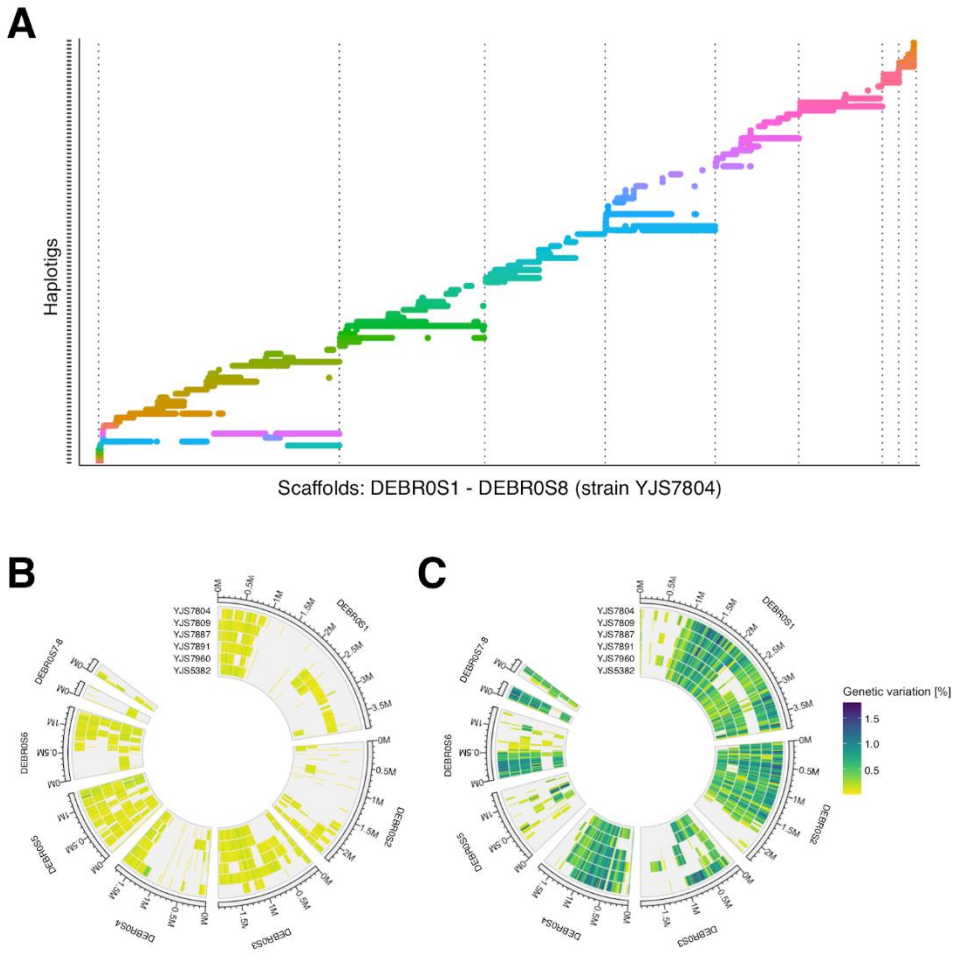

Figure S3: Phasing the polyploid wine 2 subpopulation with low intra-genomic variation.

A Separation of haplotypes. The program nPhase (Abou Saada *et al*., 2021) separated the chromosomes into haplotypes, which in most cases, resolves the chromosomes into two or more haplotigs at a given region.

B-C Intra-genomic variation. The separation of regions underlying two (**B**) or three (or more; **C**) haplotypes corresponds to different levels of intra-genomic variation. Regions with two haplotypes have on average intra-genomic variation of 0.09%, while this increases to 0.54% regions with three haplotypes.

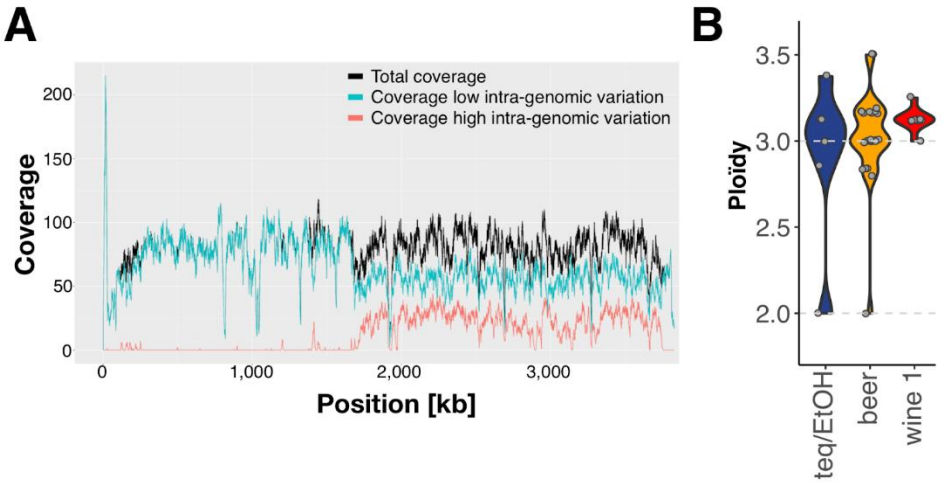

Figure S4: Coverage analysis and ploidy determination using long read sequencing data.

A Example of chromosome 1 (DEBR0S1) of a beer strain where long reads were aligned to the reference genome of *B. bruxellensis* (Fournier *et al*., 2017). First, reads have been separated based on the number of SNPs/kb, respectively into clusters of low or high intra-genomic variation to the reference genome (see Material & Methods), and then compared to the total coverage at a given site.

B With the coverage of the reads bearing low or high intra-genomic variation to the reference genome (**A**), the ploidy was estimated for strains from the three subpopulations teq/EtOH, beer and wine 1. The reads containing high intra-genomic variation contributed on average to a third of the total coverage at each site, reflecting a triploid state (3n) for these strains. Ploidy was converted from ratios (see Material & Methods).

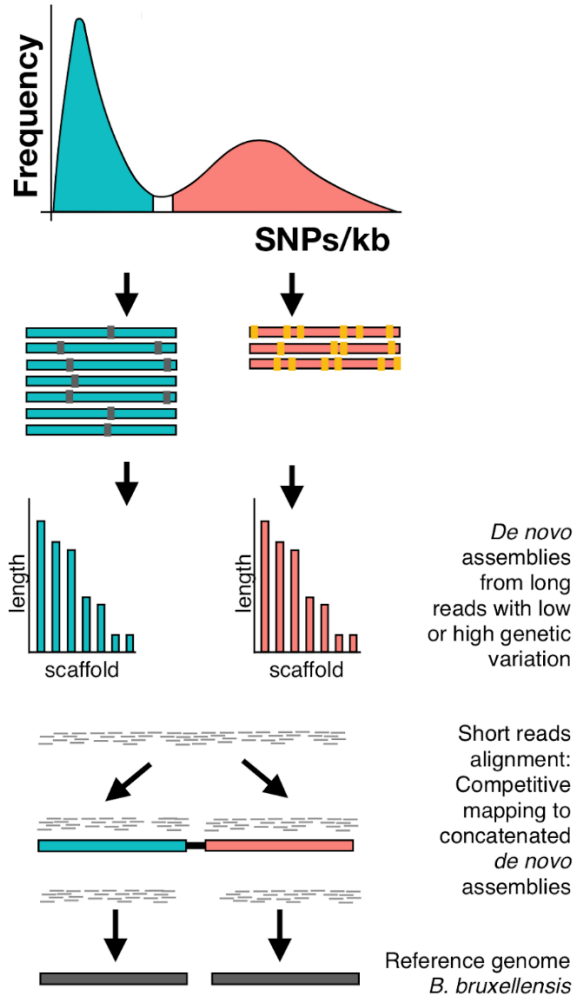

Figure S5: Competitive mapping for comparative genomic analysis (see also Figure S2).
In order to perform a comparative analysis on the different genomic copies, first independent *de novo* assemblies were constructed from reads with low or high intra-genomic variation to the reference genome (Fournier *et al*., 2017). The low and high variation *de novo* assemblies were then concatenated for three strains, one of each different subpopulation, and used as reference sequences for the other strains of the same subpopulation (see: Material & Methods). Short sequencing reads were separated based on a comparative mapping approach using the concatenated *de novo* genome assemblies. Finally, the separated short sequencing reads were aligned back to the reference genome of *B. bruxellensis* to perform comparative analyses.

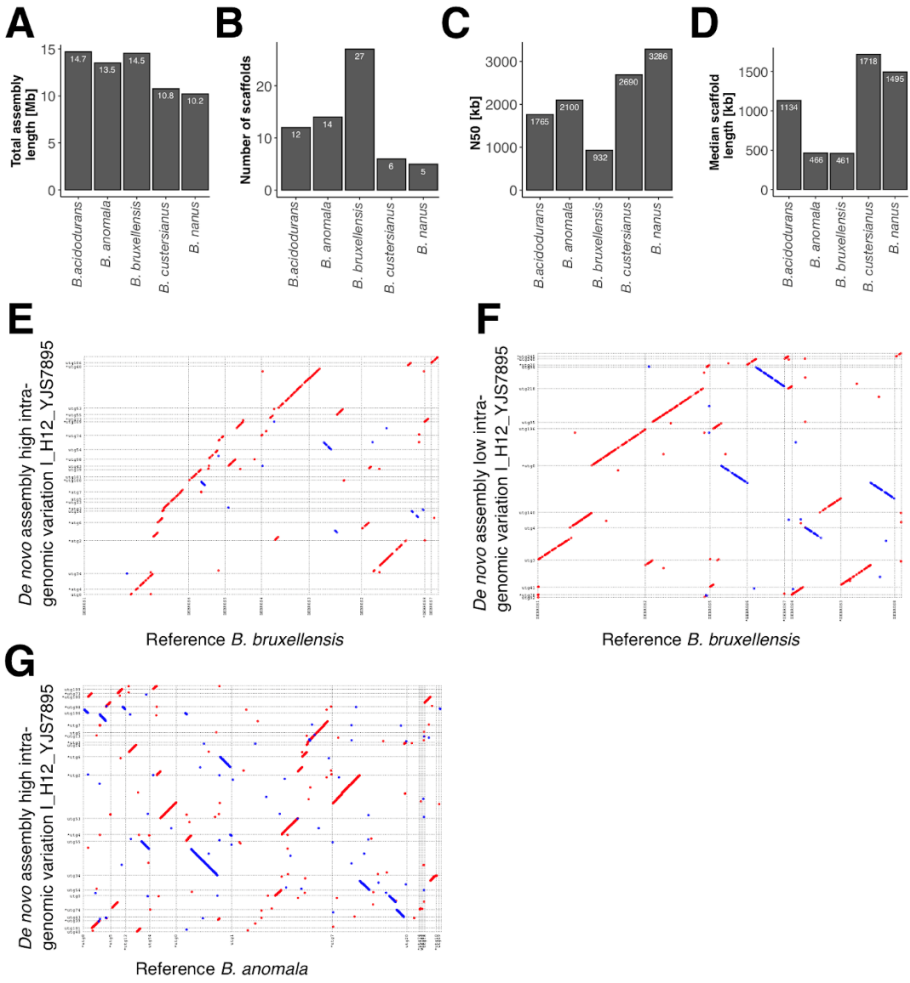

Figure S6: *De novo* genome assembly statistics for *B. bruxellensis* and four of its sister species.

The assembly statistics (**A-D**) are in accordance with those from Roach & Borneman (2020).

E-F Collinearity plots comparing synteny between *de novo* assemblies. Both assemblies, respectively performed using reads with high or low intra-genomic variation, reveal a good synteny albeit rearrangements with the reference genome *B. bruxellensis* (Fournier *et al*., 2017) can be seen (Mummer parameters: --mum -l 200).

G Collinearity plot comparing synteny between the *de novo* assembly from reads with high intra-genomic variation and *B. anomala*. Collinearity is disrupted by many small syntenic elements, which only appear using less stringent parameters (Mummer parameters: -- mum -l20 -c 30 -b 100).

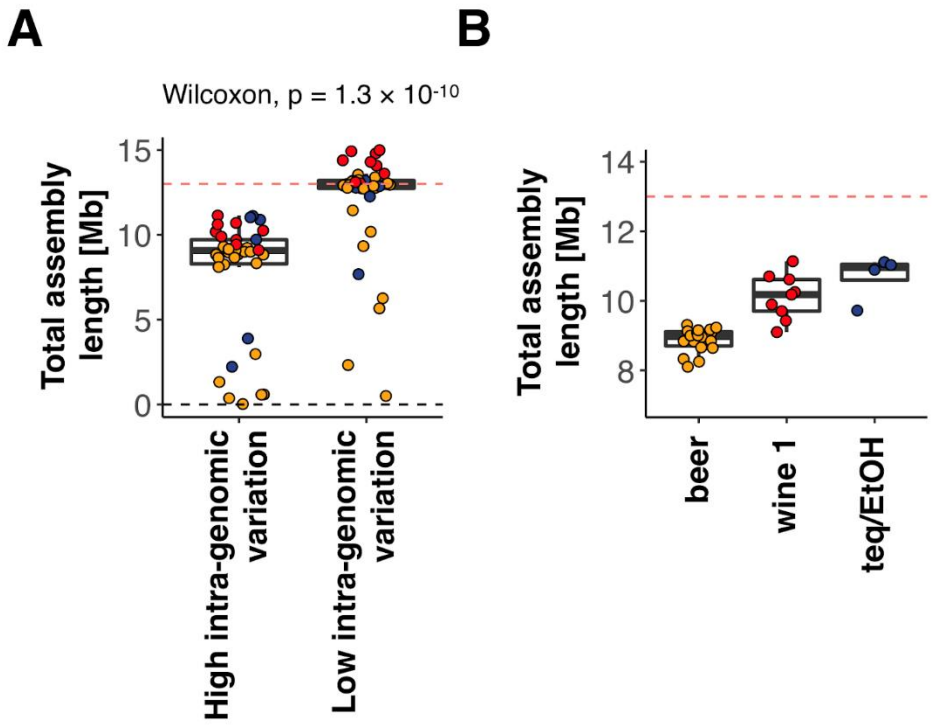

Figure S7: *De novo* genome assemblies.
A Genome assemblies were prepared for the reads harboring either low or high intra-genomic variation to the reference. The median total assembly size for the *de novo* assemblies of the high intra-genomic variation is 9.08 Mb, significantly different from the median of assemblies based on low intra-genomic variation at 12.92 Mb (median; p value = 1.3e-10).
B The total assembly sizes of strains from different subpopulations (only high intra-genomic variation). Lowest total assembly length was determined for the subpopulation beer (8.84 Mb), followed by wine 1 (10.18 Mb), and teq/ EtOH (10.34 Mb). The red dotted line represents the assembly length of the *B. bruxellensis* reference genome assembly (Fournier *et al*., 2017; 13 Mb).

A

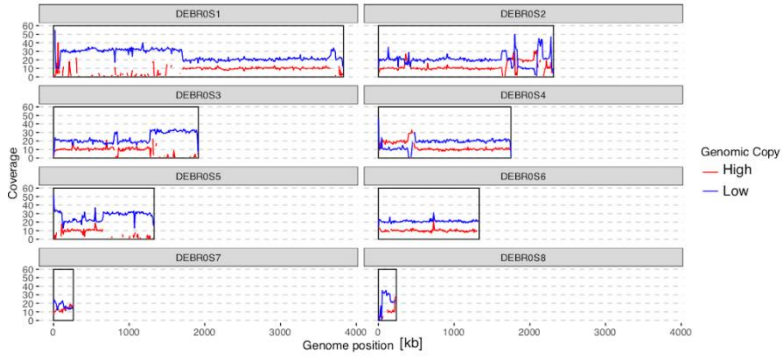
DEBR0S1
DEBR0S2
DEBR0S3
DEBR0S4
DEBR0S5
DEBR0S6
DEBR0S7
DEBR0S8
Coverage
Genome position [kb]
Genomic Copy
High
Low

B

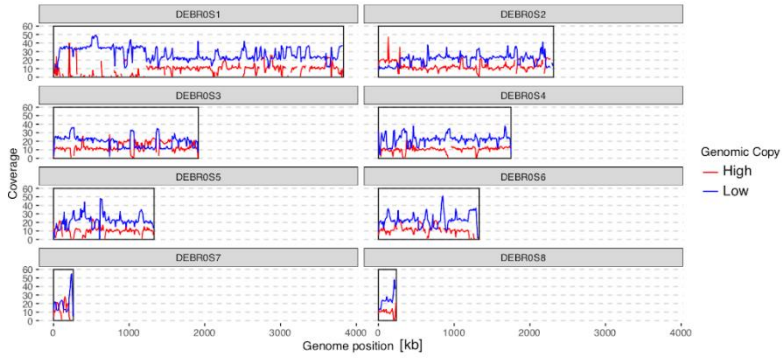
DEBR0S1
DEBR0S2
DEBR0S3
DEBR0S4
DEBR0S5
DEBR0S6
DEBR0S7
DEBR0S8
Coverage
Genome position [kb]
Genomic Copy
High
Low

C

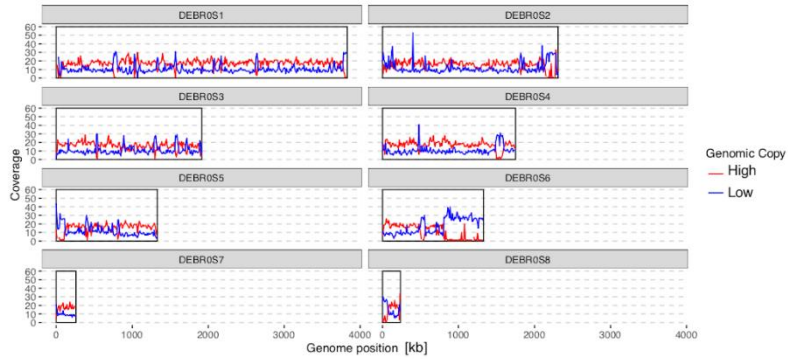
DEBR0S1
DEBR0S2
DEBR0S3
DEBR0S4
DEBR0S5
DEBR0S6
DEBR0S7
DEBR0S8
Coverage
Genome position [kb]
Genomic Copy
High
Low

Figure S8: Reciprocal shifts in coverage underlying LOH events.
A-B Example of coverage plots, calculated using 10 kb windows along the scaffolds for two strains from the subpopulations beer and wine 1. Plotted are the strains IH12_YJS7895 (**A**; beer) and III_D04_YJS8039 (**B**; wine 1), which were initially aligned to subpopulation-specific reference genomes (concatenated *de novo* assemblies) to separate reads with low or high intra-genomic variation, and then aligned back to the reference genome *B. bruxellensis* (Fournier *et al*., 2017). In red (High), the reads from the high intra-genomic copy are shown, in blue (Low), the reads from the low intra-genomic copy. Example (**A**): The average coverage of the High genomic copy is 10x (=haploid), while the Low genomic copy is 20x (=diploid). The total coverage (sum of High + Low) is 30x. This coverage of Low vs. High is not consistent across the genome, where shifts in coverage show that additional regions of a genomic copy have been acquired or were lost.

Table S1 - Set of 71 strains sequenced with Illumina and MinION technology

Library Name	Readcount Illumina 75 PE	Genome-wide coverage (X)	Genetic Group	ID	Region of Origin	Polyploid with acquired Copy
I_A01_YJS7800	3698954	19.8	teq/EtOH	CBS 5512	South Africa	Yes
I_A02_YJS7801	6392370	34.2	wine 2	CBS_74	Belgium	No
I_A03_YJS7802	7364180	39.5	wine 3	12_LT_VGC3_c_10	France	No
I_A05_YJS7804	5083294	27.2	wine 2	L1710	South Africa	No
I_A06_YJS7805	7156204	38.3	teq/EtOH	CBS_6055	USA	Yes
I_A07_YJS7806	7575208	40.6	wine 3	SJ12_4	France	No
I_A08_YJS7807	7100406	38	wine 2	L1733	France	No
I_A10_YJS7809	5899958	31.6	wine 2	ISA2211	Portugal	No
I_A11_YJS7810	5208832	27.9	beer	ISA2397	Portugal	Yes
I_A12_YJS7811	10180660	54.5	wine 2	L1739	Italy	No
I_B01_YJS7812	5555190	29.8	wine 2	VP1544	Italy	No
I_B02_YJS7813	7729348	41.4	beer	LB15110g	France	Yes
I_B03_YJS7814	10613154	56.9	beer	LB15107g	France	Yes

The full table can be found in the companion document accessible from the appendices.

Table S2: Statistics of de novo genome assemblies.

YJS Number	Genetic Group	Genome Copy	Total Assembly Size (Mb)	Scaffold Count	Average Length Scaffold (kb)	Median Length Scaffold (kb)	N50 (kb)
YJS7800	teq/EtOH	Acquired	10.9	46	237	166	395
YJS7800	teq/EtOH	Primary	13	32	406	300	570
YJS7801	wine 2	Primary	13.1	72	182	122	293
YJS7802	wine 3	Primary	0.7	24	31	27	38
YJS7804	wine 2	Primary	13.1	13	1004	1194	1395
YJS7805	teq/EtOH	Acquired	2.2	109	20	17	25
YJS7805	teq/EtOH	Primary	7.7	274	28	23	37
YJS7806	wine 3	Primary	0	2	11	5	17
YJS7807	wine 2	Primary	6.5	127	51	41	66
YJS7809	wine 2	Primary	12.9	11	1177	1142	1453
YJS7810	beer	Acquired	NA	NA	NA	NA	NA
YJS7810	beer	Primary	6.3	131	48	41	60

The full table can be found in the companion document accessible from the appendices.

Table S3: De novo assembly statistics for the sister species of Brettanomyces bruxellensis.

Species	Strain name	Strain ID	Other ID	Origin	Substrate
Brettanomyces bruxellensis	NRRL Y-12961 T	ATCC 36234=CBS 74=CCRC 21414=CCY 59-2-1=DBVPG 6706=IFO 1590=NCYC 823	Belgium	Belgium, beer Belgique, Biere, 1938 Type of Dekkera bruxellensis Van der Walt, isolated by M.T.J. Custers, LcIII, Sep 1938	Beer
Brettanomyces anomala	NRRL Y-17522 T	ATCC 58985=CBS 8139=JCM 31686=van Grinsven 10300	The Netherlands	Spoiled soft drink, The Netherlands	Soft drinks
Brettanomyces nanus	NRRL Y-17527 T	ATCC 48014=CBS 1945=CCRC 21335	Sweden	Bottled beer, Kalmar brewery, Sweden	Beer
Brettanomyces custersianus	NRRL Y-6653 T	ATCC 34446=CBS 4805=CCRC 21516=DBVPG 6709=IFO 1585=VKM Y-1419	South Africa	Bantu beer brewery, South Africa	Beer
Brettanomyces acidodurans	NCAIM Y.02178 T	CBS 14519T = NRRL Y-63865T = ZIM 2626T	Spain	Isolated from olive oil originating from Lucena, Cordoba, Spain, in 2016	Olive oil

Availability of data

Illumina and Oxford Nanopore data for the 71 *Brettanomyces bruxellensis* isolates are available under the study accession number PRJEB41126.
Oxford Nanopore sequencing data for the *B. anomala*, *B. nanus*, *B. custerianus* and *B. acidodurans* species is available under the study accession number PRJEB41125.

References

1. Adams, K. L. & Wendel, J. F. Polyploidy and genome evolution in plants. Curr. Opin. Plant Biol. 8, 135–141 (2005).
2. Gregory, T. R. & Mable, B. K. Polyploidy in Animals. in The Evolution of the Genome 427–517 (Elsevier, 2005). doi:10.1016/B978-012301463-4/50010-3.
3. Gjelsvik, K. J., Besen-McNally, R. & Losick, V. P. Solving the Polyploid Mystery in Health and Disease. Trends Genet. 35, 6–14 (2019).
4. Dehal, P. & Boore, J. L. Two Rounds of Whole Genome Duplication in the Ancestral Vertebrate. PLoS Biol. 3, e314 (2005).
5. Sacerdot, C., Louis, A., Bon, C., Berthelot, C. & Roest Crollius, H. Chromosome evolution at the origin of the ancestral vertebrate genome. Genome Biol. 19, 166 (2018).
6. Comai, L. The advantages and disadvantages of being polyploid. Nat. Rev. Genet. 6, 836–846 (2005).
7. Fox, D. T., Soltis, D. E., Soltis, P. S., Ashman, T.-L. & Van de Peer, Y. Polyploidy: A Biological Force From Cells to Ecosystems. Trends Cell Biol. 30, 688–694 (2020).
8. Mayer, V. W. & Aguilera, A. High levels of chromosome instability in polyploids of Saccharomyces cerevisiae. Mutat. Res. Mol. Mech. Mutagen. 231, 177–186 (1990).
9. Wood, T. E. et al. The frequency of polyploid speciation in vascular plants. Proc. Natl. Acad. Sci. 106, 13875–13879 (2009).
10. Van de Peer, Y., Mizrachi, E. & Marchal, K. The evolutionary significance of polyploidy. Nat. Rev. Genet. 18, 411–424 (2017).
11. Leitch, A. R. & Leitch, I. J. Genomic Plasticity and the Diversity of Polyploid Plants. Science 320, 481–483 (2008).
12. Soltis, P. S., Marchant, D. B., Van de Peer, Y. & Soltis, D. E. Polyploidy and genome evolution in plants. Curr. Opin. Genet. Dev. 35, 119–125 (2015).
13. Sanchez-Perez, G., Mira, A., Nyirő, G., Pašić, L. & Rodriguez-Valera, F. Adapting to environmental changes using specialized paralogs. Trends Genet. 24, 154–158 (2008).
14. Eberlein, C. et al. The Rapid Evolution of an Ohnolog Contributes to the Ecological Specialization of Incipient Yeast Species. Mol. Biol. Evol. 34, 2173–2186 (2017).
15. Orr, H. A. 'Why Polyploidy is Rarer in Animals Than in Plants' Revisited. Am. Nat. 136, 759–770 (1990).
16. Masterson, J. Stomatal Size in Fossil Plants: Evidence for Polyploidy in Majority of Angiosperms. Science 264, 421–424 (1994).
17. Levin, D. A. The Role of Chromosomal Change in Plant Evolution. (Oxford University Press, 2002).

18. Wertheim, B., Beukeboom, L. W. & van de Zande, L. Polyploidy in Animals: Effects of Gene Expression on Sex Determination, Evolution and Ecology. Cytogenet. Genome Res. 140, 256–269 (2013).
19. Bellon, J. R. et al. Newly generated interspecific wine yeast hybrids introduce flavour and aroma diversity to wines. Appl. Microbiol. Biotechnol. 91, 603–612 (2011).
20. Krogerus, K., Magalhães, F., Vidgren, V. & Gibson, B. New lager yeast strains generated by interspecific hybridization. J. Ind. Microbiol. Biotechnol. 42, 769–778 (2015).
21. Peter, J. et al. Genome evolution across 1,011 Saccharomyces cerevisiae isolates. Nature 556, 339–344 (2018).
22. te Beest, M. et al. The more the better? The role of polyploidy in facilitating plant invasions. Ann. Bot. 109, 19–45 (2012).
23. Bertier, L., Leus, L., D'hondt, L., de Cock, A. W. A. M. & Höfte, M. Host Adaptation and Speciation through Hybridization and Polyploidy in Phytophthora. PLoS ONE 8, e85385 (2013).
24. Morrow, C. A. & Fraser, J. A. Ploidy variation as an adaptive mechanism in human pathogenic fungi. Semin. Cell Dev. Biol. 24, 339–346 (2013).
25. Seoighe, C. & Wolfe, K. H. Extent of genomic rearrangement after genome duplication in yeast. Proc. Natl. Acad. Sci. 95, 4447–4452 (1998).
26. Gerstein, A. C. & Otto, S. P. Ploidy and the Causes of Genomic Evolution. J. Hered. 100, 571–581 (2009).
27. Gordon, J. L., Byrne, K. P. & Wolfe, K. H. Additions, Losses, and Rearrangements on the Evolutionary Route from a Reconstructed Ancestor to the Modern Saccharomyces cerevisiae Genome. PLoS Genet. 5, e1000485 (2009).
28. Marcet-Houben, M. & Gabaldón, T. Beyond the Whole-Genome Duplication: Phylogenetic Evidence for an Ancient Interspecies Hybridization in the Baker's Yeast Lineage. PLOS Biol. 13, e1002220 (2015).
29. de Barros Pita, W., Leite, F. C. B., de Souza Liberal, A. T., Simões, D. A. & de Morais, M. A. The ability to use nitrate confers advantage to Dekkera bruxellensis over S. cerevisiae and can explain its adaptation to industrial fermentation processes. Antonie Van Leeuwenhoek 100, 99–107 (2011).
30. Avramova, M. et al. Competition experiments between Brettanomyces bruxellensis strains reveal specific adaptation to sulfur dioxide and complex interactions at intraspecies level. FEMS Yeast Res. 19, (2019).
31. Avramova, M. et al. Brettanomyces bruxellensis population survey reveals a diploid-triploid complex structured according to substrate of isolation and geographical distribution. Sci. Rep. 8, 4136 (2018).
32. Gounot, J.-S. et al. High Complexity and Degree of Genetic Variation in Brettanomyces bruxellensis Population. Genome Biol. Evol. 12, 795–807 (2020).

33. Colomer, M. S. et al. Assessing Population Diversity of Brettanomyces Yeast Species and Identification of Strains for Brewing Applications. Front. Microbiol. 11, 637 (2020).
34. Schrinner, S. D. et al. Haplotype threading: accurate polyploid phasing from long reads. Genome Biol. 21, 252 (2020).
35. Abou Saada, O., Tsouris, A., Eberlein, C., Friedrich, A. & Schacherer, J. nPhase: an accurate and contiguous phasing method for polyploids. Genome Biol. 22, 126 (2021).
36. Fournier, T. et al. High-Quality de Novo Genome Assembly of the Dekkera bruxellensis Yeast Using Nanopore MinION Sequencing. G3 GenesGenomesGenetics 7, 3243–3250 (2017).
37. Borneman, A. R., Zeppel, R., Chambers, P. J. & Curtin, C. D. Insights into the Dekkera bruxellensis Genomic Landscape: Comparative Genomics Reveals Variations in Ploidy and Nutrient Utilisation Potential amongst Wine Isolates. PLOS Genet. 10, e1004161 (2014).
38. Liu, H., Wu, S., Li, A. & Ruan, J. SMARTdenovo: a de novo assembler using long noisy reads. Gigabyte 2021, 1–9 (2021).
39. Roach, M. J. & Borneman, A. R. New genome assemblies reveal patterns of domestication and adaptation across Brettanomyces (Dekkera) species. BMC Genomics 21, 194 (2020).
40. Smukowski Heil, C. S. et al. Loss of Heterozygosity Drives Adaptation in Hybrid Yeast. Mol. Biol. Evol. 34, 1596–1612 (2017).
41. Lancaster, S. M., Payen, C., Smukowski Heil, C. & Dunham, M. J. Fitness benefits of loss of heterozygosity in Saccharomyces hybrids. Genome Res. 29, 1685–1692 (2019).
42. Jackson, J. A. & Tinsley, R. C. Parasite infectivity to hybridising host species: a link between hybrid resistance and allopolyploid speciation? Int. J. Parasitol. 33, 137–144 (2003).
43. Augustine, R., Majee, M., Gershenzon, J. & Bisht, N. C. Four genes encoding MYB28, a major transcriptional regulator of the aliphatic glucosinolate pathway, are differentially expressed in the allopolyploid Brassica juncea. J. Exp. Bot. 64, 4907–4921 (2013).
44. Thompson, J. N., Nuismer, S. L. & Merg, K. Plant polyploidy and the evolutionary ecology of plant/animal interactions: PLANT POLYPLOIDY AND PLANT/ANIMAL INTERACTIONS. Biol. J. Linn. Soc. 82, 511–519 (2004).
45. Těšitelová, T. et al. Ploidy-specific symbiotic interactions: divergence of mycorrhizal fungi between cytotypes of the Gymnadenia conopsea group (Orchidaceae). New Phytol. 199, 1022–1033 (2013).
46. Selmecki, A. M. et al. Polyploidy can drive rapid adaptation in yeast. Nature 519, 349–352 (2015).

47. Wani, G. A., Shah, M. A., Reshi, Z. A. & Dar, M. A. Polyploidy determines the stage of invasion: clues from Kashmir Himalayan aquatic flora. Acta Physiol. Plant. 40, 58 (2018).
48. Ng, D. W.-K. et al. Proteomic divergence in Arabidopsis autopolyploids and allopolyploids and their progenitors. Heredity 108, 419–430 (2012).
49. Leggatt, R. A. & Iwama, G. K. Occurrence of polyploidy in the fishes. Rev. Fish Biol. Fish. 13, 237–246 (2003).
50. Barker, M. S., Arrigo, N., Baniaga, A. E., Li, Z. & Levin, D. A. On the relative abundance of autopolyploids and allopolyploids. New Phytol. 210, 391–398 (2016).
51. Istace, B. et al. de novo assembly and population genomic survey of natural yeast isolates with the Oxford Nanopore MinION sequencer. GigaScience 6, (2017).
52. Sedlazeck, F. J. et al. Accurate detection of complex structural variations using single-molecule sequencing. Nat. Methods 15, 461–468 (2018).
53. Koren, S. et al. Canu: scalable and accurate long-read assembly via adaptive k -mer weighting and repeat separation. Genome Res. 27, 722–736 (2017).
54. Li, H. & Durbin, R. Fast and accurate short read alignment with Burrows-Wheeler transform. Bioinformatics 25, 1754–1760 (2009).
55. Li, H. et al. The Sequence Alignment/Map format and SAMtools. Bioinformatics 25, 2078–2079 (2009).
56. McKenna, A. et al. The Genome Analysis Toolkit: A MapReduce framework for analyzing next-generation DNA sequencing data. Genome Res. 20, 1297–1303 (2010).
57. Danecek, P. et al. The variant call format and VCFtools. Bioinformatics 27, 2156–2158 (2011).
58. Charif, D. & Lobry, J. R. SeqinR 1.0-2: A Contributed Package to the R Project for Statistical Computing Devoted to Biological Sequences Retrieval and Analysis. in Structural Approaches to Sequence Evolution (eds. Bastolla, U., Porto, M., Roman, H. E. & Vendruscolo, M.) 207–232 (Springer Berlin Heidelberg, 2007). doi:10.1007/978-3-540-35306-5_10.
59. Schliep, K. P. phangorn: phylogenetic analysis in R. Bioinformatics 27, 592–593 (2011).
60. Rambaut, A. FigTree, a graphical viewer of phylogenetic trees. Institute of Evolutionary Biology University of Edinburgh. FigTree, a graphical viewer of phylogenetic trees http://tree.bio.ed.ac.uk/software/figtree/ (2009).
61. Jombart, T. adegenet: a R package for the multivariate analysis of genetic markers. Bioinformatics 24, 1403–1405 (2008).
62. Yin, T., Cook, D. & Lawrence, M. ggbio: an R package for extending the grammar of graphics for genomic data. Genome Biol. 13, R77 (2012).

Conclusion and perspectives

Towards accurate, contiguous and complete polyploid phasing algorithms

Despite extensive efforts, polyploid phasing algorithms have been held back by the limited read length of short read sequencing methods. The arrival of long-read sequencing methods has led to very efficient diploid phasing methods, such as WhatsHap[1] and Falcon-Unzip[2]. However, the problem of polyploid phasing remained. In part due to the non-negligible error rate of these new sequencing technologies, but also due to a euploid bias which presumes that a polyploid with n copies of its genome has n haplotypes throughout its genome. We are now in the midst of a paradigm shift, with the short read polyploid phasing methods being phased out in favor of long read methods and an increasing acknowledgement of the complexity of the genomic structures being phased. The recently published polyploid phasing tool Ranbow handles the edge case of having fewer distinct haplotypes than genomic copies in a region[3], and the long-read polyploid phasing method WhatsHap polyphase explicitly tackles this problem through its solution of "haplotype threading" which uses coverage information to determine which haplotype is present multiple times[4]. With our phasing algorithm, nPhase, we explicitly consider that ploidy is uncertain and present a ploidy agnostic method which allows for variation in the number of haplotypes, making it possible to handle aneuploidy, large LOH events and relieving the user from the task of estimating and selecting a ploidy[5]. We also question the usefulness of the SWitch Error Rate metric, which we argue is fundamentally unpredictable, and consider that more attention should be given to the inseparable notions of accuracy and contiguity in this field.

In the future, solutions to the polyploid phasing problem need to go beyond the

innovations of nPhase and tackle remaining issues and improvements. Since nPhase is a reference alignment phasing method, it does not natively resolve structural variants. Currently, the phasing results of nPhase can only be used to heterozygous structural variation by performing additional analysis, such as *de novo* assembly of the phased reads followed by comparison of the assembled sequences. Phasing indels is crucial to identifying frameshift events in polyploids to determine if there is a functional copy of a given gene, however nPhase doesn't phase these events. Further analysis is required to determine the impact of including indels in the phaseable genetic markers, particularly given the propensity of long-read sequencing methods to suffer from homopolymer errors. Finally, future methods would greatly benefit from incorporating metadata that aids in the interpretation of results such as confidence metrics or phasing quality scores. Taking base-calling quality and mapping quality into account can also serve to improve the accuracy of these methods. Finally, we also find it would be highly beneficial to generate simulated and real validation datasets against which to systematically benchmark all polyploid phasing tools with carefully selected performance metrics. This practice would not only allow for a standardization of the highly diverse methods used in the benchmarking step, it would also highlight the strengths and weaknesses of polyploid phasing tools, providing deeper insight into their differences and helping users select the most appropriate method.

Applications of polyploid phasing to population genomics

Due to the lack of effective polyploid phasing methods, there has been very little application of polyploid phasing to populations. In a paper on *S. cerevisiae* beer strains, Fay *et al.* (2019)[6] developed what is arguably the first polyploid phasing method in order to show that one of the three main clades of beer strains is composed of a polyploid admixture of Asian and European wine strains. Using nPhase and a

population of 35 beer strains of *S. cerevisiae* stemming from different clades, we were able to characterize two other groups of beer strains. The European dominant group was shown to be a similar admixture to the Asian dominant clade, but with different proportions, and the African Beer group was shown to mostly have European wine and French dairy alleles. Both French dairy strains and African Beer strains of *S. cerevisiae* share their environment with lactic acid bacteria, which we hypothesize is a driver of the allelic similarities between them. We developed the notion of intra-strain divergence, where we calculate the divergence between the different haplotypes within a strain, and the notion of estimating the divergence between the haplotypes of strains, showing that the distance between strains is typically lower than would be estimated with unphased data. Having phased genes in this polyphyletic group of strains exposed to similar environments allowed us to identify the genes with the highest levels of divergence (>4%), which we found to be enriched for GO terms relevant for adaptations to the brewing environment. Polyploid strains of *S. cerevisiae* are only found in a few clades, including all of the clades containing beer strains. Our study did not uncover any further connection between beer brewing strains and polyploidy, though this dataset may provide important insight into the mechanisms which seem to pressure *S. cerevisiae* beer-brewing strains into polyploidy.

We also studied a population of 71 diverse strains of *B. bruxellensis*, in which many triploid strains were suspected of being composed of a core diploid genome hybridized with a set of chromosomes from a different species[7]. We found that the long reads of such hybrid strains were easily identified by calculating the density of SNPs that don't match with the *B. bruxellensis* reference genome and plotting their distribution. Hybrid strains output a bimodal distribution, with a set of reads which have few mismatches relative to the reference (<10 SNPs/kb) and a set of reads, belonging to the extra set of chromosomes, which has many mismatches to the

reference (>14 SNPs/kb). We could then simply phase these strains by separating reads based on their SNP density. This phasing method could not apply to strains of another specific polyploid subpopulation (wine 3 triploids) which do not exhibit this bimodal distribution, prompting us to phase them using nPhase. This allowed us to show that while the core genomes were always very similar, even across subpopulations, the diverged set of chromosomes is not the same in any two subpopulations, and therefore was acquired independently from different species by each subpopulation of *B. bruxellensis*, potentially as adaptations to their respective environments. We ruled out known sister species of *B. bruxellensis* such as *Brettanomyces anomala* and *Brettanomyces nanus* as the hybridization candidates, prompting the need for a search to identify them.

Performing these studies highlighted the need for accessory tools and analytical methods which leverage polyploid phasing data to improve insight into the data. The tools which need to be developed range from simple ones, such as a tool which performs comparisons between haplotypes within a strain which expose simple statistics such as the similarity between haplotypes or the basecall quality and mapping quality scores throughout the genome, to more complex tools such as a tool which identifies missense, nonsense and frameshift states in genes of phased haplotypes. The latter would require a tool which handles indels at minimum, and structural variants at best. We now have the possibility to perform population genomic studies with polyploid genomes which exploit phased data, and there is significant room for the development and application of novel tools and methods to analyze this data.

In a future project, our dataset of high-quality real phased genomes could be leveraged to develop a ploidy agnostic polyploid *de novo* assembly algorithm. These real genomes, containing aneuploidies, large LOH events and highly likely to contain

structural variants, can serve as a crucial validation dataset to direct the development of such an algorithm. Our high confidence in the phasing provided by nPhase allows us to reasonably expect that improvement in the *de novo* assembly's similarity to the predictions of nPhase will translate to improvement in *de novo* assembly quality. A ploidy agnostic *de novo* assembly algorithm loses the guide of a reference genome, complexifying the problem, but also gains the freedom to faithfully reconstruct structural variants, sequences not present in the reference and duplication events. The core idea of nPhase is to allow like reads to cluster based on similarity, with an emphasis on the weight of variable positions as identified by Illumina. A first step in an endeavor to develop a novel *de novo* assembly algorithm could be to identify variable positions within similar blocks through mapping and variant calling reads, and then subsequently perform *de novo* assembly with an additional constraint based on the same rules as nPhase. If results are promising, the next phase would seek to make the identification of variable positions not require lengthy mapping and variant calling steps. Such a tool would take us closer to an accurate picture of polyploid genomes, permitting deeper insights into genotype-phenotype relationships.

The phasing out of approximations

Earlier this year, the Telomere-To-Telomere (T2T) consortium pre-published the complete human genome[8], analysis of segmental duplications[9], epigenetic patterns of the complete genome[10], the centromeres[11] and repeat elements[12]. If the genomic era is in part defined by the sequencing boom afforded by short read high-throughput sequencing methods and the promises of population genomic studies and GWAS methods, the next era may be in part defined by the unprecedented detail afforded by long-read sequencing methods. Individual molecules will be sequenced directly, obtaining high-quality *de novo* assemblies will be considered a pre-processing step, reference sequences will be replaced by genome graphs, multi-omics will routinely

be integrated in population genomics projects and approximations will become increasingly rare.

We need highly modular, integrated toolkits, analysis platforms and standardized analysis and benchmarking protocols to catch up with the immense quantity of data we routinely generate and tip the scale towards analyzing data faster than we can generate it.

References

1. Patterson, M. et al. WhatsHap: Weighted Haplotype Assembly for Future-Generation Sequencing Reads. J. Comput. Biol. 22, 498–509 (2015).
2. Chin, C.-S. et al. Phased diploid genome assembly with single-molecule real-time sequencing. Nat. Methods 13, 1050–1054 (2016).
3. Moeinzadeh, M.-H. et al. Ranbow: A fast and accurate method for polyploid haplotype reconstruction. PLOS Comput. Biol. 16, e1007843 (2020).
4. Schrinner, S. D. et al. Haplotype threading: accurate polyploid phasing from long reads. Genome Biol. 21, 252 (2020).
5. Abou Saada, O., Tsouris, A., Eberlein, C., Friedrich, A. & Schacherer, J. nPhase: an accurate and contiguous phasing method for polyploids. Genome Biol. 22, 126 (2021).
6. Fay, J. C. et al. A polyploid admixed origin of beer yeasts derived from European and Asian wine populations. PLOS Biol. 17, e3000147 (2019).
7. Borneman, A. R., Zeppel, R., Chambers, P. J. & Curtin, C. D. Insights into the Dekkera bruxellensis Genomic Landscape: Comparative Genomics Reveals Variations in Ploidy and Nutrient Utilisation Potential amongst Wine Isolates. PLOS Genet. 10, e1004161 (2014).
8. Nurk, S. et al. The complete sequence of a human genome. bioRxiv 2021.05.26.445798 (2021) doi:10.1101/2021.05.26.445798.
9. Vollger, M. R. et al. Segmental duplications and their variation in a complete human genome. bioRxiv 2021.05.26.445678 (2021) doi:10.1101/2021.05.26.445678.
10. Gershman, A. et al. Epigenetic Patterns in a Complete Human Genome. bioRxiv 2021.05.26.443420 (2021) doi:10.1101/2021.05.26.443420.
11. Altemose, N. et al. Complete genomic and epigenetic maps of human centromeres. bioRxiv 2021.07.12.452052 (2021) doi:10.1101/2021.07.12.452052.
12. Hoyt, S. J. et al. From telomere to telomere: the transcriptional and epigenetic state of human repeat elements. bioRxiv 2021.07.12.451456 (2021) doi:10.1101/2021.07.12.451456.

APPENDIX

Companion document

Some supplemental figures and tables from chapters II and III take too much space and have been added to a companion document available online at

https://doi.org/10.5281/zenodo.5207333

List of publications

- Fournier T., **Abou Saada O.**, Hou J., Peter J., Caudal E., Schacherer J.
Extensive impact of low-frequency variants on the phenotypic landscape at population-scale. eLife. 2019 Oct 24;8:e49258.

- **Abou Saada O.**, Tsouris A., Eberlein C., Friedrich A., Schacherer J.
nPhase: an accurate and contiguous phasing method for polyploids. Genome Biol. 2021 Apr 29;22(1):126.

- Eberlein, C., **Abou Saada, O.**, Friedrich, A., Albertin, W. & Schacherer, J.
Different trajectories of polyploidization shape the genomic landscape of the *Brettanomyces bruxellensis* yeast species. (Accepted for publication in Genome Research)

- Peltier, E.,Vion, C., **Abou Saada, O.**, Friedrich, A., Schacherer J., Marullo P.
Flor yeasts rewire the central carbon metabolism during wine alcoholic fermentation. (Under review in Frontiers in Fungal Biology)

- **Abou Saada, O.**, Tsouris, A., Large, C., Friedrich A., Dunham M., Schacherer J.
Phased polyploid genomes provide deeper insights into the different evolutionary trajectories of the *Saccharomyces cerevisiae* beer yeasts. (In preparation)

- **Abou Saada, O.**, Friedrich A., Schacherer J. Towards accurate, contiguous and complete polyploid phasing algorithms. (Review, in preparation)

List of oral communications

Pint of Science – scientific popularization
Strasbourg, France, May 2018
Comment trouver un gène dans une botte de foin [How to find a gene in a haystack]

Oxford Nanopore event - The state of Nanopore sequencing in 2018: technical updates and applications in Strasbourg
Strasbourg, France, October 2018
Exploration of the structural variant landscape in yeast using Oxford Nanopore sequencing

EMBO Workshop – Comparative genomics of eukaryotic microbes: Genomes in flux, and flux between genomes
Sant Feliu de Guixols, Spain, October 2019
Ploidy agnostic phasing method with short and long read sequencing,

Lightning talk for Oxford Nanopore event initially planned in Paris.
Presented online, March 2020
nPhase – Ploidy agnostic pipeline

Teaching

University of Strasbourg

2018-2020
Classes for doctoral students
o Français Langue Étrangère [French as a foreign language]

2020-2021
Classes for master's degree students
o Génétique Quantitative Appliquée [Applied Quantitative Genetics]
o Génomique Fonctionelle et Évolutive [Functional and Evolutionary Genomics]